SPECTROSCOPIC AND PHASE TRANSITION STUDIES OF SOME HEXAFLUORO SILICATES AND TITANATES OF DIVALENT METALS

SYNOPSIS OF

A THESIS
Submitted
To

The North-Eastern Hill University,
Shillong - 793001

in fulfilment of the requirement of the degree of

DOCTOR OF PHILOSOPHY

By

GANESH THAKUR

Department of Physics
School of Physical Sciences

The North-Eastern Hill University
Bijni Complex, Shillong-793003

INDIA

AUGUST, 1989

S Y N O P S I S

Title : "Spectroscopic and Phase Transition Studies of Some Hexafluoro Silicates and Titanates of Divalent Metals"

Ph.D thesis

by

Ganesh Thakur

Under the Supervision of Prof. A L Verma

There has been considerable interest in the study of metal hexahydrate compounds containing cations $[M(OH_2)_6]^{2+}$ and anions $[XF_6]^{2-}$, where M is a divalent metal ion and X stands for Si or Ti - a tetravalent element, in order to gain information about the bonding and dynamics of water molecules in these solids. Several of the hexahydrated fluorosilicates $[M(OH_2)_6SiF_6$; where M = Fe, Mg, Mn, Co etc$]$ and fluorotitanates $[M(OH_2)_6TiF_6$; where M = Zn, Ni, Co, Mg etc$]$ undergo structural phase transitions at low temperatures in which the high temperature rhombohedral phase generally changes over to a low symmetry phase. On the other hand, the Zn and Ni hexahydrated fluorosilicates are known to maintain room temperature structure down to 10k [Jenkins and Lewis, 1981] whereas Ni and Zn hexahydrated fluoro-titanates undergo structural phase transition at low temperatures [Choudhury et al, 1983].

Physics

In most of the hexaaquo-metal hexafluoro silicates, the $[SiF_6]^{2-}$ ion has a O_h molecular symmetry and, in the crystals of space group C_{3i}^2, occupies a site of symmetry C_{3i}; as for example the salts of Ni, Zn and Co fluorosilicate hexahydrates. The other salts of the series belong to the space group D_{3d}^5 and the site symmetry of the $[SiF_6]^{2-}$ ion in this type of crystals is D_{3d} [Ray et al, 1973]. Moreover, the $[M(OH_2)_6]^{2+}$ complex has the molecular symmetry T_h and occupies a site of symmetry C_{3i} or D_{3d} in the crystals of space group C_{3i}^2 or D_{3d}^5. The water molecules of the system have C_{2v} molecular symmetry and also occupy sites of symmetry C_{2v} in both types of crystals. Most of the hexaaquo metal hexafluoro silicates and titanates have a trigonally distorted CsCl type of structure and their unit cell has one formula unit. In all the salts of the series there is a disorder in the orientations of the $[SiF_6]^{2-}$ anions between two sites unrelated by any symmetry element and with unequal occupancy. In the Fe and Mg salts, there is a two-fold disorder in the $[M(OH_2)_6]^{2+}$ complex and for the $Mg(OH_2)_6SiF_6$ salt, the high temperature space group R $\bar{3}$m (D_{3d}^5) changes to $P_{2\ 1/c}$ (C_{2h}^5) at low temperature during phase transition. The structure of the low temperature phase for most of the members of the series is unknown. Although a good deal of work has been reported on phase transitions in some members of the series by X-ray [Datta et al, 1979], specific heat [Karnezos et al, 1978), EPR [J. How et al, 1974 ; Rubins et al, 1976] and other techniques [Jenkins et al, 1981; Francis et al, 1977; Poulet et al, 1978], the understanding of the mechanism of phase

transitions is still obscure in this series of salts. In particular one does not understand why among crystals of similar structure and parameters only a few show phase transitions while others do not? Moreover, some of the fluorotitanates of the series show two phase transitions while others show only one?

In order to understand the dynamics of structural phase changes in this family of salts, identify the low temperature phase, understand the bonding of water molecules and their role in the phase transition mechanism in these salts, we undertook systematic Laser Raman studies on oriented single crystals at different temperatures and infrared absorption measurements at room temperature on the following salts -

(i) $CdSiF_6:6H_2O$ (ii) $CdTiF_6:6H_2O$ and their deuterated analogues i.e. (iii) $CdSiF_6:6D_2O$ and (iv)$CdTiF_6:6D_2O$

We undertook systematic studies on these salts because, to our knowledge, no literature was available on the spectroscopic or the phase transition studies to arrive at a comprehensive picture of the mechanism of phase transitions in these systems. Although the process of growing single crystals of these salts is very difficult, we undertook the preparation of constituent materials and devised a method for growing single crystals in order to explore their properties by spectroscopic methods.

In order to elucidate the mechanism of phase transition, it is important to understand the vibrational characteristics of the system at both ends of phase transition and correct assignment of

the bands is very important. We, therefore, undertook measurements on single crystals of the above mentioned salts at various temperatures. Specifically we studied in depth the internal modes of the $[SiF_6]^{2-}$ and $[TiF_6]^{2-}$ octahedra, internal and librational modes of water molecules, variation of FWHM of some internal modes and lattice modes and the variation of peak intensities of some bands of these systems as a function of temperature. The work in this thesis is divided into the following chapters -

In Chapter I a brief review and discussion on various types of phase transitions, crystal hydrates, anharmonicity, Fermi Resonance, hydrogen bonding,isotopic substitution, previous vibrational studies (IR and Raman) on some other salts in this series and structural phase transitions on $MXF_6:6H_2O/6D_2O$ single crystals have been given.

The experimental aspects relevent for the present investigation are given in Chapter II. A brief description of preparation and purification of samples, modification in the solution method for growing single crystals are discussed. A brief description of the techniques used for recording Raman spectra at room temperature as well as at low temperature, the Ramalog 1403 double monochromator, the Argon-Ion laser source, the helium cryo-cooler unit and the method of deuteration of the samples are given in this chapter [Thakur G, 1983].

The Chapter III deals with the pertinent theoretical details for understanding these systems. A brief description of the structure of the crystals, group theoretical analysis, Bhagavantam's method, local or site symmetry approach, correlation method etc are explained for determining the vibrational modes, their activity in the IR and Raman etc.

Chapter IV gives a detailed temperature-dependent Raman spectroscopic study on single crystals of $CdTiF_6:6H_2O$. The Raman spectra at room temperature and at 10k in all the six polarization geometries are given. The IR spectrum at room temperature is also given in this chapter. The Raman spectral data at different temperatures at the intervals of 10k or 5k from room temperature to 10k are also given. The important findings on this system are summarized as follows [Thakur and Verma, 1986] .

(a) The room temperature space group of $CdTiF_6:6H_2O$ is C_{3i}^2 $(R\bar{3})$.

(b) There are two structural phase transitions, one at 200k and the other at 80k.

(c) The space group of the crystal below 80k is C_{2h}^5 in monoclinic series.

(d) The high temperature phase transition is triggered by distortions in the $[Cd(OH_2)_6]^{2+}$ octahedra.

(e) The low temperature phase transition is triggered by similar distortions in the $[TiF_6]^{2-}$ octahedra.

Chapter V deals with the detailed study on $CdSiF_6:6H_2O$ single crystals which can be summarized as follows -

(a) The Raman spectra in all the six polarization geometries of the single crystals of the salt at room temperature and 10k.

(b) IR spectra of the salt at room temperature.

(c) Raman spectra of the single crystals at different temperatures at intervals of 10k or 5k from room temperature to 10k in the $\{x(yy)z\}$ polarization geometry.

(d) Evaluation of peak intensity, measurement of FWHM of some isolated bands at different temperatures.

(e) Assignments of bands at room temperature as well as at 10k.

From the above observations, the following conclusions are drawn in this chapter [Thakur and Verma, 1989] -

(1) The space group of $CdSiF_6:6H_2O$ at room temperature is C_{3i}^2 $(R\bar{3})$.

(2) A structural phase transition at about 220k. There is no second phase transition as observed in case of $CdTiF_6:6H_2O$.

(3) The low temperature space group of the system is most likely C_{2h} in the monoclinic series.

(4) The phase transition in this case is triggered due to distortions in the $[Cd(OH_2)_6]^{2+}$ octahedra.

The temperature dependent Raman study of single crystals of deuterated Cadmium fluoro silicate ($CdSiF_6:6D_2O$) is discussed in Chapter VI. The Raman spectra at room temperature as well as at 10k in all the six polarization geometries are given.

Frequency shift, peak intensity and FWHM as a function of temperature have been measured in this system. From the above observations, we discovered a phase transition in this system at 235k which shows a rise of 15k in the transition temperature compared to the hydrogenated system [Thakur and Verma, 1989].

The anomalous behaviour of $\Delta\nu_{\frac{1}{2}}$ of ν_s(O-D) stretching mode as a function of temperature from room temperature to 10k has been explained in terms of various dephasing mechanisms.

The low temperature space group of $CdSiF_6:6D_2O$ is found to be C_{2h} which is the same as of its hydrogenated analogue $CdSiF_6:6H_2O$.

Chapter VII contains the study of the crystal of $CdTiF_6:6D_2O$ at room temperature as well as at low temperatures in all the six polarization geometries. The temperature dependent Raman study of some bands including that due to the ν_s(O-D) mode has been given in this chapter. We discovered two phase transformations in this system, at 218k and 110k [Thakur and Verma]. This shows that there is a rise in the phase transition temperatures by 18k and 30k in the high and low temperature T_c's with respect to the $CdTiF_6:6H_2O$ salt. The space group at 10k is deduced C_{2h} which remains the same as of the hydrogenated analogue. It is concluded that the pure vibrational dephasing mechanism provides a major contribution to the width of the symmetric stretching mode ν_s(O-D).

References

[1] Choudhury P, Ghosh B, Lamba O P and Bist H D, J. Phys. C 16, 1609 (1983).

[2] Choudhury P, Ghosh B, Lamba O P and Bist H D, J. Raman Spectrosc. 14, 99 (1983).

[3] Datta S K and De Debabala, Indian J. Phys. 52A, 499 (1978) and J. Cryog. 4(1), 39 (1979).

[4] Francis C L and Culvahouse, J W, J. Chem. Phys. 66, 1089 (1977).

[5] How T and Svare I, Physica Scripta, 9, 40 (1974).

[6] Jenkins T E and Lewis J, Spectrochim Acta, 37A, 47 (1981).

[7] Jenkins T E and Lewis J, Physica Scripta, 18, 351 (1978).

[8] Jenkins T E and Lewis J, J. Raman Spectrosc. 8, 111 (1979).

[9] Jenkins T E and Lewis J, J. Raman Spectrosc. 11, 1 (1981).

[10] Karnezoz M and Friedberg S A, J. Appl. Phys. 49, 1380 (1978).

[11] Majumdar M and Datta S K, J. Chem. Phys. 42(1), 418 (1965).

[12] Poulet H and Mathieu J., C.R. Acad. Sc. Paris, t-286(12) Series B, 331 (1978).

[13] Ray S, Zalkin A and Templeton D H, Acta Crystallogr. B29, 2741 (1973).

[14] Rubins R S, Griffin B C and Burris R, J. Chem. Phys. 64, 3349 (1976).

[15] Thakur G, Proc. of Second National Seminar on 'Crystal Growth' Aug. 27-30 (1984), Anna University, Madras.

[16] Thakur G, Symp. on 'Crystal Growth' Dec. 24, (1983) Anna University, Madras.

[17] Thakur G and Verma A L, J. Raman Spectrosc. 17, 207 (1986).

[18] Thakur G and Verma A L, J. Raman Spectrosc. 20, 000 (1989).

[19] Thakur G and Verma A L, Spectrochim Acta 45A, 615 (1989).

[20] Thakur G and Verma A L, to be communicated.

[21] Thakur G and Verma A L, Proc. of SSP Symp. Dec. 23-25 (1984) Vol 27C, pp. 282, BARC, Bombay.

[22] Volland U, Hösl S and Spiering H, Solid State Commun. 27, 49 (1978).

SPECTROSCOPIC AND PHASE TRANSITION STUDIES OF SOME HEXAFLUORO SILICATES AND TITANATES OF DIVALENT METALS

A THESIS
Submitted
To

The North-Eastern Hill University,
Shillong - 793001

in fulfilment of the requirement of the degree of

DOCTOR OF PHILOSOPHY

By

GANESH THAKUR

Department of Physics
School of Physical Sciences

The North-Eastern Hill University
Bijni Complex, Shillong-793003

INDIA

AUGUST, 1989

DEDICATED
IN THE MEMORY OF
MY
MOTHER

Professor A L Verma
Dean
School of Physical Sciences

Phone:
Grams : NEHU

North - Eastern Hill University

Bijni Complex
Bhagyakul, Shillong-793003 (Meghalaya)

Department of...Physics....

C E R T I F I C A T E

I certify that the thesis entitled "SPECTROSCOPIC AND PHASE TRANSITION STUDIES OF SOME HEXAFLUORO SILICATES AND TITANATES OF DIVALENT METALS" submitted by Shri Ganesh Thakur for the Degree of Doctor of Philosophy of the North-Eastern Hill University, Shillong embodies the record of original research work carried out by him under my supervision.

He has been duly registered and the thesis presented is worthy of being considered for the Award of Ph.D. Degree.

This work has not been submitted to any other University for any Degree.

A L Verma
11.8.89

Dated, August 1989
Shillong

(A L VERMA)
Thesis Supervisor

Phone:
Grams : NEHU

North - Eastern Hill University

Bijni Complex
Bhagyakul, Shillong-793003 (Meghalaya)

Head,
Department of Physics

C E R T I F I C A T E

This is to certify that Mr. GANESH THAKUR has cleared the following four courses as a requirement for Ph.D/M.Phil. programme obtaining grade 'A' on an average (on Seven Point Scale)

Course		Grade
1. Group Theory and Molecular Physics II	-	B
2. Chemical Binding	-	A
3. Laser Physics	-	A
4. Electronics II	-	B^+

(Y.S.T. Rao)
Professor and Head
Department of Physics
School of Physical Sciences
North-Eastern Hill University, Shillong
793003

A C K N O W L E D G E M E N T S

At the outset I wish to express my deepest sense of gratitude to Professor A.L. Verma for providing me an opportunity to do research work in the laser laboratories, suggesting me the research problem and guiding me throughout the course of my Ph.D programme.

I take the opportunity to thank Professor C.S. Shastry, Professor Y.S.T. Rao, Dr. Kamal Kumar and Dr. T. Chakraborty for their kind help during the course of this work.

I also extend my sincere thanks to Mr. A.K. Rathore, Mr. L.B. Rathore and B. Borgohain for assisting me in recording the Raman spectra; to Mr. Sadhu for the typing of this thesis and to all the Research Scholars in the laser laboratories for their kind co-operation.

I am grateful to U.G.C., New Delhi, for awarding me Teacher Fellowship for doing research work in N.E.H.U., Shillong, and to D.S.T., New Delhi, for providing Raman spectrometer.

Lastly I remain indebted to my wife (Shailkumari) and my Tutu, Sonu and Mary for their encouragement and understanding during the course of my research work.

Ganesh Thakur

Ganesh Thakur

S Y N O P S I S

Title : "Spectroscopic and Phase Transition Studies of Some Hexafluoro Silicates and Titanates of Divalent Metals"

Ph.D thesis

by

Ganesh Thakur

Under the Supervision of Prof. A L Verma

There has been considerable interest in the study of metal hexahydrate compounds containing cations $[M(OH_2)_6]^{2+}$ and anions $[XF_6]^{2-}$, where M is a divalent metal ion and X stands for Si or Ti - a tetravalent element, in order to gain information about the bonding and dynamics of water molecules in these solids. Several of the hexahydrated fluorosilicates $[M(OH_2)_6SiF_6$; where M = Fe, Mg, Mn, Co etc$]$ and fluorotitanates $[M(OH_2)_6TiF_6$; where M = Zn, Ni, Co, Mg etc$]$ undergo structural phase transitions at low temperatures in which the high temperature rhombohedral phase generally changes over to a low symmetry phase. On the other hand, the Zn and Ni hexahydrated fluorosilicates are known to maintain room temperature structure down to 10k [Jenkins and Lewis, 1981] whereas Ni and Zn hexahydrated fluoro-titanates undergo structural phase transition at low temperatures [Choudhury et al, 1983].

In most of the hexaaquo-metal hexafluoro silicates, the $[SiF_6]^{2-}$ ion has a C_h molecular symmetry and, in the crystals of space group C_{3i}^2, occupies a site of symmetry C_{3i}; as for example the salts of Ni, Zn and Co fluorosilicate hexahydrates. The other salts of the series belong to the space group D_{3d}^5 and the site symmetry of the $[SiF_6]^{2-}$ ion in this type of crystals is D_{3d} [Ray et al, 1973]. Moreover, the $[M(OH_2)_6]^{2+}$ complex has the molecular symmetry T_h and occupies a site of symmetry C_{3i} or D_{3d} in the crystals of space group C_{3i}^2 or D_{3d}^5. The water molecules of the system have C_{2v} molecular symmetry and also occupy sites of symmetry C_{2v} in both types of crystals. Most of the hexaaquo metal hexafluoro silicates and titanates have a trigonally distorted CsCl type of structure and their unit cell has one formula unit. In all the salts of the series there is a disorder in the orientations of the $[SiF_6]^{2-}$ anions between two sites unrelated by any symmetry element and with unequal occupancy. In the Fe and Mg salts, there is a two-fold disorder in the $[M(OH_2)_6]^{2+}$ complex and for the $Mg(OH_2)_6SiF_6$ salt, the high temperature space group $R\bar{3}m$ (D_{3d}^5) changes to $P_{2\ 1/c}$ (C_{2h}^5) at low temperature during phase transition. The structure of the low temperature phase for most of the members of the series is unknown. Although a good deal of work has been reported on phase transitions in some members of the series by X-ray [Datta et al, 1979], specific heat [Karnezos et al, 1978), EPR [J. How et al, 1974 ; Rubins et al, 1976] and other techniques [Jenkins et al, 1981; Francis et al, 1977; Poulet et al, 1978], the understanding of the mechanism of phase

transitions is still obscure in this series of salts. In particular one does not understand why among crystals of similar structure and parameters only a few show phase transitions while others do not? Moreover, some of the fluorotitanates of the series show two phase transitions while others show only one?

In order to understand the dynamics of structural phase changes in this family of salts, identify the low temperature phase, understand the bonding of water molecules and their role in the phase transition mechanism in these salts, we undertook systematic Laser Raman studies on oriented single crystals at different temperatures and infrared absorption measurements at room temperature on the following salts -

(i) $CdSiF_6:6H_2O$ (ii) $CdTiF_6:6H_2O$ and their deuterated analogues i.e. (iii) $CdSiF_6:6D_2O$ and (iv)$CdTiF_6:6D_2O$

We undertook systematic studies on these salts because, to our knowledge, no literature was available on the spectroscopic or the phase transition studies to arrive at a comprehensive picture of the mechanism of phase transitions in these systems. Although the process of growing single crystals of these salts is very difficult, we undertook the preparation of constituent materials and devised a method for growing single crystals in order to explore their properties by spectroscopic methods.

In order to elucidate the mechanism of phase transition, it is important to understand the vibrational characteristics of the system at both ends of phase transition and correct assignment of

the bands is very important. We, therefore, undertook measurements on single crystals of the above mentioned salts at various temperatures. Specifically we studied in depth the internal modes of the $[SiF_6]^{2-}$ and $[TiF_6]^{2-}$ octahedra, internal and librational modes of water molecules, variation of FWHM of some internal modes and lattice modes and the variation of peak intensities of some bands of these systems as a function of temperature. The work in this thesis is divided into the following chapters -

In Chapter I a brief review and discussion on various types of phase transitions, crystal hydrates, anharmonicity, Fermi Resonance, hydrogen bonding, isotopic substitution, previous vibrational studies (IR and Raman) on some other salts in this series and structural phase transitions on $MXF_6:6H_2O/6D_2O$ single crystals have been given.

The experimental aspects relevent for the present investigation are given in Chapter II. A brief description of preparation and purification of samples, modification in the solution method for growing single crystals are discussed. A brief description of the techniques used for recording Raman spectra at room temperature as well as at low temperature, the Ramalog 1403 double monochromator, the Argon-Ion laser source, the helium cryo-cooler unit and the method of deuteration of the samples are given in this chapter [Thakur G, 1983].

The Chapter III deals with the pertinent theoretical details for understanding these systems. A brief description of the structure of the crystals, group theoretical analysis, Bhagavantam's method, local or site symmetry approach, correlation method etc are explained for determining the vibrational modes, their activity in the IR and Raman etc.

Chapter IV gives a detailed temperature-dependent Raman spectroscopic study on single crystals of $CdTiF_6:6H_2O$. The Raman spectra at room temperature and at 10k in all the six polarization geometries are given. The IR spectrum at room temperature is also given in this chapter. The Raman spectral data at different temperatures at the intervals of 10k or 5k from room temperature to 10k are also given. The important findings on this system are summarized as follows [Thakur and Verma, 1986] .

(a) The room temperature space group of $CdTiF_6:6H_2O$ is C_{3i}^2 ($R\bar{3}$).

(b) There are two structural phase transitions, one at 200k and the other at 80k.

(c) The space group of the crystal below 80k is C_{2h}^5 in monoclinic series.

(d) The high temperature phase transition is triggered by distortions in the $[Cd(OH_2)_6]^{2+}$ octahedra.

(e) The low temperature phase transition is triggered by similar distortions in the $[TiF_6]^{2-}$ octahedra.

Chapter V deals with the detailed study on $CdSiF_6:6H_2O$ single crystals which can be summarized as follows -

(a) The Raman spectra in all the six polarization geometries of the single crystals of the salt at room temperature and 10k.

(b) IR spectra of the salt at room temperature.

(c) Raman spectra of the single crystals at different temperatures at intervals of 10k or 5k from room temperature to 10k in the $\{x(yy)z\}$ polarization geometry.

(d) Evaluation of peak intensity, measurement of FWHM of some isolated bands at different temperatures.

(e) Assignments of bands at room temperature as well as at 10k.

From the above observations, the following conclusions are drawn in this chapter [Thakur and Verma, 1989] -

(1) The space group of $CdSiF_6:6H_2O$ at room temperature is C_{3i}^2 $(R\bar{3})$.

(2) A structural phase transition at about 220k. There is no second phase transition as observed in case of $CdTiF_6:6H_2O$.

(3) The low temperature space group of the system is most likely C_{2h} in the monoclinic series.

(4) The phase transition in this case is triggered due to distortions in the $[Cd(OH_2)_6]^{2+}$ octahedra.

The temperature dependent Raman study of single crystals of deuterated Cadmium fluoro silicate ($CdSiF_6:6D_2O$) is discussed in Chapter VI. The Raman spectra at room temperature as well as at 10k in all the six polarization geometries are given.

Frequency shift, peak intensity and FWHM as a function of temperature have been measured in this system. From the above observations, we discovered a phase transition in this system at 235k which shows a rise of 15k in the transition temperature compared to the hydrogenated system [Thakur and Verma, 1989].

The anomalous behaviour of $\Delta\nu_{\frac{1}{2}}$ of $2\nu_s$(O-D) stretching mode as a function of temperature from room temperature to 10k has been explained in terms of various dephasing mechanisms.

The low temperature space group of $CdSiF_6:6D_2O$ is found to be C_{2h} which is the same as of its hydrogenated analogue $CdSiF_6:6H_2O$.

Chapter VII contains the study of the crystal of $CdTiF_6:6D_2O$ at room temperature as well as at low temperatures in all the six polarization geometries. The temperature dependent Raman study of some bands including that due to the $2\nu_s$(O-D) mode has been given in this chapter. We discovered two phase transformations in this system, at 218k and 110k [Thakur and Verma]. This shows that there is a rise in the phase transition temperatures by 18k and 30k in the high and low temperature T_c's with respect to the $CdTiF_6:6H_2O$ salt. The space group at 10k is deduced C_{2h} which remains the same as of the hydrogenated analogue. It is concluded that the pure vibrational dephasing mechanism provides a major contribution to the width of the symmetric stretching mode $2\nu_s$(O-D).

References

[1] Choudhury P, Ghosh B, Lamba O P and Bist H D, J. Phys. C 16, 1609 (1983).

[2] Choudhury P, Ghosh B, Lamba O P and Bist H D, J. Raman Spectrosc. 14, 99 (1983).

[3] Datta S K and De Debabala, Indian J. Phys. 52A, 499 (1978) and J. Cryog. 4(1), 39 (1979).

[4] Francis C L and Culvahouse, J W, J. Chem. Phys. 66, 1089 (1977).

[5] How T and Svare I, Physica Scripta, 9, 40 (1974).

[6] Jenkins T E and Lewis J, Spectrochim Acta, 37A, 47 (1981).

[7] Jenkins T E and Lewis J, Physica Scripta, 18, 351 (1978).

[8] Jenkins T E and Lewis J, J. Raman Spectrosc. 8, 111 (1979).

[9] Jenkins T E and Lewis J, J. Raman Spectrosc. 11, 1 (1981).

[10] Karnezoz M and Friedberg S A, J. Appl. Phys. 49, 1380 (1978).

[11] Majumdar M and Datta S K, J. Chem. Phys. 42(1), 418 (1965).

[12] Poulet H and Mathieu J., C.R. Acad. Sc. Paris, t-286(12) Series B, 331 (1978).

[13] Ray S, Zalkin A and Templeton D H, Acta Crystallogr. B29, 2741 (1973).

[14] Rubins R S, Griffin B C and Burris R, J. Chem. Phys. 64, 3349 (1976).

[15] Thakur G, Proc. of Second National Seminar on 'Crystal Growth' Aug. 27-30 (1984), Anna University, Madras.

[16] Thakur G, Symp. on 'Crystal Growth' Dec. 24, (1983) Anna University, Madras.

[17] Thakur G and Verma A L, J. Raman Spectrosc. 17, 207 (1986).

[18] Thakur G and Verma A L, J. Raman Spectrosc. 20, 000 (1989).

[19] Thakur G and Verma A L, Spectrochim Acta 45A, 615 (1989).

[20] Thakur G and Verma A L, to be communicated.

[21] Thakur G and Verma A L, Proc. of SSP Symp. Dec. 23-25 (1984) Vol 27C, pp. 282, BARC, Bombay.

[22] Volland U, Hösl S and Spiering H, Solid State Commun. 27, 49 (1978).

CONTENTS

C H A P T E R I

General Introduction

CHAPTER I

1.1 Phase transition

Many solids (metals, semiconductors or insulators) exhibit structural phase changes from their room temperature phase, on being subjected to change in temperature or pressure or both. The subject of structural phase transformation in crystals has been discussed by a good number of persons like Rao et al [1,2], Buerger [3], Thomas [4], Staveley [5], Tayal et al [6], Smolchowski [7], Owens et al [8], Muller et al [9], and Ubbelohde [10]. An outline of the phase transformation in solids is presented here which may be relevant with regard to this work. Here after phase transition or phase transformation means structural phase transformation.

1.1.1 Definition of phase transition in solids

The phase transformation, in general, is a change in the structure of the solid which occurs in two different ways. Firstly, the atoms of a solid reconstruct a new lattice, for example - transformation of graphite into diamond and change of amorphous to crystalline state of a solid. These reconstructive type of transformations involve transport of matter and are very slow. Moreover these transformations are not symmetry related in any way and belong to first order category.

In another kind of phase transformation, a regular lattice is distorted only slightly without disrupting the linkage of the lattice network. This kind of phase transformation occurs due to a small displacement in the lattice positions of a single atom or molecule or due to ordering of the atoms or molecules among various equivalent positions.

1.1.2(a) Classification of phase transformations

Depending upon the nature of change in internal and free energies and rate of change of phase at the transformation temperature, the phase transformations are divided into two groups - (i) first order or discontinuous transitions (ii) second order or continuous transitions.

(i) First order transition - If the change in entropy and enthalpy is discontinuous, the transformation is called first order. In this type of transformation a sharp and discrete change in the free energy and internal energy of the system at the transition temperature is observed. Hence a discontinuity is found in almost all the physical and chemical properties of the system at the transition temperature. There is no relation between the symmetries of the high and low temperature phases during transition and the order parameter also changes abruptly at the phase transition temperature.

(ii) Second order transition - This kind of transitions occur over a large temperature range and are accompanied by continuous increase in internal energy and disorder with the rise in tempera-

ture. The symmetry of one phase is higher than that of the other phase. There is no latent heat envolved. The order parameter gradually changes as the transition temperature is approached.

1.1.2(b) *The Buerger's classification* [3]

According to Buerger, the different kind of phase transformations in solids can be categorised as follows -

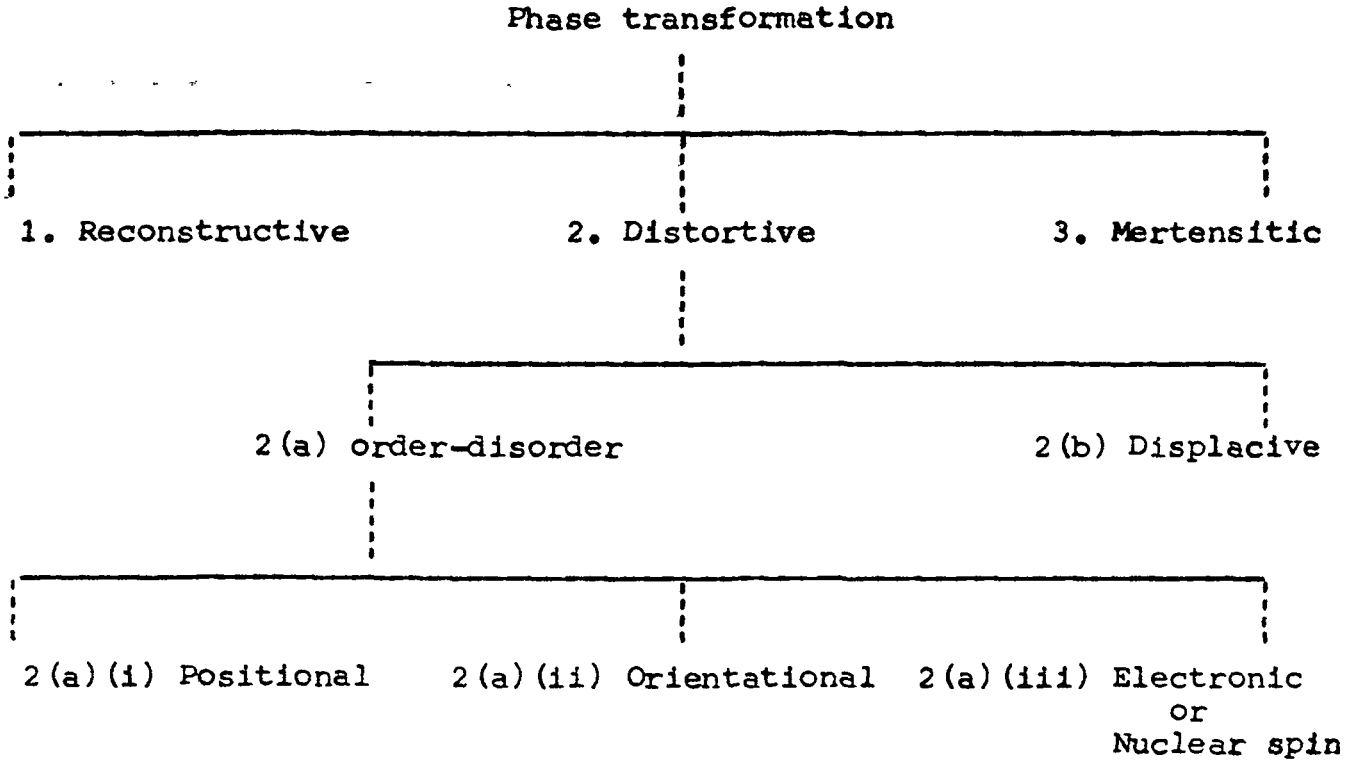

The (1) reconstructive and (3) mertensitic transformations shall not be discussed here because they are not relevant to our systems.

(2) Distortive type phase transition - In this type of transition the regular lattice is distorted slightly without disturbing the linkage among atoms or molecules. This kind of transition occurs in the following two ways :-

2(a) Order-disorder transformation - In this kind of transformation ordering of atoms or molecular units among various equivalent positions in the lattice takes place. Only at the absolute zero temperature an ideal state of crystalline arrangement, i.e., perfect order, can be realised. At higher temperatures, the extent of order is measured in terms of an order parameter. There are three kinds of order-disorder transformations :-

2(a)(i) Positional disordering - This type of transformation occurs either when atoms or ions occupy sublattice positions which are not appropriate or when more positions are available for the atoms in the lattice than are necessary. This kind of ordering has been observed in the phase transformations of AgI, Fe_3O_4, KH_2PO_4, Rb Ag_4I_5 etc [11-20].

2(a)(ii) Orientational disordering - This takes place in a situation where more than one distinguishable orientation becomes possible for a molecular unit in the lattice. This kind of disordering has been observed during the phase transitions in the following systems - NH_4Cl [21-25], $NaNO_2$ [26,27], $NaNO_3$ [28,29], NaHS [30] KNO_2 [31,32], KCN [33-36], KNCS [37-40].

2(a)(iii) Spin disordering - An ordering of spins imparts magnetism to the system. When the elementary magnetic spins flip over to other orientations setting in a disorder in the solid whose temperature has been increased, spin disordering takes place [41(a)]. The defects due to vacancies in a crystal also give rise to this kind of disordering transformations. Some order-disorder transitions have features of both the co-operative and discontinuous transitions [41].

2(b) Displacive transformation - If there is a small displacement in the lattice position of a single atom or molecular unit, or the displacement of a whole sublattice of ions of one type relative to another sub-lattice, then it is called displacive transformation. This kind of transformation is associated with very small change in the energy and is usually a fast transition. The high temperature form generally has higher specific volume, specific heat and symmetry. Examples of this type of transformations include the following :-

1) Brookite to Rutile (TiO_2)
2) Arsenolite to clandelite (As_2O_3)
3) Senarmonite to Volentinite (Sb_2O_3)
4) Pyrite to Mercasite (FeS_2)

[3, 42]

5) Tridymite to quartz (SiO_2)
6) Sphalerite to Wurtzite (ZnS)

[43-46]

The phase transitions of $BaTiO_3$ and $PbTiO_3$ often considered to be displacive can also be described as order-disorder type [47,48].

1.1.3 Mechanism of order-disorder transitions

In the order-disorder type of transitions an increase in entropy consists of configurational, vibrational, rotational and electronic contributions. In short it can be expressed as follows -

$$\Delta S = \Delta S_{con} + \Delta S_{vib} + \Delta S_{rot} + \Delta S_{elec} \quad \ldots (1.1)$$

where ΔS = change in entropy.

In case of order-disorder transitions all the terms except the ΔS_{con} are negligible. So the expression (1) reduces to

$$\Delta S = \Delta S_{con} \quad \ldots (1.2)$$

Again it is known that [1]

$$\Delta S_{con} = k \ln\left(\frac{N_2}{N_1}\right) \quad \ldots (1.3)$$

where N_1 = Total no. of configurations in the ordered phase

N_2 = Total no. of configurations in the disordered phase

k = Boltzaman constant.

The expression (1.3) provides the physical insight into the order-disorder transitions. Also the rate at which full value of the order or disorder is attained, generally, is different in different

directions. Let W be a measured property which depends on disorder and if the environment is changed so that W_f is the value of W suitable for that environment, and W_i is the instantaneous value of W, then the rate of change of W_i is given by [11]

$$\frac{dW_i}{dt} = \frac{1}{\tau} (W_f - W_i) \quad \ldots\ldots \quad (1.4)$$

where τ = relaxation time.

The expression (4) after integration becomes

$$W_i = W_f - (W_f - W_o) \exp [- t/\tau] \quad \ldots\ldots \quad (1.5)$$

where W_o = initial value of W.

The relaxation time for ordering is very sensitive to temperature and its value decreases with the temperature nearing the phase transition temperature T_c. As T_c is approached, the free energy difference between the ordered and disordered states decreases to such a value that the processes of ordering and disordering get very much retarded. This increases the relaxation time. The relaxation time is thus minimum in the region just below T_c.

1.1.4 Distinction between displacive and order-disorder transitions

On the basis of atomic single cell potential a distinction between the displacive and order-disorder type transitions can be made. The phase transitions in Ferro - or antiferro-electric

systems are connected with the rearrangement of only a few atoms in the unit cell while the position of other atoms remain unchanged. The Hamiltonian describing the structural phase transition depends on the local normal co-ordinate Q with the anharmonic potential.

$$V(Q) = AQ^2 + BQ^4 \qquad \ldots\ldots \qquad (1.6)$$

where A and B are constants, $A < 0$ and $B > 0$.

In displacive ferroelectrics, V(Q) is slightly anharmonic and can be considered to have a broad minimum at $Q = 0$ for $k T_c \gg \Delta E$, where ΔE = energy difference between the minima and maxima of the potential well. In order-disorder systems, V(Q) has large anharmonicity and in the simplest case V(Q) has two minima of equal depth at

$$Q = \pm Q_o$$

There is yet another important distinction in the soft mode dynamics between displacive and order-disorder systems. The complex frequency of the soft mode is given by

$$\tilde{\omega} = \omega' + i\omega'' \qquad \ldots\ldots \qquad (1.6a)$$

In displacive transitions the real (ω') and imaginary (ω'') parts of the complex soft mode frequency ($\tilde{\omega}$) will be generally different from zero ($\omega', \omega'', \neq 0$). In the case of order-disorder transitions, the imaginary part of the complex soft mode frequency will not be zero, but the real part will be zero ($\omega' = 0, \omega'' \neq 0$) provided the tunnel splitting of the ground state is not significant.

1.1.5 Classification of distortive phase transformations based on the translational symmetry

Based on the translational symmetry or spatial periodicity of the order parameter, the distortive structural phase transformations can be divided into two classes:

(i) Ferro-distortive or zone centre transformations, where the number of formula units per unit cell Z does not change at the transition temperature. The system in which this kind of transition takes place is called proper ferroelectrics; examples are - $NaNO_2$, KH_2PO_4, $BaTiO_3$ etc.

(ii) Anti-ferro distortive or zone boundary transitions where the number of formula units (Z) of the new low temperature phase is an integral multiple of the number of formula units (Z) of the old high temperature phase ($Z' = nZ$) where n is an integer. An example of the system in this class is the transition in $Gd_2(MoO_4)_3$; and these systems are also called improper ferroelectrics.

1.1.6 Incommensurate phase transitions

Apart from zone centre and zone boundary transitions, an unique class of transitions exists in which the distorted phase is not commensurate with the high temperature phase. This class of transitions is called incommensurate transitions. In these transitions the translational symmetry of the system is lost but the soft mode picture still holds good for the high symmetry phase.

1.1.7 Ferro-elastic transitions

The material in which ferro-elastic transition takes place is called ferro-elastic material. The ferro-elastic materials are characterised by the existence of spontaneous strain which becomes an order parameter during structural changes. A soft mode related to the distortions would be Raman active on both sides of the transition and the centre of symmetry is preserved across the phase transition. The co-operative Jahn-Teller type of transitions is a special class of ferro-elastic transition which is driven by an electron-phonon interaction.

1.1.8 Experimental techniques used for phase transition studies

A large number of experimental techniques are used in the study of phase transitions in solids, some of them are mentioned below:-

Diffraction of -

1) X-rays [17,49]
2) Neutrons [9,18]
3) Electrons [19]

Measurement of -

4) Diamagnetic susceptibility [36]
5) Hall-coefficient [33]
6) Thermo-electric power [34]
7) Electrical resistivity [20]
8) Heat capacity [35]

9) Specific heat [50]

10) Thermal expansion [50]

11) Elastic constants [30]

12) Dielectric constant [50]

13) Ultrasonic attenuation [50]

14) Magnetic anisotropy [8]

Absorption spectroscopy in the region of -

15) UV [6]

16) Visible [6]

17) IR [9]

Microscopy -

18) Electron

19) Optical

Magnetic resonances -

20) NMR

21) PMR

22) DMR

23) EPR

24) ESR

25) NQR

Spectroscopy -

26) Mössbauer spectroscopy

Chemical methods -

27) Differential Thermal Analysis (DTA) [26]

28) Differential thermal gravimetric analysis (DTG) [51]

29) Differential scanning calorimetry (DSC)

Scattering methods -

30) Neutron inelastic scattering

31) Laser Raman scattering

32) Rayleigh scattering

33) Brillouin scattering

Sometimes one method alone does not provide complete and accurate information about the system. In such cases two or more methods have to be used to gain detailed information of phase transitions in a system.

1.1.8.1 Laser Raman scattering

Laser Raman scattering will be discussed in brief because this method has been used in our investigations of phase transitions in the hexafluoro silicates and titanates of divalent metals.

The momentum energy transfer in scattering techniques is shown in Fig.1.1. Extensive work on phase transitions has been done by Raman scattering technique. The geometry of a typical light scattering system is shown in Fig. 1.2 [52]. The incident optical field can be expressed as

$$\vec{E}_i = \vec{E}_o \quad \text{Exp}\left[i\,\vec{k}_i\cdot\vec{r} - \omega_i t\right] \qquad \ldots\ldots \qquad (1.7)$$

where ω_1, $\vec{k}_1$ and $\vec{E}_1$ represent frequency, wave vector and polarization of the incident optical field.

The incident light produces the space and time dependent polarizability fluctuations $\delta\alpha_{ij}(\vec{r}, t)$ in the medium. The frequency, wave vector and polarization of the scattered light are ω_2, $\vec{K}_2$ and $\vec{E}_2$ respectively. The space-time correlation function of the polarizability tensor element

$$\langle \delta\alpha_{ij}(\vec{r}, t), \delta\alpha_{ij}(\vec{r}=0, t=0) \rangle$$

gives the information contained in the scattered field which is proportional to the qth spatial Fourier component of α_{ij}, where

$$\vec{q} = \vec{K}_2 - \vec{K}_1 \qquad \ldots\ldots \quad (1.8)$$

At $\omega_2 = \omega_1 \pm \Omega$, the Fourier component of $\delta\alpha(\vec{q}, \Omega)$ is observed. The amplitude of the scattered field has various polarization components which are proportional to

$$E_2^{(i)} \approx (\text{const})\, \vec{K}_1^{\,2}\, E_1^{(j)}\, \delta\alpha_{ij}(\vec{q}, \Omega) \ldots \quad (1.9)$$

The intensity I_1 of the ith polarization component is proportional to

$$I_1 \propto K_1^4\, E_1^{(j)}\, E_1^{(m)} \langle \delta\alpha_{ij}(\vec{q}, \Omega), \delta\alpha_{im}(\vec{q}, m) \rangle$$

$\ldots\ldots$ (1.10)

The momentum and energy conservations for the process are given by

$$\left.\begin{aligned} \hbar \vec{K}_2 &= \hbar \vec{K}_1 \pm \hbar \vec{q} \quad \text{and} \\ \hbar\omega_2 &= \hbar \omega_1 \pm \hbar\Omega \end{aligned}\right\} \quad \ldots\ldots \qquad (1.11)$$

as shown in Fig.1.2 where $\vec{q}$ is the scattering momentum transfer and Ω is the frequency shift corresponding to excitations of the medium.

There are many processes which may contribute to the fluctuating polarizability $\delta\alpha_{ij}(\vec{r}, t)$ but the fundamental relations for light scattering remain the same. The polarizability depends on different macroscopic variables such as temperature, pressure, or electric field.

The analysis of Raman scattering from single crystals in different geometries in terms of incident and scattered polarizations yields information about the six independent components of the Raman tensor. From such type of measurements the symmetry of the observed excitations can be inferred [50].

1.1.8.2 Real and symmetric polarizability tensor

We give here some details of the Raman tensor which is a real and symmetric polarizability tensor.

For most of the systems, an induced electric dipole moment $\vec{P}$ is related to the electric field $\vec{E}$ of the radiation by the power series

$$\vec{P} = \vec{P}^{(1)} + \vec{P}^{(2)} + \vec{P}^{(3)} \quad \ldots\ldots \qquad (1.12)$$

where $\vec{P}^{(1)} = \tilde{\alpha} \cdot \vec{E}$ ..... (1.12a)

$\vec{P}^{(2)} = \frac{1}{2} \tilde{\beta} \cdot \vec{E}\vec{E}$ ..... (1.12b)

where $\vec{P}$ and $\vec{E}$ are vector and $\tilde{\alpha}$ is a tensor. The magnitudes of the components of $\vec{P}$ are related to the magnitudes of the components of $\vec{E}$ by the following matrix -

$$\begin{bmatrix} P_x \\ P_y \\ P_z \end{bmatrix} = \begin{bmatrix} \alpha_{xx} & \alpha_{yy} & \alpha_{xz} \\ \alpha_{yx} & \alpha_{yy} & \alpha_{yz} \\ \alpha_{zx} & \alpha_{zy} & \alpha_{zz} \end{bmatrix} \begin{bmatrix} E_x \\ E_y \\ E_z \end{bmatrix} \quad \cdots \quad (1.13)$$

The variation of the polarizability $\tilde{\alpha}$ with vibrations of the molecule can be expressed by expanding each component α_{ij} in a Taylor series with respect to the normal co-ordinates of vibration Q as follows -

$$\alpha_{ij} = (\alpha_{ij})_0 + \sum_k \left(\frac{\partial \alpha_{ij}}{\partial q_k} \right)_0 Q_k + \frac{1}{2} \sum_{k,l} \left(\frac{\partial^2 \alpha_{ij}}{\partial Q_k \partial Q_l} \right)_0 Q_k Q_l + \cdots$$

. . . . (1.14)

where $(\alpha_{ij})_0$ is the value of α_{ij} at the equilibrium configuration; Q_k, Q_l ... are the normal co-ordinates of vibration associated with vibrational frequencies ω_k, ω_l ... and the summation is over all normal co-ordinates. The subscript 'o' on the derivatives

indicates that these are to be taken at the equilibrium configuration. [52]

1.1.8.3 Stokes and Antistokes Raman scattering

We shall, as a first approximation, neglect the terms involving higher powers of Q. This approximation is also called electrical harmonic approximation. We shall also take only one normal mode of vibration Q_k. Then the Taylor series given above reduces to -

$$(\alpha_{ij})_k = (\alpha_{ij})_o + (\alpha'_{ij})_k Q_k \quad \ldots\ (1.15)$$

where α'_{ij} indicates first derivative of α_{ij}. The above expression can be simplified as

$$\tilde{\alpha}_k = \tilde{\alpha}_o + \tilde{\alpha}'_k \cdot Q_k \quad \ldots\ (1.16)$$

where Q_k is kth normal co-ordinate, and is a function of time

$$Q_k = Q_{k_o} \cos(\omega_k t + \delta_k) \quad \ldots\ (1.17)$$

also $$\vec{E} = \vec{E}_o \cos \omega_o t \quad \ldots\ (1.18)$$

Then equation (1.12a) becomes after substituting the values from (1.16), (1.17) and (1.18) in (1.12a)

$$\vec{P}^{(1)} = \tilde{\alpha}_o \vec{E}_o \cos\omega_o t + \tilde{\alpha}'_k Q_{k_o} \vec{E}_o \cos\omega_o t \cdot \cos(\omega_k t + \delta_k)$$

$\ldots\ (1.19)$

$$\vec{P}^{(1)} = \tilde{\alpha}_0 \vec{E}_0 \cos\omega_0 t + \frac{1}{2}\tilde{\alpha}_k' \vec{E}_0 Q_{k_0} \left[\cos\{(\omega_0+\omega_k)t+\delta_k\} + \cos\{(\omega_0-\omega_k)t-\delta_k\}\right] \quad \ldots\ldots (1.20)$$

We see from the above equation that the linear induced dipole $\vec{P}^{(1)}$ has three distinct frequency components. The first term gives rise to radiation at ω_0 and is called Rayleigh scattering; second term gives rise to scattering at $(\omega_0 + \omega_k)$ and is called anti-stokes Raman scattering and the third term gives rise to scattered radiation at $(\omega_0 - \omega_k)$ and so accounts for Stokes Raman scattering.

1.2 Crystal hydrates

A large number of hydrated inorganic crystals are found which contain hydrogen bonded water molecules. The water molecules in these crystals interact strongly and their vibrational modes are coupled. Crystal hydrates and their structures have been reviewed by many workers [53-56]. In general three types of hydrates may be found - (1) In first type, the number of water molecules equal the co-ordination number of the cation. (2) In the second type, the number of water molecules is larger than the co-ordination number of the cation. (3) In the third type, the number of water molecules is smaller than the co-ordination number of the cation. Lone-pair co-ordination and hydrogen bonding are necessary

factors in determining the orientation, geometry and symmetry of water molecules in crystal hydrates.

1.2.1 Structures of hydrates

The structure of hydrates has been discussed extensively [53,57-59] and only the points relevant to the present study will be discussed here. Neutron diffraction is used to obtain the geometry of water molecules in hydrates. Ferraris and Franchini-Angela [60] have given a valuable survey of neutron diffraction studies of hydrates. They found that the actual geometry varies in various hydrates, but in general the O-H bond length, $r(O-H)$ and the interbond angle, 2α of H_2O molecules increase in the bound state. The position of hydrogen in various hydrates has also been estimated by PMR study [61-70].

1.2.2 Symmetry of water in crystal hydrates

In the absence of orientational disorder a water molecule in a crystal can occupy a site having its point group symmetry C_{2v} or any of its sub-groups C_2, C_s or C_1. If the two O-H arms of a molecule form hydrogen bonds of different strength, the C_2 axis as well as one mirror plane are lost, the symmetry is then reduced to C_s. Further more, if the spatial environments above and below the plane of the water molecule are non-equivalent, its symmetry is further reduced to C_1.

Neutron diffraction studies show that most of the water molecules lose their C_{2v} symmetry in crystal hydrates [60]. In a detailed survey by Falk and Knop [71] it was found that only a few percent of water molecules in the crystals retain C_{2v} symmetry and most of them are distorted to give C_s or C_1 symmetry. There is yet another consequence of the particular shape and symmetry of the water molecule. In true hydrates water is often found as water of co-ordination forming a fully hydrated $[M(OH_2)_6]^{n+}$ complex ion, where M is the central cation and 'n' is the number of electronic charges on the complex ion. The highest symmetries which the complex may attain in crystals are generally lower than the ideally possible octahedral symmetry for the MX_6 configuration.

1.3 Perturbation of crystalline field on vibrational spectra of crystals

Spectroscopic studies involving the emission, absorption or scattering of electromagnetic radiation are the most widely used methods to investigate the dynamics of constituents in solids. The theory of crystal vibrations will not be reviewed here because extensive reviews are available in literature [72-89]. A brief description of various topics related to the present study is given here.

1.3.1 The crystal potential

In harmonic approximation the potential energy of a unit cell of the crystal can be written as [65] -

$$V = V_L + \sum (V_j^{\circ} + V_j') + \sum_{jk} (V_{jk} + V_{Lj}) + \ldots. \quad \ldots. \quad (1.21)$$

where summation extends over all the molecular units in the unit cell. The various terms in the above expression are as follows -

V_L = Lattice potential, it contains terms involving the relative displacements and quasi rotational orientations of molecular groups with respect to each other and lead to rotatory and translatory modes.

V_j° = the potential at the jth molecular ion when the external field is zero. It has symmetry of the unperturbed molecular ion.

V_j' = the perturbation to V_j° due to the equilibrium field of the crystal at the site of the jth molecular group.

$\sum V_j'$, therefore, gives the static field shifts of frequencies from their free state values determined by $\sum V_j^{\circ}$. Also the change in the symmetry of the potential field can lead to changes in the selection rules and hence lift the degeneracy of the internal vibrations.

V_{jk} = interaction between vibrations of different molecular units within the unit cell. This term gives rise to dynamic coupling among the vibrations of different molecules. Such an interaction between the corresponding vibrations of molecules at equivalent sites in the unit cell lifts the degeneracy and gives rise to splitting of bands. This splitting is often called the correlation or dynamic field splitting. This splitting is in addition to the site or static field splitting arising from the inequality of V_j at different sites.

V_{Lj} = the perturbation to V_L and it involves interaction of lattice with the jth molecule. This may lead to multiphonon processes involving lattice and internal modes, but this term is very small in comparison to the other terms in the expression and is generally neglected.

Most often crystals are anharmonic and hence give rise to many modifications in the vibrational spectra. Moreover in order to include modifications in the charge distribution of nuclei due to interactions with neighbours, an anisotropic short range potential has to be added [90]. These anharmonic considerations make the actual crystal potential very complex. We shall discuss anharmonicity in the next section.

1.3.2 Anharmonicity

When the amplitude of a vibration is very small, only the quadratic terms in the potential energy need be considered for normal vibrations; but for accurate calculations cubic, quartic

or higher order terms in the potential energy must be taken into account. In such cases the vibrations become anharmonic [91]. The anharmonicity manifest itself in two ways. Firstly the selection rules derived for harmonic oscillator $\Delta\nu = \pm 1$ do not hold strictly and transitions with $\Delta\nu = \pm 2, \pm 3, \ldots$ etc become allowed. Secondly the vibrational levels are not equally spaced and so overtones will have different energy than twice the energy of the fundamental modes.

Deviations from the harmonic potential lead to mechanical anharmonicity whereas asymmetric variation in the dipole moment of a molecule leads to electrical anharmonicity. In case of crystals, anharmonicity is responsible for providing coupling for energy decay processes and controls the temperature dependence of the properties of the crystal i.e. frequencies and half widths of the vibrational modes of the crystal [92-94] etc. Sood et al [95] have deduced expressions for the temperature dependence of half width of vibrational modes in cases where the cubic or quartic anharmonic process dominates. The cubic anharmonic terms contribute to half width as

$$\Delta\nu_{1/2} = A \left\{ \exp\left[\pm \hbar\omega_0 / 2k_B T \right] \right\}^{-1} \quad \ldots\ (1.22)$$

while the contribution from quartic terms is given by

$$\Delta\nu_{1/2} = B\left\{\left[\left\{\exp(\hbar\omega_0/3k_BT)-1\right\}^{-1}+1/2\right]^2+\frac{1}{12}\right\} \quad \ldots\ldots (1.23)$$

where A and B are constants.

At high temperatures, these equations reduce to

$\Delta\nu_{\frac{1}{2}} \approx T$ for cubic terms

$\Delta\nu_{\frac{1}{2}} \approx T^2$ for quartic terms in potential energy.

A completely temperature-independent half-width would indicate absence of anharmonicity.

1.3.3 Fermi Resonance

Fermi resonance also perturbs a normal vibrational spectrum. This may occur when two vibrational modes, one fundamental and other overtone, have nearly the same energy, and belong to the same symmetry species. In such cases the overtone steals some intensity from the fundamental, and instead of appearing as a weak band, it becomes nearly equally strong as the fundamental [96]. Moreover the two energy levels repel each other, so that the one with greater energy moves to higher frequency and the one with lower energy moves to lower frequency. A great deal of research work has been reported in the literature where Fermi resonance processes cause intra and intermolecular energy transfer [97-99].

The separation of the unperturbed levels 'd_o' and the Fermi coupling co-efficient, Ω, can be calculated by the following equations [100, 101].

$$d_o = d\left(\frac{R - 1}{R + 1}\right) \quad \cdots\cdots \quad (1.24)$$

$$\Omega = \frac{(d^2 - d_o^2)^{1/2}}{2} \quad \cdots\cdots \quad (1.25)$$

where d = observed frequency separation

R = observed ratio of intensities of the two bands

In case of fundamental frequencies (ν_1 and ν_2) for water, the frequencies of ν_1 and $2\nu_2$ are very near, and resonance may occur. Then the unperturbed frequencies of the doublet can be calculated by the following equation -

$$(\nu_1^{\circ}, 2\nu_2^{\circ}) = \frac{\nu_1 + 2\nu_2}{2} \pm \frac{d_o}{2} \quad \cdots\cdots \quad (1.26)$$

where ν_1 and ν_2 are the observed frequencies and ν_1° and ν_2° are unperturbed frequencies of water molecule. The displacement parameter $\Delta F = d - d_o$ is the energy separation between the two perturbed levels.

1.3.4 Hydrogen Bonding

A hydrogen bond is said to exist when the distance between the atoms H and Y in the structure O-H...Y is shorter by at least 0.20 Å than the sum of their van der Waals contact radii r_H and r_Y where Y represents an electro-negative atom such as O, F, Cl, Br, I, etc. In the process of formation of

such a bond, the distribution of charge may be O^{-}-H...Y^{+} and the electrostatic interaction may lead to the formation of Hydrogen bond [71]. The exact nature of this bond is not completely known. Much work has been done to understand the hydrogen bonds and their significance in vibrational spectra [102-109].

Formerly the hydrogen bonds were considered to be straight and single, but later it was found that both linear and bent (bifurcated, trifurcated) hydrogen bonds exist [105]. From deformation energy calculations [110-113] and neutron diffraction studies [102] it has been confirmed that the bent and bifurcated hydrogen bonds are more common in different systems.

Spectroscopic techniques are capable of providing information regarding the nature and formation of the bond. Some of the effects of hydrogen bonding on vibrational modes are given below -

(i) The fundamental and overtone vibrational bands due to the O-H stretching modes shift to lower frequency as compared to those in free molecules with increase in hydrogen bond strength.

(ii) The shifted vibrational bands are much broader than the corresponding non-hydrogen bonded O-H group bonds due to the presence of several different hydrogen bonded molecular species undergoing anharmonic coupling, frequency modulation and Fermi resonance.

(iii) The O-H-O deformation modes slightly shift to the higher frequency side but the shift is very small compared to the

shift in case of O-H stretch. There is no definite correlation between the frequency of the bonding mode and the strength of hydrogen bond.

(iv) The temperature variation of the stretching mode $(\frac{\partial \nu_i}{\partial T})$ indicates the multi-function or bent nature of hydrogen bonds. If $(\frac{\partial \nu_i}{\partial T}) < 0$ the bond must be bent but if $(\frac{\partial \nu_i}{\partial T}) > 0$ the bond must be straight [107].

(v) The integrated intensity of the fundamental O-H stretching mode increases where as that of overtones decreases on formation of hydrogen bond.

(vi) Corresponding to the H...Y stretch and deformation modes, weak new bands may appear at lower temperatures.

(vii) The vibrational modes of H...Y shift in frequency but the shift is much smaller than that of the (O-H) stretches.

1.3.5 Lone-pair co-ordination

The water molecule has two tetrahedrally directed lone-pair orbitals. These orbitals form cation-oxygen bond through ion dipole interactions which provides a suitable environment to water for forming hydrogen bonds in crystals. The geometry in which the bisector of the lone-pair is directed towards a polyvalent metal ion is generally found in $FeSiF_6 : 6H_2O$ type of compounds [112]. The charge donated by the water molecules attached with cation shortens the O-H...Y hydrogen bond length and therefore it contributes to the spectroscopic effects observed in hydrogen

bonding. The length of the hydrogen bond varies inversely with the electrostatic bond strength [114]. In most of the cases, however, the lone-pair co-ordination may be considered weaker as compared to the hydrogen bonding strength [115,116] provided a correlation between hydrogen bond strength and O...O distance exists.

The lone-pair on oxygen play an important role in determining the strength and direction of hydrogen bonds and calculations on water indicate that the shortest bond is formed when the O-H axis of one molecule is collinear with lone-pair axis on the oxygen atom of a neighbouring water molecule.

1.4 Isotopic dilution

The isotopic dilution method provides an important way for uncoupling the vibrations of neighbouring molecules, and thus eliminates the interactions arising from correlation field splittings. By this technique it is possible to distinguish between static and correlation field effects [117,118]. The static field for the molecule remains almost unchanged, but the dynamic coupling of the vibrations of a molecular group with its neighbours is eliminated provided the transition frequencies of the two species are sufficiently apart. This method was applied to crystal hydrates by J. Schiffer [119]. In the crystal, H_2O is replaced by D_2O which is of great help in the assignment of vibrational bands due to water molecules.

Table 1.1

1·5 Previous Vibrational Studies (IR and Raman) of the Systems of General Formula

$MXF_6 : 6(H_2O/D_2O)$, M = divalent metal ion; X = Si, Ti

M	X	H_2O/D_2O	Workers	Raman/ IR	Year	Ref.
1	2	3	4	5	6	7
Zn	Si	H_2O -	M^{me} Annette et al	Raman	1955	1
Ni,Mn,Fe	Si	H_2O -	Ichiro Nakagawa et al	IR	1964	2
Zn,Cd,Cu	Si	H_2O -	R.B. Badachhape et al	Raman and IR	1966	3
Mn,Co,Ni	Si	H_2O -				
$(NiSnCl_6)^*$		H_2O -	J. Jager and G. Schaack	IR and Raman	1973	4
Mn,Zn,Fe	Si	H_2O -	Sunil K. Datta and Debbala De	NIR	1976	5
Mn,Co,Fe	Si	H_2O -	Debbala De and Sunil K. Datta	NIR	1977	6
(Co,Mg)≠ (Co,Zn)	Si	H_2O -	Debbala De and Sunil K. Datta	NIR	1978	7
Mn,Fe,Co, Ni,Zn	Si	H_2O -	Debbala De and Sunil K. Datta	NIR	1978	8
Ni	Si	H_2O -	T.E. Jenkins and Lewis	Raman	1978	9

Table 1.1 continued...

Table 1.1 continued

1	2	3	4	5	6	7
Mn,Fe,Co	Si	H_2O -	Debbala De and Sunil K. Datta	NIR	1979	10
Fe,Ni	Si	H_2O -	Lewis and Jenkins	Raman	1979	11
Ni	Si	- D_2O				
Ni,Zn	Ti	H_2O -	Jenkins and Lewis	Raman	1981	12
Ni,Fe, Mg,Zn	Si	H_2O -				
Ni	Si	H_2O -	Jenkins and Lewis	Raman	1981	13
Ni	Si	H_2O -	T.E. Jenkins	IR Tunable Laser	1982	14
Mn,Zn	Ti	H_2O -	P. Choudhury et al	Raman	1983	15
Mn,Zn	Ti	- D_2O	P. Choudhury et al	Raman	1983	16
Mn	Ti	- D_2O	P. Choudhury et al	Raman	1984	17

* $NiSnCl_6$: $6H_2O$ - is a similar salt in this series.

≠ Cobalt is diluted with Mg and Zn.

References for Table 1.1

[1] M^me Annette Weil-Marchand, C.R. Acad. Sci. 240, 509 (1955).

[2] Nakagawa I and Shimanouchi T, Spectrochim. Acta 20, 429 (1964).

[3] Badachhape R B, Hunder G, McCory LD and Margrave J L, Inorg. Chem. 5(5), 929 (1966).

[4] Jager J, Schaack G, Z. Naturforsch, 28(a), 738 (1973).

[5] Datta Sunil K, and De Debabala, Indian J. Cryog. 1(1), 45 (1976).

[6] De Debabala and Datta Sunil K, Indian J. Cryog. 2, 26 (1977).

[7] Datta Sunil K, and De Debabala, Indian J. Physics. 52A, 499 (1978).

[8] De Debabala and Datta Sunil K, J. Chem. Phys. 68 (4), 1865 (1978).

[9] Jenkins T E and Lewis J, Physica Scripta, 18, 351 (1978).

[10] De Debabala and Datta Sunil K, Indian J. Cryog., 4(1), 39 (1979).

[11] Lewis J and Jenkins T E, J. Raman Spectrosc. 8(2), 111 (1979).

[12] Jenkins T E and Lewis J, Spectrochim Acta 37A, 47 (1981).

[13] Jenkins T E and Lewis J, J. Raman Spectrosc. 11(1), 1 (1981).

[14] Jenkins T E, J. Phys. C. Solid State Phys. 15, L1205 (1982).

[15] Choudhury P, Ghosh B, Raghuvanshi G S and Bist H D, J. Raman Spectrosc. 14(2), 99 (1983).

[16] Choudhury P, Ghosh B, Patel M B, and Bist H D, Proc of 3rd Symp. on "Laser and its application" Bist H D and Goel J S (Eds.) pp. 307, Dec. 16 (1983). I.I.T. Kanpur.

[17] Choudhury P, Ghosh B, Patel M B and Bist H D, J. Phys. C : Solid State Phys. 17, 5827 (1984).

Table 1.2

1.5 Previous Studies of Phase Transitions in the System of General Formula $MXF_6 : 6(H_2O/D_2O)$; where M = divalent metal ion, X = Si, Ti; critical temperature T_c is shown

M	X	$\frac{H_2O}{D_2O}$	T_c in K Cooling-Heating cycles	Workers	Method/ Technique	Year	Ref.
1			2	3	4	5	6
Zn	Si	H_2O	No No	H. Poulet et al	I.P.O.C.P.L.	1978	1
Zn	Si	H_2O	No No	T.E. Jenkins et al	Raman	1981	2
Zn	Ti	H_2O	180 ± 2 180 ± 2	R.S. Rubins	EPR	1974	3
Zn	Ti	H_2O/D_2O	182 ± 1 -	M.L. Afanasyev et al	NMR	1979	4
Zn	Ti	H_2O	182,217 -	P. Choudhury et al	Dielectric mea.	1981	5
Zn	Ti	H_2O	173 ± 2 -	Geetha Jayaram et al	EPR	1983	6
Zn	Ti	H_2O	185 203	P. Choudhury et al	Raman	1983	7
Zn	Ti	D_2O	180-200,245-250	P. Choudhury et al	Raman	1983	8
Zn	Ti	D_2O	182,230 -	M. Bose et al	NMR	1983	9

Table 1.2 continued..

Table 1.2 continued

1			2		3	4	5	6
Ni	Si	H_2O	100-270K	-	R. Rammetveit et al	Dielectric mea.	1978	9(a)
Ni	Si	H_2O	No	-	H. Poulet et al	I.P.O.C.P.L.	1978	1
Ni	Si	H_2O	No	-	T.E. Jenkins et al	Raman	1978	10
Ni	Si	D_2O	No	-	R.S. Rubins et al	EPR	1981	11
Ni	Ti	H_2O	121	-	J. How and I Svare	ESR	1974	12
Ni	Ti	H_2O	134-137	-	Rubins et al	EPR	1976	13,14
Ni	Ti	H_2O	136.5	-	M. Karnezos et al	Magnetic Suscep.	1978	15
Ni	Ti	H_2O	120	-	T.E. Jenkins et al	Raman	1981	2
Ni	Ti	D_2O	129 ± 2	-	M. Bose et al	NMR	1984	16
Ni	Ti	H_2O	122-126,131-134		Cheung et al	NMR	1985	12(a)
Co	Si	H_2O	246 ± 2 259 ± 1		M. Majumdar	Magnetic Anisotropy(MA)	1964	17
Co	Si	H_2O	143-173	-	E. Kodera et al	Xray	1972	18
Co	Si	H_2O	259	-	McLellan et al	MA	1975	19
Co	Si	D_2O	263 ± 2 278 ± 2		B. Ghosh et al	MA & IR	1977	20

Table 1.2 continued...

Table 1.2 continued

1			2		3	4	5	6
Co	Si	H_2O	246	-	H. Poulet et al	I.P.O.C.P.L.	1978	1
Co	Si	D_2O	262 ± 2	-	M. Bose et al	DMR	1979	21
Co	Ti	D_2O	262	-	M. Bose et al	2D NMR	1980	22
Co	Si	H_2O	240	-	J. Sthanapati et al	EPR	1981	23
Co	Si	H_2O	230	265	Manasi Raychoudhury	EPR	1981	24
Co	Ti	D_2O	261 ± 2	-	M. Bose et al	2D NMR	1981	25
Mn	Si	H_2O	223 ± 4	233 ± 2	T. Sujikawa et al	O.B.	1955	26
Mn	Si	H_2O	143-173		E. Kodera et al	Xray	1972	18
Mn	Si	H_2O	No Ist Order P.T. but second order		Sunil K. Datta et al	NIR	1976	27
Mn	Si	H_2O	230	-	H. Poulet et al	I.P.O.C.L.	1978	1
Mn	Ti	H_2O	144	169	P. Choudhury et al	IR	1983	7
Mn	Ti	D_2O	175-200		P. Choudhury et al	Raman	1983	8
Mn	Ti	D_2O	200 ± 3,	228 ± 3	P. Choudhury et al	Raman	1984	28
Fe	Si	H_2O	240	-	R.S. Rubins	EPR	1974	29
Fe	Si	H_2O	240	-	Jehanno et al	Xray	1975	30
Fe	Si	H_2O	225	-	R.S. Rubins et al	EPR	1977	31

Table 1.2 continued...

Table 1.2 continued

1			2		3	4	5	6
Fe	Si	H_2O	225	-	Chappert et al	Xray	1977	32
Fe	Si	H_2O	225	-	R.S. Rubins et al	DSC	1977	35
Fe	Si	H_2O	240	-	H. Poulet et al	I.P.O.C.P.L.	1978	1
Fe	Si	H_2O	225	-	Volland et al	Xray & DSC	1978	34
Fe	Si	H_2O	240	-	R.S. Rubins	EPR	1979	35
Fe	Si	H_2O	240	-	Chevrier	Xray	1981	36
Fe	Si	H_2O	240	-	J. Sthanapati et al	EPR	1981	23
Fe	Si	H_2O	230 ± 0.5	-	Orlandi et al	D.T.A.	1984	37
Fe	Ti	H_2O	275	-	R.S. Rubins	DSC	1977	33
Mg	Si	H_2O	-	298 ± 1	Syoyama and Osaki	Xray;DSC	1972	38
Mg	Si	H_2O	301 ± 1	302 ± 1	R.S. Rubins et al	EPR	1977	31
Mg^+ Ni	Si 20%	H_2O	305 ± 1	307 ± 1	R.S. Rubins et al	EPR	1977	31

Table 1.2 continued...

Table 1.2 continued

1	2		3	4	5	6
Mg	Si	H_2O	-	302 ± 1	R.S. Rubins et al	DSC	1977	31
Mg	Ti	H_2O	301 ± 1	318 ± 1	R.S. Rubins et al	EPR	1977	31
Mg	Si	H_2O	298	-	H. Poulet et al	I.P.O.C.P.L.	1978	1
Cu (diluted with Zn ion)	Si	H_2O	255-283		Sukharivskii et al	DSC	1982	39
(Co,Mg)	Si	H_2O	253-243	-	S.K. Datta et al	NIR	1978	40

I.P.O.C.P.L. = Interference pattern of convergent polarized light ,

O.B. = Optical Birefrigerence.

References for Table 1.2

[1] Poulet H and Mathieu J, C.R. Acad. Sc. Paris, t-286(12) Series B, 331 (1978).

[2] Jenkins T E and Lewis J, Spectrochim. Acta 37A, 47 (1981).

[3] Rubins R S, Chem. Phys. Lett. 28, 273 (1974).

[4] Afanasyev M L, Lybzikov A F, Menshikov V V and Zeer E P, Chem. Phys. Lett. 60, 279 (1979).

[5] Choudhury P, Bal B, Saha S, and Ghosh B, Proc. of Nucl. Phys. and Solid State Phys. Vol 24C, pp 323, Dec. 28 (1981) BARC, Bombay.

[6] Jayaram Geetha and Sivarama Sastry G, Chem. Phys. Lett. 97, 431 (1983).

[7] Choudhury P, Ghosh B, Lamba O P. and Bist H D, J. Phys. C 16, 1609 (1983).

[8] Choudhury P, Ghosh B, Patel M B and Bist H D, Proc of 3rd Symp. on "Laser and its application" Bist H D and Goel J S (eds.) Dec. 16 (1983), I.I.T. Kanpur.

[9] Bose M, Roy K and Ghoshray A, J. Phys. C 16, 645 (1983).

[9a] Rammetveit R and Svare I, Physica Scripta 17, 27 (1978).

[10] Jenkins T E and Lewis J, Physica Scripta 18, 351 (1978).

[11] Rubins R S and Haghighatijou T, J. Phys. Chem. Solids 43 (5), 491 (1982).

[12] How T and Svare I, Physica Scripta 9, 40 (1974).

[12a] Cheung H M and Lichti R L, J. Phys. C 18, 6157 (1985).

[13] Rubins R S, Griffin B C and Burris R, J. Chem. Phys. 64 (8), 3349 (1976).

[14] Rubins R S, Bull. Ann. Phys. Soc. 20, 386 (1975).

[15] Karnezos M and Friedbero S A, J. Appl. Phys. 49, 1382 (1978).

[16] Bose M, Roy K and Ghoshray A, J. Phys. C 17 (30), 5277 (1984).

[17] Majumdar M and Datta S K, J. Chem. Phys. 42(1), 418 (1965).

[18] Kodera E, Torii A, Osaki K and Watanabe T, J. Phys. Soc. Japan, 32, 863 (1972).

[19] McLellan A G, and Datta S K, Nat. Seminar on Cryogenics, New Delhi, Abst No - 18. (1975).

[20] Ghosh B, Chatterjee N, Das A N, Datta Roy S K, and Pal A, J. Phys. C 10, L627 (1977).

[21] Bose M, Ghoshray A, Basu A and Roy K, J. Phys. C 12, L771 (1979).

[22] Bose M, Roy K, and Ghoshray A, Proc. of DAE Symp. 23C, pp 834 (1980) New Delhi.

[23] Sthanapati J and De D K, Phys. Stat. Sol(a) 68, K123 (1981).

[24] Roychoudhury Manashi and Pal A K, Indian J. Phys. 55A, 419 (1981).

[25] Bose M, Roy K and Ghoshray A, Proc. of DAE Symp. 24C, 389 (1981).

[26] TSujikawa I and Couture L, J. Phys. Radium 16, 430 (1955).

[27] Datta Sunil K and De Debabala, Indian J. Cryog. 4(1), 39 (1979).

[28] Choudhury P, Ghosh B, Patel M B, and Bist H D, J. Phys. C 17, 5827 (1984).

[29] Rubins R S, J. Chem. Phys. 60, 4189 (1974).

[30] Jehanno G and Varret F, Acta Cryst. A 31, 857 (1975).

[31] Rubins R S and Jani S K, J. Chem. Phys. 66, 3297 and 3948 (1977).

[32] Chappert , J. Physique, 38, 411 (1977).

[33] Rubins R S, unpublished data.

[34] Vollard U, Hösl S and Spiering H , Solid State Commun., 27, 49 (1978).

[35] Rubins R S, J. Chem. Phys. 70, 4383 (1979).

[36] Chevrier , Acta Cryst. A 37, 578 (1981).

[37] Orland P and Rigamonti A, Phys. Stat. Sol. (a) 82, K129 (1984).

[38] Syoyama S and Osaki K, Acta Cryst. B 28, 2626 (1972).

[39] Sukhariviskii , Ukr. Fiz. Zh., 27 (9), 1418 (1982) Chem. Abst. 98 (4) Abst No. 25759.

[40] Datta S K, and De Debabala, Indian J. Phys. 52A, 499 (1978).

1.6 References (sec 1.1 to 1.4)

[1] Rao C N R and Rao K J, "Phase Transition in Solids", McGraw-Hill Inc. (1978).

[2] Rao C N R and Rao K J, in "Progress in Solid State Chemistry" ed. by H. Reiss Vol. 4, Pergamon Press, Oxford (1967).

[3] Buerger M J, in "Phase Transition in Solids" pp. 133, John Wiley, New York (1957).

[4] Thomas H, in "Structural Phase Transformations and Soft Modes" pp. 15, Universitat Sforlaget, Oslo (1971).

[5] Staveley L A K, Quart. Rev., 3, 64 (1949).

[6] Tayal V P; Srivastava B K, Khandelwal, D P and Bist, H D, Appl. Spectrosc. Rev. 16, 89 (1980).

[7] Smolchowski R (ed) "Phase Transformation in Solids" John Wiley and Sons Inc. New York (1957).

[8] Owens F J; Poole C P, Jr and Farach, H A (eds.) "Magnetic Resonance of Phase Transitions" Academic Press, New York.

[9] Muller K A and Thomas H (eds.) "Structural Phase Transitions" Springer-Verlag, Berlin, Heidelberg, New York (1981).

[10] Ubbelohde A R, Quart. Rev. 11, 246 (1957).

[11] Krivoglaz M A and Smirnov A, in "The Theory of Order-disorder in Alloys", Warlimont, H (ed.) pp 148, Springer-Verlag, Berlin (1974).

[12] Cowley J M, J. Appl. Phys. 21, 24 (1950).

[13] Lipson H, "Progress in Metal Physics" Chalmers, B (ed.) Vol. 1, Pergamon Press, New York (1957).

[14] Guttman L, in "Solid State Physics" Seitz F and Turnball D (eds.) Vol. 3, Academic Press, New York (1956).

[15] Yamouchi H and deFontaine D, in "Order-disorder Transformation in Alloys" Warlimont, H (ed.) pp 148.

[16] Kear B H; Sims T; Stoloff N S and Westbrook J H, (eds.), "Ordered Alloys-Structural Applications and Physical Metallurgy", Claitors Publishing Division, Baton Rouge (1970).

[17] Van Gool W, in "Fast Ion Transport in Solids", Van Gool (ed.), North-Holland, Amsterdam, (1973).

[18] Geller S, Science, 157, 310 (1967).

[19] Wiedersich H and Geller S, in "The Chemistry of Extended Defects in non-metallic Solids", Eyring L and Keefe M O (eds.) pp 629, North-Holland, Amsterdam (1970).

[20] Kamigaki K; Okashi M and Kanekto T, in "Ferrites", Hoshino Y; Iida S and Sugimoto M (eds.) pp. 598, Univ. Park Press, Baltimore (1971).

[21] Arell A, Ann. Acad. Sci. Fenn. Ser. A 6 (57), 204 (1966).

[22] Schwartz P, Phys. Rev. B4, 902 (1971).

[23] Levy H A and Peterson S W, Phys. Rev. 86, 766 (1952) and J. Chem. Phys. 21, 366 (1953).

[24] Bersohn R and Gutowsky H S, J. Chem. Phys. 22, 651 (1954).

[25] Wang C H and Wright R B, J. Chem. Phys. 58, 1411 (1973).

[26] Yamada Y; Shibuya I and Hoshino S, J. Phys. Soc. Japan, 18, 1594 (1963).

[27] Chisler E V and Shur M S, Phys. Stat. Solidi 17, 163 and 173 (1966).

[28] Kracek F C, J. Amer. Chem. Soc. 53, 2609 (1931).

[29] Schroeder R A, Weir C E and Lippincott E R J. Res. Natl. Bur. Standards, 66A, 407 (1962).

[30] Rush J J; de Graaf L A and Livington R C, J. Chem. Phys. 58, 3439 (1973).

[31] Solbakk J F and Stromme K O, Acta Chem. Scand. 23, 300 (1969).

[32] Stromme K O, Z. Anorg. Allg. Chem. 389, 315 (1972).

[33] Suga H, Matsno T and Seki S, Bull. Chem. Soc. Japan, 38, 1115 (1965).

[34] Aloji M, J. Chem. Phys. 54, 3514 (1971).

[35] Fukishima E, J. Chem. Phys. 49, 4721 (1968).

[36] Reilly D E O; Peterson E M; Scheie C E and Kadaba P K, J. Chem. Phys. 58, 3018 (1973).

[37] Akers C Peterson S W and Willett R D, Acta Cryst. B24, 1125 (1968).

[38] Sakiyama M, Suga H and Seki S, Bull. Chem. Soc. Japan, 36, 1025 (1963).

[39] Savoie R and Pezolet M, Can. J. Chem. 45, 1677 (1967).

[40] Iqbal Z, Sarma L H and Moller K D, J. Chem. Phys. 57, 4728 (1972).

[41] Staveley L A K, "Technica Revista de Engenharia", Separate 10 (414), 173 (1972) Lisbon.

[41a] Scott J F in "Advances in Raman Spectrosc., Mathieu J P (ed.) pp 353, Heyden, London.

[42] Buerger M J, Fortscher. Miner, 39, 9 (1961).

[43] Robert A L, "Kinetics of High Temperature Processess" Kingery W D (ed.) John Wiley, New York (1959).

[44] Yoganarasimhan S R and Rao C N R, Trans. Farad. Soc. 58, 1579 (1962).

[45] Rao C N R, Canad. J. Chem., 39, 498 (1961).

[46] Kroger F A, Z. Krist. A 102, 136 (1939).

[47] Scott J F, Rev. Mod. Phys. 46, 33 (1974).

[48] Shirane G, Rev. Mod. Phys. 46, 437 (1974).

[49] Ubbelohde A R, "Reactivity of Solids" de Boor J H (ed.), Elsevier Publishing Co. Amsterdam (1961).

[50] Verma A L, "Phase Transitions in Insulators" in Proc. Nucl. Phys. and Solid State Phys. Symp. Vol. 25A, Dec. 27 (1982) pp. 159, BHU, Varanasi (India).

[51] Bartenev G M and Ramizova A A, Zhur. Fiz. Khim. 31, 2534 (1957).

[52] Long D A, "Raman Spectroscopy" McGraw-Hill International Book Co. New York, London (1977).

[53] Wells A F, "Structural Inorganic Chemistry" pp 565, Oxford, (1962).

[54] Schiffer J, Ph.D. Thesis, Michigan University (1964).

[55] Fifer R A, Ph.D. Thesis, Temple University (1970).

[56] Chiari G and Ferraris G, Acta Cryst. B 38, 2331 (1982).

[57] Wells A F, Quart. Rev. 8, 380 (1954).

[58] Fuller W J. Phys. Chem. 63, 1705 (1959).

[59] Hadzi D (ed.) "Hydrogen Bonding", pp 187, Pergamon Press, New York (1959).

[60] Ferraris G and Francheni-Angela, Acta Cryst. B 28, 3572 (1972).

[61] Pake G E, J. Chem. Phys. 16, 327 (1948).

[62] McGrath J W and Silvidi A A, J. Chem. Phys. 34, 322 (1961).

[63] Benedict W S, Gailer N and Plyler E K, J. Chem. Phys. 24, 1139 (1956).

[64] Franks F (ed.) "Water a Comprehensive Treatise" Vol. 2 Chap. 2, Plenum Press, New York (1973).

[65] Tayal V P, Srivastava B K, Khandelwal D P and Bist H D, Appl. Spectrosc. Rev. 16, 43 (1980).

[66] Gabrichidge Z A and Dnhaparidge I N, Chem. Abst. 69, 6925b (1968).

[67] Klewe B and Pedersen B, Acta Cryst. B 30, 2363 (1974).

[68] Simonsen S H and Muller M H, J. Inorg. Nucl. Chem. 27, 309 (1965).

[69] Sikka S K, and Chidambaran R, Acta Cryst. B 25, 310 (1969).

[70] Sequeina A, Srikanta S and Chidambaram R, Acta Cryst. B 26, 77 (1970).

[71] Falk M and Knop O, in "Water- a Comprehensive Treatise" Vol. 2. Franks F (ed.) Plenum Press, New York (1973).

[72] Menzies A C, Rept. Prog. Phys. 16, 83 (1953).

[73] Bhagavantam S, Proc. Indian Acad. Sci. A 37, 350 (1953)

[74] Mathieu J P, Phys. Soc. Year book, pp. 23 (1956) and "Spectre de vibration et Symetrie des Molecules et des Cristaux", Paris Hermann (1945).

[75] Marten L, Z. Naturf. A 15, 47 (1960).

[76] Mitra S S, Solid State Phys. 13, 1 (1962).

[77] Loudon R, Proc. Phys. Soc. London, 82, 393 (1963a)

[78] Loudon R and Johnson F A, Proc. Roy. Soc. A 281, 274 (1964).

[79] Metselaar R, "Lattice Vibration of Solid Solution" Ph.D. Thesis, University of Amsterdam (1967).

[80] Pauling L, J. Am. Chem. Soc. 57, 2680 (1935).

[81] Vedder W and Horning D F, "Infrared Spectra of Crystals" in 'Advances in Spectroscopy', Vol. 2, Thompson H W (ed.) pp. 189, Interscience, New York (1961).

[82] Turrel G, "Infrared and Raman Spectra of Crystals" Academic Press, London and New York (1972).

[83] Halford R S, J. Chem. Phys. 14, 8 (1946).

[84] Horning D F, J. Chem. Phys. 16, 1063 (1948).

[85] Winsten H and Halford R S, J. Chem. Phys. 17, 607 (1949).

[86] Margenau H and Kestner N R, "Theory of Inter Molecular Forces", Pergamon Press, Oxford (1969).

[87] Kibra T, "Intermolecular Forces" John Wiley, New York (1977).

[88] Califano S, Schettino V and Neto N, "Lattice Dynamics of Molecular Crystal", Springer-Verlag, Berlin (1981).

[89] Schettno V and Califano S, in "Advances in Infrared and Raman Spectroscopy", Clark H J and Hester R E (eds.) Vol. 10, Heyden, London (1978).

[90] Schettino V and Califano S, J. Mol. Struc. 100, 459 (1983).

[91] Foldes F and Sandorfy C, J. Mol. Spectrosc. 20, 262 (1966).

[92] Wallis R F and Maradudin A A, Phys. Rev. 125, 1277 (1962).

[93] Maradudin A A and Fein A E, Phys. Rev. 128, 2589 (1962).

[94] Sakurai T and Sato T, Phys. Rev. B4, 583 (1971).

[95] Sood A K, Arora A K, Umadevi V and Venkat Raman, Pramana, 16, 1(1981) and J. Phys. C. 14, 5215 (1981).

[96] Herzberg G, "Infrared and Raman Spectra of Polyatomic Molecules", Vol. 2 pp. 215, Van Nostrand, NJ (1945).

[97] Duncan J L, Ellis D and Wright I J, Mol. Phys. 20, 673 (1971).

[98] Schever J R, "The Vibrational Spectroscopy of Water", in 'Advances in Infrared and Raman Spectroscopy" Clark R J H and Hestor R E (eds.) Vol. 5, pp 149, Heyden, London (1978)

[99] Rice S A in "Advances in Laser Chemistry" Zewail A (ed.), Springer, New York (1978).

[100] Bertran J F, Ballester L, Dorriholova L, Sanches N and Arrieta R, Spectrochim. Acta 24A, 1765 (1968).

[101] Overent J, "Infrared Spectroscopy and Molecular Structure" pp. 350, Davies M (ed.), Elsevier (1963).

[102] Taylor R, J. Mol. Struct. 70, 255 (1981), 71, 311 (1981) 73, 125 (1981).

[103] Huang P V, "Band Shapes and Molecular Dynamics in Liquids" in 'Advances in Infrared and Raman Spectroscopy' Clark R H and Hester R E(eds.) Vol. 4, Heyden, London (1978).

[104] Berglund B, Lindgren J and Tegenfelat J, J. Mol. Struct. 43, 169 and 179 (1978).

[105] Baur W H, Acta Cryst. B19, 909 (1965).

[106] Falk M, Huang C H and Knop O, Can. J. Chem. 52, 2380 and 2928 (1974), 53, 3394 (1975), 57, 404 (1979) and 58, 270, 867 (1980).

[107] Lutz L D, Pobitschka W, Frifchemier B and Becher R A, J. Raman Spectrosc. 7, 130 (1978).

[108] Lutz H D and Christian H, J. Mol. Struct. 96, 61 (1982).

[109] Lamba O P, Khandelwal D P and Bist H D, J. Mol. Struct. 101, 223 (1983).

[110] Heath D F and Linnet J W, Trans. Faraday Soc. 44, 556 (1948).

[111] Lippincott E R and Schronder R, J. Chem. Phys. 23, 1099 (1955).

[112] Chidambaran R, Sequeira A and Sikka S K, J. Chem. Phys. 41, 3616 (1964).

[113] Joesten M D and Schaad L J, "Hydrogen Bonding", Chap. 2, pp. 53, Marcel Dekkar, New York (1974).

[114] Tillmanns E and Baur W H, Acta Cryst. B27, 2124 (1971).

[115] Well A F, "Structural Inorganic Chemistry" pp 565, Oxford, England (1962).

[116] Schiffer J, Ph.D. Thesis, Michigan University (1964).

[117] Hiebert G L and Horning D F, J. Chem. Phys. 20, 918 (1952).

[118] Hrostowski H J and Pimental G C, J. Chem. Phys. 19, 661 (1951).

[119] Schiffer, Ph.D. Thesis, Princeton University (1963).

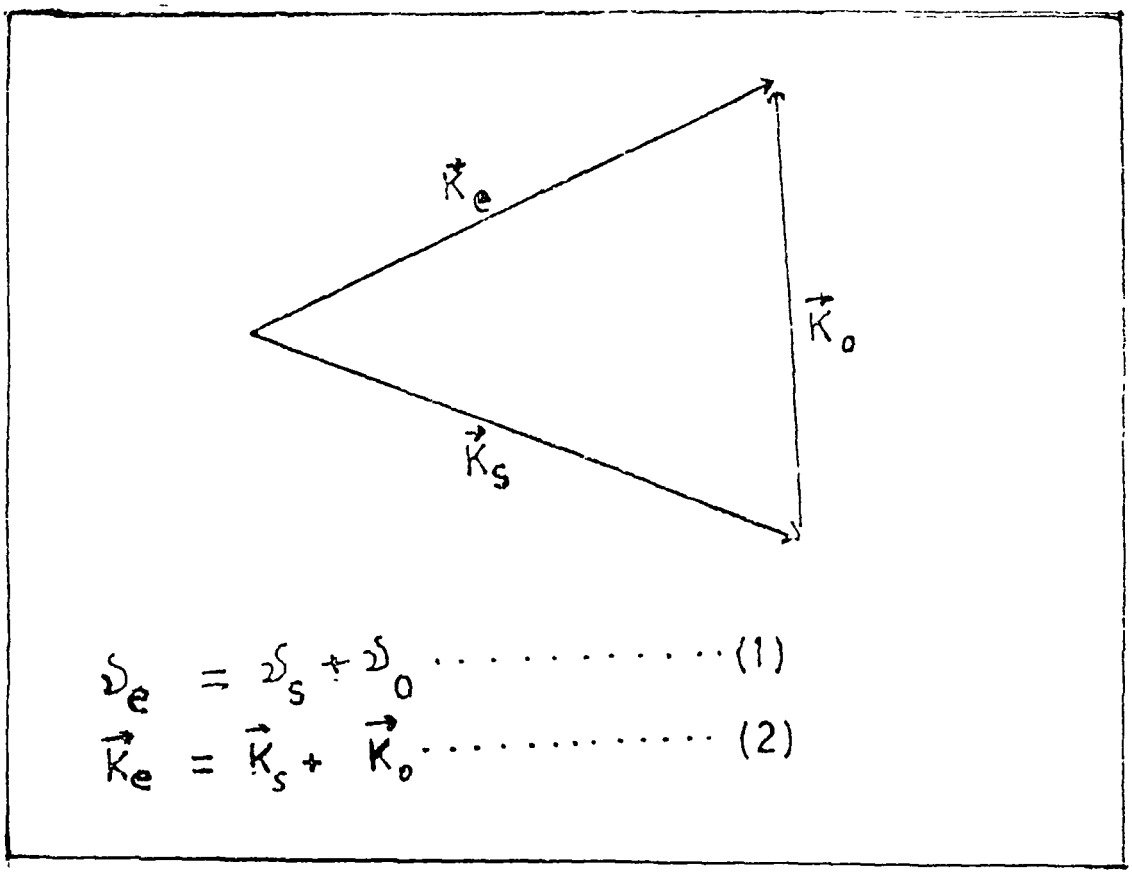

Fig. 1.1

Momentum energy transfer in Raman scattering. $\vec{K}_e$ and $\vec{K}_s$ are wave vectors of exciting and scattered radiations and $\vec{K}_o$ is a wave vector of a given lattice mode ν_e and ν_s are frequencies of exciting and scattered radiations and ν_o frequency of the lattice mode.

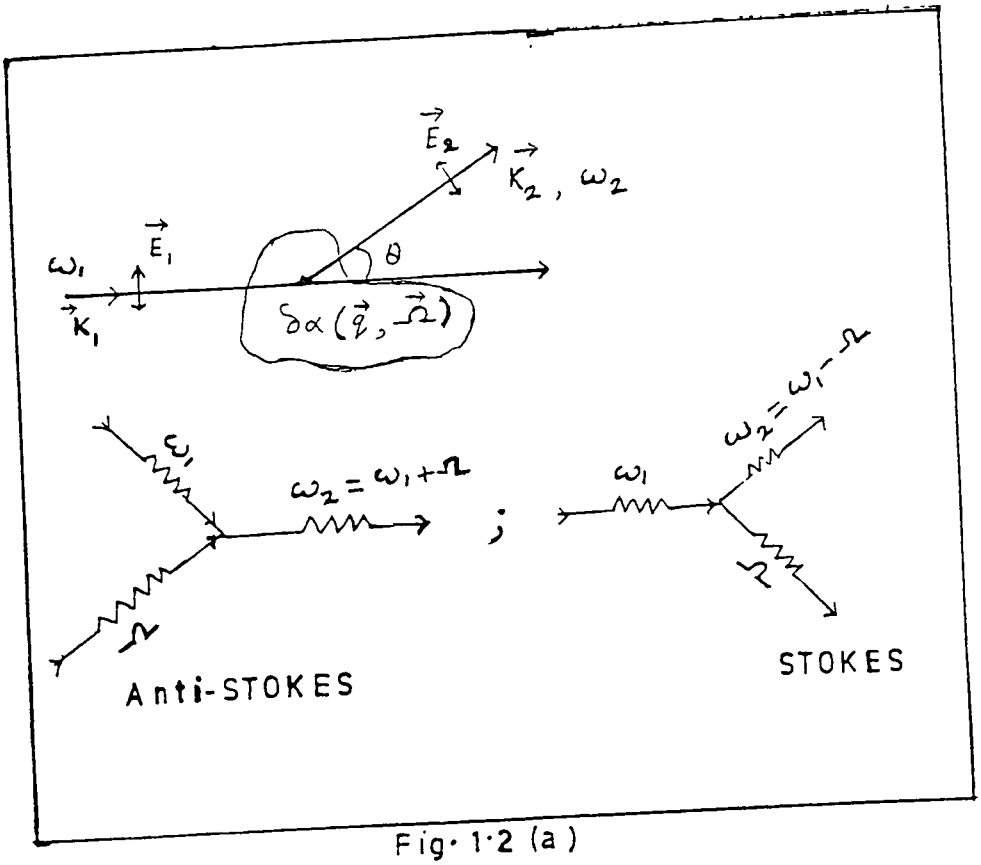

Fig. 1.2 (a)

Geometry of a typical light scattering experiment

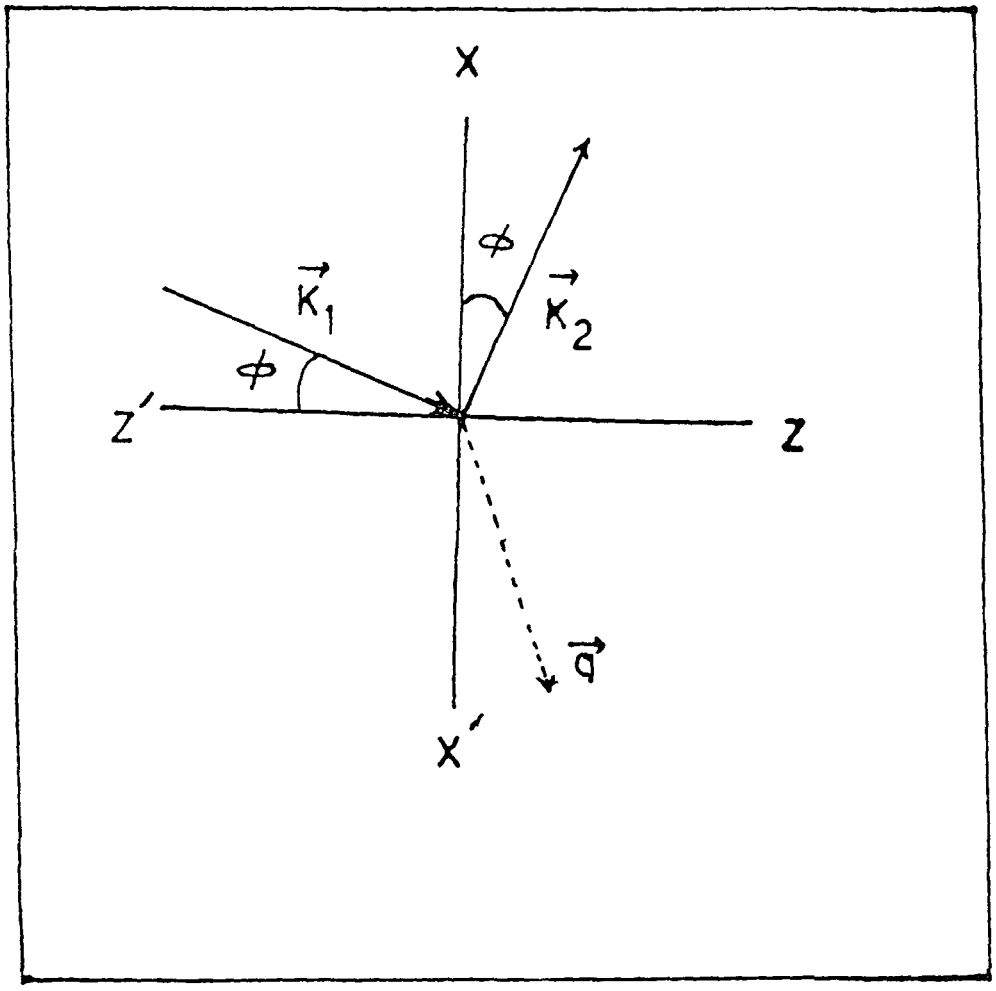

Fig. 1·2 (b)

Geometry of typical light scattering (Perpendicular scattering geometry). $\vec{K}_1$ and $\vec{K}_2$ are incident and scattered wave vectors respectively and $\vec{q}$ is the scattering momentum transfer vector.

CHAPTER II

C H A P T E R II

Experimental

2. Introduction*

The crystal growth is the science and technology of controlling phase transitions which lead to a crystalline solid. The solution growth method is probably the oldest, but this method does not always give good results in many cases. Hence other methods and techniques such as melt, vapour and gel methods were developed from time to time.

In the case of cadmium fluoro silicate hexahydrates (CFSH) and cadmium fluoro titanate hexahydrate (CFTH) which are very hygroscopic and decompose at about 70°C before melting, the solution growth method has been adopted.

2.1 A brief account of the theory of crystal growth

Many theories have been proposed to explain the mechanism of crystal growth based on different concepts like surface energy theory [1-4], diffusion theory [5-11] and surface absorption theory [12-15]. The surface energy theory is briefly discussed here. This theory was first proposed by Curie [1] based on the postulation of Gibbs which states that an isolated droplet of a fluid is most stable when its surface free energy

---

*Papers based on part of this chapter have been accepted for presentation: (1) in the Symposium on 'Crystal Growth' Dec. 24, 1983, Anna University, Madras; and (2) in the Second National Seminar on 'Crystal Growth' Aug. 27-30, 1984. 'Crystal Growth Centre' Anna University, Madras.

is minimum. In a super saturated system when a few atoms or molecules join together a change in energy takes place in the process of formation of the cluster. This cluster is termed as embryo. An embryo may grow or disintegrate and disappear completely depending upon its size. If the embryo grows to a particular size called critical size, then there is a greater probability of the embryo to grow to become a crystal. Thus the birth of a critical nucleus is called nucleation which is an important phenomenon in the crystal growth. There are four stages in the birth of a stable nucleous. The first stage is the development of super-saturated stage. The second stage is the birth of an embryo (nucleation). The nucleation may be either homogeneous in which atoms or molecules build themsleves in the interior of the parent system or heterogeneous in which the molecules or atoms build up on an impurity atom or dust particle or on the surface of the container or on any other imperfections. The third stage is the growth of embryo from unstable to stable state. The fourth stage is the relaxation processes in which the texture of the newly born nucleous changes.

The nucleation is not an easy process. Not only the atoms or molecules have to coagulate resisting the tendency to redissolve but they also have to orient to occupy a fixed lattice.

A crystal is normally bounded by different faces and each face has surface energy characteristic of that face. According to Curie, when the volume free energy per unit volume is constant

then the sum of the surface energies of all faces of the crystal will be a minimum [1] i.e.

$$\sum_{i=1}^{n} A_i \gamma_i = \text{minimum} \qquad \ldots\ldots \qquad (2.1)$$

where A_i = area of the ith face

γ_i = surface energy per unit area of the ith face

n = the number of faces of the nucleous of the crystal.

When the number of molecules associated with a critical nucleus is not large, the critical nucleus will not have a regular morphology of a crystal. So it is considered to be spherical to a first approximation.

If ΔG is the free energy change due to the formation of an embryo, then [16]

$$\Delta G = 4\pi r^2 \gamma + \frac{4}{3} \pi r^3 \Delta g \qquad \ldots\ldots \qquad (2.2)$$

where r = radius of the embryo

γ = the surface energy per unit area of the interface separating the parent and product phases.

Δg = Gibbs free energy change per unit volume and is negative = $g_s - g_l < 0$.

g_s = free energy of solid phase

g_l = free energy of liquid phase

Since $\triangle g$ is negative, the $\triangle G$ passes through a maximum. The values of the radius 'r' by setting $\frac{d(\triangle G)}{dr} = 0$, is called the critical radius and is denoted by r^*

$$r^* = - \frac{2\gamma}{\Delta g} \quad \ldots\ldots \quad (2.3)$$

2.2 Experimental methods for the growth of crystals

As already mentioned in the introduction of this chapter, there is a good number of methods for growing single crystals (monocrystals) only solution method has been tried by us.

2.2.1 Solution method [17,18]

In the solution method the techniques developed and modified by the following persons can not be applied here in our systems (CFSH and CFTH) because in all of the methods evaporation technique at constant temperature is used. A few of them are mentioned below -

(1) Johnsen (Johnsen's rotating crystal method)

(2) Barlett (Barlett single chamber method)

(3) Kruger and Finke (Kruger and Finke U-tube method) and

(4) Valeton (Valeton's method).

The main reason for discarding the methods of evaporation at constant temperature or slow cooling is the high humidity at this place and hygroscopic nature of the materials. The preparation of the constituent components for the crystals used in this study is described below.

2.3 Preparation of the constituent substances

The cadmium fluorosilicate hexahydrate (CFSH) and cadmium fluorotitanate (CFTH) were not available commercially. Therefore we synthesised the same in our laboratory. For this purpose H_2SiF_6 and H_2TiF_6 acids were prepared in our laboratory from HF acid, because these acids were not available easily.

2.3.1 Preparation of H_2SiF_6 acid [18(a)]

This acid was prepared from commercially available HF acid 48% dilute (S.D.'s electronic grade) and 99.99% pure quartz powder (SiO_2) from FLUKA company of West Germany.

The stoichiometric amount of SiO_2 powder was dissolved in HF acid in a polyethylene beaker (50 gm of SiO_2 was dissolved in 200 ml of HF acid). The reaction was exothermic and therefore to control the heat evolved, the beaker was placed in cold water bath and left over night.

The chemical reaction is -

$$6HF + SiO_2 = H_2SiF_6 + 2H_2O$$

The H_2SiF_6 acid was gently warmed to make the solute (SiO_2) dissolve completely, and then filtered by using Whatman No-40 filter paper. The presence of the $[SiF_6]^{2-}$ ions in the H_2SiF_6 acid was confirmed by IR spectra. By this method 500 ml of H_2SiF_6 acid was prepared and its specific gravity was found to be 1.446.

2.3.2 Preparation of H_2TiF_6 acid

The preparation of this acid was similar to the preparation of H_2SiF_6 acid except with some modifications. The TiO_2 in powder form was obtained commercially. The stoichiometric amount of TiO_2 (55 gm) was mixed with 200 ml of HF acid (48% and specific gravity 1.175). The chemical reaction is similar to the former reaction -

$$6HF + TiO_2 = H_2TiF_6 + 2H_2O$$

The reaction was very slow in this case. The polythene beaker containing acid was placed in water bath whose temperature initially was kept below room temperature. The mixture was stirred with a magnetic stirrer. The temperature of the bath was very slowly increased, by regulating the heating current in the electrical heater attached to the magnetic stirrer, and raised to 50°C within two days. The experimental arrangement is shown in the Fig. 2.1a. The stirring was done continuously. This slow heating was necessary to check the evaporation of HF acid. The excess amount of TiO_2 was filtered out and the filtrate was H_2TiF_6 acid. Its specific gravity was found to be 1.382 and its strength in percentage was 62%. The $[TiF_6]^{2-}$ ions were monitored by IR spectra.

2.3.3 Preparation of $CdSiF_6:6H_2O$ and $CdTiF_6:6H_2O$ salts

150 ml of H_2SiF_6 acid prepared by us was taken in a 500 ml polythene beaker. Then 100 gm of $CdCO_3$ was added slowly to the H_2SiF_6 acid stirring the solution constantly with a solid rod of polyethylene. The reaction was vigorous and the beaker was filled with foam. The reaction was complete when evolution of CO_2 gas ceased. The solution was then diluted, filtered and warmed, and left for crystallisation overnight. The chemical reaction is -

$$H_2SiF_6 + CdCO_3 = CdSiF_6 + CO_2 + H_2O$$

The needle shaped, extremely fine crystals were collected from the solution and the mother liquid was warmed again and left for further crystallization. In this way crystals were collected from the mother liquid.

The $CdTiF_6:6H_2O$ was prepared in a similar manner starting from H_2TiF_6 acid and $CdCO_3$.

Similarly, starting with different salts like $MnCO_3$, $CoCO_3$, pure Fe-powder, and $ZnCO_3$ and dissolving them in H_2SiF_6 or H_2TiF_6 acids, the following substances were also prepared in the laboratory :- $MnSiF_6:6H_2O$, $MnTiF_6:6H_2O$, $CoSiF_6:6H_2O$, $CoTiF_6:6H_2O$, $FeSiF_6:6H_2O$, $FeTiF_6:6H_2O$ and $ZnSiF_6:6H_2O$ and $ZnTiF_6:6H_2O$.

2.4 Growth of single crystals (Monocrystals)

The solution-growth method with some modifications in the procedure of controlling the evaporation and maintaining slow and constant temperature gradient has been adopted in growing single crystals of $CdSiF_6:6H_2O$ (CFSH) and other members of the system $MSiF_6:6H_2O$, where M = Zn, Mn, Co and Fe.

2.4.1 Growth of single crystals of CFSH

The compound CFSH prepared in the laboratory was recrystallized several times and its purity was checked by IR spectroscopy. The CFSH is highly hygroscopic and its saturated solution also absorbs moisture when the humidity of the environment is above 65%. A slight variation of temperature and humidity dissolved the seed in the solution disallowing the growth of single crystals.

To overcome these difficulties the concentrated solution of CFSH was taken in a polyethylene beaker of 100 ml capacity and was warmed in a water bath to 30°C. Then the beaker was immersed in another beaker of bigger size and was wrapped with cotton to check the rapid heat dissipation. The whole system was then put in a descicator (3 litre capacity) containing 150 gm. of blue solid silica gel of medium size grains at the bottom. The descicator itself was placed in a constant temperature water-bath. The experimental arrangement is shown in Fig. 2.1(b).

From the initial temperature of 25°C, the temperature of the bath was lowered at the rate of 2°C per 12 hours. After 4 days crystals having nearly 5 mm diameter and 20 mm length were obtained.

The single crystals of other compounds such as $ZnSiF_6:6H_2O$, $MnSiF_6:6H_2O$, $CoSiF_6:6H_2O$ and $FeSiF_6:6H_2O$ were also grown in a similar way.

2.4.2 Growth of single crystals of CFTH

The single crystals of CFTH ($CdTiF_6:6H_2O$) were also grown in the same manner as those of CFSH crystals with slight modifications. The most difficult part of the solution-growth method is the preparation of proper saturated solution to prevent dissolution of the nucleous or seed and to prevent rapid initial mushroom growth of small crystals.

A general common technique is to make a slightly unsaturated solution and allow evaporation to bring it to exact saturation (super saturation) point. But in case of very hygroscopic substances like CFTH, this technique cannot be used, for the slightly under saturated solution exposed for evaporation absorbs moisture and becomes less saturated instead of being super-saturated.

The solubility characteristics of a solute-solvent system have very profound influence on the selection of a method of crystallization as shown in Fig.2.2.

In case of CFTH therefore, the following arrangements were made. The concentrated solution of CFTH in a polyethylene beaker was warmed in a water bath to 30°C. The beaker containing CFTH was then placed inside another beaker of bigger capacity which was insulated from outside by cotton. Both of these beakers were placed inside a descicator containing 150 gm. of blue solid silica gel of fine size grains. The ventilator of the descicator was attached with a side-tube filled with the same kind of blue silica gel. The experimental arrangement is shown in Fig. 2.3. The whole system was placed in a BOD Incubarator. From the initial temperature of 30°C the temperature of the Incubarator was lowered at the rate of 1°C per day. After about 10 days, good quality single crystals were obtained.

Similarly, single crystals of other compounds like $ZnTiF_6:6H_2O$, $MnTiF_6:6H_2O$, $CoTiF_6:6H_2O$ and $FeTiF_6:6H_2O$ were also grown [19-22].

2.5 Crystal structure of $MTiF_6:6H_2O$ [23]

The table 2.1 gives the crystal structure data of systems having general formula $MTiF_6:6H_2O$, where M stands for divalent metal ion. In the table 2.1, a_o, C_o and α are the unit cell parameter. Z is the number of formula units per unit cell.

Table 2.1

M	Rhombohedral Unit			Hexagonal Pseudo Cell		
	a_o A^o	α^o	Z	a_o A^o	C_o A^o	Z
Zn	6.410	96° 20'	1	9.610	9.940	3
Mg	6.520	96° 57'	1	9.750	9.830	3
Ni	6.40 ±.03	96° ± 18'	1	-	-	-
Mn	6.51	96° 42'	1	-	-	-

2.5.1 Crystal structure data of the systems having general formula $MSiF_6:6H_2O$

The Table 2.2 shows the structural data of the systems, where M stands for divalent metal ion such as Zn, Mn, Co, etc.

2.6 Measurement of Spectra

The Raman and IR spectra were measured in our laboratory at room and low temperatures. The Raman spectra were measured on a SPEX Raman Spectrometer using lasers as excitation sources. Here we give only brief discussion of the equipment used in our studies.

2.6.1 Laser source

The commercially available Spectra-Physics Model 165-09 Argon-Ion Laser was used as excitation source in our studies. This model is a CW Argon-ion laser of maximum 5 watts output power in all the lines. The assembly consists of mainly two units; one laser head and the other, exciter (Spectra-Physics Model 265). The plasma

Table 2.3

Crystal structure data of the systems having general formula $MSiF_6:6H_2O$

M	Rhombohedral Cell Unit			Hexagonal Pseudo Cell Unit			Space Group
	a_o A°	o	Z	a_o A°	C_o A°	Z	
Co	6.27 ± 0.05	96°.0 ± 0.5	1	9.366 ± 0.002	9.730 ± 0.04	3	R $\bar{3}$
Mn	6.51 ± 0.06	96°.7 ± 0.2	1	9.700 ± 0.03	9.800 ± 0.03	3	P $\bar{3}$ m1
Zn	6.297 ± 0.003	96°.3 ± 0.1	1	9.363 ± 0.003	9.690 ± 0.005	3	R $\bar{3}$
Fe	6.418 ± 0.005	97°.1 ± 0.1	1	9.621 ± 0.008	9.648 ± 0.008	3	R $\bar{3}$ m
Ni	6.255 ± 0.002	96°,1 ± 0.1	1	9.310 ± 0.003	9.618 ± 0.002	3	R $\bar{3}$
Mg	6.430 ± 0.002	96°.05 ± 0.1	1	9.50 ± 0.003	9.88 ± 0.005	3	R $\bar{3}$ m

A° = Angstron Unit

tube is cooled by circulating chilled, deionized and distilled water at constant temperature of 15°C at a pressure of 40 PSIG. The water supply source used was NESLAB Model HX-500 water chiller plant.

The input power stabilization for the laser source was achieved by using three single phase 8.3 KVA capacity NELCO Voltage Stabilizers.

2.6.2 Raman Spectrometer (Details in SPEX manual)

The Raman spectrometer used in our studies was a SPEX Model 1403. This is a f/7.8 instrument covering frequency range from 31×10^3 to 11×10^3 cm^{-1} with an accuracy of $\pm$ 1 cm^{-1} in the 10×10^3 cm^{-1} range. The spectral repeatibility and resolution of the instrument are $\pm$ 0.2 cm^{-1} and 0.15 cm^{-1} respectively. The holographic gratings having 1800 groves/mm are mounted on a modified C-Zerny-Tunner mount which utilizes the fundamental grating equation:

$$m\lambda = d(\sin\alpha + \sin\beta) \qquad (2.4)$$

where m = spectral order , λ = wave length

d = grating spacing

α = angle of incidence

β = angle of diffraction

By substituting $\alpha = (\theta + \phi)$ and $\beta = (\theta - \phi)$ the above equation may be reduced to

$$m\lambda = 2d \sin\theta \cos\phi \qquad (2.5)$$

where θ = angle of grating rotation

ϕ = the angle-dependent constant of the instrument design.

Since in the Ramalog 1403 model the Raman peaks are observed as frequency shift in cm^{-1} on a linear scale, it utilizes a cosecant drive for the grating rotation with $\phi = 10°$.

Before exciting the sample by the laser beam, the laser light was passed through the SPEX 1459 UVISIR illuminator and lasermate, a small grating monochromator, to isolate the background plasma lines. The filtered laser beam is deflected upwards by a mirror and focussed onto the sample by a fused silica condensing lens. The diameter of the beam on the sample was approximately 10×10^{-6} m. Fig. 2.4(a) and 2.4(b).

2.6.3 Spectrometer control and data processing

The SPEX DATAMATE is used for controlling the spectrometer and for data acquisition. The DATAMATE is a 8-bit dedicated microcomputer which is capable of manipulating the spectral data by background subtraction, division, differentiation and integration, whenever necessary. The incoming and the manipulated data could be stored in the 8 files of variable length. The stored data can be plotted on a strip-chart recorder or can be transferred to external peripherials to a general computer through the standard IEEE interface for further data manipulation.

2.6.4 Low temperature cryogenics device (Details in the manual of Air Products Model CSA 202 E)

An Air Products closed-cycle helium cryo-cooler Model - Displex CSA 202E was used for low temperature studies upto 10k.

The helium gas is circulated by compression pump. The expander module DE 202 of the system is shown in Fig. 2.5 in which the principal parts are labelled. The Figs. 2.6 and 2.7 show helium gas flow and displacer movement during the intake and exhaust phases of the expander's operating cycle. The cycle is phased and timed by rotating valve disc.

The high pressure helium gas admitted by the rotating valve disc flows through passages in the slack cap and at the same time enters the regenerators. The regenerators cooled during the previous exhaust stroke, cool the incoming gas. The helium gas flowing through the slack cap passages pushes up the slack cap which, in turn, lifts the displacer, thereby an space for expansion is created at the heat-stations. As the displacer lifts the gas above the slack cap, it is partially compressed and pushed through the orifice into the surge volume.

Before the displacer reaches the valve-stem, the valve closes. The compression of helium gas becomes slow above the slack cap and therefore stops the displacer before it can collide with the valve stem.

The exhaust stroke is shown in Fig. 2.7. When the valve opens to exhaust, high pressure gas at the heat-station is free to expand and refrigerate them. The regenerators are also cooled by the outgoing gas. As the pressure drops, partially compressed gas comes out from the surge volume, pushes the slack cap and

displacer towards the heat-stations and to position the displacer for the next cycle. The valve closes again and the residual gas acts as a cushion to decelerate and to stop the displacer before it collides with the heat-stations. In this way after a good number of cycles, the temperature is gradually reduced to a minimum (10k) after about one and half an hour of operation of the cryo-cooler.

The sample holder is attached with the second stage heat-station having a cold finger not shown in the Fig. 2.7.

A Digital temperature controller model APD-E, was used with gold-chromel thermo-couple to control and measure the temperature of the heat-station.

2.6.5 Recording of IR spectra

The IR spectra of polycrystalline samples were recorded using a Perkin-Elmer Model- 983-IR Spectrometer. A small amount of the compound $MXF_6:6H_2O$ was grounded into fine powder and then mixed with a suitable amount of KBr to keep the absorption within scale. A pellet was made by a press-machine and the spectra were recorded by placing a pellet of pure dry KBr of the same thickness in the path of the reference beam. Nujol oil was used in place of KBr for the deuterated compounds. The IR spectra of $CdSiF_6:6D_2O$ and $CdTiF_6: 6D_2O$ in Nujol medium are given in Figs. 2.8 and 2.9.

2.7 References

[1] Curie P, Bull. Soc. France, Mineral 8, 145 (1885).

[2] Wulff G, Z. Krist., 34, 449 (1901).

[3] Marc R and Ritzel A, Z. Physik. Chem. 76, 584 (1911).

[4] Nacken R, Neues Jahrb Mineral Geol. 2, 133 (1915).

[5] Noyes A A and Whitney W R, Z. Physik. Chem. 23, 689 (1897).

[6] Nernst W, Z. Physik. Chem. 67, 470 (1909).

[7] Wagner C L, Z. Physik. Chem. 71, 401 (1910).

[8] Lebrum J, Bull. Classe Sci. Acad. Roy. Belge., 970 (1913).

[9] Marc R, Z. Physik. Chem. 61, 385 (1908), 67, 470 (1909) and 73, 685 (1910).

[10] Leblanc M and Schmandt W, Z. Physik. Chem. 77, 614 (1911).

[11] Berthound A, J. Chem. Phys. 10, 624 (1912).

[12] Volmer M, Z. Physik. Chem. 102, 267 (1922).

[13] Brandes H, Z. Physik. Chem. 126, 196 (1927).

[14] Bravais A, "Etudes Cristallographique", Paris, Gaunthier Villars (1966).

[15] Kossel W, Nachr. Ges. Wiss. Gottingen Jahresber Math-Physik. Klasse, 135 (1927).

[16] Raghavan V, "Material Science and Engineering" 2nd ed., pp. 186, Prentice-Hall of India (1982).

[17] Balman A A and Laudise R A, in "The Art and Science of Growing Crystals", Gilman J J (ed.), John Wiley and Sons Inc. (1963).

[17a] Rabenau A, "Crystal Growth : An Introduction", Hartman P (ed.), North Holland Publishing Co. (1973).

[18] Badachhape R B, Hunter G, McCory L D and Margrave J L, Inorg. Chem. 5(5), 929 (1966).

[18a] Brauer G, "Hand Book of Preparation of Inorganic Reagents", Academic Press, New York (1963).

[19] Rosenberger F, "Fundamental of Crystal Growth" Springer Series in Solid State Sciences Cardona M (ed.), New York (1979).

[20] Verma A R, "Crystal Growth and Dislocations", Butterworth, London (1953).

[21] Thakur G, Symp. on "Crystal Growth" Dec. 24 (1983), Crystal Growth Centre, Anna University, Madras.

[22] Thakur G, Second National Seminar on 'Crystal Growth' Aug. 27 (1984), Anna University, Madras.

[23] Wyckoff R W G, "Crystal Structure" 2nd ed. Vol. 3, Wiley Interscience, New York. (1965)

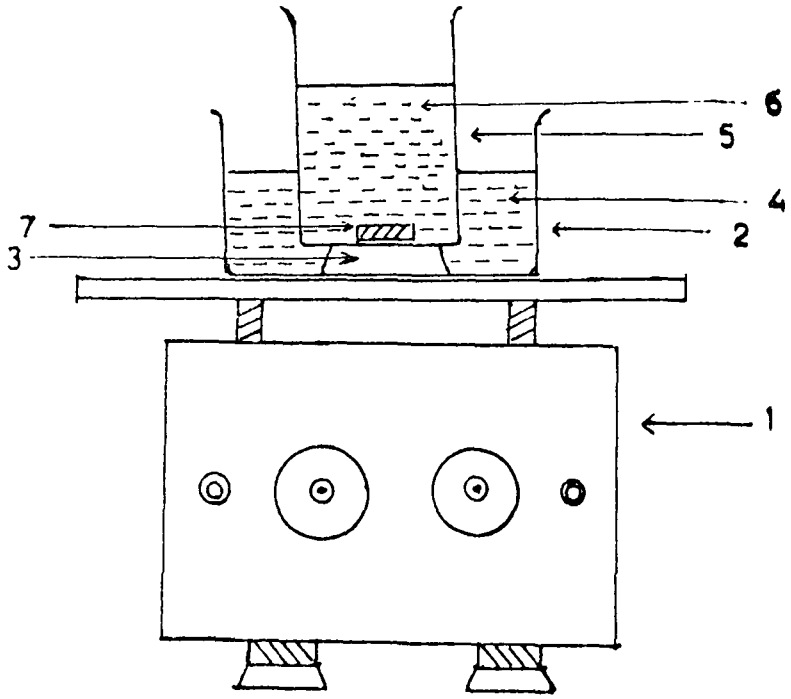

1. Magnatic Stirrer, 2. Glass Beaker
3. Ruber pad, 4. Water, 5. Polyethylene Beaker
6. Sol. of HF and TiO_2
7. Magnet coated with Teflon

Fig. 2.1(a)

Experimental arrangement for preparation of H_2TiF_6 acid in the laboratory.

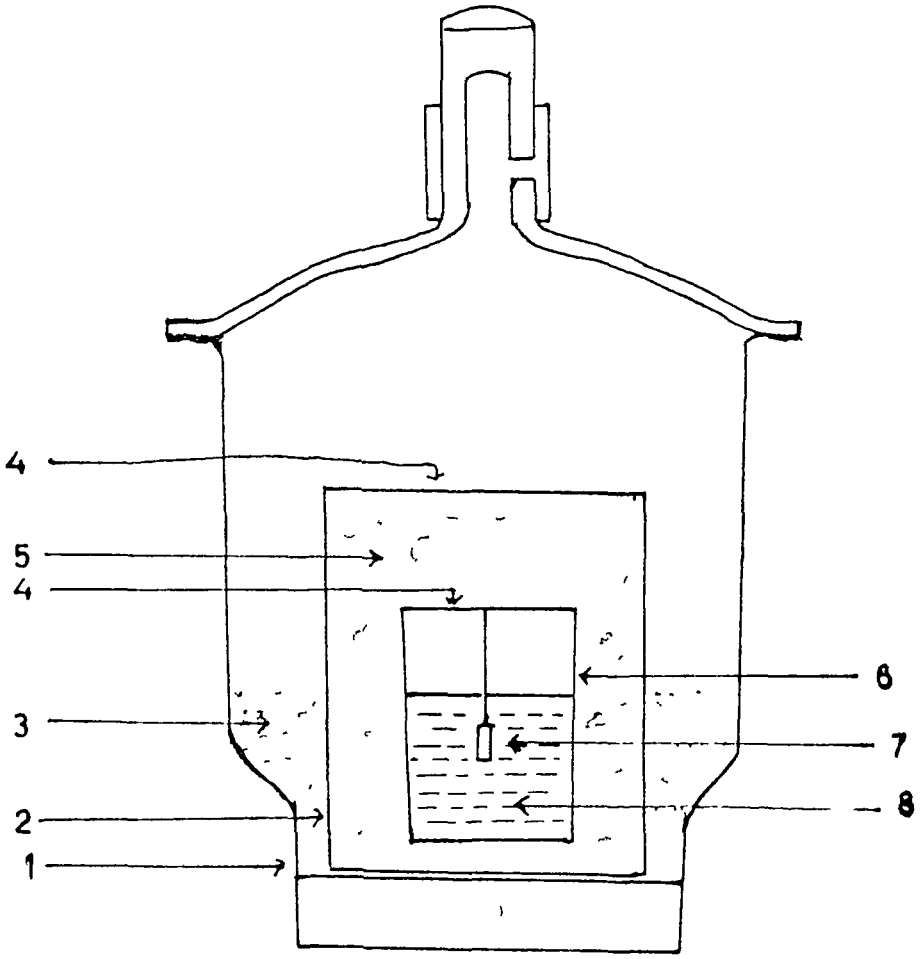

1-DESCICATOR, 2.POLYTHENE BEAKER
3-SILICA GEL, 4-POLYTHENE SHEET COVER,
5.COTTON, 6.POLYTHENE BEAKER,
7-SEED OF THE SAMPLE ($CdSiF_6:6H_2O$)
8-SOLUTION OF THE SAMPLE.

Fig.2.1(b)

Experimental arrangement for growing single crystals of $CdSiF_6:6H_2O$.

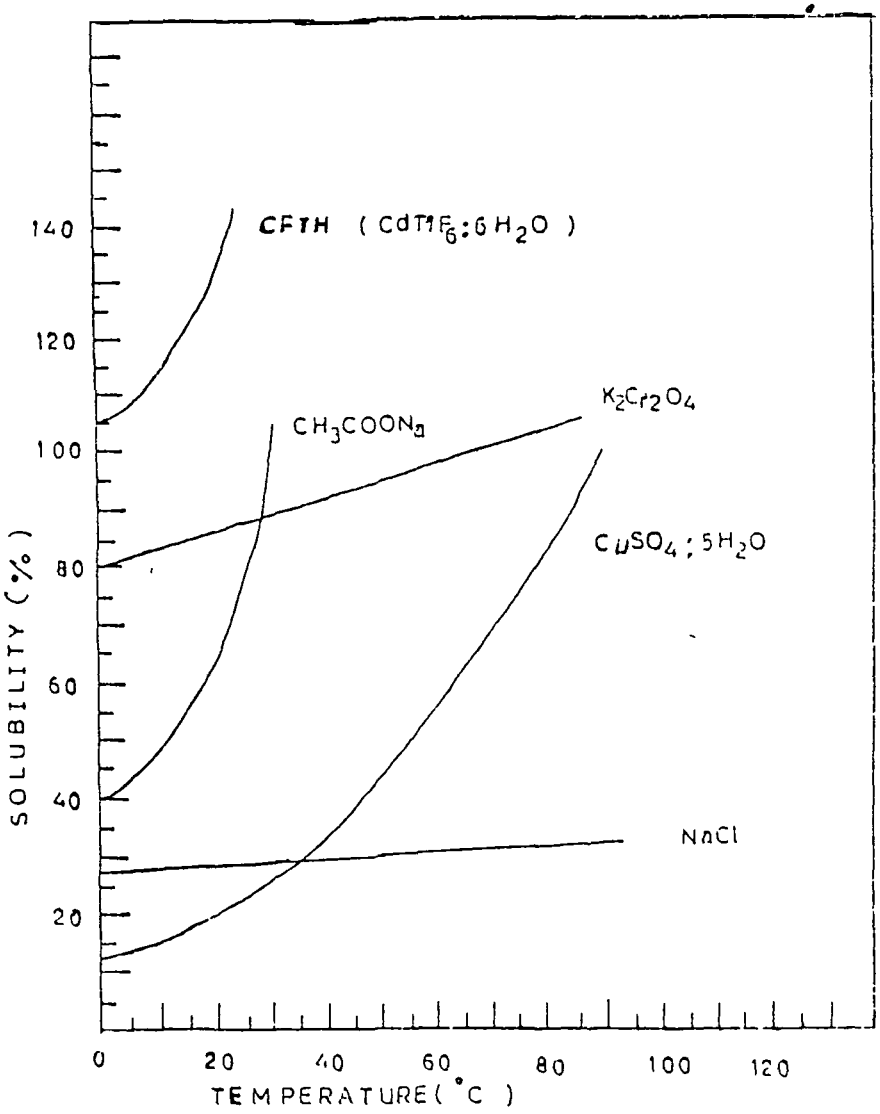

Fig·2·2

A comparison in the variation of solubility with temperature of CFTH ($CdTiF_6:6H_2O$) with the corresponding variation in case of other salts such as CH_3COONa, $K_2Cr_2O_4$, $CuSO_4:5H_2O$ and NaCl is shown in the figure.

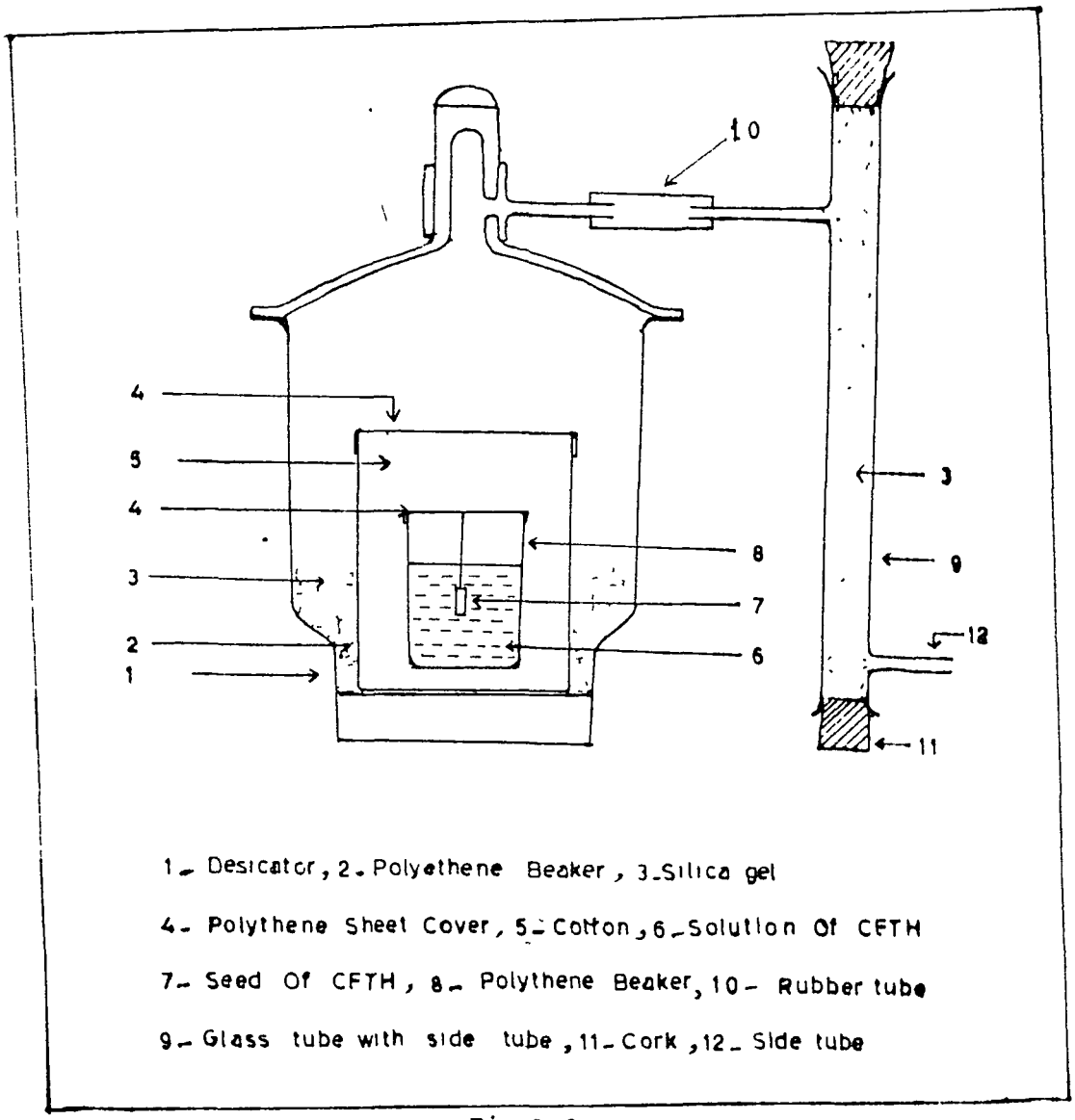

Fig·2·3

Experimental arrangement for growing single crystals of CFTH ($CdTiF_6:6H_2O$).

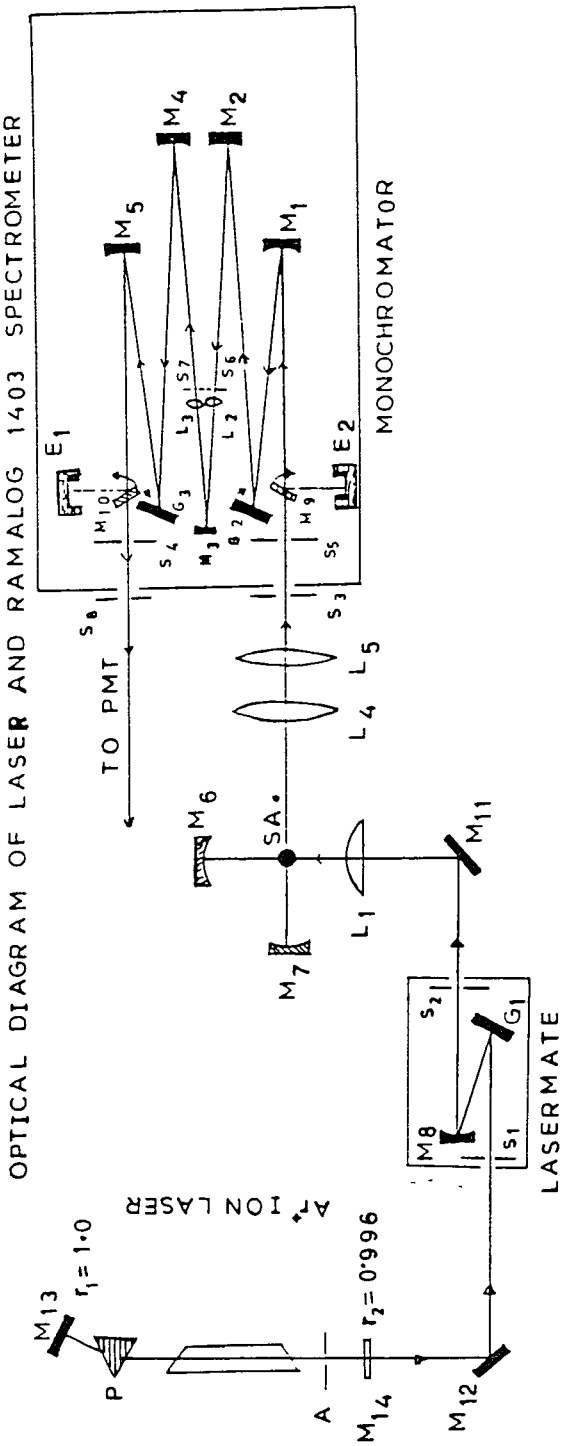

L_1 = CONDENSER LENSE .

L_4, L_5 = FOCUSING LENSES .

A = APERTURE .

P = PRISM .

r_1, r_2 = reflectance .

SA = SAMPLE HOLDER .

$M_{1,2,3,4,5,6,7 \& 8}$ = CONCAVE MIRRORS .

$M_{9,10,11,12,13 \& 14}$ = PLANE MIRRORS .

$G_{1,2,3}$ = PLANE GRATINGS .

$S_{1,2,3,4,5,6,7 \& 8}$ = SLITS .

L_2 , L_3 = OPTICAL FILTERS.

Fig 2·4(a)

Optical line diagram of Laser and Ramalog 1403 spectrometer

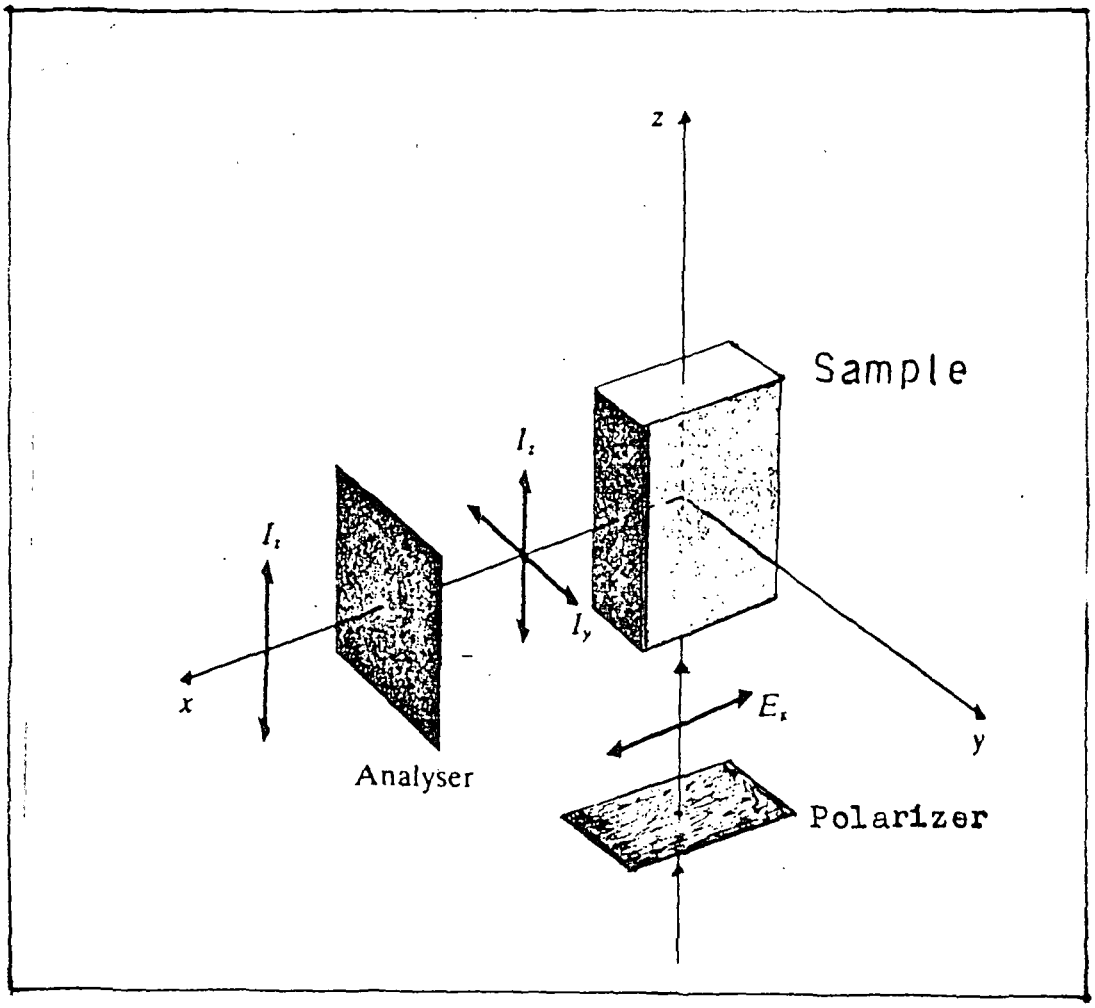

geometry for $z(xz)x$ measurement

Fig·2·4(b)

Fig·2·4(b)·The arrangement for $\{z(xz)x\}$ polarization geometry is shown in this figure. The x,y and z-axes are orthogonal co-ordinate axes.

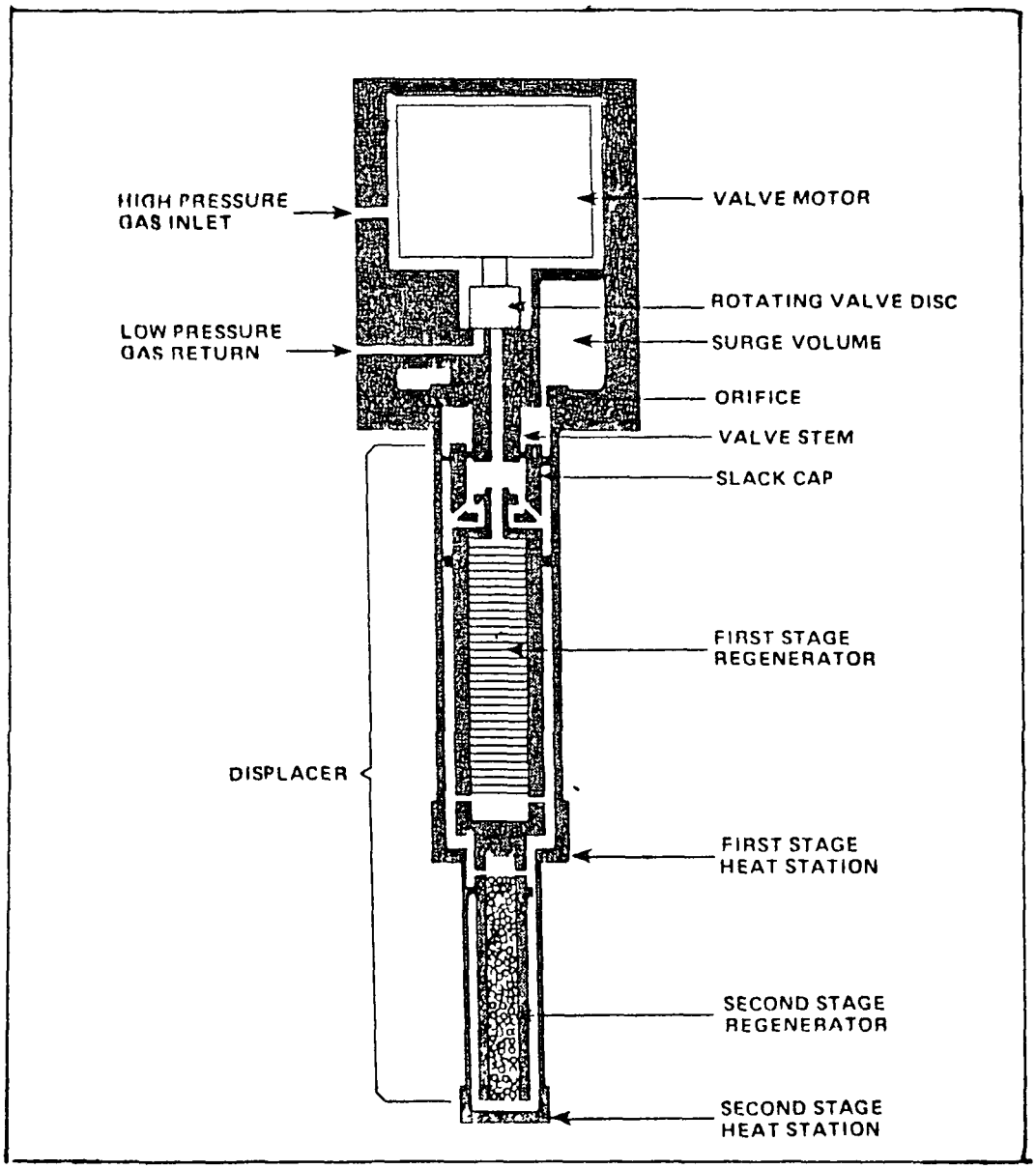

Fig·2·5

The section diagram of the expander module DE 202 of the helium cryo-cooler Model Displex CSA 202 E. The principal parts are labelled.

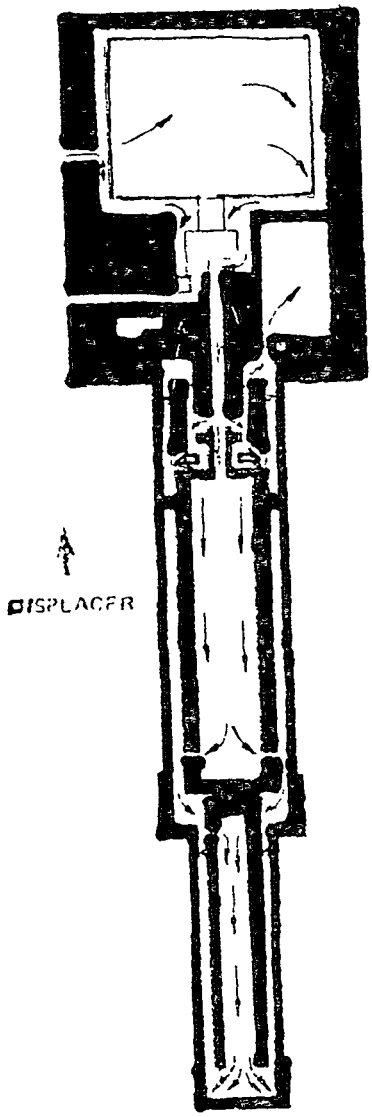

Fig. 2·6

The section diagram of the expander module when the displacer movement is upward during intake phase. The arrows indicate the flow of helium gas during the intake.

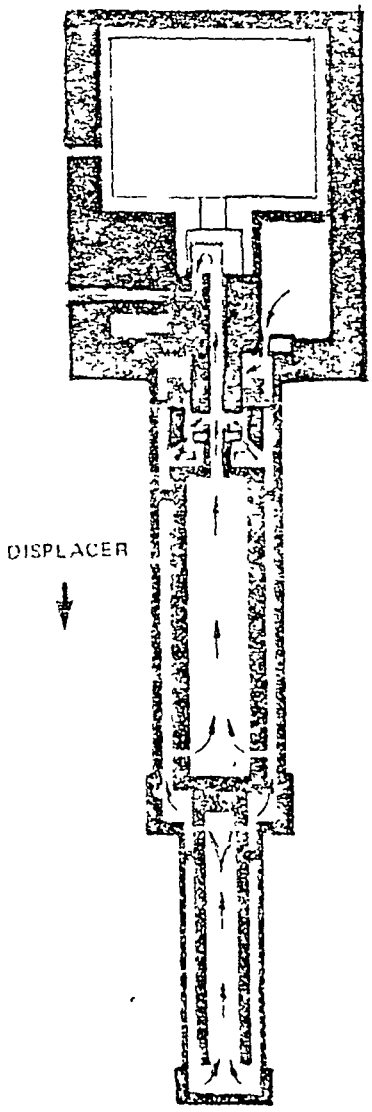

Fig·2·7

The section diagram of the expander module during exhaust phase. The arrows indicate the flow of helium gas during the exhaust process.

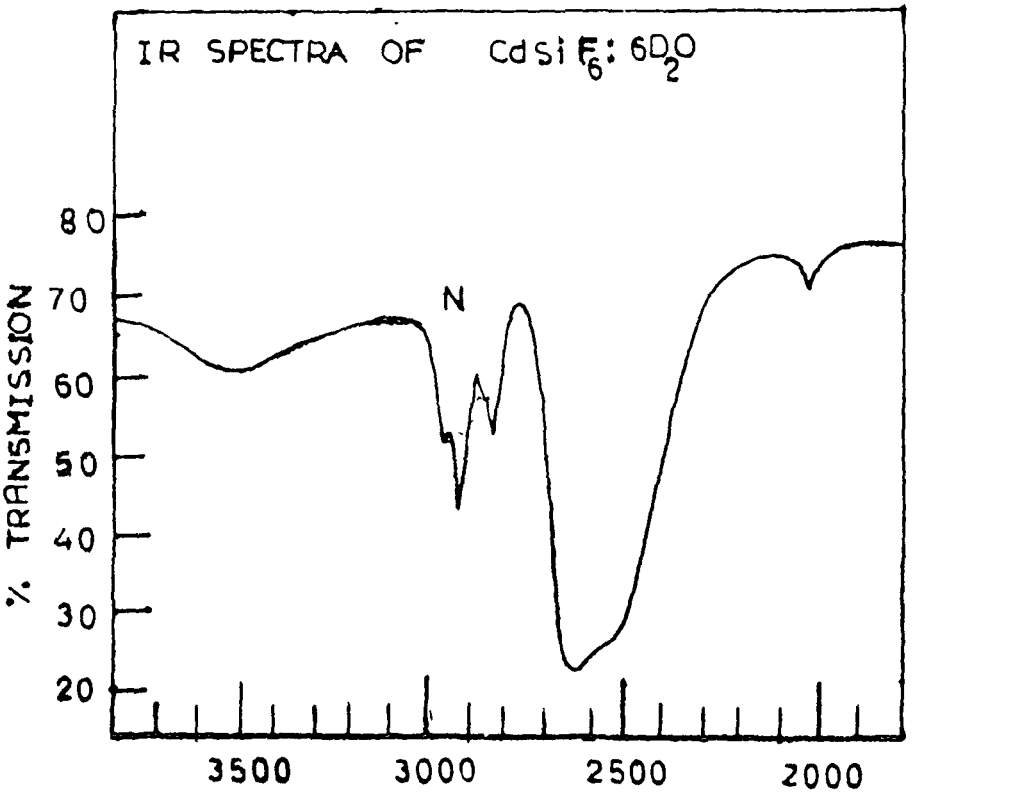

Fig·2·8

The IR spectra of $CdSiF_6:6D_2O$ in Nujol medium at room temperature.

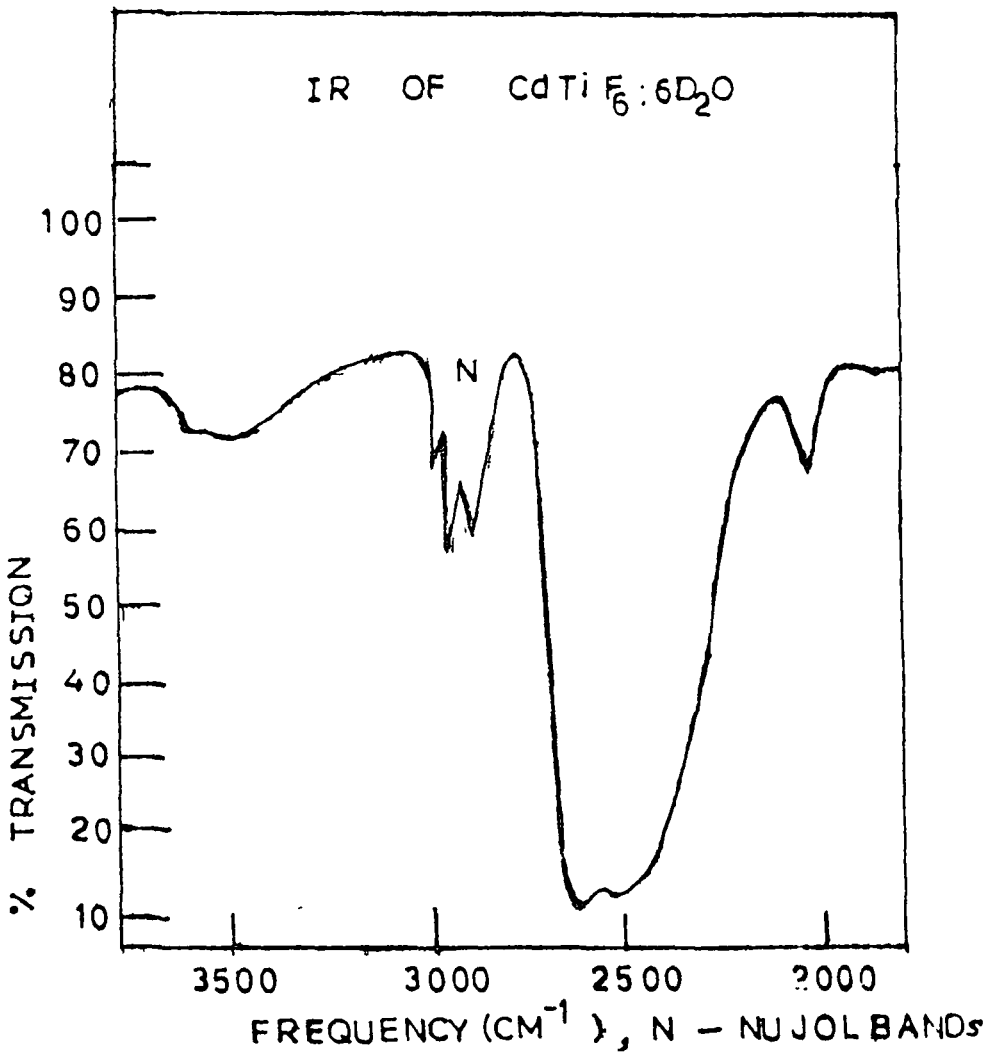

Fig. 2.9

The IR spectra of $CdTiF_6:6D_2O$ in Nujol medium at room temperature.

CHAPTER III

C H A P T E R III

Theoretical Aspects

3. Group Theoretical Analysis

The different approaches for analysing normal modes of crystals have been suggested by many workers, namely by Horning, Winston, and Bhagavantam [1-3]. The correlation method which was suggested by Fately et al [4] is commonly used in the factor group analysis of the crystal vibrations. A few of them are briefly discussed below:

3.1 Factor Group Analysis (Unit cell approach)

This method was suggested by Bhagavantam et al in 1951 [3]. In this method the problem of analysis of 3Nm normal modes of a crystal in which there are N units cells and 'm' atoms in each cell is reduced to the problem of classifying 3m modes of the unit cell. The assumption in this case is that atoms or molecules at equivalent lattice positions are in the same state of vibration. Therefore in this approach the total character representation for the unit cell is worked out. When the inter-atomic forces within a polyatomic group in the unit cell are stronger than the inter-molecular forces between the groups, the distinction is made between internal and external group motions. The external modes are librational and translational in nature. In order to classify the translational modes, each group of atoms, i.e., ion or molecule, is treated as if it were a single entity. Thus for a total of 'p' polyatomic groups and 'q' mono-atomic groups, the chracter representations associated with these vibrations are given by:

$$\chi_j = m_j(p)(2\cos\theta_j \pm 1) \quad (3.1)$$

$$\chi_j(ta) = (2\cos\theta_j \pm 1) \quad (3.2)$$

$$\chi_j(te) = (m_j(p) - 1)(2\cos\theta_j \pm 1) \quad (3.3)$$

and

$$\chi_j(l) = m_j(p-q)(\pm 2\cos\theta_j + 1) \quad (3.4)$$

where

χ_j = character representation

χ_{ta} = acoustic modes

χ_{te} = translational modes (external modes)

χ_l = librational modes

m_j = number of atoms which remain invariant by an operation of class 'j'.

In the above expression, (+) sign is taken for proper rotation where as (-) sign is for improper rotation. For symmetry operation σ_h, θ is taken as 0° and 'i' (inversion) is considered as improper rotation with $\theta = 180^\circ$.

The number of modes belonging to a particular species is found by reducing the above character representation using the following formula [2]

$$N^{(\gamma)} = \frac{1}{g}\sum_j g_i \chi_i(\gamma)\,\chi_j \quad (3.5)$$

where g = order of the group of symmetry operations

g_i = order of the ith class

$N^{(\gamma)}$ = number of modes in the symmetry species

$\chi_i^{(\gamma)}$ = the character of irreducible representation for the species 'γ' of jth class

χ_j = character of reducible representation in the jth class.

The summation sign $\sum$ indicates that the sum goes over all the classes in the point group of the unit cell.

3.2 Site Symmetry Approach

R.S. Halford in 1946 proposed this method [4] based on the assumption that the local potential is responsible for the dynamics of the mono or polyatomic groups in the crystal. The vibrational modes are obtained by correlating the symmetry species of the free molecular point group to those of the local symmetry point group. This method, however, neglects the interaction between different groups in the same unit cell.

3.3 Correlation method

Fately et al in 1971 [5] proposed an alternative method called the correlation method. This is a quick and simpler method which provides information about vibrational modes of a crystal without any ambiguities and has been followed by us in our analysis of different systems. The different terms and symbols, used in the correlation method, are defined here:-

t^{γ} = the number of translations in a site species 'γ'. This number may take values zero, one, two or three depending on whether none, one, two, or three translations are contained in the site species 'γ' respectively. This information is obtained from the character table.

r^{γ} = the number of rotations included in the site symmetry species 'γ'.

f_{v}^{γ} = the degrees of vibrational freedom present in each site species 'γ'. ($= t^{\gamma} \cdot n$. where 'n' is the number of atoms or molecules in an equivalent site.)

f_{r}^{γ} = $r^{\gamma} \cdot n$ = degree of rotational freedom present in each species 'γ'.

a_{γ} = the degree of freedom contributed by each site species γ to a factor group species δ

$$a_{\gamma} = \frac{f_{v}^{\gamma}}{\sum_{\delta} C_{\delta}} = \frac{f_{r}^{\gamma}}{\sum_{\delta} C_{\delta}} \quad \ldots \quad (3.6)$$

where C_{δ} = the degeneracy of the species 'δ'.

Species	A	B	E	F	G	H
C_{δ}	1	1	2	3	4	5

The following steps are followed for finding out the reducible representation corresponding to the various degrees of freedom of atoms or molecular units in the primitive cell:-

1) The crystal structural data of the system should be known or can be assumed and group theoretical predictions of vibrational spectra can be made and compared with experimental observations to confirm the structure.

2) In case of a molecular crystal, the lattice (translational and librational) modes of both the +ve and -ve ions are calculated. Then the intra-molecular (internal) vibrations of the ions are calculated.

3) These are combined to obtain all the modes in the unit cell.

3.4 The crystal structure of $MXF_6:6H_2O$

The class of compounds having general formula $MXF_6:6H_2O$ contain two octahedral ions $[M(OH_2)_6]^{2+}$ and $[XF_6]^{2-}$ as shown in Fig. 3.1(a)-(g), where M = divalent metallic ions (Cd, Zn, Fe etc) and X = Si or Ti.

Most of the members in this series have the space group R $\bar{3}$ (C_{3i}^2) where as some of them have space group R $\bar{3}$m (D_{3d}^5) at room temperature [6]. From crystal structure data given in Chapter II (Sec. 2.5 to 2.5.1) the Zn and Ni salts of the systems are known to have a unimolecular rhombohedral unit cell of space group R $\bar{3}$ (C_{3i}^2). No structural data are available for $CdSiF_6:6H_2O$ or $CdTiF_6:6H_2O$ to our knowledge.

3.4.1 The structure of the $[XF_6]^{2-}$ ions

In most of the compounds, the $[XF_6]^{2-}$ ion (where X = Si, Ti) is a regular octahedron having O_h molecular symmetry, see Fig. 3.1(a)-(g).

3.4.2 The structure of $[M(OH_2)_6]^{2+}$ ions

The complex ion $[M(OH_2)_6]^{2+}$ is normally a distorted octahedron of T_h molecular symmetry and occupies a site of symmetry C_{3i} in a crystal of space group C_{3i}. The H_2O molecules have C_{2v} symmetry and also occupy sites of symmetry C_{2v} [7], see Fig. 3.1(a)-(g).

3.5 Calculation of lattice vibrations of $[M(OH_2)_6]^{2+}$ ion and $[XF_6]^{2-}$ ions

By applying the correlation method (Sec. 3.3) we obtain the vibrations as given in the following Table:-

f^γ	t^γ	Site Symmetry C_{3i}	Factor Group C_{3i}	C	a
2	$2(T_{xy})$	E_u ⟶	E_u	2	1
1	$1(T_z)$	A_u ⟶	A_u	1	1

Therefore the lattice vibrations (external modes) belong to the A_u and E_u symmetry species.

The ion $[XF_6]^{2-}$ has O_h molecular symmetry and in a crystal of space group C_{3i} it occupies a site of symmetry D_{3d}. Therefore the number of lattice vibrations of this ion is the same as that of the ion $[M(OH_2)_6]^{2+}$ as explained in Sec. 3.5. Therefore the lattice vibrations of the crystal having these two ions are:-

$$(A_u + E_u) + (A_u + E_u) - (A_u + E_u) = A_u + E_u$$

Lattice vibr. of $[M(OH_2)_6]^{2+}$ + Lattice vibr. of $[XF_6]^{2-}$ - Acoustical vibr.

So the lattice vibrations of $MXF_6:6H_2O$ are classified as $A_u + E_u$.

3.5.1 Internal vibrations of $[M(OH_2)_6]^{2+}$ ions.

This complex ion has the molecular symmetry T_h whose internal modes are classified as [8] -

$$3A_g(R) + 3E_g(R) + 5F_g(R) + A_u(ia) + E_u(ia) + 8F_u(IR)$$

In the crystal of space groups C_{3i}^2 its internal modes are shown in the following correlation diagram:-

Free ion molecular symmetry	Site and Factor group
T_h	C_{3i}
A_g	A_g
E_g	E_g
F_g	
A_u	A_u
E_u	E_u
F_u	

The triply degenerate modes of F_g and F_u symmetries split into A_g and E_g and A_u and E_u species respectively under C_{3i} site symmetry.

Thus the total internal modes of the complex ion $[M(OH_2)_6]^{2+}$ are:-

$$8A_g(R) + 8E_g(R) + 9A_u(IR) + 9E_u(IR) = 51$$

Therefore the Raman inactive modes of symmetries A_u and E_u in case of free ion become active in the crystalline form.

3.5.1.1 Internal vibrations of $[XF_6]^{2-}$ ion

The internal modes of the complex ion $[XF_6]^{2-}$ having point group symmetry O_h are:-

$$A_{1g}(R) + E_g(R) + F_{2g}(R) + 2F_{1u}(IR) + F_{2u}(ia) = 15$$

In the crystal of space group C_{3i}^2 or D_{3d}, the internal modes are classified as given in the following correlation diagram because only D_{3d} site is possible-

Free ion symmetry	Site and Factor group
O_h	D_{3d}
A_{1g}	A_{1g}
E_g	A_{2g}
F_{2g}	E_g
F_{1u}	A_{1u}
	A_{2u}
F_{2u}	E_u

Therefore in a crystal of space group D_{3d}, the internal modes are:-

$$2A_{1g} + 2E_g(R) + A_{1u}(ia) + 2A_{2u}(IR) + 3E_u(IR) = 15$$

3.5.2 Symmetry and selection rules for $MXF_6:6H_2O$

As shown in the above sections 3.5 to 3.5.1.1, there are 78 phonon branches expected for the crystal $MXF_6:6H_2O$. The symmetries and selection rules are given below for a crystal with space group C_{3i}^2 -

Species	Lattice modes	Acoustical modes	Rotation or Librations	Internal vibrations	Spectral activity	Total modes
A_g	-	-	2	10	R	12
E_g	-	-	2	10	R	12
A_u	1	1	-	12	IR	14
E_u	1	1	-	12	IR	14

$$12A_g(R) + 12E_g(R) + 14A_u(IR) + 14E_u(IR)$$

$$12 + (12 \times 2) + 14 + (14 \times 2) = 78 \text{ modes.}$$

Similarly for a crystal of space group D_{3d} the following table gives the details-

Species	Lattice modes	Acoustical modes	Rotation or Libration	Internal vibration	Spectral activity	Total modes
A_{1g}	-	-	-	5	R	5
A_{2g}	-	-	2	5	ia	7
E_g	-	-	2	10	R	12
A_{1u}	-	-	-	2	ia	2
A_{2u}	1	1	-	10	IR	12
E_u	1	1	-	12	IR	14

$$5A_{1g}(R) + 7A_{2g}(ia) + 12E_g^{(R)} + 2A_{1u}^{(ia)} + 12A_{2u}(IR) + 14E_u(IR)$$

$$5 + 7 + (12 \times 2) + 2 + 12 + (14 \times 2) = 78.$$

3.6 Frequencies of normal modes of $[XF_6]^{2-}$

The frequencies of the normal modes of the hexahalide ions of the general formula $[XY_6]^{2-}$ where X = Si, Ti, Zr or Sn and Y = F, Cl, Br or I were obtained by Peacock et al in 1959 [9]. Since the mass of the central metal is large, all the vibrations are expected to be observed below 660 cm^{-1}.

The following table gives the frequencies of $[XF_6]^{2-}$ (where X = Si, Ti) and $[TiCl_6]^{2-}$ ion observed by Griffith et al [10] and Evans et al [11-11(a)].

ion	$\nu_1 A_{1g}$(R)	$\nu_2 E_g$(R)	$\nu_3 F_{1u}$(IR)	$\nu_4 F_{1u}$(IR)	$\nu_5 F_{2g}$(R)
$[SiF_6]^{2-}$	655 cm^{-1}	474 cm^{-1} 510* cm^{-1}	740 cm^{-1}	485 cm^{-1}	395 cm^{-1}
$[TiF_6]^{2-}$	613 cm^{-1}	-	560 cm^{-1}	-	275 cm^{-1}
$[TiCl_6]^{2-}$	321-331cm^{-1}	284,271cm^{-1}	302-330cm^{-1}	188-193cm^{-1}	186-94 cm^{-1}

*Reported by Nakagawa Ref. [8]

3.7 Resolution of the overlapping bands

The neighbouring bands overlap generally in the IR absorption and Raman spectra. It is necessary therefore to resolve such spectral features geometrically on the basis of the expected shapes of the overlapping components. In the condensed phase the Lorentzian shape for the band contours is justified [12] while for the electronic absorption bands, Gaussian band shape is a reasonable approximation [13]. In many cases neither Lorentzian nor Gaussian curves provide a complete fit to the experimental curves. Hence the Voiget like functions are generally used [14].

However, in cases where the actual band width is much larger than the instrumental slit width, the Lorentzian shape gives a reasonably good fit, especially if one is not interested into the tail of the band.

A Lorentzian function is given by the expression -

$$I(\nu) = I(\nu_0) \frac{b^2}{b^2 + (\nu - \nu_0)^2} \qquad (3.7)$$

where ν_o is the frequency at peak intensity $I(\nu_o)$ and '2b' is the FWHM intensity ($\Delta\nu_{1/2}$). Similarly the full band width at 0.1, 0.2, 0.3 ..... 0.8, 0.9 of the maximum intensity are 6b, 4b, 3.06b ..... b, 0.66b respectively. The Fig. 3.2 shows the relationship between $I(\nu_o)$ and 'b'. The product of $I(\nu_o)$ and $\Delta\nu_{1/2}$ is a measure of the intensity of a band, usually called integrated intensity. It is useful to evaluate the relative integrated intensities (RII) of different bands assigning RII = 100 to one typical band.

3.7.1 Selection of a base line

The selection of a proper base line is essential for the analysis of overlapping bands. The following considerations are necessary in the selection of the base line:-

(a) the base line should not touch the tail of a absorption profile or a scattering profile.

(b) A base line with increasing absorption towards lower frequency region is avoided.

Analysis is then made choosing the more obvious components first, and then affixing $I_o(\nu)$ and $\Delta\nu_{1/2}$ parameters for them. The residues were then found. The following main criteria were used in this analysis:-

(a) The minimum number of the Lorentzian components warranted by the observed contour was found,

(b) Minor residues or deviations were neglected for the bands with doubtful existence,

(c) In case of alternative analysis giving equally good fit, the one which maintained the peak positions nearer the observed ones was preferred.

(d) An indistinct component in the band contour was introduced only in those cases where repeated Lorentzian trials failed by wide margins.

3.8 Correlation of ν_{OH} and ν_{OD} frequencies

The correlation between the ν_{OH} and ν_{OD} frequencies for single OH and OD oscillator as a function of O...O distance has been extensively studied [15,16]. The following correlation was suggested by Falk [15] -

$$\nu_{OD}^{HOD} = 2727 - \exp [20.96 - 5.539\ R_{O...O}]\ cm^{-1} \qquad (3.8)$$

where ν_{OD}^{HOD} are the decoupled ν_{OD} frequencies of HOD oscillator whose gas phase limit is $\nu_{OD} = 2727\ cm^{-1}$ and $R_{O...O}$ is the distance between the hydrogen bonded oxygen atoms in Angstrom unit.

At present no useful correlations between the $R_{O...O}$ and force constant for the O-H bond are available. A typical correlation obtained by Berglund et al [17] on deutron quadrupole coupling parameter is as follows -

$\nu_{OD} = 2727 - 7.0 \times 10^4 \exp [-3.02\ R_{H...O}]$ and

$\nu_{OD} = 2727 - 8.97 \times 10^4 \exp [-3.73\ R_{O...O}]$.

The value of $r_{(OH)}$ - the bond length of O-H, can be obtained using Badger's rule [18].

$$r_{(OH)} = 0.335 + [(1.86 \times 10^5)/4\pi^2 \mu c^2 \nu_{OH}]^{\frac{1}{3}} \qquad (3.9)$$

where $C = 2.998 \times 10^{10}$ cm sec^{-1}

$\mu = 1.562 \times 10^{-24}$ gm

and ν_{OH} = frequency of the symmetric stretch in cm^{-1}

A rough estimate of $r_{(O-H)}$ can also be made from the $R_{O....O}$ value using empirical correlation [15] given below -

$$r_{(O-H)} = (1.376 \pm 0.193) - (0.143 \pm 0.069)\ R_{O....O} \qquad (3.10)$$

Statistically in a hydrate-deuterate mixture the molar percentage of H_2O : HOD : D_2O would be X^2 : 2x(1-x) : $(1-x)^2$ where 'x' is the molar fraction of H. For 20%, 80% and 95% deuteration of the sample the following shall be the proportion of D_2O, H_2O and HOD in the sample [18(a)] -

	Sample	% D_2O	% H_2O	% HOD
I	20% deuterated	4%	64%	32%
II	80% deuterated	64%	4%	32%
III	95% deuterated	90.25%	0.25%	9.5%

The first (I) sample shall have most of its D_2O surrounded by HOD and H_2O to exclude other D_2O's. Hence one expects the OD oscillators of D_2O to be dynamically uncoupled. Similar arguments apply for OH

oscillators of H_2O molecules in the II sample. In the III sample, the OD and OH oscillators of HOD are surrounded by D_2O and hence dynamical coupling is absent again. In this case the decoupled modes belong to vibrations of indivisual OH and OD oscillators of HOD. These yield a degree of asymmetry in a particular H_2O molecule.

Although the isotopic dilution technique has been used by many workers on tacit assumptions to study modes of water in crystal-hydrates, formal attempts to justify the techniques theoretically by calculating potential functions and the isotopic frequency shift ratio has been made only recently [19].

3.9 References

[1] Horning D F, J. Chem. Phys. 16, 1063 (1948).

[2] Winston H and Halford R S, J. Chem. Phys. 17, 607 (1949).

[3] Bhagavantam S and Venkatarayudu T, "Theory of groups and its application to Physical Problems", 2nd ed. Bangalore Press, Bangalore (1951).

[4] Halford R S, J. Chem. Phys. 14, 8 (1946).

[5] Fately W G, McDevitt N T and Bentley F F, Appl. Spectrosc. 25 (2), 155 (1971).

[6] Hamilton W C, Acta Cryst. 15, 353 (1962).

[7] Lewis J and Jenkins T E, J. Raman Spectrosc. 8, 111 (1979).

[8] Nakagawa I and Shimanouchi T, Spectrochimi Acta, 20, 429 (1964).

[9] Peacock R D and Sharp D W A, J. Chem. Soc. (A), 2762 (1959).

[10] Griffith J E and Irish D E, Inorg. Chem. 3, 1134 (1964).

[11] Evans D F and Dean P A W, J. Chem. Soc. (A), 698 (1967).

[11a] Shurrell H F, Can. Spectrosc. 12, 156 (1967).

[12] Lorentz H A, Ned. Akad. Welenschap, Proc. 8, 591 (1960).

[13] Vitek and Czachoslov A, Chem. Commun. 39, 366 (1974).

[14] Voigt W, Munch. Berg. 1912, 603 (1912).

[15] Falk M and Knop O, in "Water" Vol. 2 Franks F (ed.) Plenum Press, New York (1973).

[16] Huang P V, "Band Shapes and Molecular Dynamics" in "Advances in IR and Raman Spectrosc. Vol. 4, Heyden, London (1978).

[17] Burglund B, Lindgren J and Tegenfeldt J, J. Mol. Struc. 43, 163 and 179 (1978).

[18] Badger R M, J. Chem. Phys. 2, 128 (1934).

[18a] Patel M B, Ph.D. Thesis, I.I.T. Kanpur (1982).

[19] Wojcik M J, Lindgren J and Tegenfeldt J, Chem. Phys. Lett. 99, 1012 (1983).

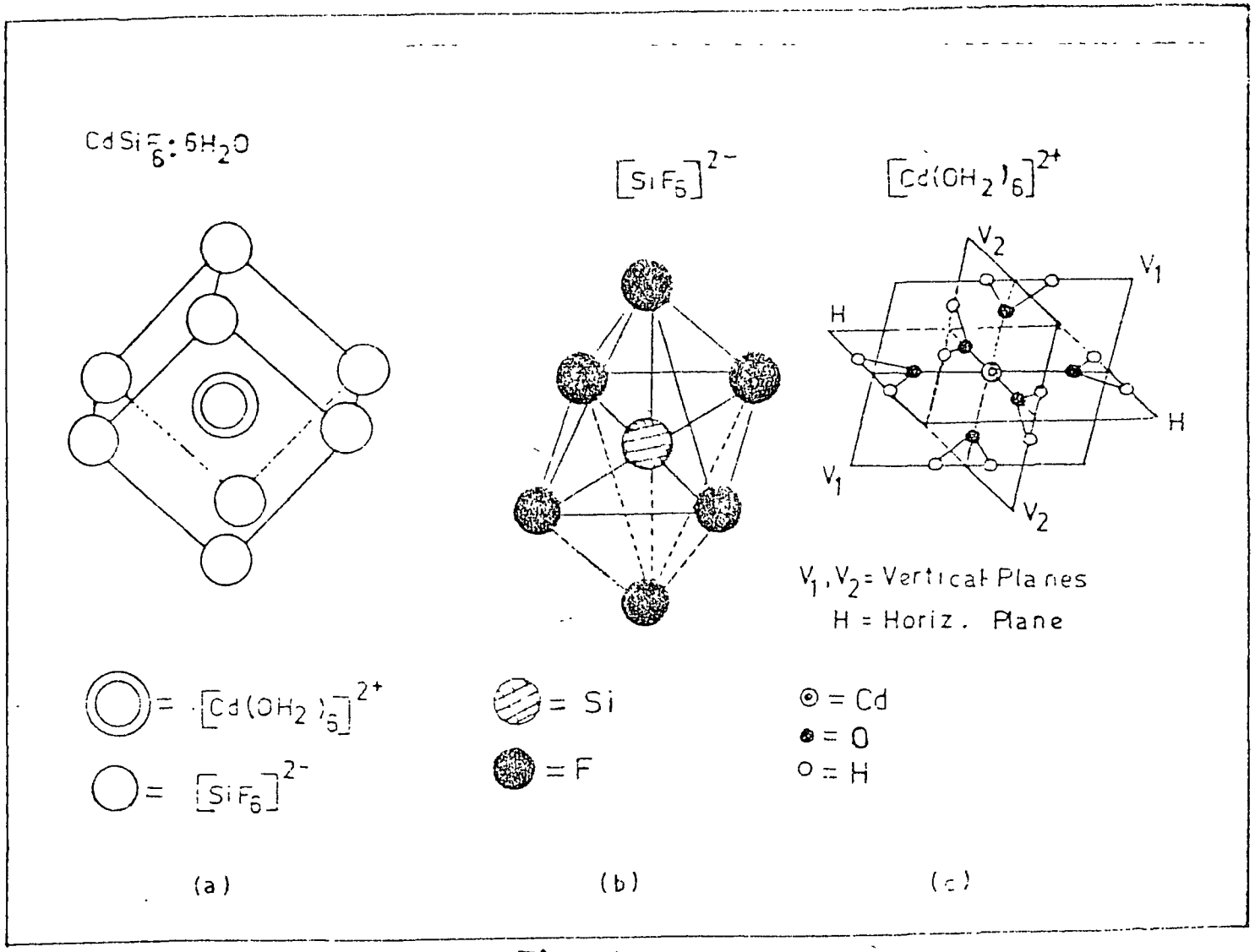

Fig·3·1

Crystal structure of $CdSiF_6:6H_2O$ based on C_{3i}^2 Space group -

(a) Rhombohedral unit cell of $CdSiF_6: 6H_2O$

(b) Octahedral $\angle SiF_6 \rangle^{2-}$ ion of O_h symmetry

(c) Octahedral $\angle Cd(OH_2)_6 \rangle^{2+}$ ion of T_h symmetry.

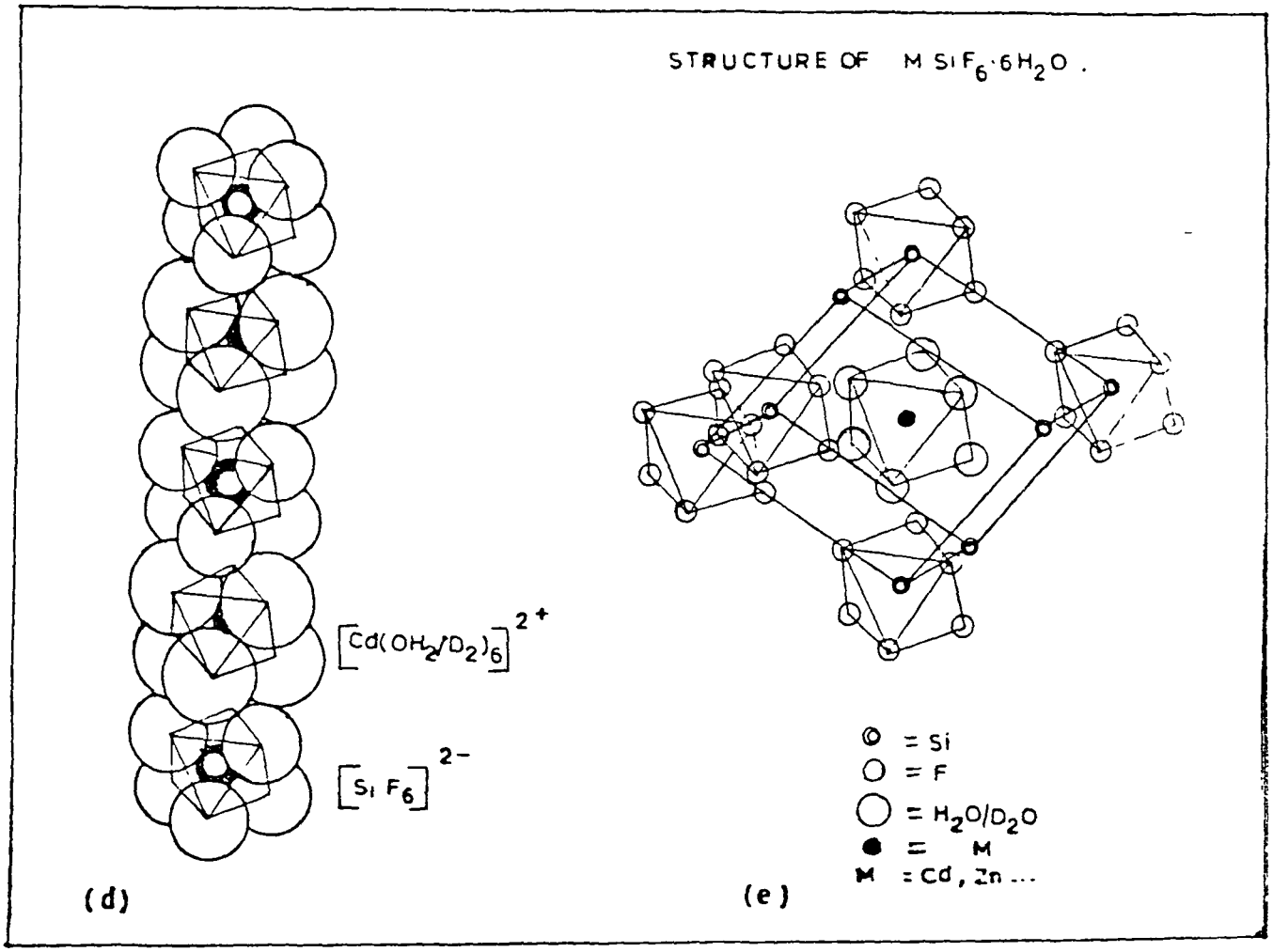

Fig·3·1

Crystal structure of $CdSiF_6:6H_2O$ based on C_{3i}^2 space group -

(d) A vertical column of $\left[SiF_6\right]^{2-}$ and $\left[Cd(OH_2)_6\right]^{2+}$ ions. The ions are alternate.

(e) The details of the arrangement of $\left[SiF_6\right]^{2-}$ and $\left[Cd(OH_2)_6\right]^{2+}$ ions in one unit cell of rhombohedral of fig. 3.1(a).

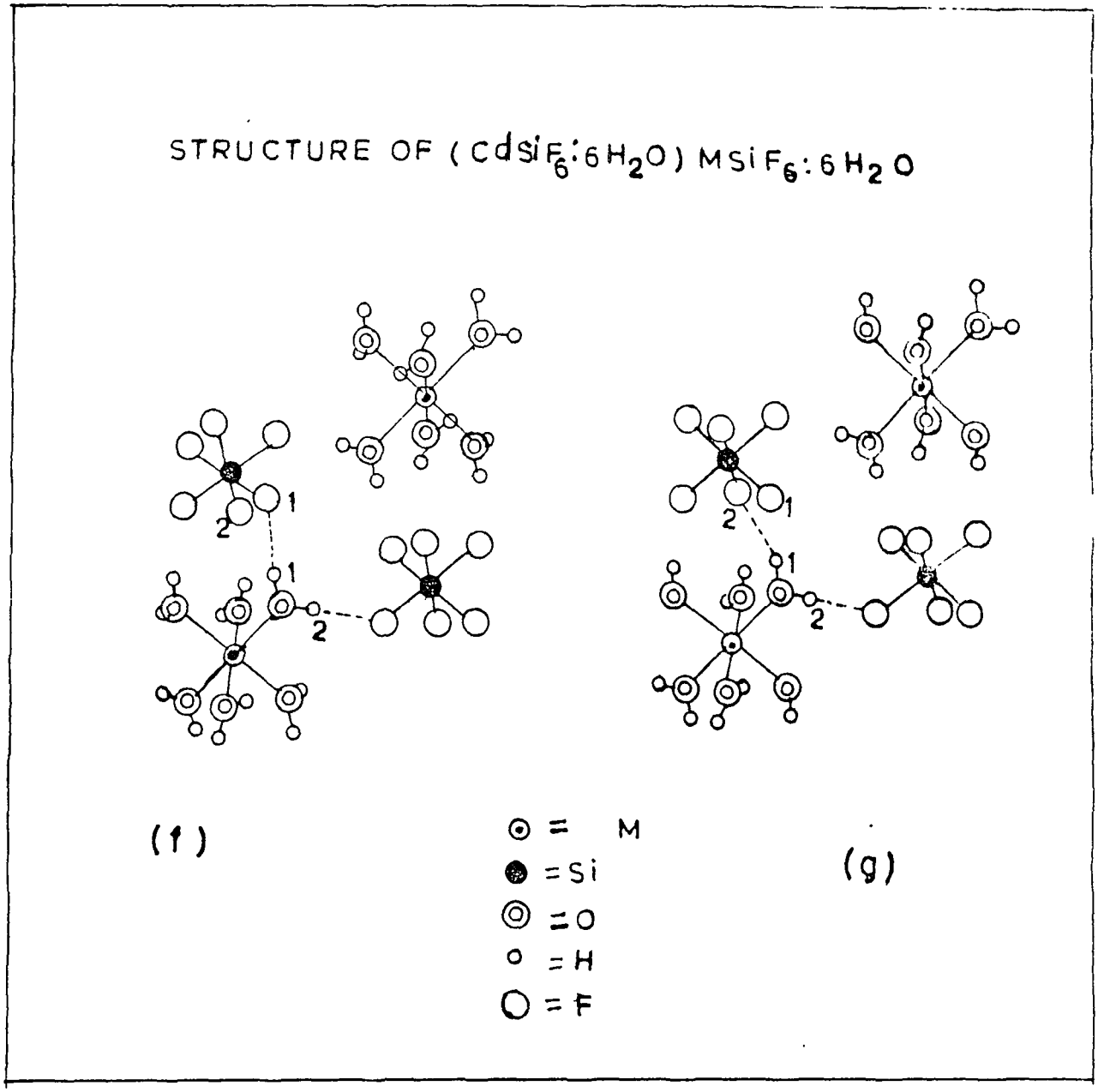

Fig. 3·1

Crystal structure of $CdSiF_6: 6H_2O$ based on C_{3i}^2 Space group -

(f) Structure of the crystal showing hydrogen bond between the two ions $\left[SiF_6\right]^{2-}$ and $\left[Cd(OH_2)_6\right]^{2+}$; O-H...F in 1-1 position

(g) Structure of the crystal showing hydrogen bond in 1-2 position.

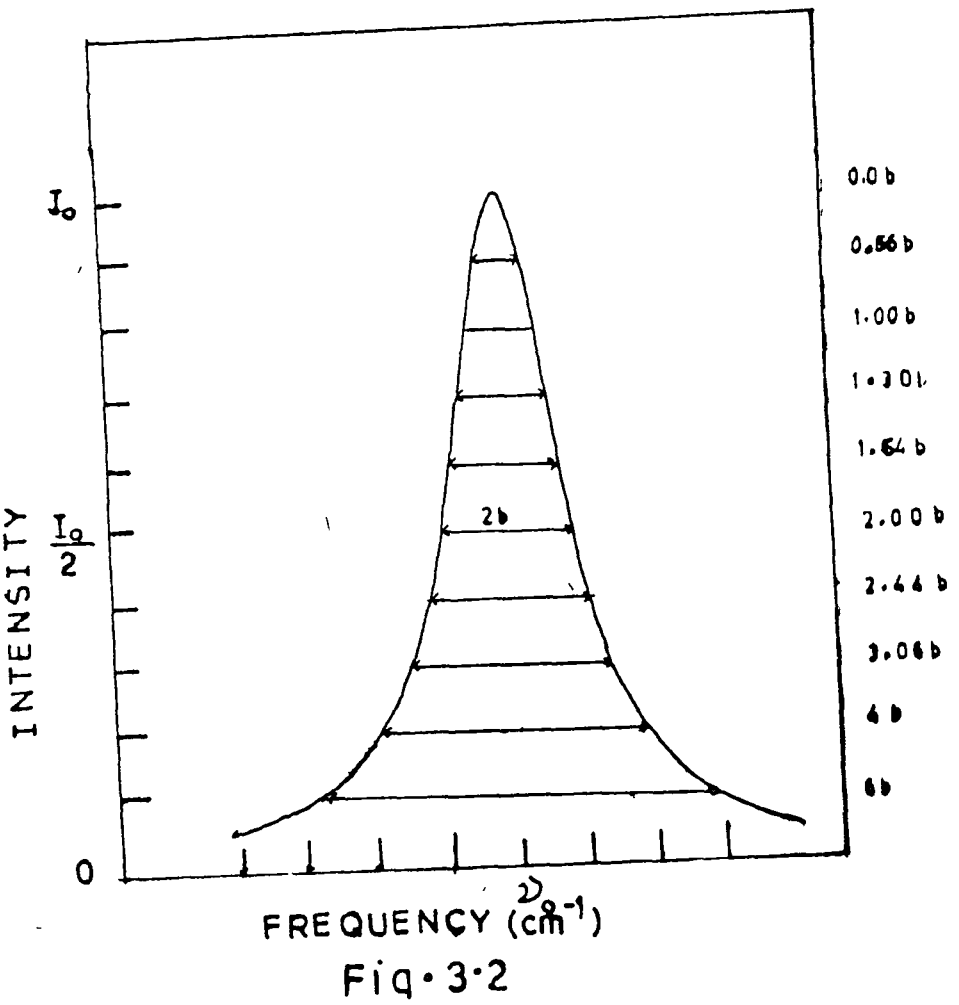

Fig·3·2

Lorentzian shape of the band contour. I_o is peak intensity and '2b' is the FWHM intensity ($\Delta\nu_{1/2}$) The figure shows the relationship between I_o and 'b'.

CHAPTER IV

C H A P T E R IV

Laser Raman Study of Phase Transformation in Single Crystals of Cadmium Fluoro-titanate Hexahydrate (CFTH)

Chapter IV

Laser Raman Study of Phase Transformation in Single Crystals of Cadmium Fluoro-titanate Hexahydrate ($CdTiF_6:6H_2O$)*

4.1 Abstract

A detailed temperature dependent Raman study of oriented single crystals of $CdTiF_6:6H_2O$ down to the temperature of 10k was carried out in the regions of internal vibrations and lattice modes. The line width, frequency shift and intensities of the modes associated with the $[Cd(H_2O)_6]^{2+}$ and $[TiF_6]^{2-}$ octahedra show abrupt changes at temperatures around 200 and 80k respectively, and many doubly degenerate modes split into two components. These studies suggest that this system undergoes two structural phase transitions at 200 and 80k. A mechanism for these phase transitions is suggested.

4.2 Introduction

As stated in the synopsis of this work, during the last few years there has been considerable interest in the study of metal hexahydrate complexes containing the anions $[XF_6]^{2-}$ and cations $[M(OH_2)_6]^{2+}$. Some members of the series of general formula $MXF_6:6H_2O$ where M = divalent metal ions and X = Si or Ti are known to undergo structural phase transitions from their room temperature space group C_{3i}^2 ($R\bar{3}$) to the space group C_{2h}^5 ($P2_1/C$) at low temperature. The metal hexahydrate complexes having X = Si and M =

---

* Paper based on this chapter has been published:
Thakur G and Verma A L, J. Raman Spectrosc. 17(2), 207 (1986).

Mg, Mn, Fe and Co are known to undergo structural phase transitions at 298, 230, 240 and 246k respectively, whereas the complexes having X = Si and M = Zn and Ni do not undergo any phase transition upto temperatures of 10k [1]. Moreover, the complex with X = Ti and M = Zn undergoes two successive phase transitions at 217 and 182k, whereas the complex with X = Ti and M = Co shows only one phase transition at 244 ± 2k [2,3]. We could not find any report on the vibrational studies of $CdTiF_6:6H_2O$ except an EPR study of Petrakovskoya et al in 1984 [3(a)].

It is clear from this brief survey that the dynamics of structural phase transitions in different metal hexahydrate complexes is quite different. Vibrational spectroscopy can play an important role in elucidating the mechanism of structural phase changes in solids and we therefore undertook a systematic study of the Raman spectra of oriented single crystals of $CdTiF_6:_6H_2O$ and $CdSiF_6:6H_2O$ at different temperatures. From a temperature-dependent study of half width, frequency shift and splitting of some bands at different temperatures, we found two structural phase transitions in the $CdTiF_6:6H_2O$ system at 200 and 80k, whereas there is only one phase change in the $CdSiF_6:6H_2O$ system at about 200k. In this chapter we give the results of the experimental studies on CFTH (Cadmium Fluorotitanate hexahydrate $CdSiF_6:6H_2O$).

4.3 Experimental details

As given in section 2.4.2 of Chapter II the single crystals of Cadmium fluoro titanate hexahydrate (hereafter abbreviated as

CFTH) were grown from solution through controlled evaporation by maintaining a slow and constant temperature gradient [4]. The crystals grew in the form of hexagonal pillars elongated along the c-axis.

Taking the c-axis as the z-axis and the line passing through the two opposite edges of the hexagonal as the y-axis, the crystals were cut in rectangular cross-sections making the y- and x-axes perpendicular to the adjacent faces of the rectangular cross-section [5]. Fig. 4.1 illustrates the cross-section for cutting the crystals.

The crystal was cut by rubbing the edges on a filter paper (Whatman No. 40) which was made wet with few drops of triply distilled water. After cutting, the crystals were polished on a dry filter paper (Whatman No. 40) and then on a 'Rayon' cloth.

For low temperature measurements, where the crystals have to be mounted on a cold-finger in a vacuum chamber, the crystals were rubbed on a paper slightly soaked with mineral oil (white oil), to prevent surface dehydration of the crystals during experiments.

The Raman spectra of the crystals were measured in all the six orientations, the details of which have been given in Chapter II sections 2.6.1 to 2.6.4.

The Raman spectra were excited by linearly polarized 514.5 and 488.0 nm radiation from a Spectra-Physics Model 165 Argon-Ion laser. The laser power at the sample was approximately 200 mW.

A SPEX Laser-mate was employed to remove plasma lines. The scattered light in the 90° scattering geometry was analysed with a SPEX Ramalog triple monochromator equipped with a cooled photomultiplier tube and a SPEX Datamate photon counting arrangement. The spectra in different geometries were recorded with a resolution varying between 2 and 4 cm^{-1}. The low-temperature spectra were measured down to *10k. The low temperature was achieved with the help of an Air-* Products closed-cycle helium cryo-cooler, the details of which have already been mentioned in Chapter II.

4.4 Theoretical analysis and crystal structure

The theoretical analysis in detail has been given in Chapter III. However, here we give only the correlation diagram for C_{3i}-O_h-D_{3d} and C_{3i}-T_h (Fig. 4.2) and the total number of Raman bands expected in the spectra. One excepts 12 A_g and 12 E_g = 12 + 24 = 36 modes. If E_g irreducible representation is counted as giving one band, the total number of Raman bands expected is 24.

Again for a crystal belonging to the space-group D^5_{3d}, the Raman active bands would be of species - 5 A_{1g} + 12 E_g = 5 + 24 = 29. If the E_g is taken to contribute one band the total bands will be 17. Experimentally it is difficult to observe all the modes in the Raman spectra [6-8].

4.5 Results and discussion

It is expected that when the CFTH system belongs to the space group C^2_{3i}, one should observe 16 Raman active modes for the

$[Cd(OH_2)_6]^{2+}$ ion and 4 Raman modes for the $[TiF_6]^{2-}$ ion in the internal vibration region of the ions. When the space group is D^5_{3d}, the number of internal vibrational modes expected in Raman scattering for the above ions are 11 and 4 respectively. Here doubly degenerate modes are counted as one mode.

As will be explained subsequently, the similarity of the Raman spectra of CFTH with that of $ZnTiF_6:6H_2O$ and polarization measurements on single crystals in different geometries make it clear that the CFTH system can exist in the space group C^2_{3i} only at room temperature as D_{3d} is not a sub-group of the free molecular ion group T_h of the $[Cd(OH_2)_6]^{2+}$ ion.

4.5.1 Room temperature spectra

Representation spectra of single crystals of CFTH at room temperature in four geometries are shown in Figs. 4.3 and 4.4 with the polarization of the incident and scattered radiations given in Porto's notation with the z-direction parallel to the c-axis of the crystal. Under the space group C^2_{3i} the A_g and E_g components of the vibration are expected to be present in all the orientations except that the E_g components should not be observed in the $\{x(zz)y\}$ orientation as the polarization tensors for the C^2_{3i} space group are:-

$$\begin{pmatrix} a & o & o \\ o & a & o \\ o & o & b \end{pmatrix} \qquad \begin{pmatrix} c & d & e \\ d & -c & f \\ e & f & o \end{pmatrix} \qquad \begin{pmatrix} d & -c & -f \\ -c & -d & e \\ -f & e & o \end{pmatrix}$$

A_g E_g E_g

We measured the polarization behaviour of Raman bands in different orientations of single crystals of CFTH and found it to be consistent with the C_{3i}^2 space group for this system. Moreover, the room temperature Raman spectra of single crystals of CFTH in different orientations resemble very closely to those of $ZnTiF_6:6H_2O$ measured under the same experimental conditions in our laboratory. The spectra observed by us for the $ZnTiF_6:6H_2O$ system are the same as reported by Chaudhury et al [9].

One would expect 4 Raman bands in the lattice mode region out of which 2 modes are of A_g species and 2 are of E_g species under the C_{3i}^2 space group, but only two lattice modes ($2E_g$) would be allowed under the D_{3d} space group. We have observed at least four distinct Raman bands in the lattice mode region, and thus supporting the C_{3i}^2 space group for the CFTH system.

The frequencies of the Raman bands in different polarizations for the single crystal of CFTH are given in Table 4.1 together with the assignment of the bands. The spectral correlations are based on group theoretical predictions, group frequencies and available assignments in the literature for similar systems [10].

At room temperature (RT) in the lattice mode region we obtained 4 Raman bands in the $\{y(xx)z\}$ and $\{x(yy)z\}$ orientations of the crystal. All the bands are very weak but distinct in this region with the frequencies at 56, 67, 82 and 125 cm^{-1} in the $\{y(xx)z\}$ orientation and are of A_g+E_g species.

We got only one band in the $\{x(zz)y\}$ orientation at 131 cm^{-1} and this band is of A_g species.

A clear shoulder at 183 cm^{-1} in the $\{y(xx)z\}$ geometry is the deformation mode δ(O-Cd-O) of the Cd-O bonds which is not observed in other geometries. The bands at 265, 304 and 354 cm^{-1} are associated with the ν_{as}(Cd-O) (asymmetric stretch of Cd-O bond and is of E_g type), δ(F-Ti-F) (A_g + E_g type) and ν_s(Cd-O) modes respectively. The band at 611 cm^{-1} is very strong compared to the other bands in the spectrum. This band arises due to symmetric stretch of Ti and F, ν_s(Ti-F). This band belongs to the A_g species but it appears in the $\{y(zy)z\}$ geometry also due to polarization leakage, as its intensity in this geometry is very low, where as in the $\{x(zz)y\}$ geometry it is very strong.

The bands arising from the water stretching modes are very broad and appears at 3477 cm^{-1} (peak) in the $\{y(xx)z\}$ orientation but in other orientations, $\{x(yy)z\}$ and $\{x(zz)y\}$, they appear at 3480 cm^{-1} and 3485 cm^{-1} respectively. At RT the bands due to the ν_1 and ν_3 modes of water are superimposed to give a single broad band centred at around 3480 cm^{-1} for CFTH.

The assignments suggested by different authors for the systems $ZnTiF_6:6H_2O$, $NiTiF_6:6H_2O$ and $MnTiF_6:6H_2O$ are compared with our assignment for the CFTH system, as shown in Table 4.2.

4.5.2 Low temperature spectra

In an attempt to resolve the closely spaced lines, we recorded the Raman spectra of a single crystal of CFTH at 10k and found that the spectra showed a complicated structure. The Table 4.3 shows the Raman bands in 4 selected orientations of the crystal at 10k. Therefore, we undertook a systematic temperature-dependent study of the Raman spectra of CFTH from room temperature to 10k at intervals of 10-20k. The spectral data are shown in Table 4.4. The main features of the temperature evolution of the Raman spectra of CFTH are summerized as follows:-

1. Most of the bands became sharp and many shoulders and unresolved components appeared as distinct features with decreasing temperature.
2. The frequency shifts, half-widths and intensities of some bands showed anomalous and sudden changes at temperatures around 210 and 80k.
3. Several modes of E_g species in the internal vibration and lattice mode regions split into two components around 210 and 80k.
4. The broad band associated with the (O-H) stretching modes at RT splits into six sharp components at 10k.

These observations strongly suggest that the system undergoes two successive structural phase transitions around 200 and 80k. We shall return later to the nature and mechanism of these phase transitions, but let us first elaborate on the temperature variation of the Raman spectra.

Fig. 4.5 shows the Raman spectra of a_k single crystal of CFTH in the $\{x(yy)z\}$ geometry at a few selected temperatures. The frequencies of the vibrational modes at different temperatures are given in Table 4.4. The Raman spectra in different geometries at 10k are shown in Fig. 4.6. The deformation mode δ(O-Cd-O) associated with the $\left[Cd(OH_2)_6\right]^{2+}$ ion is found at 176 cm^{-1} in the room temperature spectrum consisting of $A_g + E_g$ components. Around 200k, the bands become sharper and appear at 176 cm^{-1} (A_g) and 180 cm^{-1} (E_g).

At 200k, the E_g component at 180 cm^{-1} splits into two bands at 185 cm^{-1} and 199 cm^{-1} but the A_g component remains at 176 cm^{-1}. Similarly, the lattice mode of E_g symmetry associated with the libration of the $\left[Cd(OH_2)_6\right]^{2+}$ ion at 83 cm^{-1} splits into two components at 84 and 90 cm^{-1} at 200k. The vibrational modes associated with the $\left[TiF_6\right]^{2-}$ ion do not show any splitting or anomalous behaviour in this temperature range.

When the temperature is reduced further, many bands associated with the $\left[TiF_6\right]^{2-}$ ion either show abrupt changes in frequency, half-width and intensity around 80k, or some degenerate modes split into two components. The 300 cm^{-1} room temperature band associated with the δ(F-Ti-F) mode having $(A_g + E_g)$ symmetries split into three components at 301 (A_g), 284 and 310 cm^{-1} at 80k. The ν_s(Ti-F) stretching mode at 612 cm^{-1} shifts abruptly to 605 cm^{-1} at 80k. The half-widths and intensities of many vibrational bands show

anomalous behaviour in this temperature range. Figs. 4.7 - 4.11 show frequency shift (splittings), full-width at half-maximum (FWHM) and intensity variations as a function of temperature for some selected and isolated bands in the Raman spectra of single crystals of CFTH.

4.5.3 Structural phase transformations

From the above described temperature dependent Raman studies on oriented single crystals of CFTH, we have discovered two structural phase transformations in this system at 200 and 80k. The higher temperature transition is triggered by distortions in the geometry of the $[Cd(OH_2)_6]^{2+}$ ions as most of the bands associated with this ion show either splittings of the modes of E_g symmetry or anomalous behaviour of half-width, etc. There is no such sudden change in the vibrational modes associated with the $[TiF_6]^{2-}$ ion and therefore it retains its octahedral symmetry in this temperature range.

As the temperature is reduced further, the vibrational modes of E_g species associated with the $[TiF_6]^{2-}$ ion show splittings into two components. The frequencies, half-widths and intensities of most of the bands associated with the $[TiF_6]^{2-}$ ion change abruptly and show anomalous behaviour around 80k. Before 80k, there are gradual and minor changes in the band positions and half-widths. These changes indicate that there is a distortion in the geometry of the $[TiF_6]^{2-}$ ion around 80k and the space group of the system changes to a lower symmetry in which there are no degenerate vibrational species.

Both of these transitions appear to be first order, characterised by abrupt changes in frequency shifts, FWHM and intensities of some of the bands at the phase transition temperatures.

Without any structural information available on this system, it is not possible to say much about the low-temperature space group of this system in the temperature regions around 200 and below 80k.

There are at least eight components observed in the lattice mode region around 10k and all the doubly degenerate modes split into two components. These similarities with the low-temperature Raman spectra of $MgSiF_6:6H_2O$ indicate that the lowest temperature space group of CFTH crystal may also be C_{2h}^5 $(P_{2\ 1/C})$ in the monoclinic series [10].

It appears that, as the system is cooled from room temperature, the lattice contracts and around 200k the water molecules lose their reorientational freedom to some extent resulting in distortion of the $[Cd(OH_2)_6]^{2+}$ octahedra. The lattice dimensions and crystalline field in this temperature range are such that they do not distort the $[TiF_6]^{2-}$ octahedra.

As the temperature is further reduced, the lattice further contracts and a situation arises when around 80k the Ti^{4+} ion does not fit into the octahedra of the $6F^-$ ions. Therefore, this octahedron distorts and triggers another phase transformation at 80k [11].

This mechanism of the phase transitions in this system is consistent with our Raman studies on single crystals of $CdSiF_6:6H_2O$ where we have discovered only one phase transition due to distortions in the $[Cd(OH_2)_6]^{2+}$ octahedra around 220k [12-13]

The details of the study on $CdSiF_6:6H_2O$ are given in Chapter V.

4.6 References

[1] Poulet H and Mathieu J, C R Acad. Sci. Ser. B286, 331 (1978).

[2] Choudhury P, Paul B, Saha S and Ghose B, Proc. of Nucl. Phys. and Solid State Phys. Symp. Vol. 24C, pp 323, Dec. 28 (1981), BARC, Bombay.

[3] Bose M, Roy K and Ghoshray A, Proc. of Nucl. Phys. and Solid State Phys. Symp. Vol. 24C pp. 389, Dec. 28 (1981), BARC, Bombay.

[3a] Petrakovskaya E A, Abakumova V S, Kocharova A G, Yad. Magn. Rezon. Strukt. Krist. (Russ.) pp. 116 (1984) Ed. by E P Zeer. Chem. Abs. 103 (26) Abs No. 226032u (1985).

[4] Thakur G, Proc. of Symp. on Crystal Growth, Dec 24 (1983) Anna University, Madras.

[5] Patel M B, Agarwal A and Bist H D, J. Raman Spectrosc. 14, 406 (1983).

[6] Wyckoff R W G, "Crystal Structure" Vol. 3, 2nd ed., Wiley Interscience, New York (1965).

[7] Hamilton W C, Acta Crystallogr., 15, 353 (1962).

[8] Lewis J and Jenkins T E, J. Raman Spectrosc. 8, 111 (1979).

[9] Choudhury P, Ghosh B, Raghuvanshi G S and Bist H D, J. Raman Spectrosc. 14, 99 (1983).

[10] Jenkins T E and Lewis J, Spectrochimica Acta 37A, 47 (1981).

[11] How T and Svare I, Phys. Script. 9, 40 (1974).

[12] Thakur G and Verma A L in Proc. of DAE Solid State Phys. Symp. Vol. 27C, pp. 282 Dec 23 (1984), BARC, Bombay.

[13] Thakur G and Verma A L, J. Raman Spectrosc. 17, 207 (1986).

Table 4·1

Raman spectral data at room temperature of $CdTiF_6 \cdot 6H_2O$[a]

Raman bands (cm^{-1}) observed in different polarizations								Assignments
$(y(xx)z)$		$(y(zy)z)$		$(x(yy)z)$		$(x(zz)y)$		
56	VVW	—		55	VVW	—		Lattice modes
67	VVW	66	VVW	67	VVW	—		
82	VW	84	VVW	83	S	—		
125	VVW	134	VVW	131	VVW	131	VVW	
172	VVW	—		172	VVW	172	VVW	restricted H_2O trans., A_g
176	M	180	VW	176	M	178	VVW	δ(O–Cd–O), $A_g + E_g$
183	(sh)			—		—		
265	S	261	W	261	M	—		ν_{as} (Cd–O), E_g
						275	(sh)	δ(F–Ti–F), $A_g + E_g$
304	M	293	W	300	S	305	S	
354	M	—	W	354	W	354	VW	ν_s (Cd–O), A_g
				453	VVW	—		ν_{as} (Ti–F), E_g
611	VS	611	M	613	VS	614	VS	ν_s (Ti–F), A_g
3477	S	—		3480	S	3485	S	ν_w (H–O)

[a] VVW = very very weak, VW = very weak, W = weak, M = medium, S = strong, VS = very strong

Table 4·2

Assignments of Raman bands for $MTiF_6 \cdot 6H_2O$ (where M = Cd, Mn, Zn, Ni) by different authors

Our observation, Cd	Observation of Chaudhury *et al*[9]		Observation of Jenkins *et al*[10]		Assignments of bands		
	Mn	Zn	Zn	Ni	By Chaudhury *et al*[9]	By Jenkins *et al*[10]	By present authors
56				15			
67				35	Lattice modes	Lattice modes	Lattice modes
82			82	87			
121			112	118			
172	180	202	—	—	Restricted	—	Restricted
					H_2O trans	—	H_2O trans
176	—	—	—	—	—	—	δ(M–O), $A_g + E_g$
261	260	260	—	—	ν_{as}(M–O)	—	ν_{as}(M–O), E_g
275, 300	300	304	262, 300	272	δ(Ti–F)	δ(Ti–F)	δ(Ti–F), $A_g + E_g$
	—			306	—	ν_{as}(M–O), E_g	—
354	—	380	385	402	ν_s(M–O)	ν_s(M–O)	ν_s(M–O), A_g
453	—	452	—	450	ν_{as}(Ti–F), E_g	ν_{as}(Ti–F), E_g	ν_{as}(Ti–F), E_g
613	600	612	610	613	ν_s(Ti–F), A_g	ν_s(Ti–F), A_g	ν_s(Ti–F), A_g
3480	3480	3480	3480	3481	ν_w(H–O), $A_g + E_g$	ν_w(H–O)	ν_w(H–O)

δ (Ti-F) and δ (M-O) mean δ (F-Ti-F) and δ (O-M-O) respectively

Table 4·3

Raman spectral data at 10 K for $CdTiF_6 \cdot 6H_2O$[a]

Raman bands (cm^{-1}) observed in different polarizations								
{y(xx)z}		{y(zy)z}		{x(yy)z}		{x(zz)y}		Assignments
58	VVW	58	VVW	56	VVW			
68	VW	—		67	VVW	—		
80	VVW	80	VVW	80	VW	—		
98	M	97	VW	95	M	95	VW	Lattice modes
113	W	112	VVW	114	VVW	114	VW	
121	VW	—		121	VW	—		
—		—		131	VVW	131	VVW	
171	VW	172	VW	171	W	172	M	Restricted H_2O trans
182	M	181	W	181	M	183	M	
192	sh	—		190	W	200	VVW	δ(O–Cd–O)
215	VVW	—		—		211	VW	
254	M	254	W	254	S	255	W	ν_{as}(Cd–O)
266	M	268	W	268	S	269	VVW	
285	W	286	W	285	S	286	VW	
300	M	301	W	300	S	299	S	δ(F–Ti–F)
313	W	314	M	314	M	318	VW	
365	M	364	W	363	S	362	W	ν_s(Cd–O)
389	VVW	—		—		381	VW	
418	VW	—		419	W	—		ν_{as}(Ti–F)
454	VW	—		—		—		
604	VS	603	W	603	S	604	S	ν_s(Ti–F)
—		—		—		3429	VVW	
3446	S	3444	W	3446	S	3446	VW	
3452	S	3451	W	3451	S	3451	W	ν_3 (H–O)*
3461	W	3461	W	3461	W	3462	M	
3488	sh	3487	VW	3486	VW	3487	M	
3503	VS	3497	M	3497	VS	3497	VS	
3506	sh	—		3506	sh	—		
3530	M	3529	W	3529	M	3530	W	

[a] Abbreviations as in Table 4.1

ν_1 and ν_3 modes of H_2O

Table 4·4

Raman spectral data at different temperatures in the $\{x(yy)z\}$ geometry of single crystals of $CdTiF_6 \cdot 6H_2O$[a]

Temperature (K)										
260	220	210	200	180	130	90	80	70	10	Assignments
48 VVW	—	—	—	—	48	—	—	—	—	
58 VVW	57	—	55	—	—	—	—	—	56 VVW	Lattice modes
67 VVW	67	67	67	66	67	68	68	67	67 VVW	
83 M	83	84	84	83	79	80	80	80	80 VW	
—	—	—	90	91	89	89	93	94	95 M	
—	—	—	—	—	—	—	—	116	114 VVW	
—	—	—	—	—	—	—	—	—	121 VW	
130 VVW	131	131	130	131	131	131	—	—	131 VVW	
168 VVW	170	165	165	168	170	170	168	169	171 W	Restricted H_2O trans
179 W	176	178	177	178	178	178	177	178	181 M	δ(Cd–O)
—	180	181	185	183	187	185	186	188	190 W	
—	—	196	199	198	200	199	201	200	—	
						—	253	254	254 S	ν_{as}(Cd–O)
259 M	259	261	262	262	259	259	265	267	268 S	
						—	284	284	285 S	δ(Ti–F)
300 M	301	302	302	302	302	302	301	301	300 S	
						—	310	311	313 M	
356 W	357	357	359	359	358	358	360	362	363 S	ν_s(Cd–O)
—	—	—	—	—	—	—	—	—	419 W	ν_{as}(Ti–F)
	—						610			
612 V	612	612	612	611	611	612	605	604	603 S	ν_s(Ti–F)

[a] Abbreviations in Table 4.1.

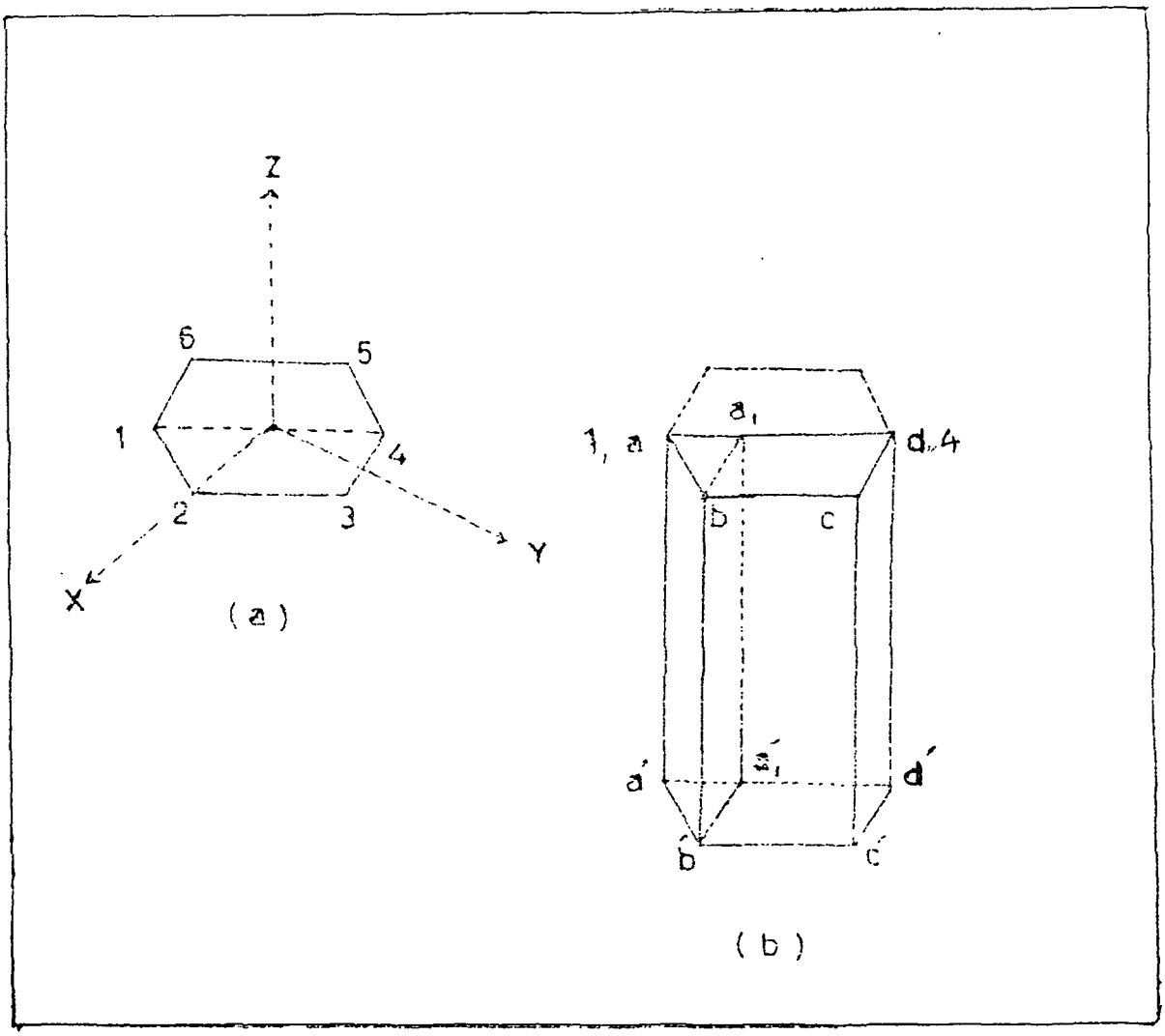

Fig. 4.1

Section of hexagonal pillar of CFTH ($CdTiF_6:6H_2O$) crystal. z-axis is perpendicular to the plane of the paper. After cutting the crystal it becomes a parallelopiped whose diagonal is a_1 c'.

Correlation diagram

(a) $[M(OH_2)_6]^{2+}$

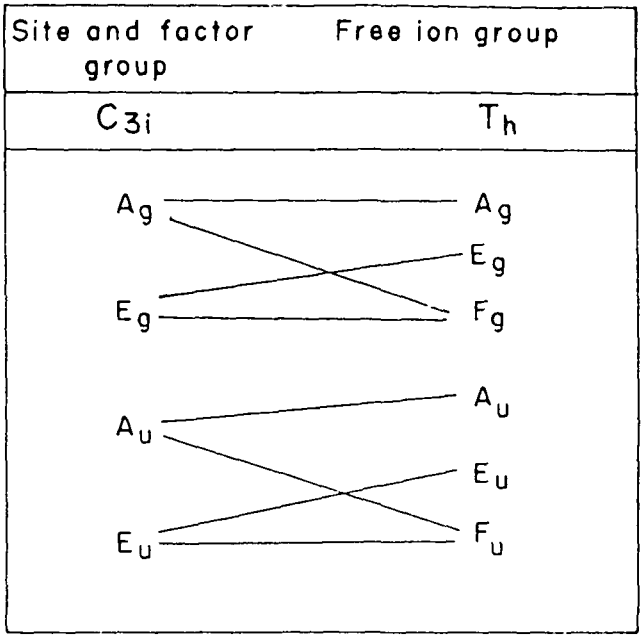

(b) $[XF_6]^{2-}$

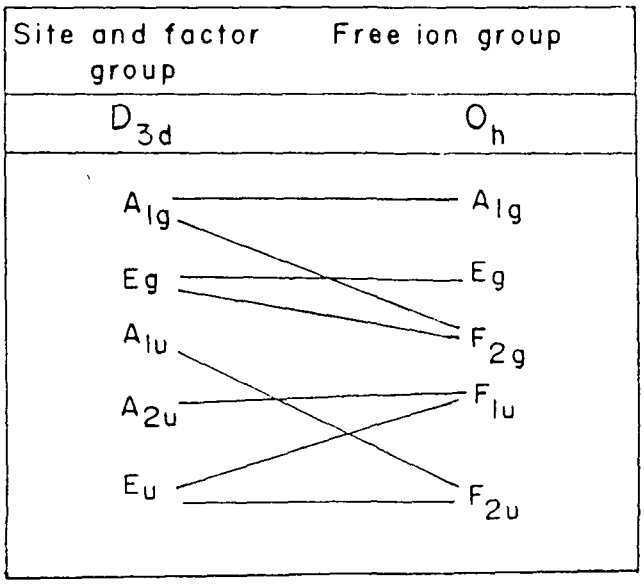

Fig. 4.2

Correlation diagram for C_{3i} - T_h and D_{3d} - O_h groups.

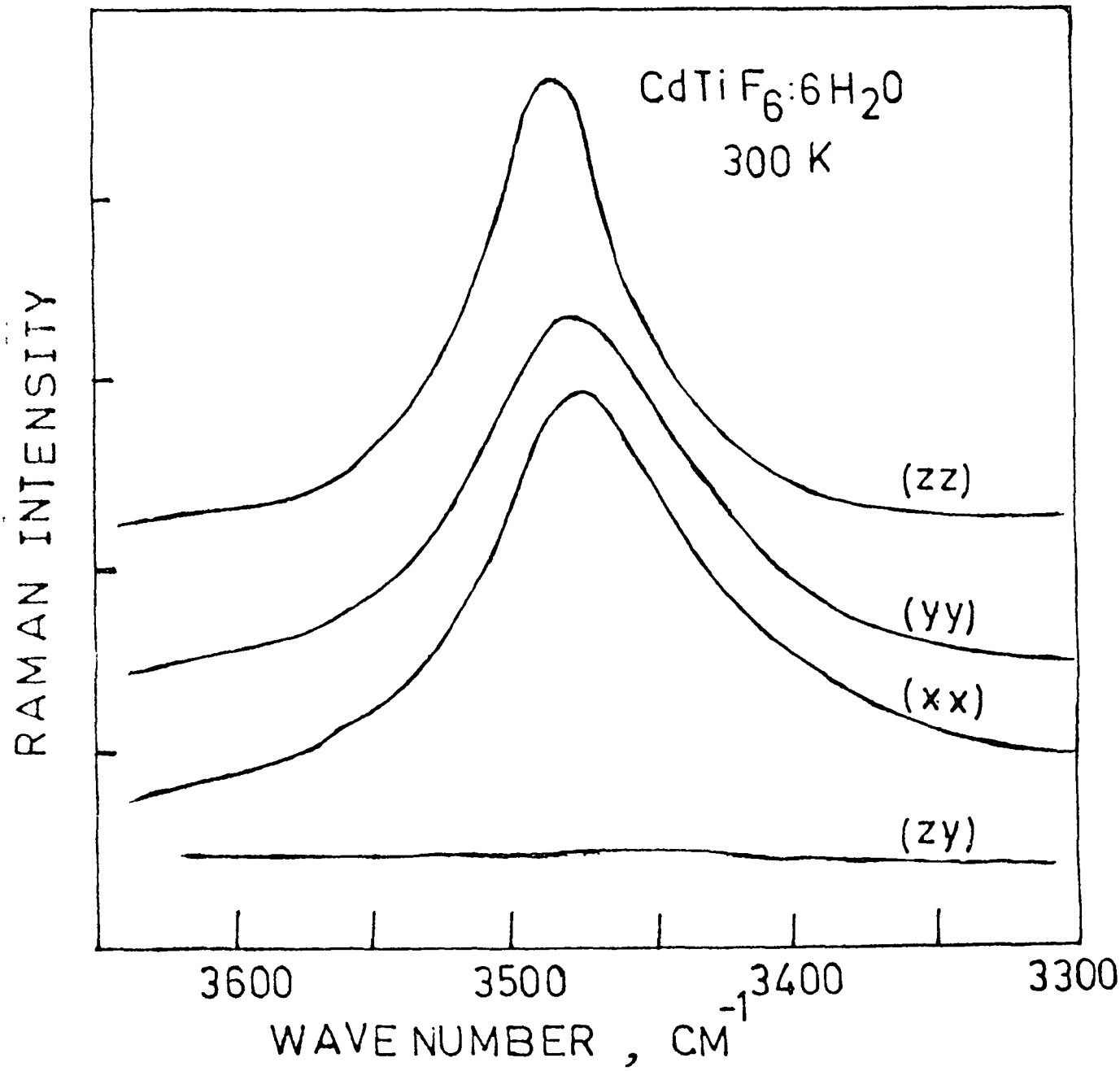

Fig. 4·3

Raman spectra of single crystal of CFTH at room temperature in a few selected polarization geometries in the region 3300 to 3600 cm^{-1}.

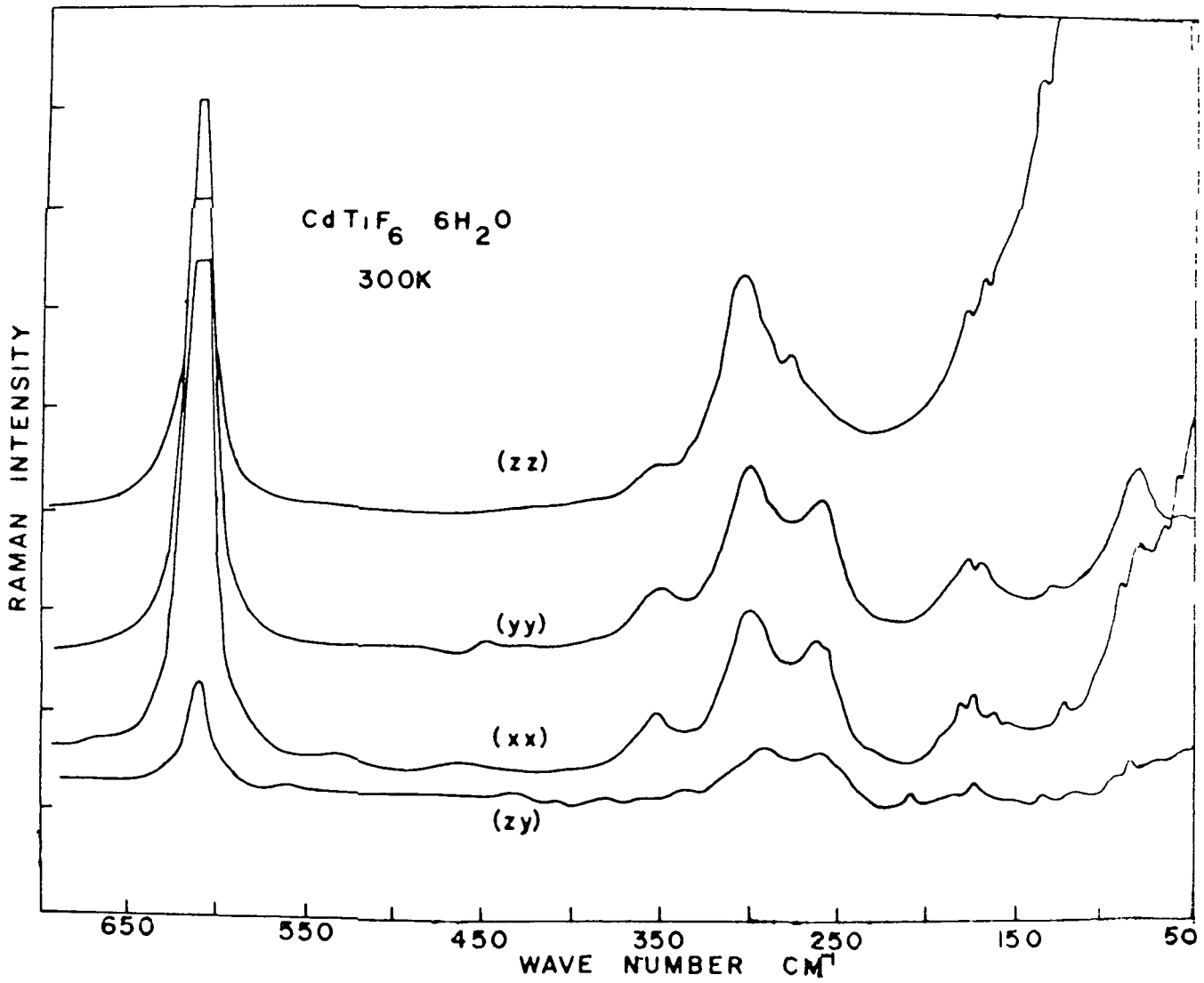

Fig. 4-4

Raman spectra of single crystal of CFTH at room temperature in a few selected polarization geometries in the region 50 to 650 cm^{-1}.

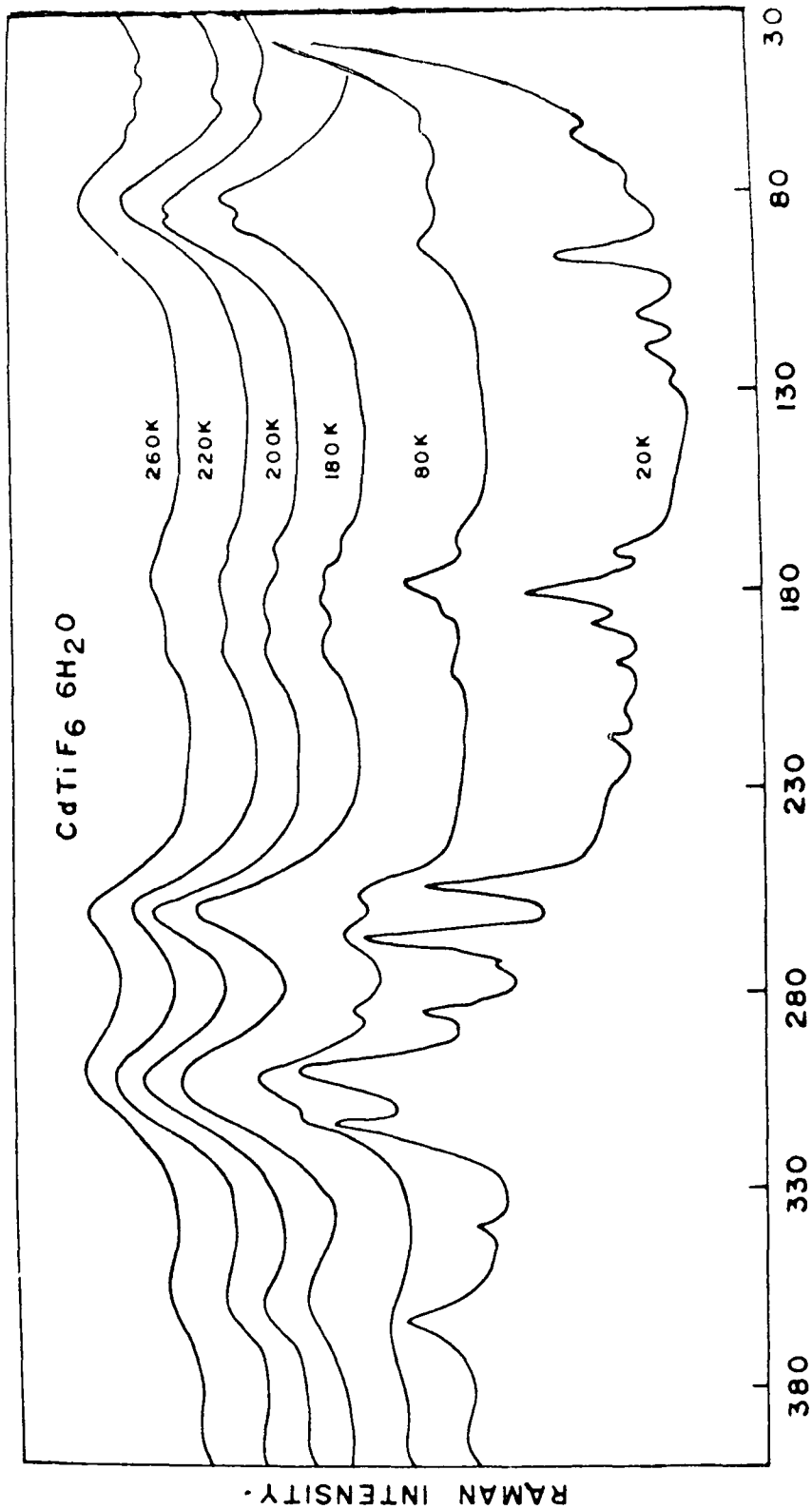

Fig. 4·5(a)

Raman spectra of single crystal of CFTH at different temperatures in the region 30 to 400 cm^{-1}.

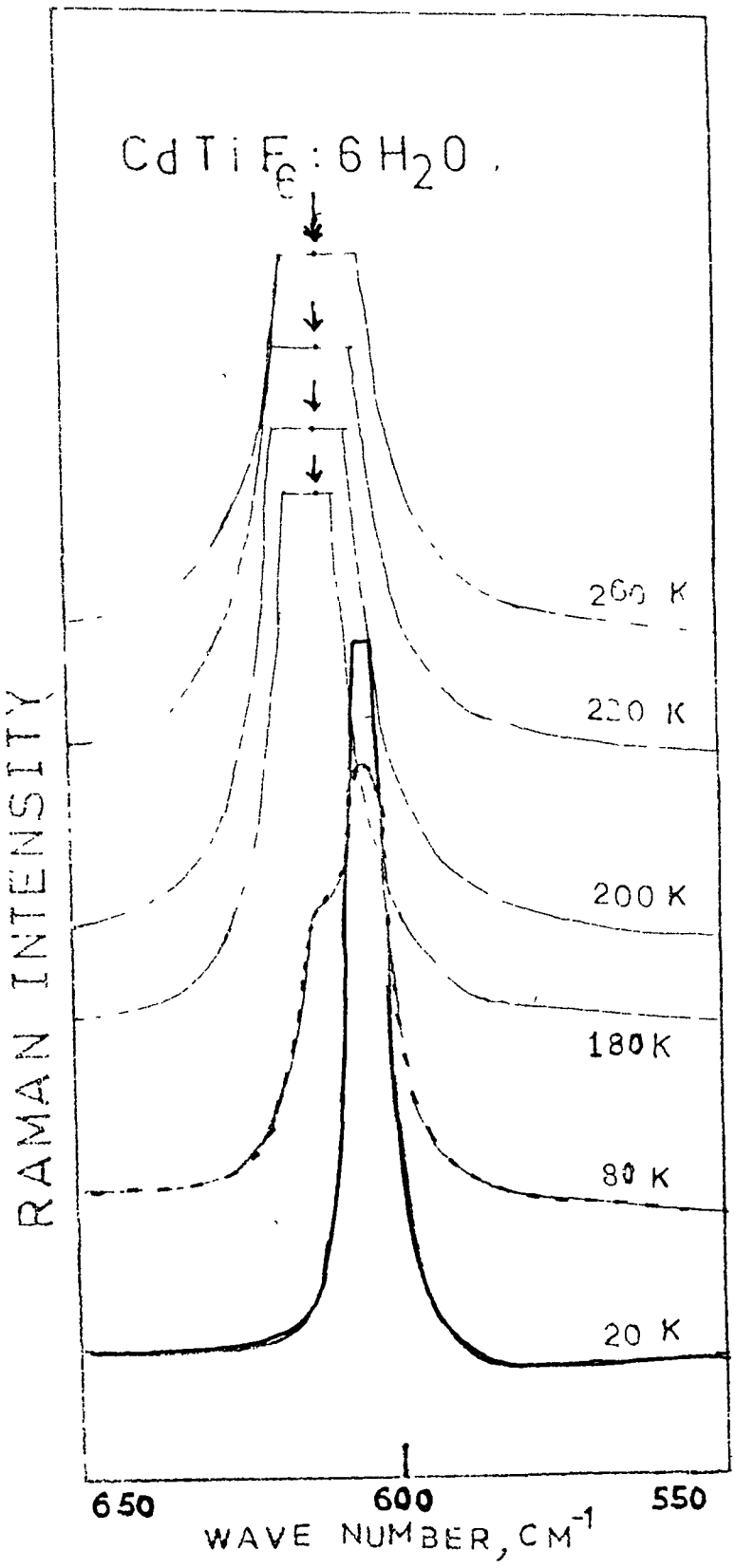

Fig·4·5(b)

Raman spectra of single crystal of CFTH at different temperatures in the region 550 to 650 cm^{-1}. ν_s(Ti–F).

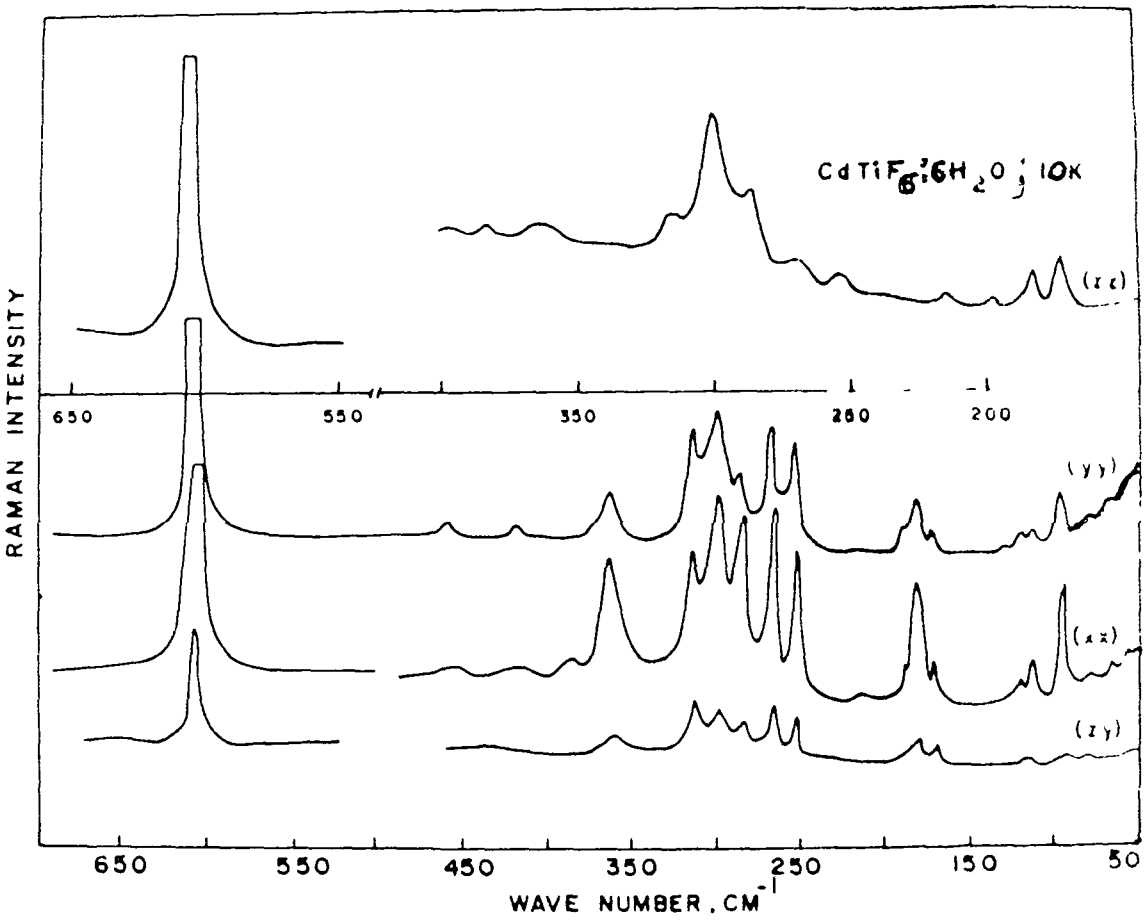

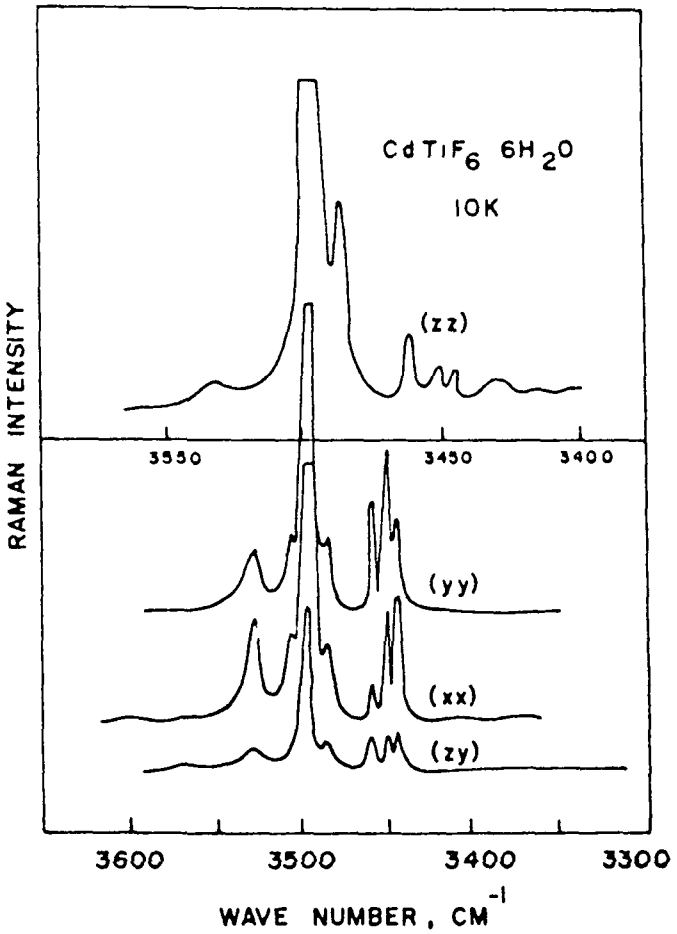

Raman spectra of single crystals of $CdTiF_6$ $6H_2O$ in selected orientations at 10 K (xx), (yy) (zz) and (zy) orientations

Fig. 4.6

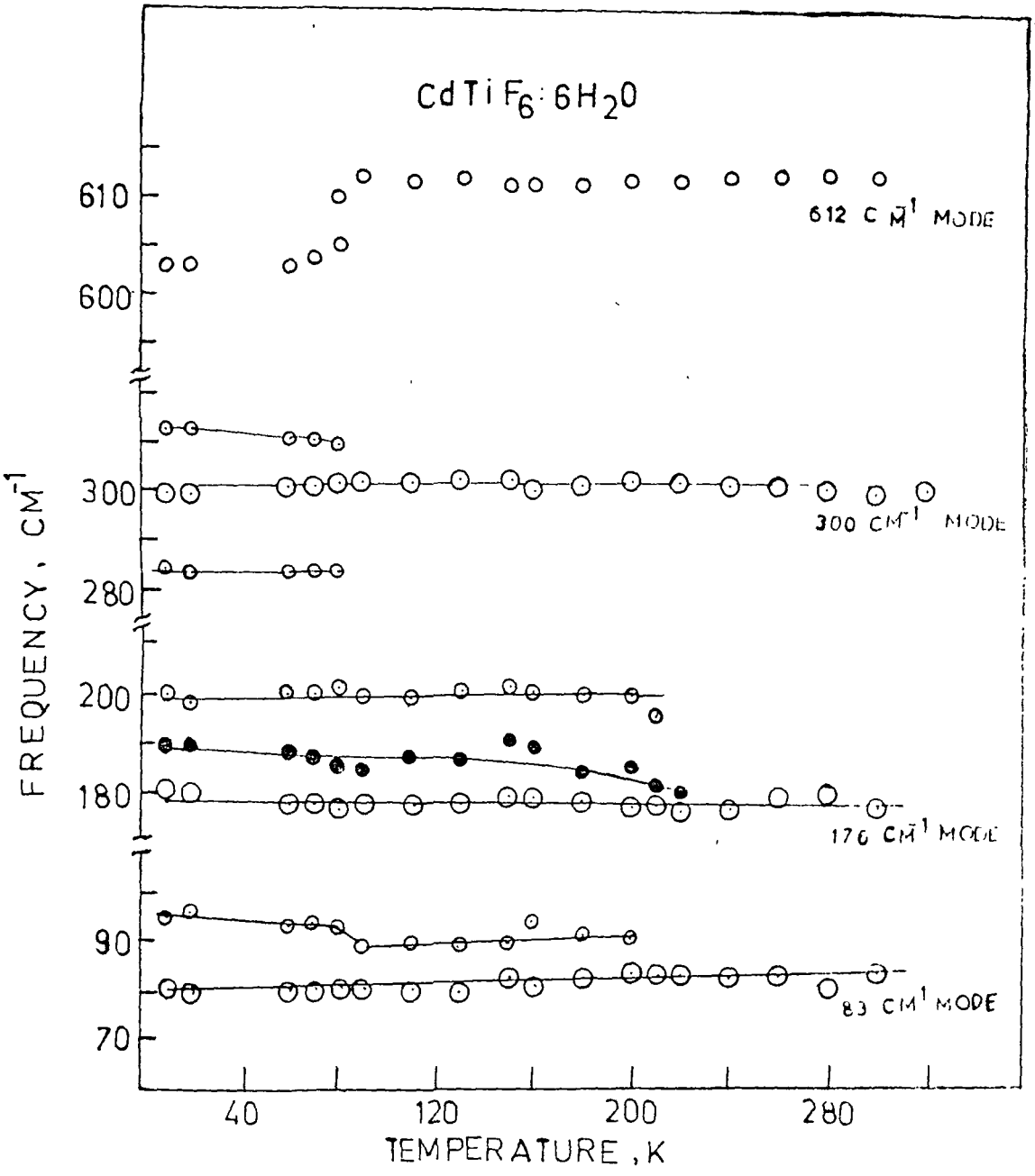

Fig. 4·7

Shift in frequency ($\Delta\delta$) as a function of temperature in case of 83, 176, 300 and 612 cm^{-1} modes of the crystal CFTH

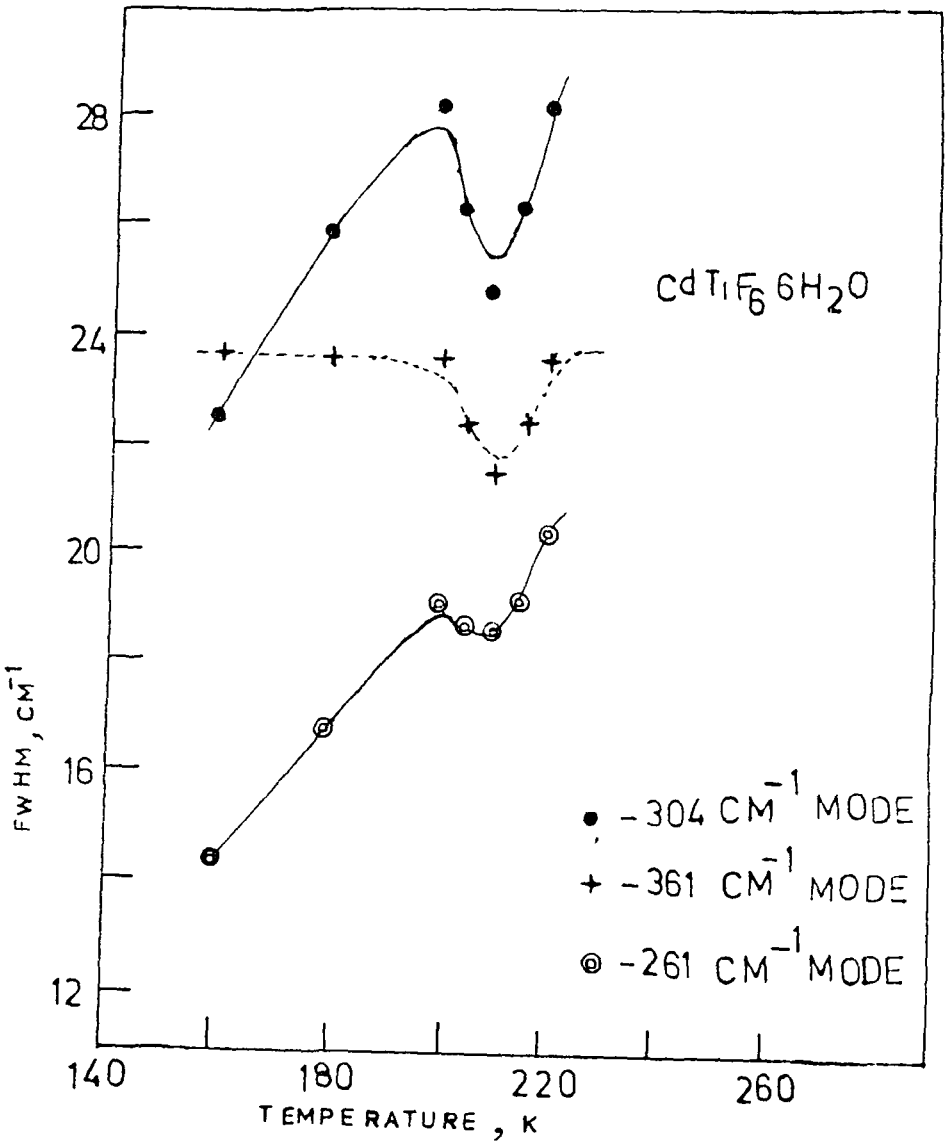

Fig·4·8

The FWHM as a function of temperature of a few isolated bands : 261, 361 and 300 cm^{-1}.

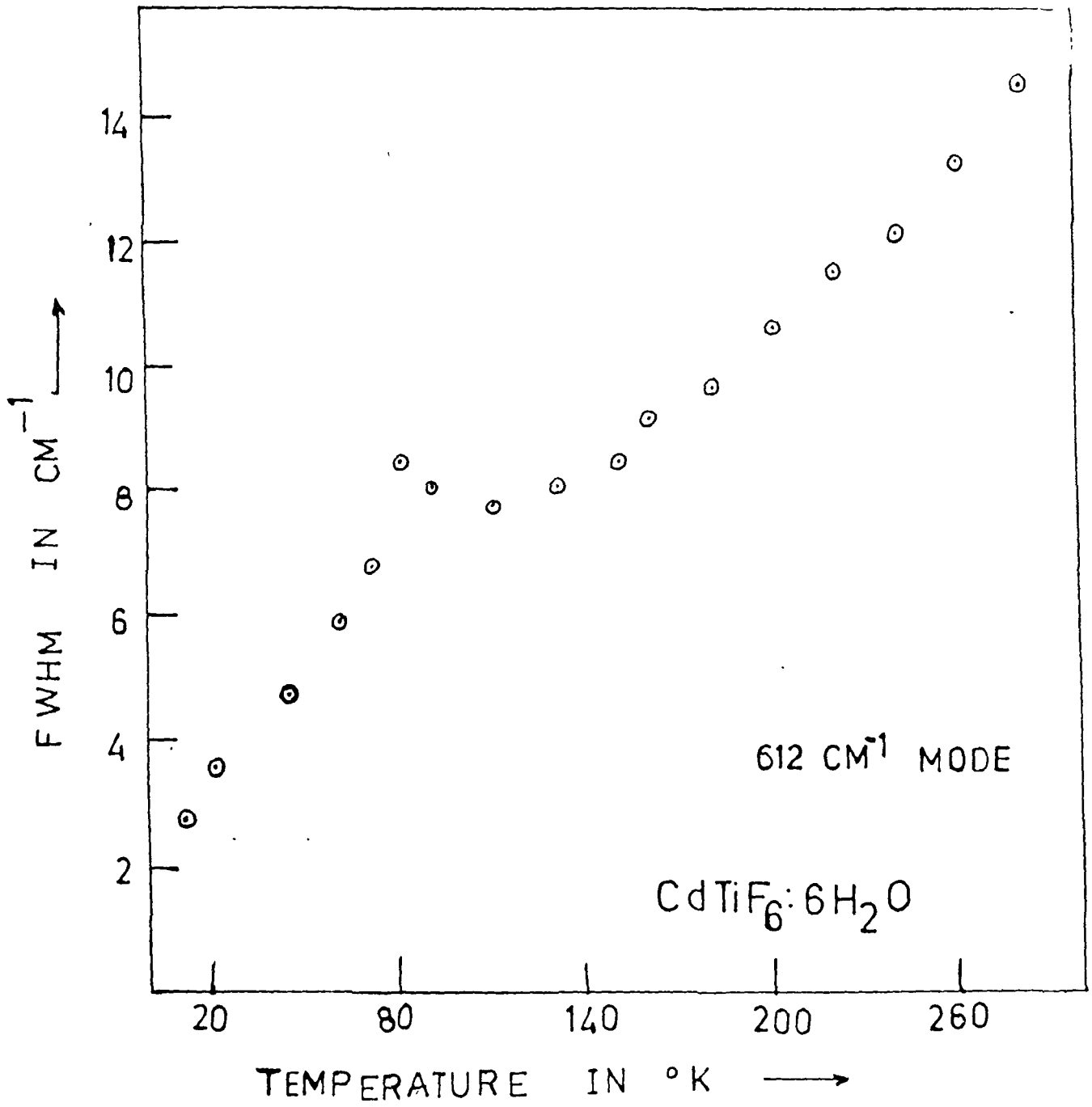

Fig. 4·9

The FWHM as a function of temperature of 612 cm^{-1}, ν_s(Ti-F) mode of the crystal CFTH.

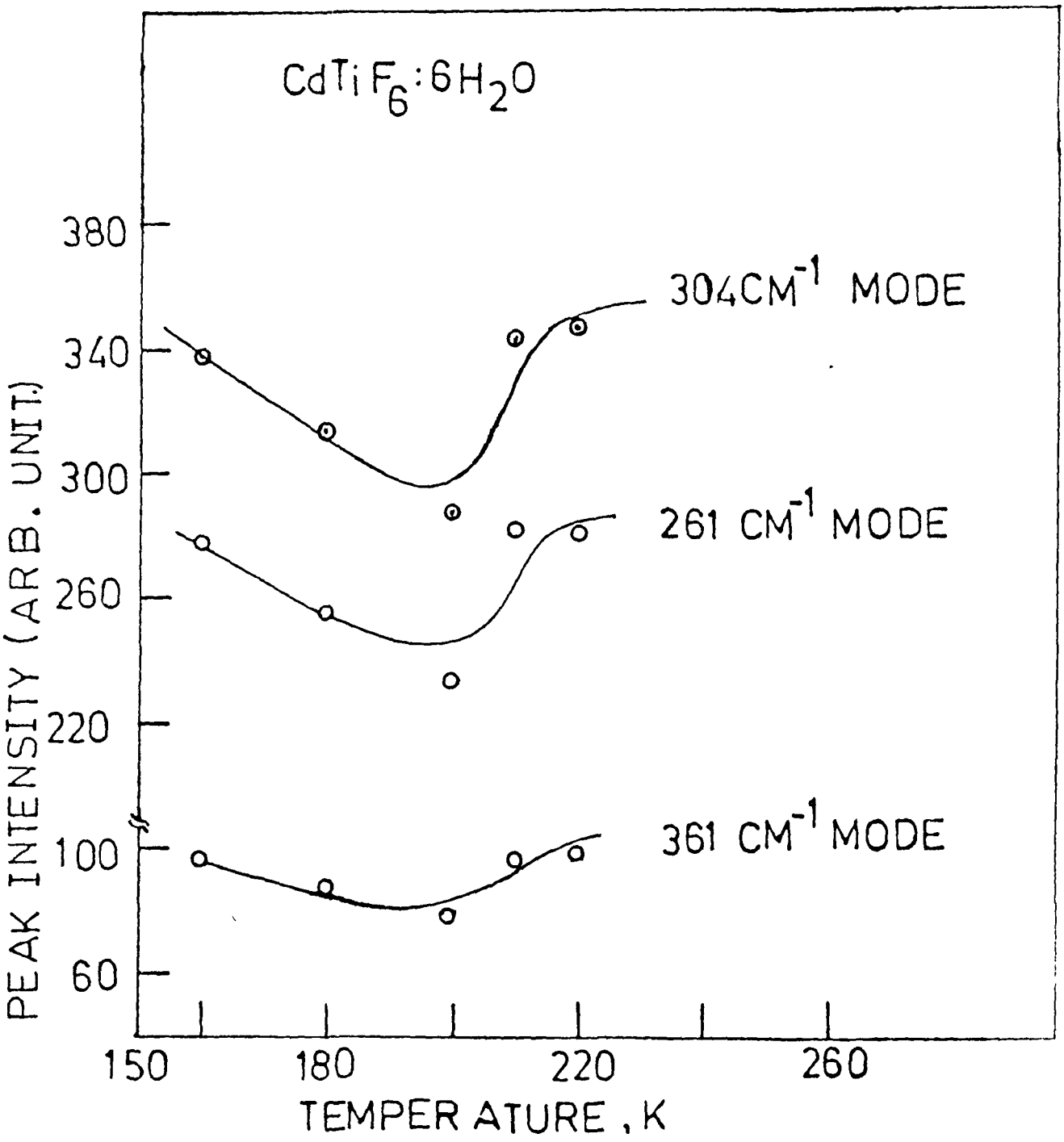

Fig. 4.10

The peak intensity as a function of temperature of a few selected modes : 361, 261 and 300 cm^{-1} modes of the crystal CFTH.

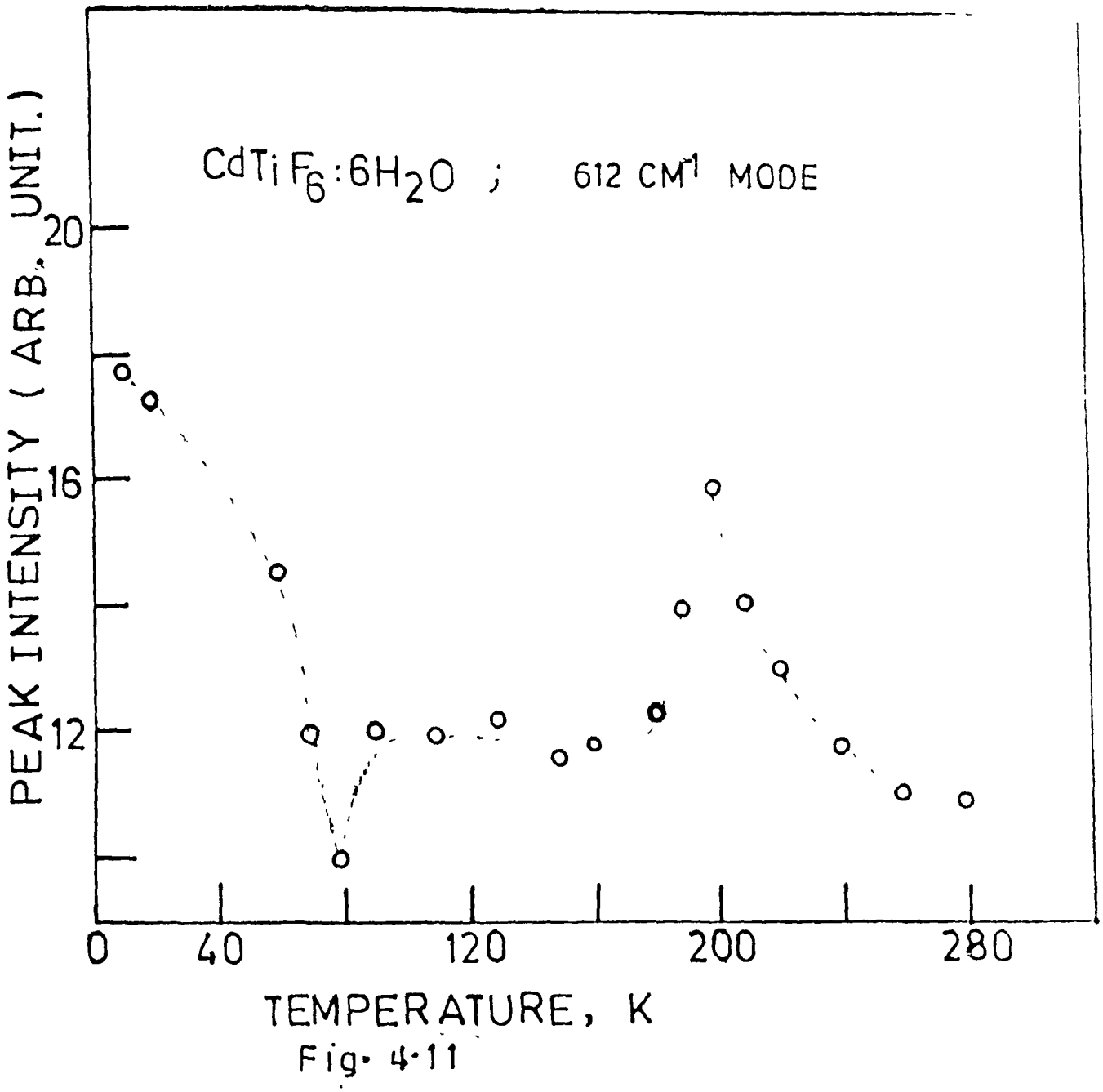

Fig. 4.11

The peak intensity as a function of temperature of 612 cm^{-1} mode of the crystal CFTH.

CHAPTER V

C H A P T E R V

Laser Raman Study of Phase Transformation in Single Crystals of Cadmium Fluoro-Silicate-hexahydrate ($CdSiF_6:6H_2O$)

Chapter V

Laser Raman Study of Phase Transformation in Single Crystals of Cadmium Fluoro-Silicate Hexahydrate ($CdSiF_6:6H_2O$)*

5.1 Abstract

A detailed temperature dependent Raman study of the oriented single crystals of $CdSiF_6:6H_2O$ upto 10k has been made in the region of internal vibrations and lattice modes. Frequency shift, line-width and intensity of some of the Raman bands associated with the modes of the $\left[Cd(OH_2)_6\right]^{2+}$ and $\left[SiF_6\right]^{2-}$ ions show abrupt changes in the temperature range around 220k, and some doubly degenerate modes split into two components. These studies suggest that this system undergoes structural phase transition at 220k. A mechanism for this transition has been suggested.

5.2 Introduction

Considerable effort has been made in understanding the phase transitions in the metal hexahydrate complexes containing the $\left[XF_6\right]^{2-}$ anions and $\left[M(OH_2)_6\right]^{2+}$ cations during the last few years, but the behaviour of some of the complexes is not yet properly understood. As mentioned in Chapter IV some of the members in the general formula $MXF_6:6H_2O$ (where M = divalent metal ions and

---

*Paper based on this study was accepted for presentation in the DAE Symp. on Solid State Phys. Vol 27C pp 282, Dec. 23 (1984), BARC, Bombay, and also paper based on part of this study is accepted for publication in J. Raman Spectrosc. 20, 00 (1989).

X = Si or Ti) undergo structural phase transitions from their room temperature space group C_{3i}^{2} (R $\bar{3}$) to the space group C_{2h}^{5} ($P_{2\ 1/c}$), but a few members of the series do not show phase transition upto very low temperatures [1-3].

We could not find any literature on $CdSiF_6:6H_2O$ regarding its structural phase transition. Badachhape et al [4] have reported two Raman bands in saturated aqueous solution of $CdSiF_6:6H_2O$ at room temperature. From the literature survey on this system, it is clear that the dynamics of structural phase transitions in different metal hexahydrate complexes is quite different.

The vibrational techniques play an important role in elucidating the mechanism of structural phase changes in solids. We, therefore, undertook a systematic study of the Raman spectra of oriented single crystals of $CdSiF_6:6H_2O$ at different temperatures in order to gain an insight about the behaviour of this system. We have detected only one phase transition in this system whereas we found two phase transitions in case of $CdTiF_6:6H_2O$ as discussed in Chapter IV [5].

The results on the study of deuterated analogues of these systems are given in Chapter VI and VII.

5.3 Crystal structure and group theoretical analysis

Most of the members of the series $MXF_6:6H_2O$, have space group R $\bar{3}$ (C_{3i}^{2}) where as some of them have space group R $\bar{3}$m (D_{3d}^{5}) at room temperature [6,7]. No structural data are available for CFSH in

the literature to our knowledge. The crystal structure data for the $ZnSiF_6:6H_2O$ mentioned in section 2.5.1 of Chapter II show that this system has a uni-molecular rhombohedral unit cell of space group $R\bar{3}$ (C_{3i}^2). We can start from the assumption that the $CdSiF_6:6H_2O$ is iso-structural with the $ZnSiF_6:6H_2O$ system and may belong to either the $R\bar{3}$ or the $R\bar{3}m$ space group because most of the members of the general formula $MXF_6:6H_2O$ belong to a rhombohedral system. On this assumption, group theoretical predictions can be made and compared with the experimental observations based on both the space groups and then it can be seen which space group can explain the experimental data correctly. The Fig. 3.1(a — g) illustrate the possible structure of $CdSiF_6:6H_2O$.

The detailed group theoretical analysis has been given in Chapter III for this system also. However, we only mention in this chapter the total number of Raman bands expected in the spectra if the system belongs to either the space group C_{3i}^2 or D_{3d}^5. The total number of Raman bands is expected 24 ($12A_g + 12E_g$ counting E_g species as giving only one band) in case of space group C_{3i}^2; and if the space group is D_{3d}^5, the total number of expected Raman bands would be 17 ($5A_{1g} + 12E_g$). Experimentally it is sometimes difficult to observe all the bands at room temperature [6-8].

5.4 Experimental Procedure

The single crystals of $CdSiF_6:6H_2O$ were grown from aqueous solution by maintaining a slow and constant temperature gradient.[9]

The details are given in Chapter II. The growth of the crystal was like hexagonal pillars elongated along the c-axis. The crystals of $CdSiF_6:6H_2O$ are very hygroscopic and therefore extra care was taken for preserving them. The crystals were taken out from the mother liquid in a dehumidified room.

The crystals were cut $\langle 10 \rangle$ and polished in the same manner as stated in Chapter IV, section 4.3.

The Raman spectra of the crystals were measured in the same manner at room temperature as explained in the case of single crystal of $CdTiF_6:6H_2O$. The details of the procedure are mentioned in Chapter II, sections 2.6.1 to 2.6.4. The linearly polarized 4880 and 5145 Å laser lines from the Spectra-Physics model 165 Argon-Ion laser were used for excitation of the Raman spectra. The scattered light in the 90° scattering geometry was analysed with a Spex Ramalog Triple Monochromator equipped with a cooled photomultiplier tube.

5.5 Results and Discussion

It is expected from the group theoretical analysis that if the CFSH belongs to the space group C_{3i}^2 one would expect to observe 16 Raman active modes for the $\langle Cd(OH_2)_6 \rangle^{2+}$ ion and only 3 Raman modes for the $\langle SiF_6 \rangle^{2-}$ ion in the internal vibration region. Here doubly degenerate modes are counted as one. If the CFSH belongs to the space group D_{3d}^5 the internal modes expected are 11 and 4 for the $\langle Cd(OH_2)_6 \rangle^{2+}$ and $\langle SiF_6 \rangle^{2-}$ ions respectively. As it will be explained later on, the similarity of the Raman spectra of the CFSH with that of the $ZnSiF_6:6H_2O$ under the same experimental conditions

at room temperature do not leave any doubt that CFSH also belongs to the space group C_{3i}^2 at room temperature.

We also recorded the IR spectrum of CFSH at room temperature. (Fig. 5.1) A comparison of the room temperature IR and Raman spectra of CFSH (Table 5.1) shows that the system gives different frequencies for IR absorption and Raman scattering bands for the same (Si-F) stretching mode. Therefore, from the principle of mutual exclusion, the CFSH possesses a centre of symmetry. This does not, however, rule out the possibility of D_{3d} space group for CFSH because both the C_{3i}^2 and D_{3d}^5 space groups have centre of symmetry. But if we look at the Raman scattering tensors and irreducible representations of Raman active modes, we find that the polarization study in different orientations does not help in distinguishing between the D_{3d} and C_{3i} space groups because in both the cases E_g modes are expected to be present in the (xx), (yy), (xy), (yz) and (zx) orientations but absent in the (zz) orientation. However the intensities corresponding to the E_g modes in the C_{3i} and D_{3d} space groups are expected to be different. Therefore one way is to record the spectra of the systems having the space groups C_{3i} and D_{3d} under the same experimental conditions as that of CFSH and compare the spectra of CFSH with the spectra of these systems and see with which the intensity of the E_g modes of CFSH resemble. The otherway is the group theoretical analysis for both the C_{3i} and D_{3d} space groups and from this predict the number of Raman active modes.

Hence a group theoretical analysis for the two groups was made to eliminate the possibility of D_{3d} space group.

We followed both the approaches and concluded that CFSH belongs to the system having space group C_{3i}^2. The Raman tensors for the C_{3i} and D_{3d} groups are given here:-

$R\ \bar{3}m\ (D_{3d})$

$$\begin{pmatrix} a & o & o \\ o & a & o \\ o & o & b \end{pmatrix} \quad \begin{pmatrix} c & o & o \\ o & -c & d \\ o & d & o \end{pmatrix} \quad \begin{pmatrix} o & -c & -d \\ -c & o & o \\ -d & o & o \end{pmatrix}$$

A_{1g} $\qquad$ E_g $\qquad$ E_g

$R\ \bar{3}\ (C_{3i} \equiv S_6)$

$$\begin{pmatrix} a & o & o \\ o & a & o \\ o & o & b \end{pmatrix} \quad \begin{pmatrix} c & d & e \\ d & -c & f \\ e & f & o \end{pmatrix} \quad \begin{pmatrix} d & -c & -f \\ -c & -d & e \\ -f & e & o \end{pmatrix}$$

A_g $\qquad$ E_g $\qquad$ E_g

5.5.1 *The room temperature spectra*

Fig. 5.2 shows the representative spectra of single crystals of CFSH at room temperature in 4 orientations expressed in Porto's notation. Under the space group C_{3i}^2 the A_g and E_g species of the vibrations are expected to be present in all the six geometries except in the $\{x(zz)y\}$ geometry where E_g species are absent.

Under the C_{3i}^2 space group one would expect 4 Raman bands $(2A_g + 2E_g)$ in the lattice mode region, but only two lattice modes

($2E_g$) would be expected under the D_{3d}^5 space group. Experimentally, only one distinct band has been observed by us, as we also got only one band in case of $ZnSiF_6:6H_2O$, in the lattice mode region at room temperature.

The position of the Raman bands in different polarizations for the single crystals of CFSH are given in Table 5.2 along with an assignment for the observed bands. The spectral correlations are based on group theoretical expectations, group frequencies and available assignments in literature on similar systems [11].

The half width of most of the bands associated with the $[SiF_6]^{2-}$ ion in the room temperature Raman spectra is 20-22 cm^{-1} while those associated with the ν(Cd-O) and δ(O-Cd-O) modes is 30 cm^{-1}. This indicates a larger disorder of the cations compared to those of anions in the lattice. The site symmetry splittings of the δ(F-Si-F) mode of T_{2g} symmetry is almost negligible while the δ(O-Cd-O) mode of the cation shows 6 cm^{-1} splitting into the A_g and E_g components under C_{3i}^2 space group. The maximum site splitting of 20 cm^{-1} is observed with the IR active ν(Si-F) mode of T_{1u} symmetry while the δ(F-Si-F) mode does not show any detectable site splitting. The ν(O-H) modes show only one broad feature. The absence of the twisting and any detectable librational modes associated with the water molecules support the view that H_2O molecules are almost freely rotating or reorientating in the lattice and all the six H_2O molecules are equivalent at room temperature.

5.5.2 The low temperature spectra

In order to resolve the closely spaced lines, we recorded the Raman spectra of a single crystal of CFSH at 10k and found that the spectra contain a complicated structure. The spectral data at 10k are presented in Table 5.3. We therefore undertook a systematic temperature dependent study of the Raman spectra of oriented crystals of CFSH from room temperature down to 10k. The spectral data at intervals of 20 or 10k are shown in Table 5.4. The Raman spectra of a single crystals of CFSH in the $\{x(yy)z\}$ geometry at few selected temperatures are shown in the Fig. 5.4, while the spectra at 10k in different geometries are displayed in the Fig. 5.3a and b in different spectral regions.

The variation of band positions and the full width at half maximum intensity (FWHM) as a function of temperature for some selected and isolated bands is shown in Fig. 5.5 and Fig. 5.6. The FWHM was calculated taking into account of slit width correlation by using the formula [12]

$$\delta_t = \delta_a \left[1-\left(\frac{s}{\delta_a}\right)^2\right] \quad \ldots\ldots\ldots\ldots \quad (5.1)$$

where δ_t = true line width

δ_a = observed line width

s = slit width

The probable errors in the measurements of FWHM is $\pm$ 1.0 cm^{-1}.

As the temperature of the system is reduced, many spectral changes take place. The important features of the temperature dependent Raman spectra of the system are given below:-

(1) Most of the bands became sharp and the shoulders and unresolved components appeared as distinct features;

(2) The frequencies, FWHM and intensities of some bands showed anomalous changes around 220k;

(3) The frequencies of the bands associated with the internal modes δ(O-Cd-O) (182 cm^{-1}), ν(Cd-O) (353 cm^{-1}) and the lattice mode at 88 cm^{-1} showed abrupt discontinuties at $\sim$ 220k (Fig. 5.5 and 5.8) while the frequencies of the bands associated with the $[Si-F_6]^{2-}$ ions did not show any change at $\sim$ 220k;

(4) The FWHMs of most of the bands show discontinuity around 220k (Fig. 5.6);

(5) The broad band associated with the ν(O-H) vibrational modes at room temperature splits into 4 sharp components below 60k;

(6) Several new features appear in the low temperature spectra below 60k in the lattice mode region and weak features at 556, 622, 675, 703 cm^{-1} which are mainly related with the H_2O librations and other water modes.

The deformation mode of (A_g + E_g) species associated with the $[Cd(OH_2)_6]^{2+}$ ions is found at 183 cm^{-1} at room temperature; but at about 220k the frequency suddenly rises to 187 cm^{-1} and as the temperature goes down the band broadens (Fig. 5.4). The E_g and A_g

components are not clearly resolved upto the temperature 210k, but below this they separate out. The A_g component is observed at 173 cm^{-1} while the E_g component is observed at 182 cm^{-1}. Although the 187 cm^{-1} band is not resolved clearly at 220k but its broad pattern indicates that the two components of the E_g mode are very close. The A_g component of the δ (O-Cd-O) vibrational mode is mixed with the 181 cm^{-1} (E_g) band. Similarly the frequency of the lattice mode at 88 cm^{-1} of E_g species suddenly increases to 93 cm^{-1} at 220k and there after its value increases slowly and gradually as the temperature is lowered from 220 to 10k. The frequency variation as a function of temperature for some bands is shown in Fig. 5.5.

The 658 cm^{-1} ν_s(Si-F) symmetric stretching mode gives the strongest band which is well isolated from the other bands. The FWHM in this case rises suddenly at about 220k. Before reaching this transition temperature the rise is gradual and smooth and also after T_c the rise is gradual following more or less Arrhenius type of relation [13]

$$\Delta\nu_{\frac{1}{2}} = A + B \exp(-U/T) \qquad (5.2)$$

where A and B are constants, U is potential barrier or activation energy, T is temperature.

Moreover, the 356 cm^{-1} band ν_s(Cd-O), is also strong and symmetrical. The FWHM of this band also increases suddenly at about 220k, then as the temperature rises it decreases and then again rises rapidly. The 397 cm^{-1} band is associated with the deformation mode

of (F-Si-F). We have also plotted its FWHM as a function of temperature and found that it suddenly increases at about 220k.

The peak intensities of the 397, 356 and 658 cm^{-1} bands were plotted against temperature (Fig. 5.7). In all the three cases the intensities decrease suddenly at about 220k. When the temperature rises the intensity rises again in all the three cases. The relative intensities of the bands are compared in terms of the count rates for different Raman bands. The variation of peak intensities as a function of temperature also confirms a phase transition at about 220k. As the temperature decreases the peak intensity increases gradually and becomes maximum at 10k in all the three cases due to sharpening of the bands.

5.5.3 Structural phase transformation

The sharp changes and discontinuties observed in the frequency shift and half width of some of the bands at 220k are typical features associated with structural phase transitions of first order type involving ordering of the ions. As most of the modes associated with the $[Cd(OH_2)_6]^{2+}$ ions show either splitting, change in frequency or anomalous behaviour of FWHM at the critical temperature, this transition is mostly associated with the changes in these ions. Since there is only a gradual and uniform change in the frequencies of the $[SiF_6]^{2-}$ ions in going to lower temperatures which may arise due to thermal changes in lattice parameters, these ions do not play any major role in the phase transformation.

The appearance of 4 sharp components associated with the ν(O-H) vibrational modes and modes related to H_2O librations below 60k indicate that the H_2O molecules become ordered only well below T_c. This also indicates that the equivalence of the H_2O molecules in the $[Cd(OH_2)_6]^{2+}$ octahedra is destroyed below the T_c and at least two different types of H_2O units can be inferred. The large number of lines observed below 150 cm^{-1} in the lattice mode region and other parts of spectra and splitting of all the E_g modes indicates that the space group symmetry of the system has reduced from C_{3i}^2 to the stage where there are no degeneracies and/or the unit cell has at least doubled in size.

5.5.4 Structure of the low-temperature phase

The polarization behaviour of Raman features in the low temperature phase does not provide unambiguous information about the space group of the system below phase transformation temperature. The crystals were cut and mounted in the helium cryo-cooler chamber consistent with the room temperature space group C_{3i}^2 of the system. When the temperature is lowered below 220k, the system undergoes structural phase transition and the crystallographic axes of the crystal in the new phase may be at different angles with respect to the laser beam polarization direction. This may give rise to intensity leakage for certain modes in specific geometries otherwise forbidden in those geometries if the crystals were cut and mounted consistent with the new geometries after phase transformation.

However, an increase in the number of Raman bands in the lattice mode region and the splitting of most of the modes of the E_g species manifest a lowering of the symmetry of the system below 220k.

If one has to infer about the space group of the low-temperature phase, one must recognise the fact that the space group of the low-temperature phase need not necessarily be a sub-group of the disordered phase for a first order transition.

We have established that the space group of CFSH at room temperature is C_{3i}^2 and is a disordered phase. It is possible for this system that the room temperature C_{3i}^2 phase has a high temperature parent phase (prototypic) having space group D_{3d}. Within the limitations of polarization leakage, the polarization measurements of Raman bands in different geometries at 10k (see Table 5.3) and in analogy with the reported results for the $MgSiF_6:6H_2O$ system, it is likely that the low temperature phase of CFSH also belongs to the C_{2h} space group in the monoclinic series. This is only a tentative proposal and with the available data it is difficult to draw any firm conclusion about the symmetry of the low-temperature phase.

It appears that as the system is cooled the lattice contracts and at about 220k the water molecules loose their orientational freedom to some extent by occupying ordered positions. This may destroy equivalence of the six H_2O molecules with the distortion of the $[Cd(OH_2)_6]^{2+}$ octahedra triggering a phase transition in this system [14-19].

5.6 References

[1] Poulet H and Mathieu J, C R Acad. Sci. Paris, t-286(12) Series B, 331 (1978).

[2] Choudhury P, Paul B, Saha S and Ghose B, Proc. of Nucl. Phys. and Solid State Phys. Vol. 24C pp 323, Dec. 28 (1981), BARC, Bombay.

[3] Bose M, Roy K and Ghoshray A, Proc. of Nucl. Phys. and Solid State Phys. Vol. 24C pp 389, Dec 28 (1981).

[4] Badachhape R B, Hunter G, McCory L D and Margrave J L, Inorg. Chem. 5(5), 929 (1966).

[5] Thakur G and Verma A L, J. Raman Spectrosc. 17, 207 (1985).

[6] Wyckoff R W G, "Crystal Structure" Vol. 3, 2nd ed. Wiley Interscience (1965).

[7] Hamilton W C, Acta Crystallogr. 15, 353 (1962).

[8] Lewis J and Jenkins T E, J Raman Spectrosc. 8, 111 (1979).

[9] Thakur G, Proc. of Symp. on Crystal Growth, Dec. 24 (1983), Anna University, Madras.

[10] Patel M B, Agarwal A and Bist H D, J. Raman Spectrosc. 14, 406 (1983).

[11] Choudhury P, Ghosh B, Raghubanshi G S and Bist H D, 14, 99 (1983).

[12] Tanabe K, Spectrochimi Acta, 40A, 437 (1984).

[13] Jenkins T E and Lewis J, J. Raman Spectrosc. 11, 1 (1981).

[14] Jenkins T E and Lewis J, Spectrochim. Acta 37A, 47 (1981).

[15] How T and Suare I, Phys. Scripta, 9, 40 (1974).

[16] Thakur G and Verma A L, Proc. of Solid State Phys. Symp. Vol. 27C pp 282 Dec. 23 (1984), BARC, Bombay.

[17] Tsujikawa P I and Couture L, J. De Physi.et Radium 16, 430 (1955).

[18] Long D A, "Plenary Lecture", "Colloquium Spectroscopium Internationale XVI" Helger, London (1971).

[19] Ben Ghozlen M H, Daoud A, Mlik Y, Poulet H, Le Postollec M and Toupry N, J. Raman Spectrosc. 16(4), 219 (1985).

Table 5.1

IR and Raman bands for $CdSiF_6:H_2O$ at room temperature (RT)

IR bands (cm^{-1})	Assignment of IR bands	Raman band (cm^{-1})	Assignment of Raman bands
-	-	88m	Lattice mode
-	-	182m	δ (O-Cd-O)
358vw	ν (Cd-O) F_{1u}	353s	ν_s (Cd-O) A_g
483vs	ν_4 (F-Si-F) F_{1u}	397m	δ (F-Si-F)
-	-	457w	ν_{as} (Si-F)
608vw	(O-H) wag	-	-
743vs	ν_3 (Si-F) F_{1u}	660vs	ν_s (Si-F) A_g
763sh			
1080vvw	-	-	-
1120w	-	-	-
1120w	-	-	-
1382vw	-	-	-
1585m sharp	-	-	-
1622m	-	-	-
2915vvw	-	-	-
3550m,b	ν_s (O-H)	3505vs	ν_s (O-H)
3640m	ν_{as} (O-H)		

vs = very strong, s = strong, m = medium, w = weak, vw = very weak, b = broad, sh = shoulder.

Table 5.2

Raman bands (cm^{-1}) observed in different polarization geometries on single crystals of $CdSiF_6:6H_2O$ at room temperature (298°K)

$\{y(xx)z\}$	$\{x(yy)z\}$	$\{x(yx)z\}$	$\{x(zy)z\}$	$\{x(zx)z\}$	$\{x(zz)y\}$	Assignment
88m	88m	88m	87w	87m	-	Lattice mode
-	-	-	-	-	176m	E_g, A_g } δ (O-Cd-O)
182m	182m	183m	182w	182w	-	E_g
353s	353s	353m	-	-	353m	A_g — ν_s (Cd-O)
397m	397m	397m	399vw	398vw	-	E_g } δ (F-Si-F)
-	-	-	-	-	400s	A_g
457w	457w	457vw	457vvw	457vvw	-	E_g — ν_{as} (Si-F)
660vs	659vs	660m	660vw	660vw	660vs	A_g ... ν_s (Si-F)
3505vs	3505vs	3505m	3505sh 3508w	-	-	E_g
-	-	-	-	-	3513vs	A_g } ν (O-H)
-	-	-	3517w	-	-	E_g

vs = very strong; s = strong; m = medium; w = weak; vw = very weak; vvw = very very weak; b = broad; sh = shoulder; ms = medium strong.

Table 5.3

Raman bands (cm^{-1}) observed in different polarizations for single crystals of $CdSiF_6:6H_2O$ at 10 K.

{y(xx)z}	{x(yy)z}	{x(yx)z}	{x(zy)z}	{x(zx)z}	{x(zz)y}	Assignment	
1	2	3	4	5	6	7	
48vvw	48vvw	-	-	-	-	B_g	
64w	64w	64vw	-	-	-	B_g	
83w	83w	83w	83m	83m	-	B_g	
93vvw	93vvw	-	-	-	93vvw	A_g	Lattice modes
108ms	108ms	108ms	108m	108m	108vw	B_g	
117s	117s	117m	116vw	117vw	117s	A_g	
137vw	137vw	137vvw	-	-	137vw	A_g	
147vw	147vw	-	-	-	-	B_g	
171s	171s	171m	171m	171m	171vs	A_g	δ (O-Cd-O)
201ms	201ms	201ms	201m	201m	-	B_g	
273vw	273vw	273w	273vw	273vw	-	A_g	ν_{as} (Cd-O)
-	-	-	293vvw	293vvw	-	B_g	
348s	348s	348ms	348m	348m	348s	A_g	ν_s (Cd-O)
391ms	391ms	391ms	391ms	391ms	391s	A_g	δ (F-Si-F)
424w	424w	424vw	424vw	-	-	B_g	δ (F-Si-F)
447m	447m	447m	447vw	447vw	-	B_g	ν_{as} (Si-F)
468vw	468vw	468vw	-	-	468vw	A_g	ν_{as} (Si-F)

Table 5.3 continued...

Table 5.3 continued

1	2	3	4	5	6		7
-	-	-	482vvw,b	482vvw,b	-	B_g	
556vvw	556vvw,b	558vvw,b	552vvw,b	556vvw,b	-	A_g	H_2O
-	622vvw	607vvw	-	-	623vvw	A_g	Libration
653vs	653vs	653s	653m	653m	653vs	A_g	ν_s(Si-F)
-	-	675vw	676vw	676vw	-	B_g	H_2O
-	703vw	-	-	703vw	703w,b	A_g	Libration
3469s	3469s	3469s	3469m	3469m	-	B_g	
3510vs	3510vs	3510vs	3510m	3510m	3510vs	A_g	
3524m	3524w	3524vvw	3524w	3524w	3524vvs	A_g	
3540s	3540m	3540w	3540m	3540ms	-	B_g	ν(H-O)
3557w	3557w	3557vw	3557vw	-	3557w	A_g	
-	-	-	3568vw	-	-	B_g	

Assignment is made based on C_{2h} space group for the low temperature phase.

Table 5.4

Spectral data of $CdSiF_6:6H_2O$ at selected temperatures in the $\{x(yy)z\}$ orientation (Frequency in cm^{-1} and temperature in K)

270K	230K	220K	215K	210K	200K	190K	10K	Assignment
							48vvw	
							64w	
87m	87m						83w	
		91m	91m	93m	93m	93m	93vvw	Lattice modes
							108ms	
							117s	
							137vw	
							147vw	
							171s	
182m	183m				182m	182m		
		187m,b	187m,b	187m,b				δ(O-Cd-O)
					196m	195m	201ms	
							273vw	ν_{as}(Cd-O)
353s	353s	356s	356s	356s	355s	355s	348s	ν_s(Cd-O)
397m	397m	398m,b	398m,b	398m,b	399m,b	400m,b	391ms	δ(F-Si-F)
							424w	
457w	457w	456vwb	456vwb	456vwb	456vwb	456vwb	447m	ν_{as}(Si-F)
							468vw	
							556vvw,b	H_2O Libr.
							622vvw	
659vs	660vs	660vs	659vs	658vs	658vs	658vs	653vs	ν_s(Si-F)
							703vw	H_2O Libr.

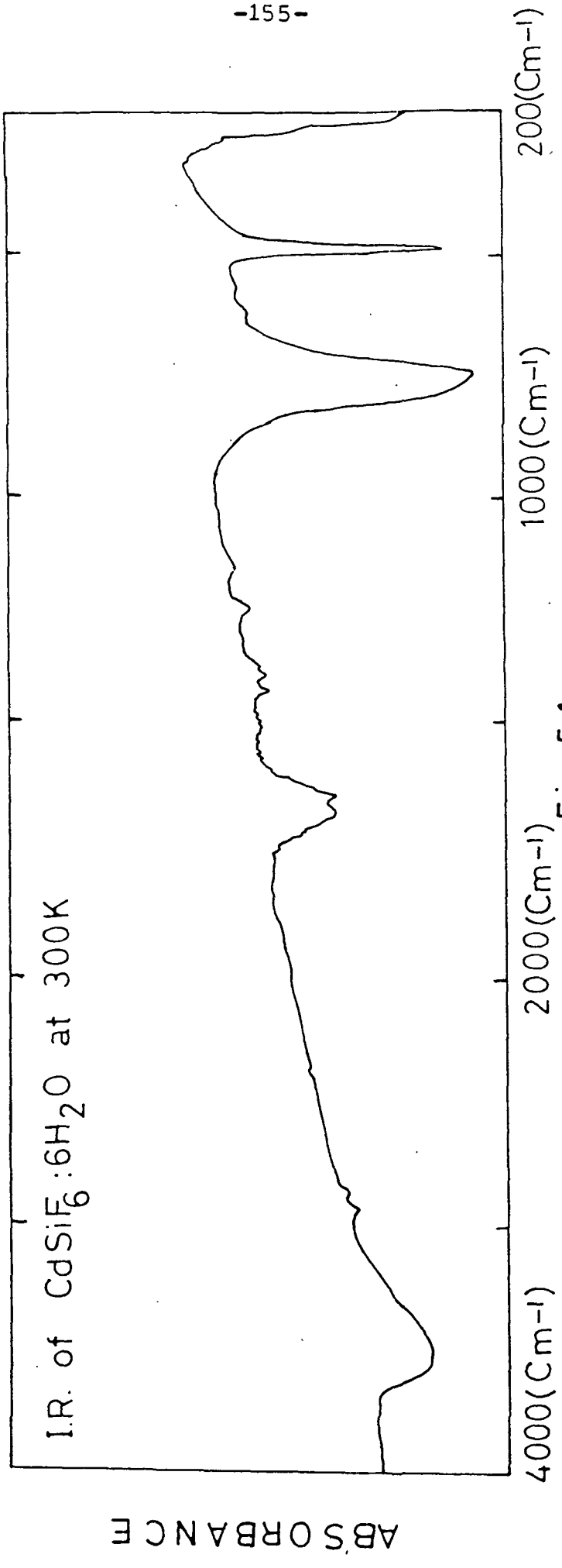

Fig. 5.1

The IR spectrum of $CdSiF_6:6H_2O$ at room temperature

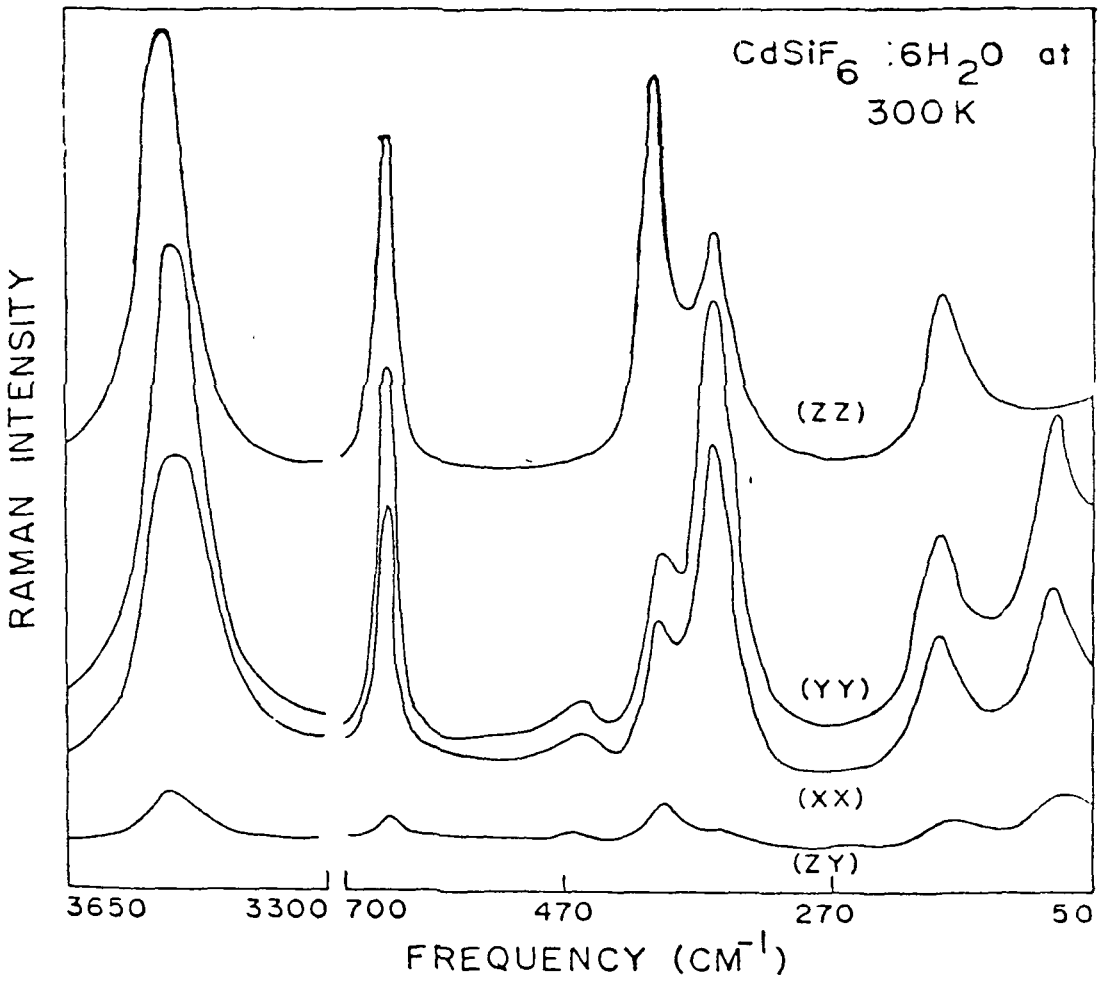

Fig. 5·2

Raman spectra of a single crystal of $CdSiF_6:6H_2O$ at room temperature in a few selected orientations.

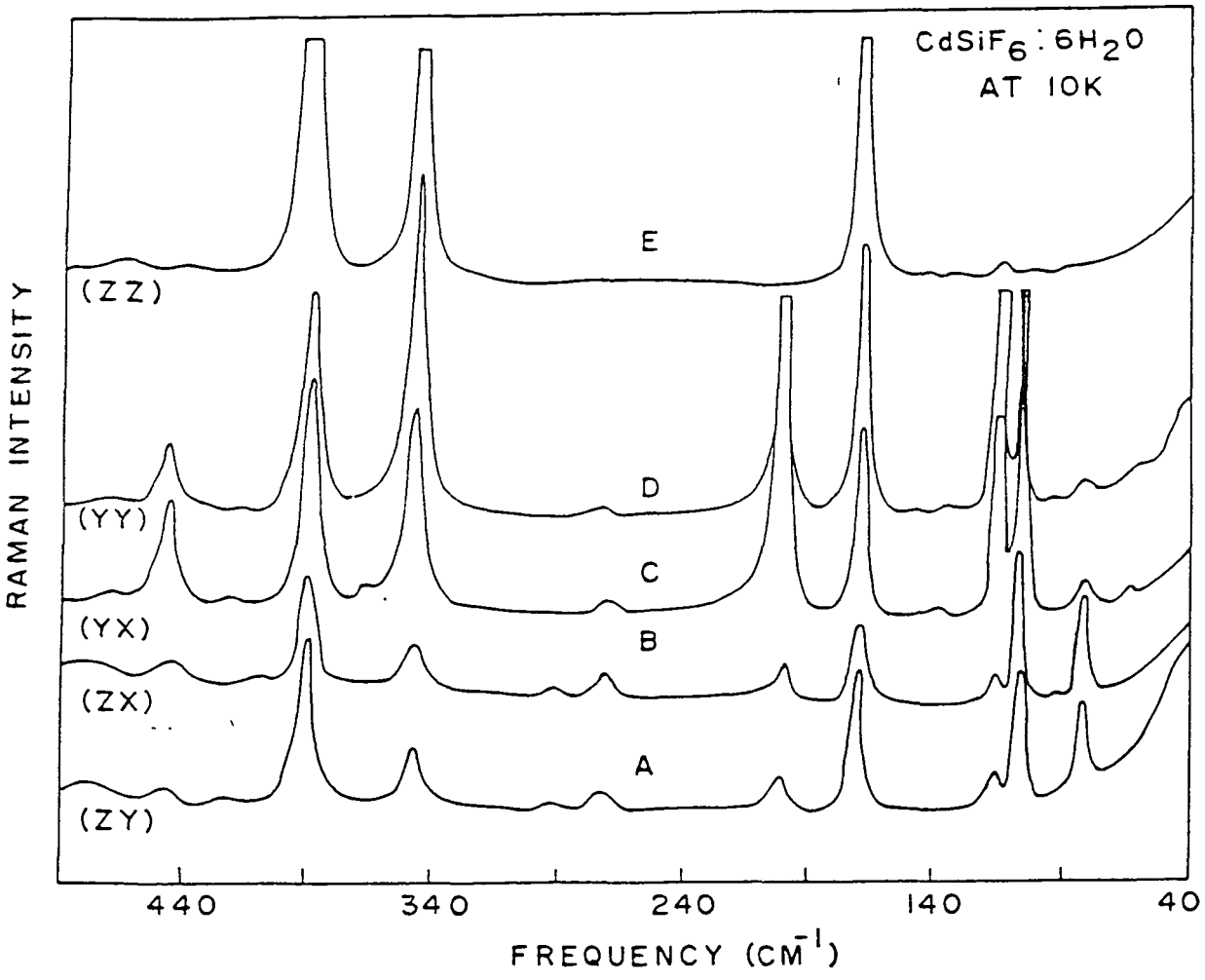

Fig. 5.3(a)

Raman spectra of a single crystal of $CdSiF_6:6H_2O$ at 10k in a few selected orientations in the 40-500 cm^{-1} region. Full scale count rates for the spectra A-C is 2 x 10^3 C/sec while for D and E, it is 5 x 10^3 and 6 x 10^3 C/sec respectively.

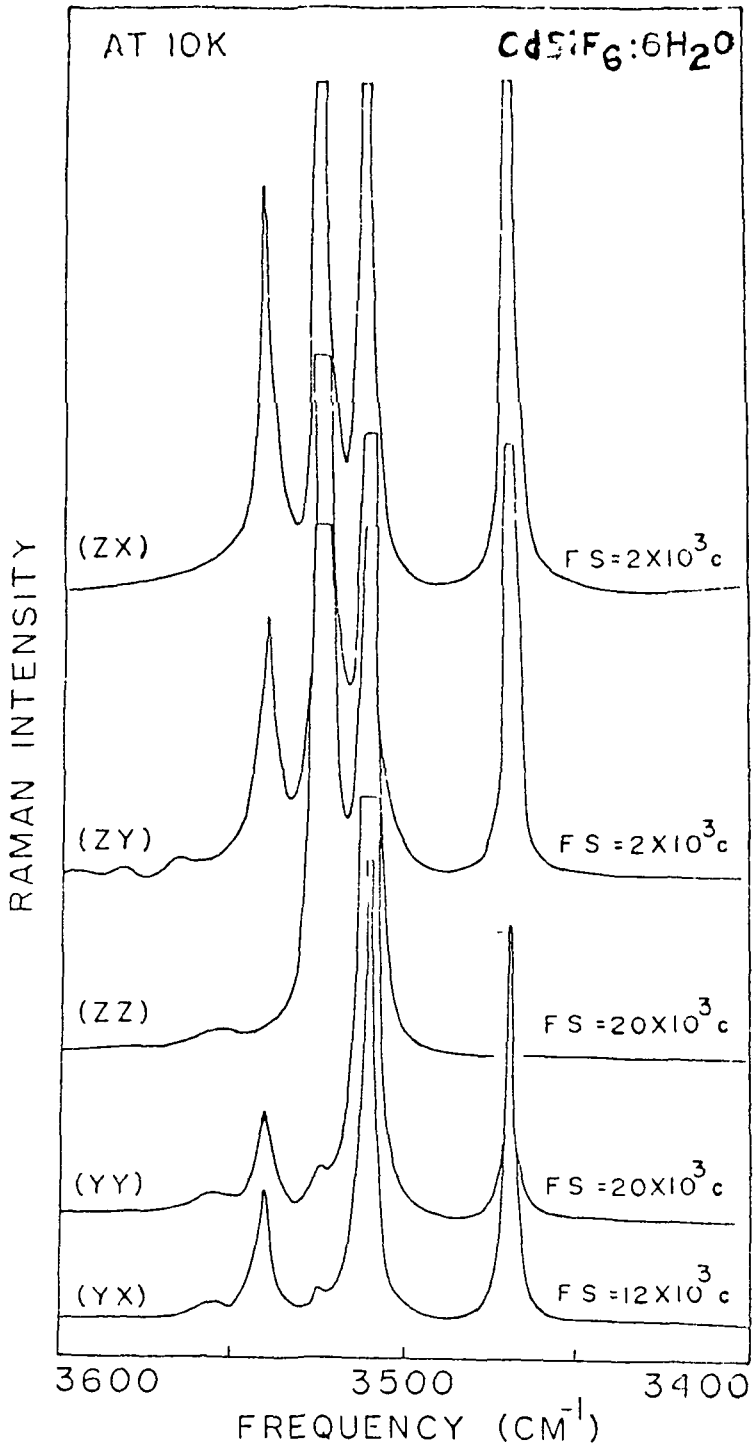

Fig. 5.3(b)

Raman spectra of a single crystal of $CdSiF_6:6H_2O$ at 10k in a few selected orientations in the 3400-3600 cm^{-1} region. The spectral conditions are the same as in Fig. 5.3(a) except the full scale count rates, which are indicated in the figure.

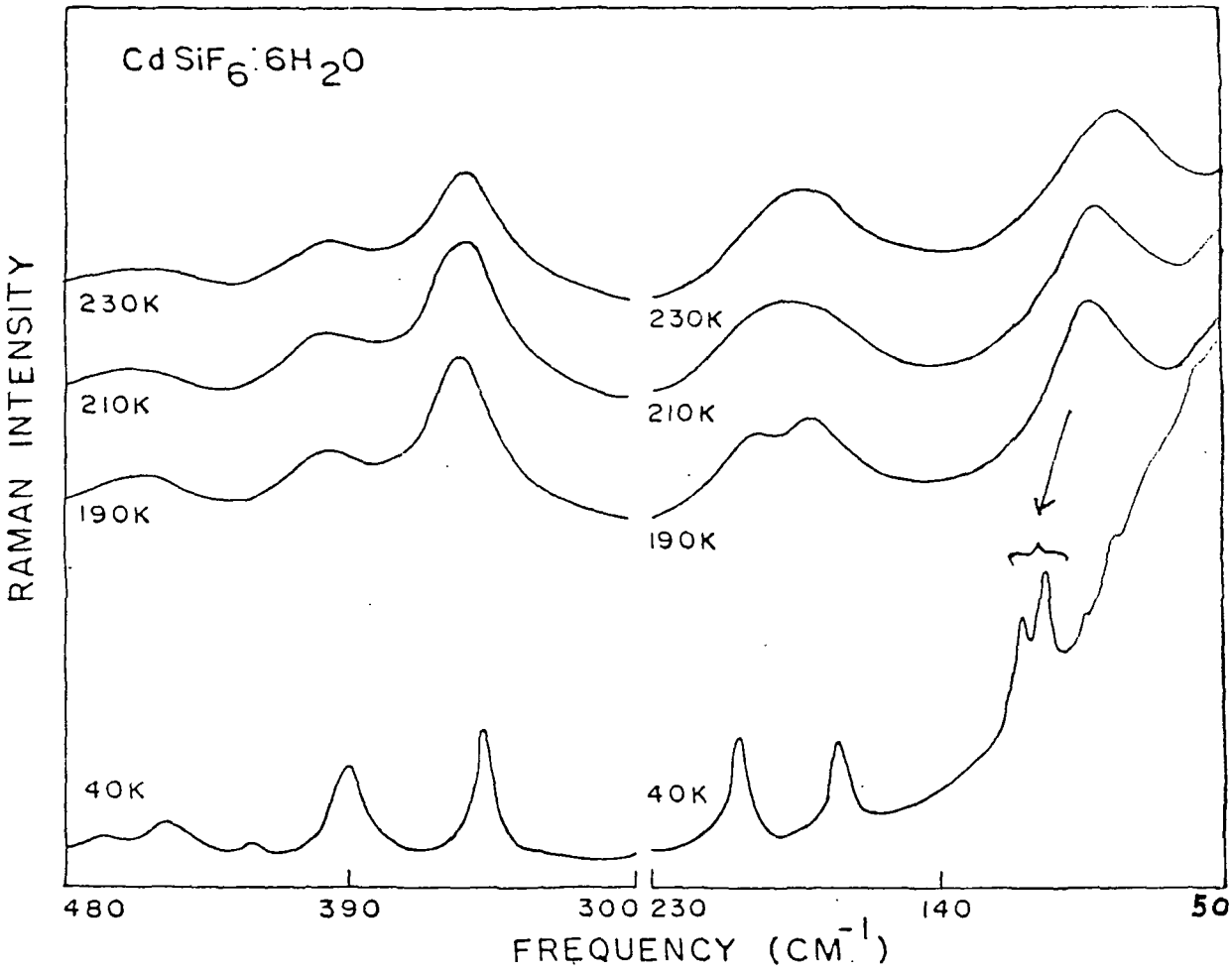

Fig. 5.4

Raman spectra of a single crystal of $CdSiF_6:6H_2O$ in the $\{x(yy)z\}$ orientation at some selected temperatures.

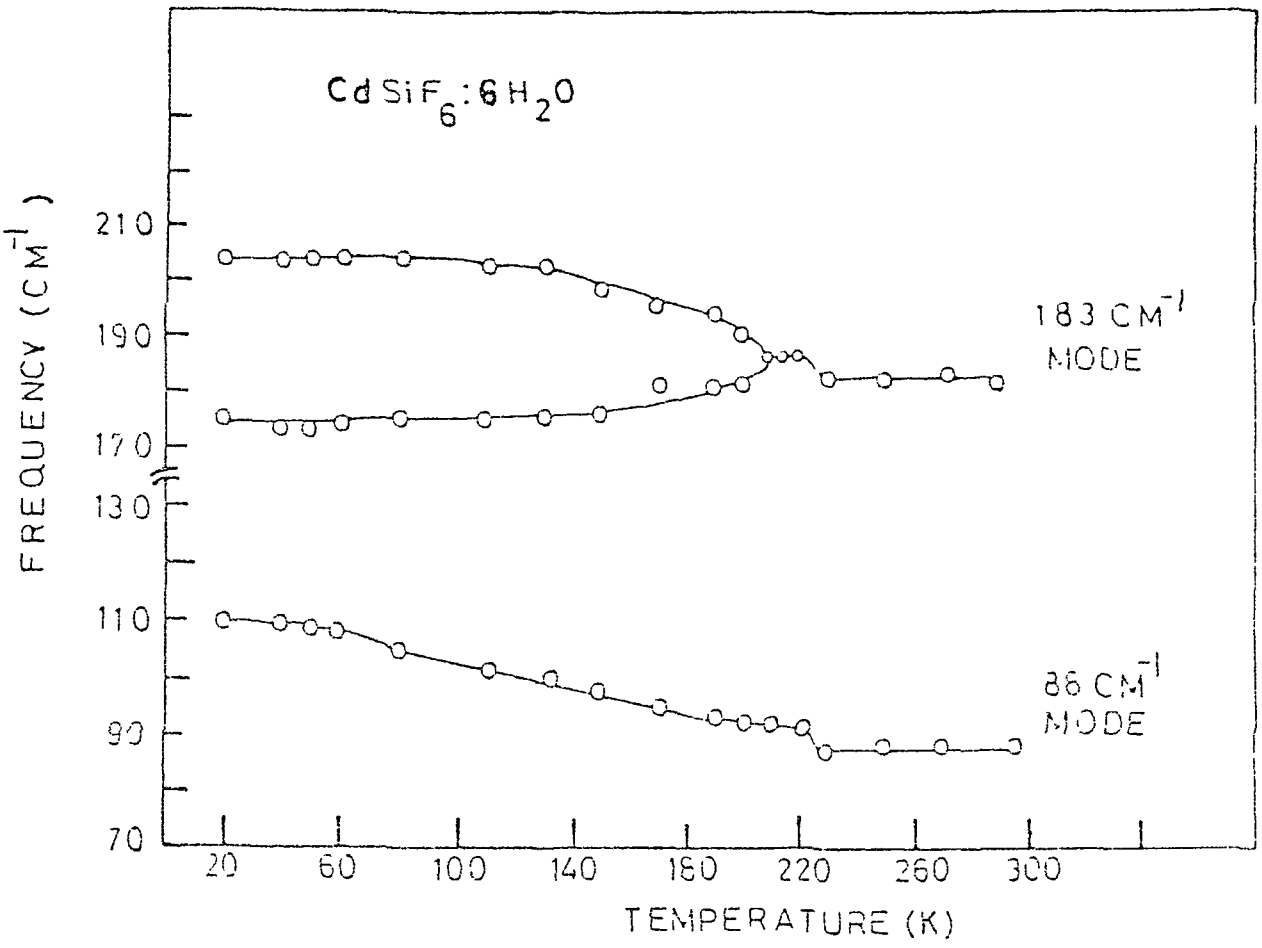

Fig. 5·5

Frequency shift of the 88 and 183 cm^{-1} bands and splitting of the 183 cm^{-1} band as a function of temperature.

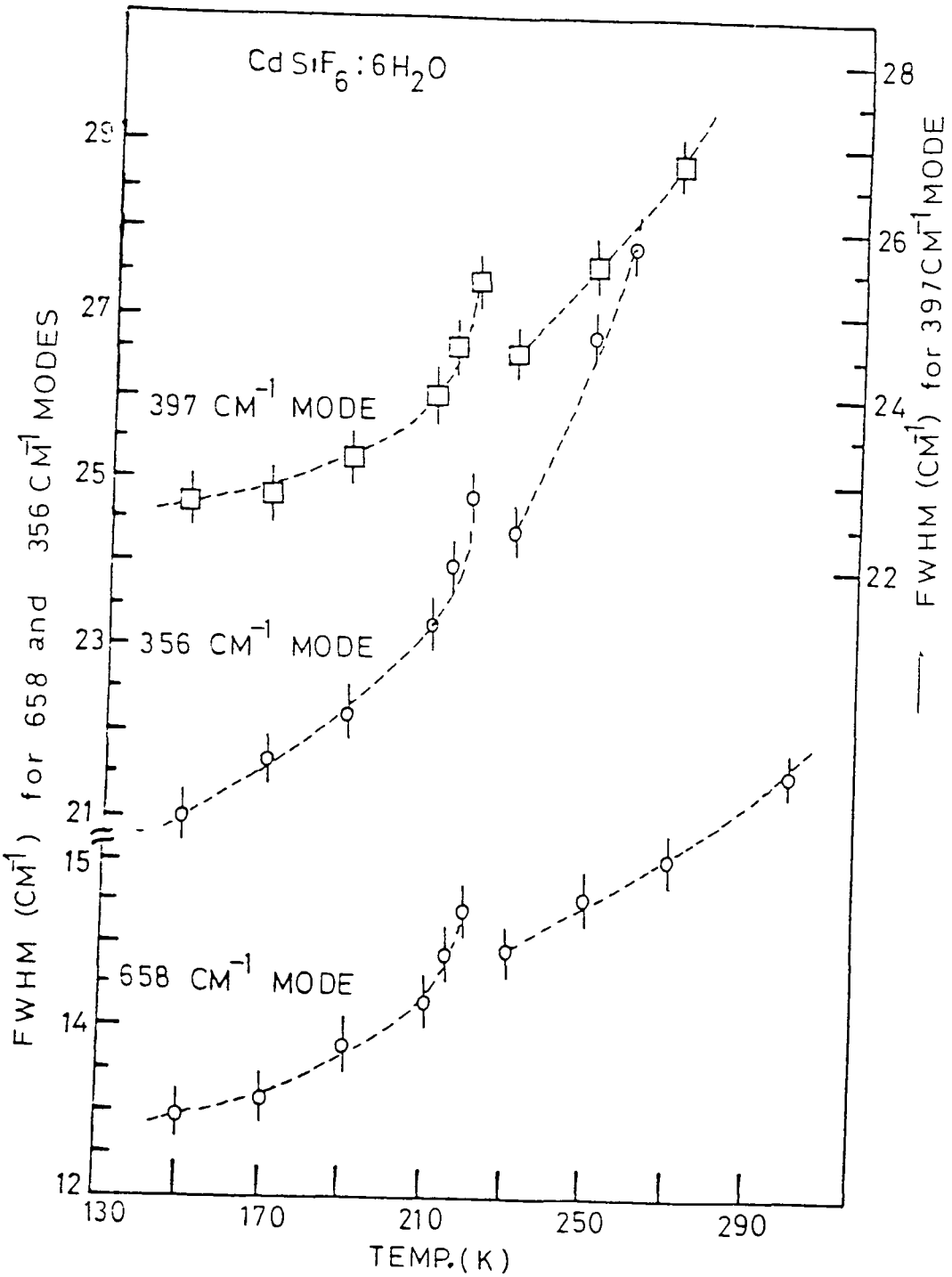

Fig. 5.6

Variation of FWHM as a function of temperature for a few selected bands.

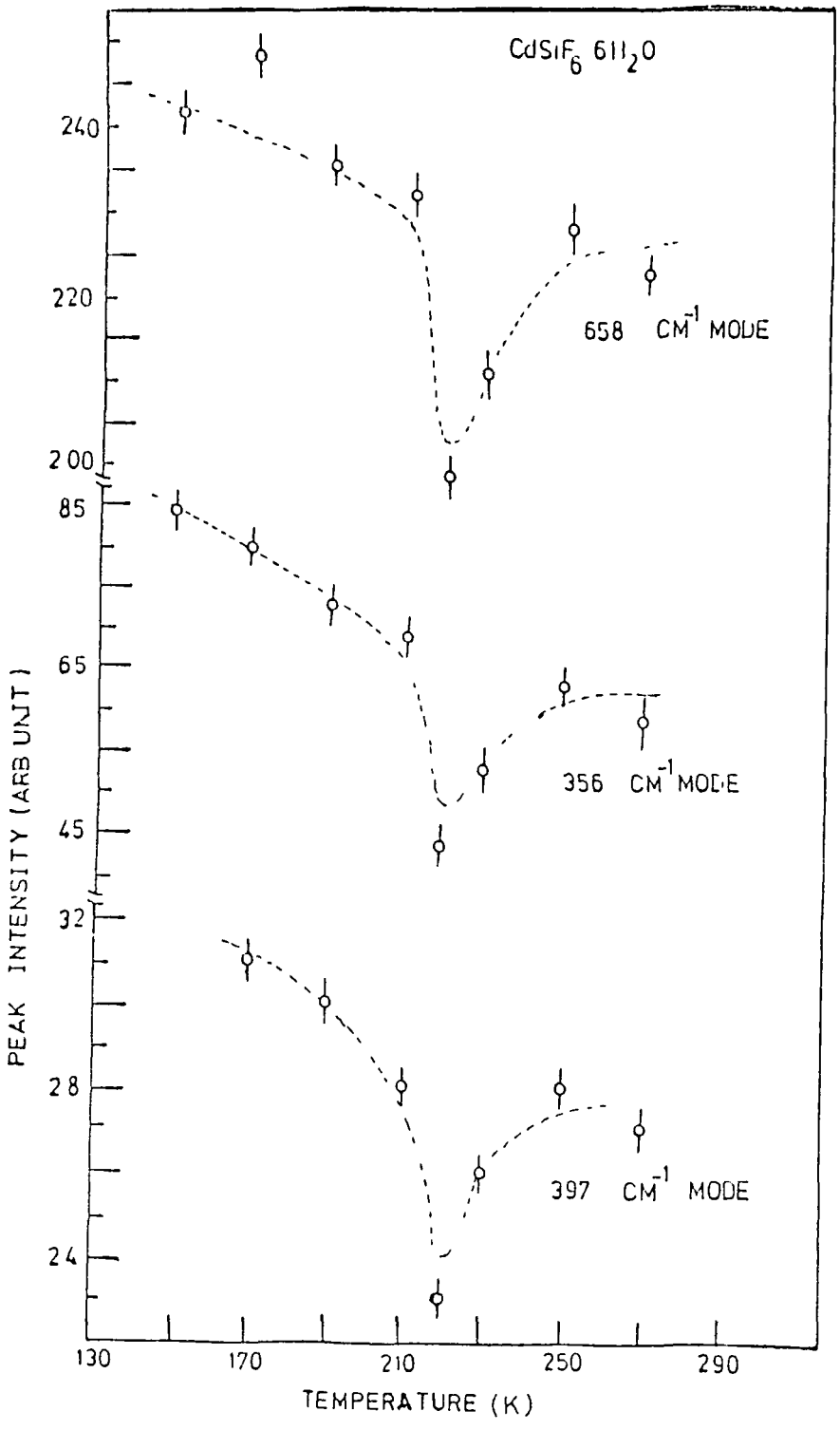

Fig. 5·7

Relative peak intensity variation as a function of temperature for a few selected bands.

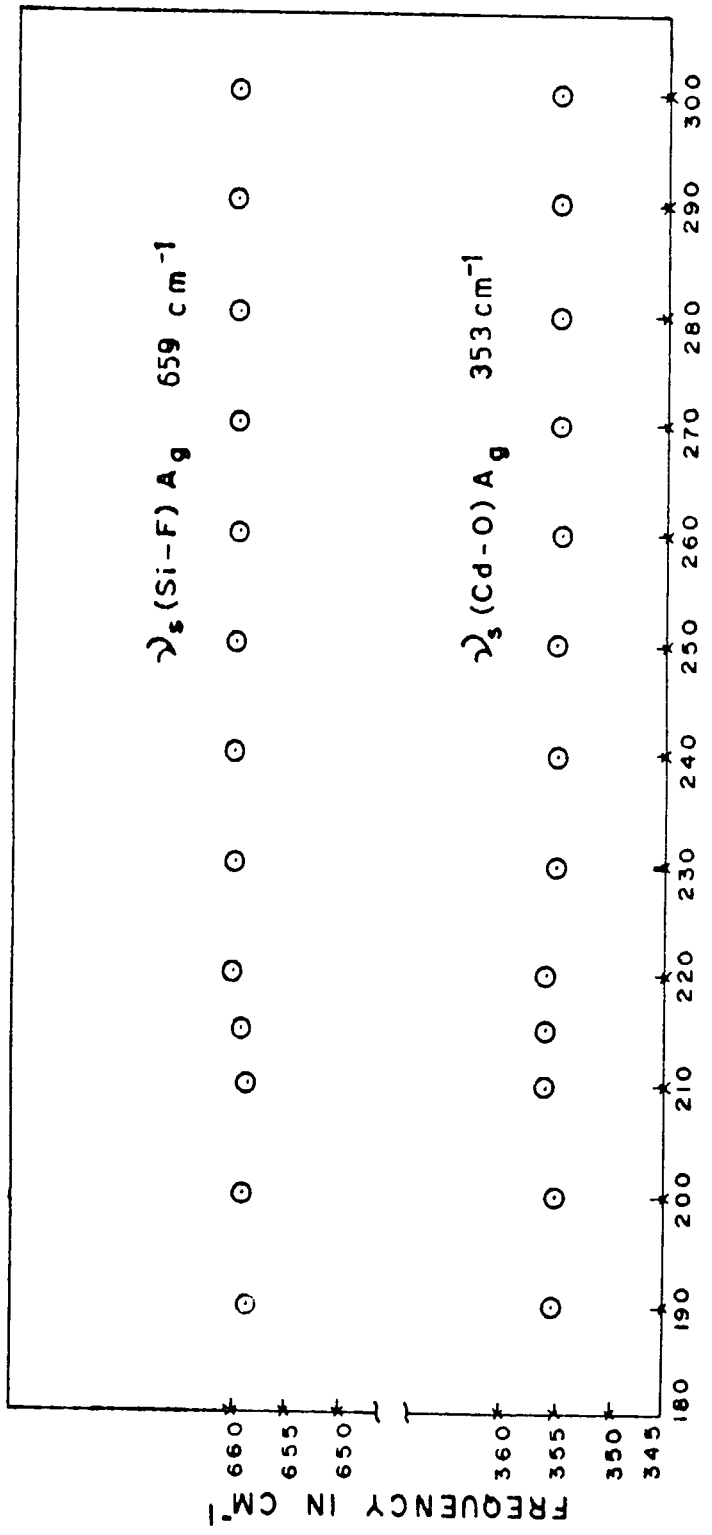

Fig·5·8

Frequency shift of the 353 and 659 cm^{-1} bands as a function of temperature.

CHAPTER VI

C H A P T E R VI

Laser Raman and Phase Transformation Studies of Single Crystals of Deuterated Cadmium Fluoro-Silicate ($CdSiF_6:6D_2O$)

Chapter VI

Laser Raman and Phase Transformation Studies of Single Crystals of Deuterated Cadmium Fluoro-Silicate ($CdSiF_6:6D_2O$)

6.1 Abstract

Laser Raman study of oriented single crystals of $CdSiF_6:6D_2O$ at room temperature as well as at 10k in all the six polarization geometries has been made. A detailed temperature dependent Raman study from room temperature to 10k in the $\{x(yy)z\}$ polarization in the region of internal vibrations and lattice modes has also been made. Abrupt changes as a function of temperature have been observed in frequency shift, line-width and intensity of some of the bands around 235k while some doubly degenerate modes show splitting at this temperature. From these observations, a phase change at about 235k is inferred for this salt. It has been suggested that when the system is cooled the lattice contracts and the water molecules lose their reorientational freedom to some extent resulting in the distortion of the $[Cd(OD_2)_6]^{2+}$ octahedra which may trigger a phase transition.

6.2 Introduction

$CdSiF_6:6H_2O/D_2O$ systems belong to a class of compound of general formula $MXF_6:6H_2O/D_2O$, where M = divalent metal ion and X = Si or Ti. Much effort has been made to understand the mechanism of phase transition in this class of compounds.

When $6H_2O$ is substituted by $6D_2O$ in the compound of the general formula mentioned above, there is a rise in the T_c (critical temperature) in most of the salts, but in case of the Zn-salt there is no change in T_c (182k), but the second critical temperature T_c (217k) is changed to 230k on deuteration. [1,2]. We, therefore, undertook this study to monitor the effect of deuteration on the critical temperature for structural phase transition in case of $CdSiF_6:6H_2O$ replacing H_2O by D_2O and to confirm the assignment of bands in the Raman spectra of the salt. The critical temperatures at which some members of this class of compound show structural phase transition detected by Raman and IR studies are given in Table 1.2 in Chapter I.

We have not found any literature on $CdSiF_6:6H_2O/D_2O$ regarding its phase transition or single crystal study, except that Badachhape et al [3] in 1966 observed two Raman bands (656 cm^{-1} strong and 395 cm^{-1} medium) in the spectra of saturated aqueous solution of $CdSiF_6:6H_2O$. We, therefore, discuss the variable temperature laser Raman studies of the deuterated single crystals of $CdSiF_6:6H_2O$ in this chapter.

6.3 Crystal structure and group theoretical analysis

This class of compounds has two octahedra $[M(OD_2)_6]^{2+}$ and $[XF_6]^{2-}$. These octahedra are arranged in trigonally distorted structure of CsCl type as in the case of

$CdSiF_6:6H_2O$ [4], the details of which have been explained in its hydrated analogue in section 6.2.

The group theoretical analysis has been given in Chapter III for this system. However, we only mention here the total number of Raman bands expected in the spectra if this salt also has the same structure as its hydrated analogue $CdSiF_6:6H_2O$ which belongs to the space group C_{3i}^2 at room temperature [5]. The total number of Raman bands expected is 24 ($12A_g + 12E_g$) counting E_g species as giving only one band.

6.4 Experimental procedure for deuteriation

The single crystals of $CdSiF_6:6D_2O$ were grown by repeated crystallization of the crystals of $CdSiF_6:6H_2O$ dissolved in D_2O in a polythene tube (dia. 1.5 cm and length 5 cm). The procedure of growing single crystals was the same as in case of $CdSiF_6:6H_2O$ salt [6-8] except that the temperature was maintained constant at 28°C in an incubator. The recrystallization was done several times and the IR spectra of the sample were measured in an environment of 50% humidity. The percentage of D_2O was calculated by measuring the ratio of the integrated intensities of the absorption bands of D_2O and H_2O in the IR spectra.

About 95% of the H_2O was replaced by D_2O. The growth of the crystals was like a platlet elongated along the c-axis of the crystal. The platlet looked like a section of a hexagonal pillar through a plane parallel to the c-axis and passing through the 1st and 4th edges of the hexagonal cross-section. From the plate like section a b c d d c b a, the d c b a_1 a_1' b' c' d' edges were

cut by rubbing out the edge a a' so that it became a figure a_1 b b' a'_1 as shown in Figs. 6.1a-b. The cross-section of the resulting figure became a parallelograme whose obtuse angle is 120°. The X, Y and Z axes were chosen as per convention given in ref. [9]

The linearly polarized 4880 and 5145Å Laser Lines from the 'Spectra-Physics' model 165 Argon Ion Laser were used for excitation of the Raman spectra. The scattered light in the 90° scattering geometry was analysed with a SPEX Ramalog Triple Monochromator equipped with a cooled photo-multiplier and a SPEX DATAMATE photon counting device.

The SPEX laser-mate was also used to eliminate any plasma lines from the Raman spectra. An Air Products closed-cycle helium cryo-cooler was used for measuring Raman spectra at lower temperatures.

6.5 Results and discussion

The group theoretical analysis is the same as in the case of the hydrated salt of the system. Therefore both the systems should display nearly similar spectral patterns except for some changes related to the H_2O/D_2O modes.

6.5.1 The room-temperature spectra

The spectral data of single crystals of $CdSiF_6:6D_2O$ at room temperature (290k) are shown in Table 6.1. Under the space group

C_{3i}^2 ,the A_g and E_g species are expected to be present in the Raman spectra in the five-orientations of the crystal, except in the $\{x(zz)y\}$ orientation where only A_g species of the vibrations are expected.

Although 4 Raman bands ($2A_g + 2E_g$) are expected in the lattice mode region, but only one band is observed in the spectrum, as we also got only one band in the case of hydrated salt in the lattice mode region at room temperature under similar experimental conditions. The relative intensities and assignment of bands are given in the Table 6.1. The frequency shift in the Raman bands associated with the lattice modes, δ(O-Cd-O), ν_s(Cd-O) and the symmetry stretch of D_2O molecule have been observed as per expectation on deuteration. There is practically no shift in the Raman bands corresponding to the δ(F-Si-F) ν_{as}(Si-F) and ν_s(Si-F) modes upon deuteration.

In case of deuterated salt $CdSiF_6:6D_2O$, the δ(O-Cd-O) and ν_s(Cd-O) modes are associated with the Raman bands at 171 and 345 cm^{-1} where as in case of hydrated salt the corresponding bands appear at 182 and 353 cm^{-1} respectively.

6.5.2 The low temperature spectra

In order to resolve the closely spaced lines and to compare the spectra of the hydrated and deuterated systems, we recorded the Raman spectra at 10k and found that the lines became sharp and intensities of some of them changed very rapidly. In order to probe the structural changes at low temperature, the Raman

spectra in all the six orientations of the crystal were recorded at 10k. The spectral data is given in the Table 6.2. The polarizations were not sharply distinct except that a few lines were absent in the $\{x(zz)y\}$ polarization geometry. The Raman bands associated with E_g species showed splitting and six bands were observed in the lattice mode region. A Raman band at 268 cm^{-1} corresponding to ν_{as}(Cd-O) appeared at low temperature which was not seen in the room temperature spectra. The deuteriation showed a very clear shift in the librational modes of water molecules from 703 cm^{-1} to 511 cm^{-1} and from 623 cm^{-1} to 453 cm^{-1}. The change in the stretching modes of D_2O molecules was as expected.

The Raman spectra in the $\{x(yy)z\}$ polarization geometries were recorded at different temperatures at the intervals of 10k from room temperature to 10k. Near the phase transition the intervals were narrowed down to 5k. The spectral data is shown in the Table 6.3. The representative spectra at a few selected temperatures are shown in the Fig. 6.2. There is no significant change from 215k to 10k except that broad bands are resolved. The 176 cm^{-1} band at 235k is clearly resolved at 215k. The 81 and 171 cm^{-1} bands show frequency shift between the temperatures 240 and 235k as shown in Fig. 6.3. The broad band associated with the ν(O-D) vibrational modes at room temperature splits into 4 components at 235k, and then into 5 components at 230k. There after down to 10k these components become more and more sharp as shown

in Fig. 6.4. The peak intensities and FWHM of some of the bands at 345, 397 and 600 cm^{-1} showed anomalous changes at about 235k as shown in Figs. 6.5 and 6.6.

The intensity variation with temperature has been plotted in Fig. 6.5 for the temperature near the phase transition. The Raman bands at 345 cm^{-1}, 397 and 660 cm^{-1} change their intensities drastically at the same temperature of 235k. This indicates that there is a change in the structure of the crystal at about 235k.

The full width at half maximum (FWHM) has been plotted against temperature for the same bands at 345, 397 and 600 cm^{-1} in Fig. 6.6. It is found that the change in FWHM occurs for all the three bands at the same temperature. From these observations it is inferred that $CdSiF_6:6D_2O$ undergoes a phase transition at 235k, where as its hydrated analogue ($CdSiF_6:6H_2O$) undergoes a phase transition at 220k. Hence there is a rise in T_c of 15k in the case of the deuterated salt [10].

6.5.3 Temperature dependence of the $2\nu_s$ (O-D) band

We have studied the temperature dependence of the symmetric stretch vibrational band $2\nu_s$ (O-D) which appears at 2567 cm^{-1} at 10k. As the temperature of the crystal is gradually increased from 10k, the intensity of the band decreases gradually upto 235k. After this temperature the intensity of the band decreases very rapidly upto 240k. Thereafter upto room temperature (290k), the intensity decreases gradually. The Raman spectra of the crystal in the 2ν (O-D) region at few selected temperatures are

shown in the Fig. 6.4. There is a sudden discontinuity in the intensity between 235 and 240k indicating a phase transition at about 235k.

The variation of FWHM of the ν_s(O-D) mode of the crystal with temperature is shown in Fig. 6.7. The slit width correction to the FWHM has been made using the formula 5.1 in chapter V The formula provides a fairly accurate value of the true line width because the observed line width of the band was much larger than the slit width even at 10k.

The symmetric stretching band ν_s(O-D) of A_g type appears at 2567 cm^{-1}. This band is not completely isolated. Therefore the graphical (geometrical) method was adopted for its resolution and then its FWHM was measured. The error in the measurement is expected to be $\pm$ 1 cm^{-1}. The half width (FWHM) decreases rapidly below room temperature upto 100k. Below 100k it remains almost constant. The asymptotic value of the $\Delta\nu_{\frac{1}{2}}$ (FWHM) of D_2O band in the crystal at very low temperature is interpreted as the vibrational relaxation-width. The variation of $\Delta\nu_{\frac{1}{2}}$ with temperature was fitted to the Arrhenious type of relation -

$$\Delta\nu_{\frac{1}{2}} = A + B \exp\left[- U/T \right] \qquad \ldots\ (6.1)$$

where A is a constant and incorporates the inelastic decay, inhomogeneous broadening etc. of the ν_s(O-D) mode and the

constant 'B' is related to the inelastic decay of low frequency mode of energy 'U'. It turns out that 'U' is related to activation energy for D_2O reorientation and T is temperature in k.

A good fit to our experimental curve was achieved for $A = 5.62\ cm^{-1}$, $B = 155\ cm^{-1}$ and $U = 480k$ values of the parameters in the Arrhenious type of expression (6.1). We believe that the activation energy of 480k obtained in this case is the energy of the first excited vibrational level of D_2O molecules. The value of 'U' obtained in our case is very nearly equal to the corresponding value obtained in case of water molecules in the $NiSiF_6:6H_2O$ salt, by Jenkins and Lewis [11]. We believe that the anomalous temperature variation of FWHM of the ν_s(O-D) mode is due to a pure vibrational dephasing process caused by elastic scattering of the molecules in the excited vibrational state and some low frequency vibrational state. The thermal activation from a well in the ground state to the first excited state separated by the barrier to D_2O re-orientation would restrict the life-time of the ground state and give rise to a damping of the ν_s(O-D) vibration. The value of the average time between re-orientations of the D_2O molecules at room temperature (290k) has been obtained from the following relation considering the spectral band shape as a Lorentzian -

$$\tau = \frac{1}{\pi c \Delta\nu_{\frac{1}{2}}} \qquad \ldots \quad (6.2)$$

where τ = average time

c = velocity of light

$\Delta\nu_{\frac{1}{2}}$ = half width

The average time calculated is 3.013×10^{-13} seconds. This reorientation time is again very similar to the reorientation time of water molecules at room temperature found in the $NiSiF_6:6H_2O$ salt [11].

6.5.4 Structural phase transformation

The changes and discontinuities observed in the frequency shift, intensity and half-width of many bands at 235k are typical characteristics of a first order type phase transformation involving ordering of the ions. The FWHM of most of the bands associated with the $(SiF_6)^{2-}$ ion is 20-22 cm^{-1} at room temperature while that associated with the ν (Cd-O) and δ (O-Cd-O) modes is 30 cm^{-1} indicating a larger disorder of the cations compared to those of anions in the lattice. The ν (O-D) modes show only two broad features associated with the symmetric and asymmetric stretch and no librational modes related to D_2O molecules are detected at room temperature. This indicates that the D_2O molecules are almost freely reorienting in the lattice and all the six molecules are equivalent at room temperature. However, at temperature below 50k, the two broad bands associated with the ν (O-D) vibrational modes split into six components and one low frequency band related to D_2O librational mode also appears. These observations indicate that the D_2O molecules become ordered

only well below T_c, the equivalence of the six D_2O molecules in the $[Cd(OD_2)_6]^{2+}$ octahedra is destroyed and at least three different types of D_2O units can be inferred.

On the other hand, there is only a small and gradual change in the vibrational modes associated with the $(SiF_6)^{2-}$ octahedra as a function of temperature. It is therefore clear that the phase transition in this system is triggered by distortions in the geometry of $[Cd(OD_2)_6]^{2+}$ ions. The appearance of more bands in the lattice mode region and splitting of most of the E_g modes into two components suggest disappearance of three-fold axis and lowering of symmetry of the system to the stage where there are no degenerate modes in the system.

6.5.5 Structure of the low temperature phase

In lieu of X-ray or neutron diffraction data on the crystal structure of this salt, it is not possible to say much about its space group at low temperature below the critical point from the Raman polarization measurements alone. From the above discussion in section 6.5.3, it is obvious that the space group must be lower than C_{3i} having no degenerate representations. The crystal systems having lower symmetry than the trigonal or hexagonal are orthorhombic and mono-clinic. In the orthorhombic series, there are only three groups D_2, C_2 and D_{2h}. None of these is either a sub-group of the possible high temperature prototypic parent phase of space group D_{3d} or a sub-group of room temperature symmetry C_{3i} of the system. Therefore it is unlikely that the low temperature

phase corresponds to the orthorhombic system. In the mono-clinic system, there are three groups C_2, C_s and C_{2h}. By similar arguments, the C_2 and C_s space groups can be eliminated as they are also not the sub-groups of either D_{3d} or of C_{3i}. The remaining possibility is that the system belongs to the C_{2h} space group which is a sub-group of the prototypic phase having the D_{3d} space group. Independent support for the mono-clinic series is provided by our polarization measurements at 10k. The symmetric stretching mode ν_s(Si-F) appears in the (zx) polarization geometry with medium intensity at 10k which is forbidden under any point group within the orthorhombic system but it can appear in the mono-clinic series.

From a comparison of the vibrational pattern of $CdSiF_6:6D_2O$ with other systems ($NiSiF_6:6D_2O$) in this series, we find that there is no structural phase transition in the $NiSiF_6:6D_2O$ system and we observe only one band at room temperature and at 10k in the ν(O-D) stretch vibrational region [1,11, 12].

A comparison of the Raman bands of the systems is shown in the Table 6.4. In case of $MgSiF_6:6H_2O$, six bands are observed in the ν(O-H) vibrational region at 15k [13] which undergoes a structural phase transition at 298k to the C_{2h}^5 space group, well characterized by X-ray and vibrational studies [14]. Our experimental data are consistent with the C_{2h} space group for the

low temperature phase of $CdSiF_6:6D_2O$. We therefore suggest that the low temperature space group of this system is C_{2h}.

6.6 References

[1] Poulet H and Mathieu J, C.R. Acad. Sc. Paris, t-286(12) Series B, 331 (1978).

[2] Bose M, Roy K and Ghoshray A, Proc. Nucl. Phys. and Solid State Phys. Vol 24C, pp. 389, Dec. 28 (1983) BARC, Bombay.

[3] Badachhape R B, Hunter G, McCory L D and Margrave J L, Inorg. Chem., 5(5), 929 (1966).

[4] Wyckoff R W G, "Crystal Structure" Vol. 3, 2nd ed. Wiley Interscience (1965).

[5] Hamilton W C, Acta Crystallogr. 15, 353 (1962).

[6] Thakur G, Proc. Symp. on "Crystal Growth" Dec. 24 (1983) Anna Univ. Madras.

[7] Thakur G and Verma A L, J. Raman Spectrosc. 17, 207 (1986).

[8] Thakur G and Verma A L, J. Raman Spectrosc. 20, 000 (1989).

[9] Turrell G, "Infrared and Raman Spectra of Crystals", Appendix F, Academic Press, London and New York (1972).

[10] Thakur G and Verma A L, Proc. DAE Symp. Vol 27C, pp. 282, Dec. 23-25 (1984), BARC, Bombay.

[11] Jenkins T E and Lewis J, Physica Scripta 18, 351 (1978).

[12] Rubins R S and Haghighatjou T, J. Phys. Chem. Solids 43 491 (1982).

[13] Jenkins T E and Lewis J, Spectrochim Acta 37A, 47 (1981).

[14] Jehanno G and Varret F, Acta Crystallogr. A31, 857 (1975).

Table 6.1

Raman bands in cm^{-1} observed in different polarization geometries at room temperature (20°c). ($CdSiF_6:6D_2O$)

y(xx)z	x(yy)z	x(yx)z	x(zy)z	x(zx)z	x(zz)y	Assignment
81m	81m	81m	80w	80m	-	Lattice mode (A_g, E_g)
171m	171m	172m	171w	171w	166m	(A_g, E_g) δ(O-Cd-O)
345s	345s	345m	-	-	345m	A_g, ν_s(Cd-O)
397m	397m	397m	399vw	398vw	400s	δ(F-Si-F), (A_g, E_g)
453w	453w	453vw	453vvw	453vvw	-	E_g, ν_{as}(Si-F)
660vs	660vs	660m	660vw	660vw	660vs	A_g, ν_s(Si-F)
2565s	2565s	2565m	2565w	2567w	2571s	ν(D-O), (A_g, E_g)

vs = very strong;
s = strong;
m = medium;
w = weak;
vw = very weak;
vvw = very very weak;
b = broad;
sh = shoulder;
ms = medium strong;
sp = sharp.

Table 6.2

Spectral data of $CdSiF_6:6D_2O$ at 10K in different polarization geometries

{y(xx)z}	{x(yy)z}	{x(yx)z}	{x(zy)z}	{x(zx)z}	{x(zz)y}	Assignment
1	2	3	4	5	6	7
63w	63w	63w	-	-	-	
77w	77w	77w	77m	77m	-	
88vw	88vw	-	-	-	88vvw	Lattice mode
102ms	102ms	102ms	102m	102m	102vw	
111s	111s	111m	110vw	111vw	111s	
130vw	130vw	130vvw	-	-	130vw	
162s	162s	162m	162m	162m	162vs	δ (O-Cd-O)
190ms	190ms	190ms	190m	190m	-	
268vw	268vw	268vvw	268vvw	-	268vw	ν_{as} (Cd-O)
338s	338s	338ms	338m	338m	338s	ν_s (Cd-O)
391ms	391ms	391ms	391ms	391ms	391s	δ (F-Si-F)
-	410vvw	-	-	410vvw	-	
424w	424w	424vw	424vw	-	-	
-	-	-	-	-	443vw	
447m	447m	447m	447vw	447vw	-	ν_{as} (Si-F)
468vw	468vw	468vw	-	-	468vw	

Table 6.2 continued...

Table 6.2 continued

1	2	3	4	5	6	7
653vs	653vs	653s	653m	653m	653vs	ν_s (Si-F)
-	-	-	350vvw	350vvw	-	D_2O
410vvw	-	-	409vvw	410vvw	-	
-	511vw	-	-	-	453vvw	Libration
2544m	2544m	2544m	2544w	2544w	-	
2567vs	2567vs	2567vs	2562m	2562m	2567vs	
2581s	2581s	2581s	2581m	2581m	2581vvs	δ (D-O)
2601m	2601m	2601w	2601w	2601m	-	
2619s	2619s	2619s	2619m	-	2619s	
-	2631w	-	2630vw	-	-	

Table 6.3

Spectral data of $CdSiF_6:6D_2O$ at selected temperatures in the $\{x(yy)z\}$ orientation

(Frequency in cm^{-1} and temp. in K)

270	240	235	230	225	215	220	50	10	Assignment
1	2	3	4	5	6	7	8	9	10
81m	81m	87m	87m	87m	87m	87m	63w 77w 88vw 102s 111ms 130vw	63w 77w 88vw 102s 111ms 130vw	Lattice mode
171m	171m	176m,b	176m,b	176m,b	171m 184m	171m 183m	162s 190ms	162s 190ms	δ (O-Cd-O)
-	-	-	-	-	-	-	-	268vw	ν_{as} (Cd-O)
345s	346s	346s	345s	345s	345s	345s	338s	338s	ν_s (Cd-O)
397m	399m	398m,b	398m,b	399m,b	399m,b	399m	391ms 410vvw 424w	391ms 410vvw 424w	δ (F-Si-F)

Table 6.3 continued...

Table 6.3 continued

1	2	3	4	5	6	7	8	9	10
453w	453w	452vw,b	452vw,b	452vw,b	452vw,b	452vw,b	447m 468vw	447m 468vw	ν_{as} (Si-F)
659vs	660vs	660vs	659vs	658vs	658vs	658vs	653vs	653vs	ν_{s} (Si-F)
							511vw	511vw	D_2O Libration
–	–	–	2550sh	2550sh	2550sh	2550sh	2544m	2544m	
2567m	2567m	2567vs	2567vs	2567vs	2567vs	2567vs	2567vs	2567vs	
2638vw	2637vw	2585sh	2585sh	2585	2585	2585s	2581s	2581s	ν (D-O)
–	–	2601sh	2600sh,sp	2600	2600	2600	2601m	2601m	
–	–	2619sh,sp	2617sh,sp	2617	2617	2617	2619s	2619s	
–	–			–	–	–	–	2631w	

Table 6.4

Comparison of Raman bands of different members of the general formula $MSiF_6:6(H_2O/D_2O)$

	$Mg(OH_2)_6SiF_6$		$Fe(OH_2)_6SiF_6$		$Zn(OH_2)_6SiF_6$		$Ni(OH_2)_6SiF_6$		$Ni(OD_2)_6SiF_6$		$Cd(OH_2)_6SiF_6$		$Cd(OD_2)_6SiF_6$	
	300K	15K	300K	15K	300K	15K	300K	15K	300K	10K	300K	10K	300K	10K
1	2		3		4		5		6		7		8	
Lattice modes	44	41	27	18 36	27	-	27	38	-	38	48	48 64	-	63
	82	75	63	68 73	-	66	66	68	-	68	-	83 93	-	77 88
	-	-	-	78 83	80	89	90	94	81	94	88	108 117	81	102
	113	101	102	107 118	114	130	137	138	120	130	-	137 147	-	111 130
δ (O-M-D)	200 220	200 224	187 198	210 231	209 216	207 228	- 220	215 235	- 207	203 225	182 -	201 -	171 -	162 190
ν_{as} (M-O)	300	300	300	296	-	278	300	305	300	300	-	273	-	268
ν_s (M-O)	377	374	380	379	384	380	405	405	382	380	353	348	345	338 391
∂ (F-Si-F)	- 402	392 400	- 405	389 400	410	401	395	391	405	405	397	391	397	410 424

Table 6.4 continued..

Table 6.4 continued

1	2		3		4		5		6		7		8	
ν_{as} (Si-F)	465	467	462	462	462	462	457	460	460	457	457	468	453	447 468
ν_{s} (Si-F)	655	654	651	651	658	658	661	661	661	661	659	653	659	653
ν (H-O)/(D-O)	-	3491										3469	-	-
		3493				3461						3510	-	2544
	3504	3502		3527	3514	3501		3500			3505	3524	2567	2567
	-	3530	3530	3535	-	3519	3518	3518	2560	2560		3540		2581
	-	3533			3493	3533						3557	2638	2601
	3540	3542											-	2619
	-	3559												2631

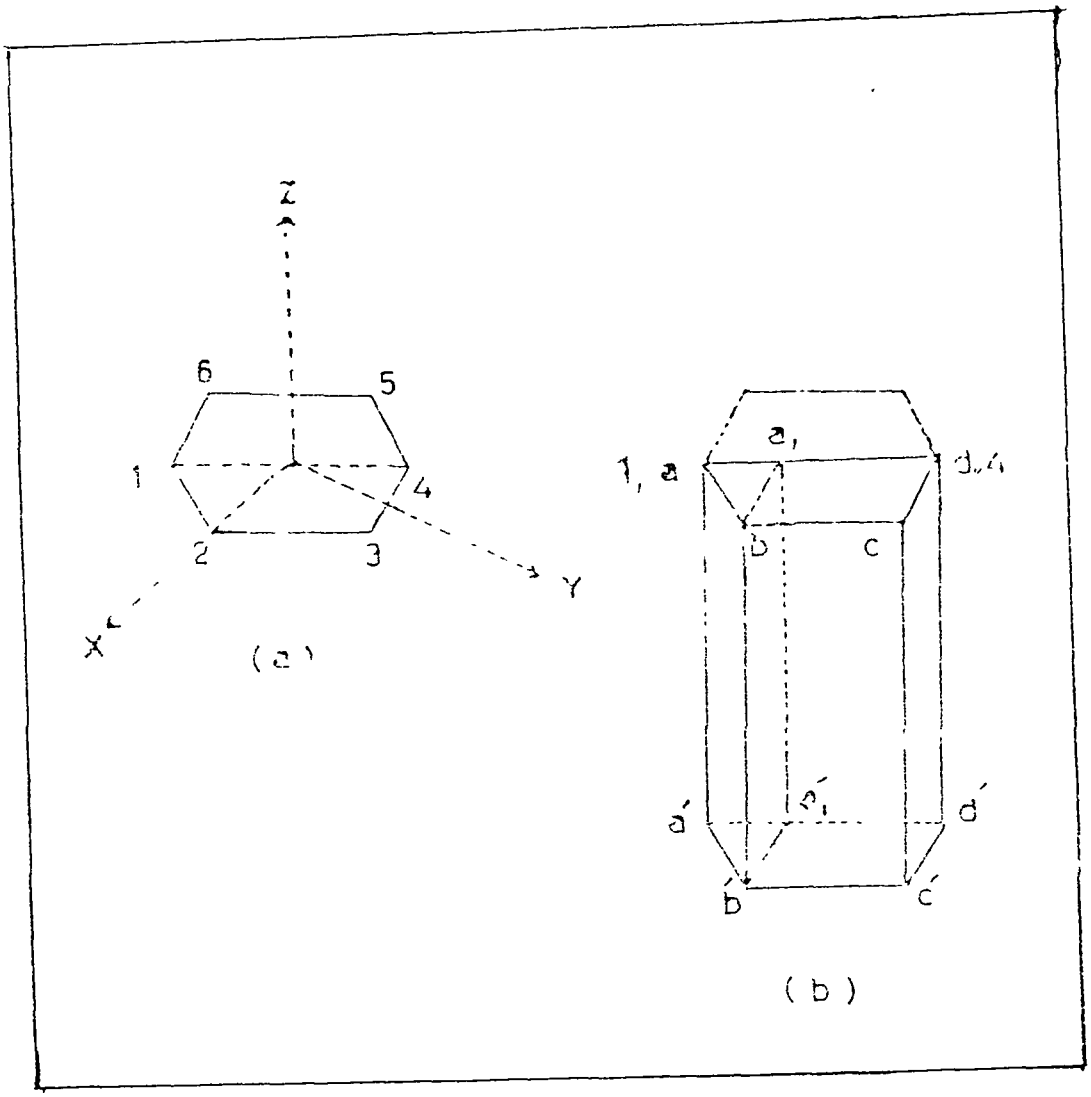

Fig. 6.1

(a) The cross-section of the hexagonal pillar of a crystal of $CdSiF_6:6(H_2O/D_2O)$. The edges are marked as 1,2,3,4,5 and 6. The z-axis is perpendicular to the plane of the paper.

(b) The vertical section cut by a plane passing through the z-axis and the 1 and 4 edges of the hexagonal pillar.

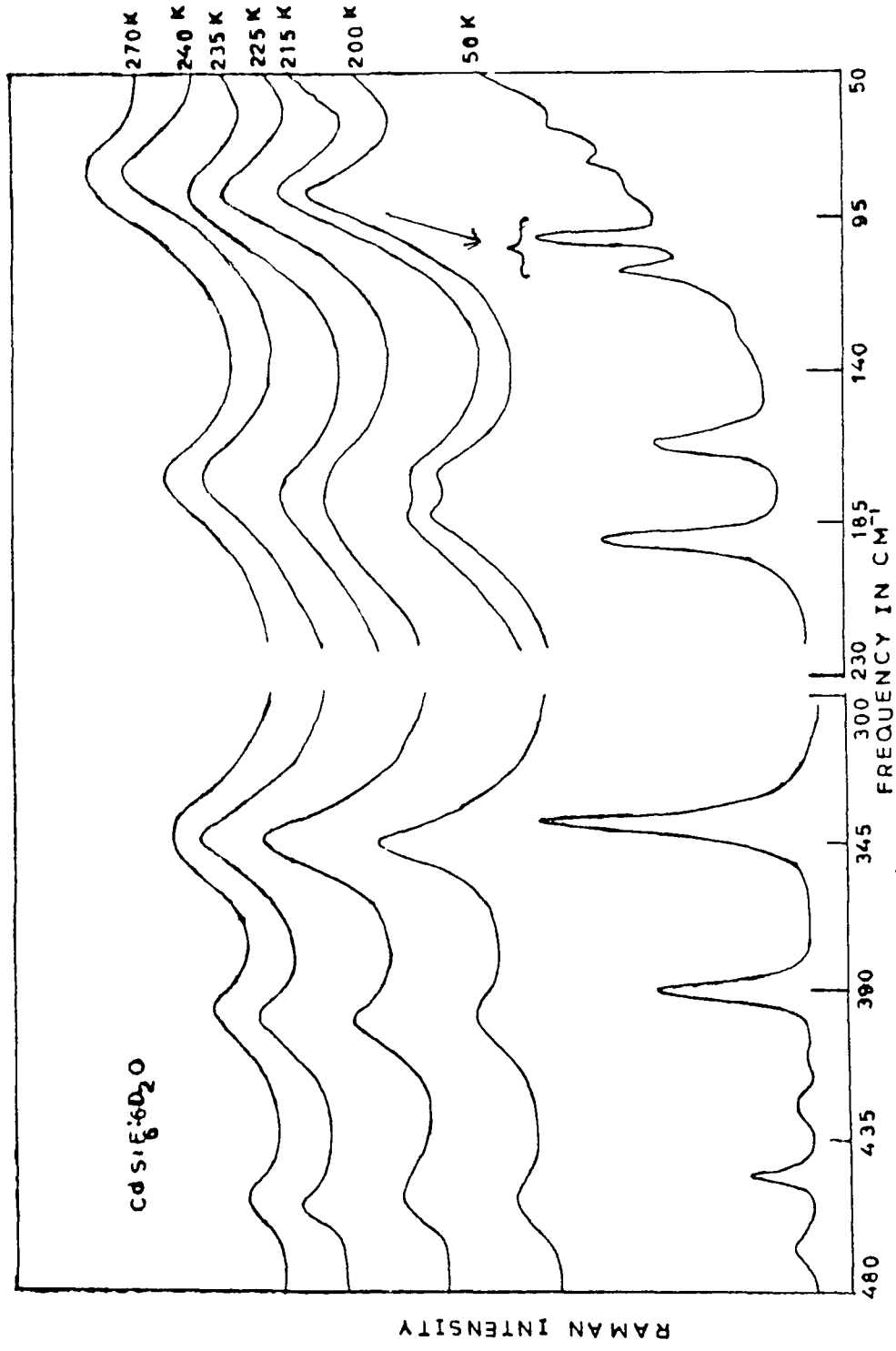

Fig·6·2

Raman spectra of $CdSiF_6:6D_2O$ in the $\{x(yy)z\}$ polarization geometry at a few selected temperatures. Only 50-230 cm^{-1} and 300-480 cm^{-1} parts of the spectra are shown

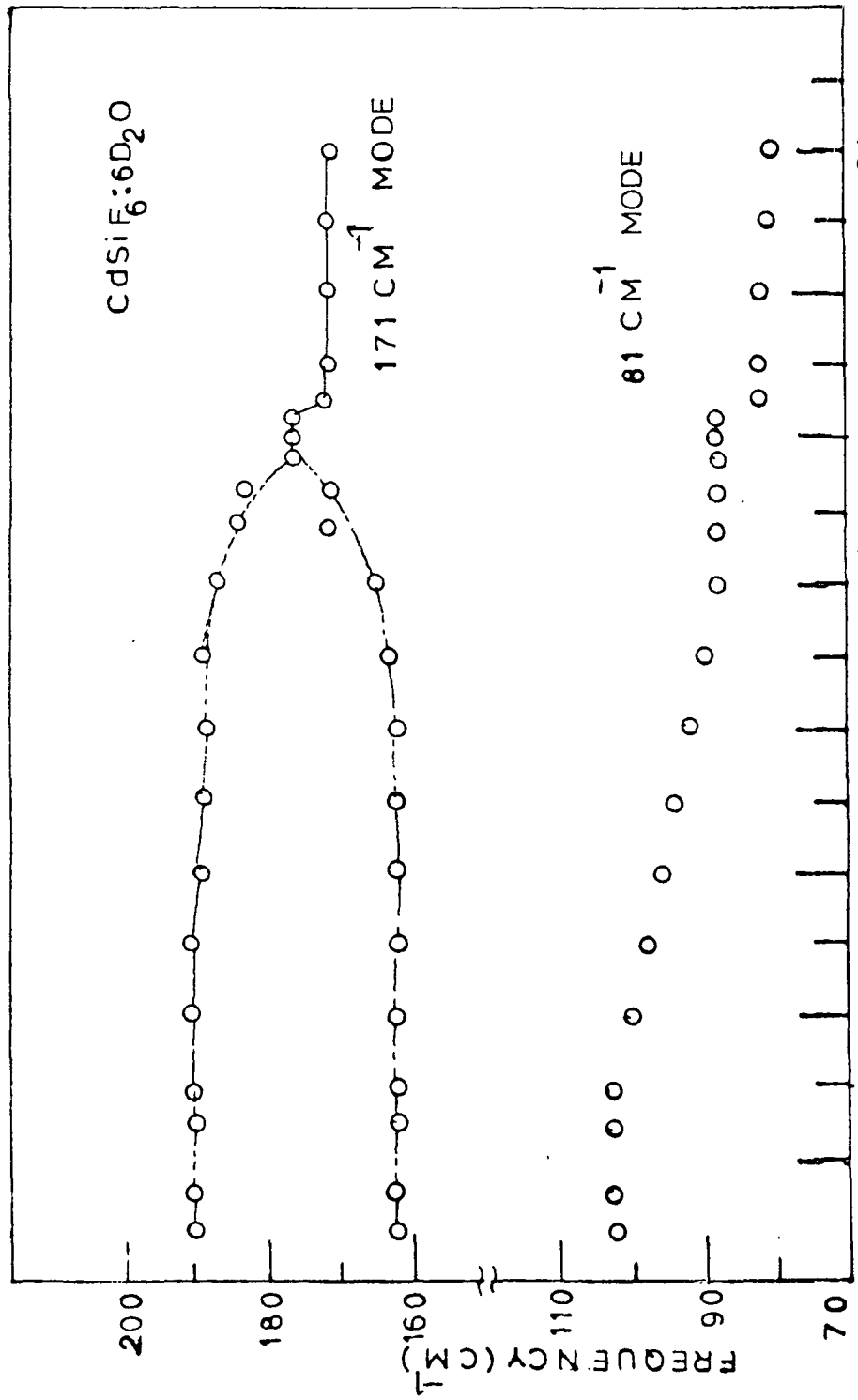

Fig. 6-3

Variation of frequency with temperature of the 81 and 171 cm^{-1} bands. The plots show a clear enhancement of frequencies around 235k.

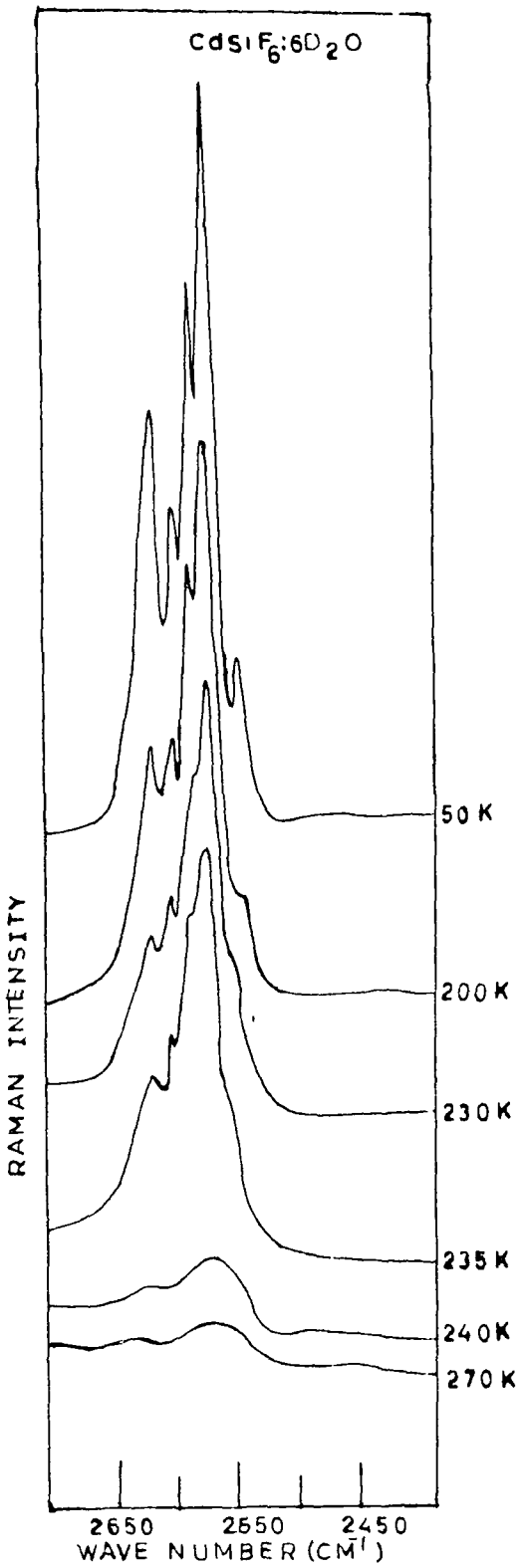

Fig. 6.4

Raman spectra of $CdSiF_6 \cdot 6D_2O$ in the ν_3(O-D) stretching region in the $\{x(yy)z\}$ orientation of the crystal at a few selected temperatures.

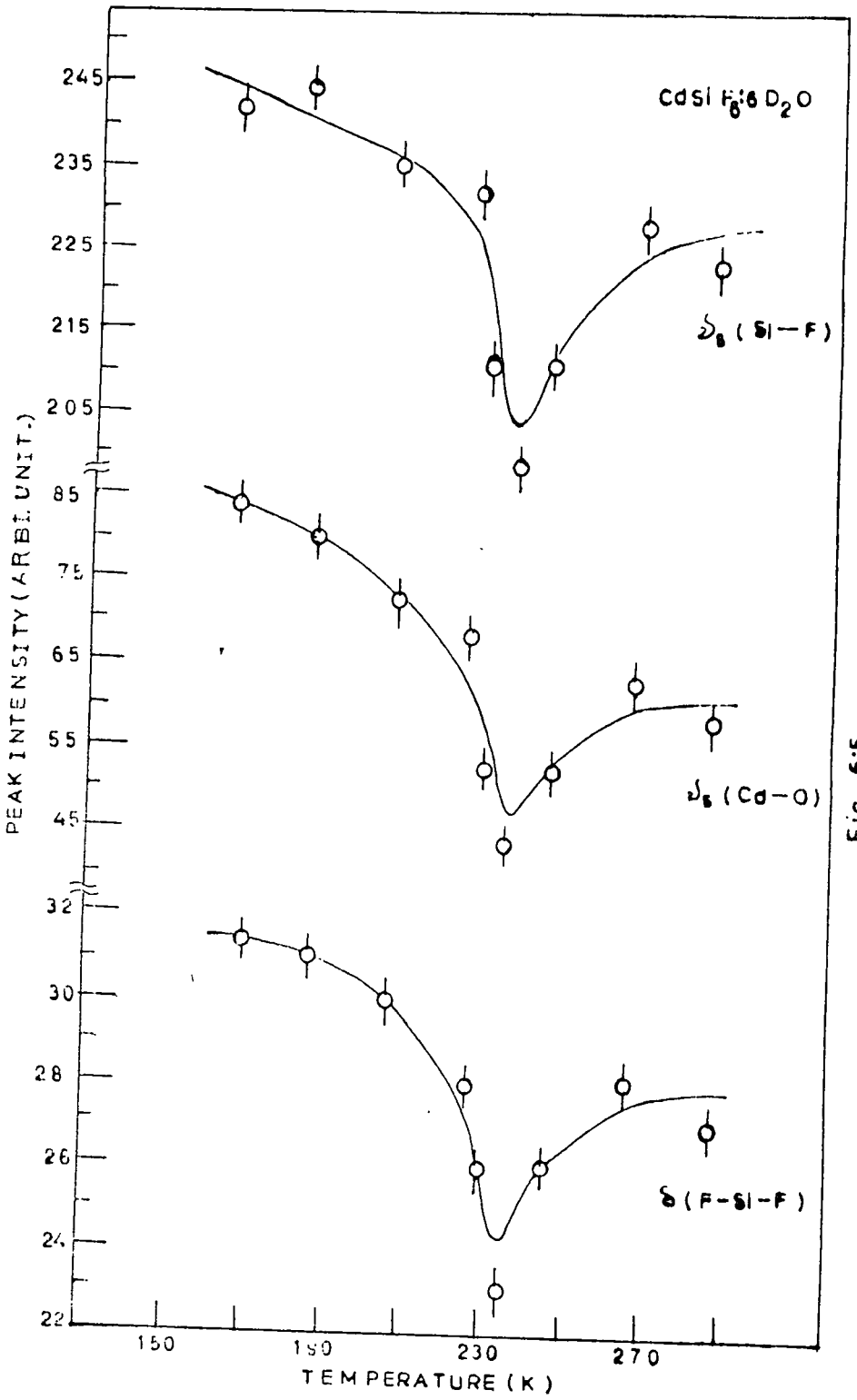

Fig. 6·5

Fig. 6·5

Variation of peak intensity with temperature of a few selected Raman bands of the crystal [ν_s (Si-F) at 660, ν_s (Cd-O) at 345 and (F-Si-F) at 397 cm^{-1}]

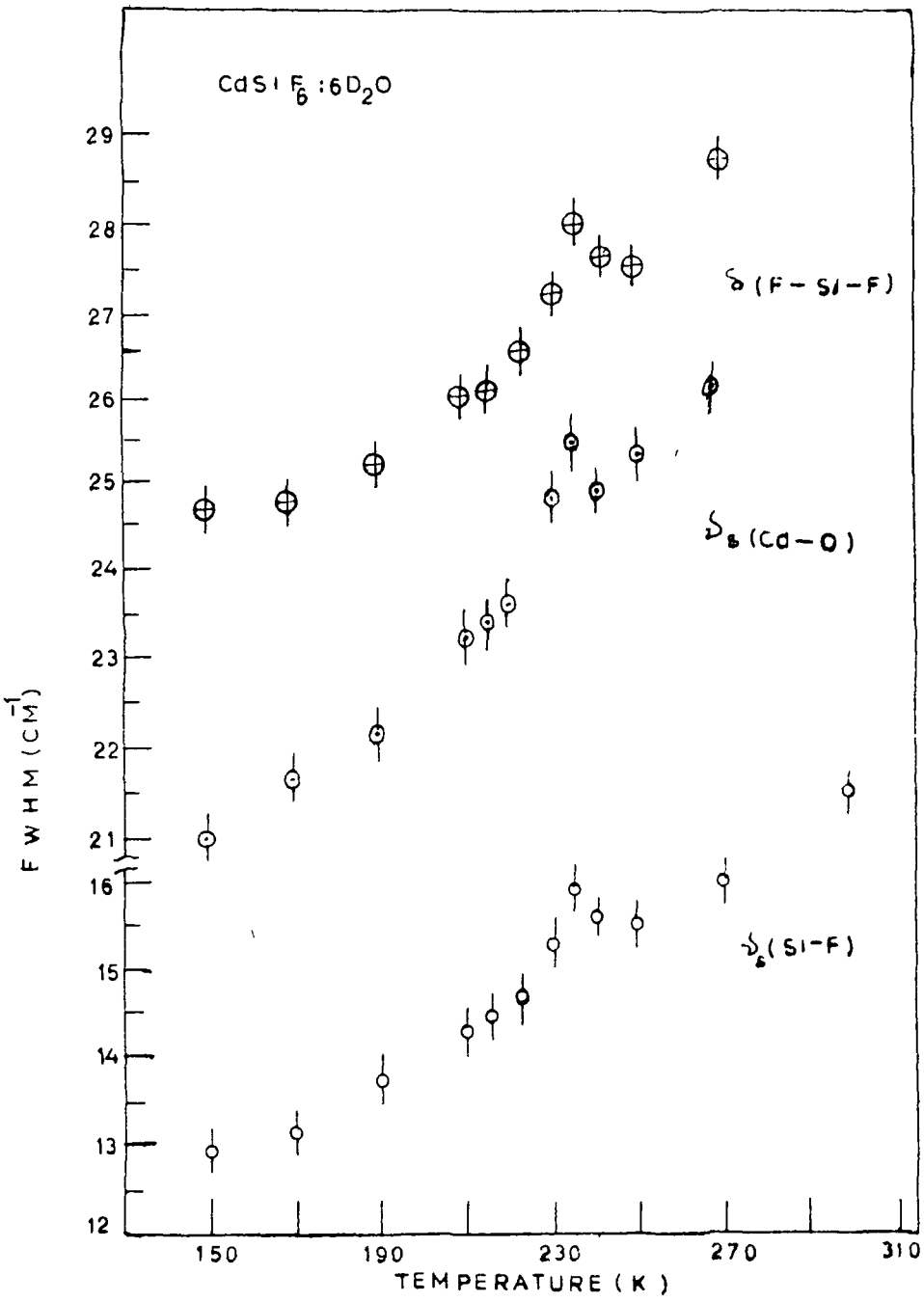

Fig. 6·6

Variation of full width at half maximum (FWHM) with temperature of a few isolated bands after slit width correction.

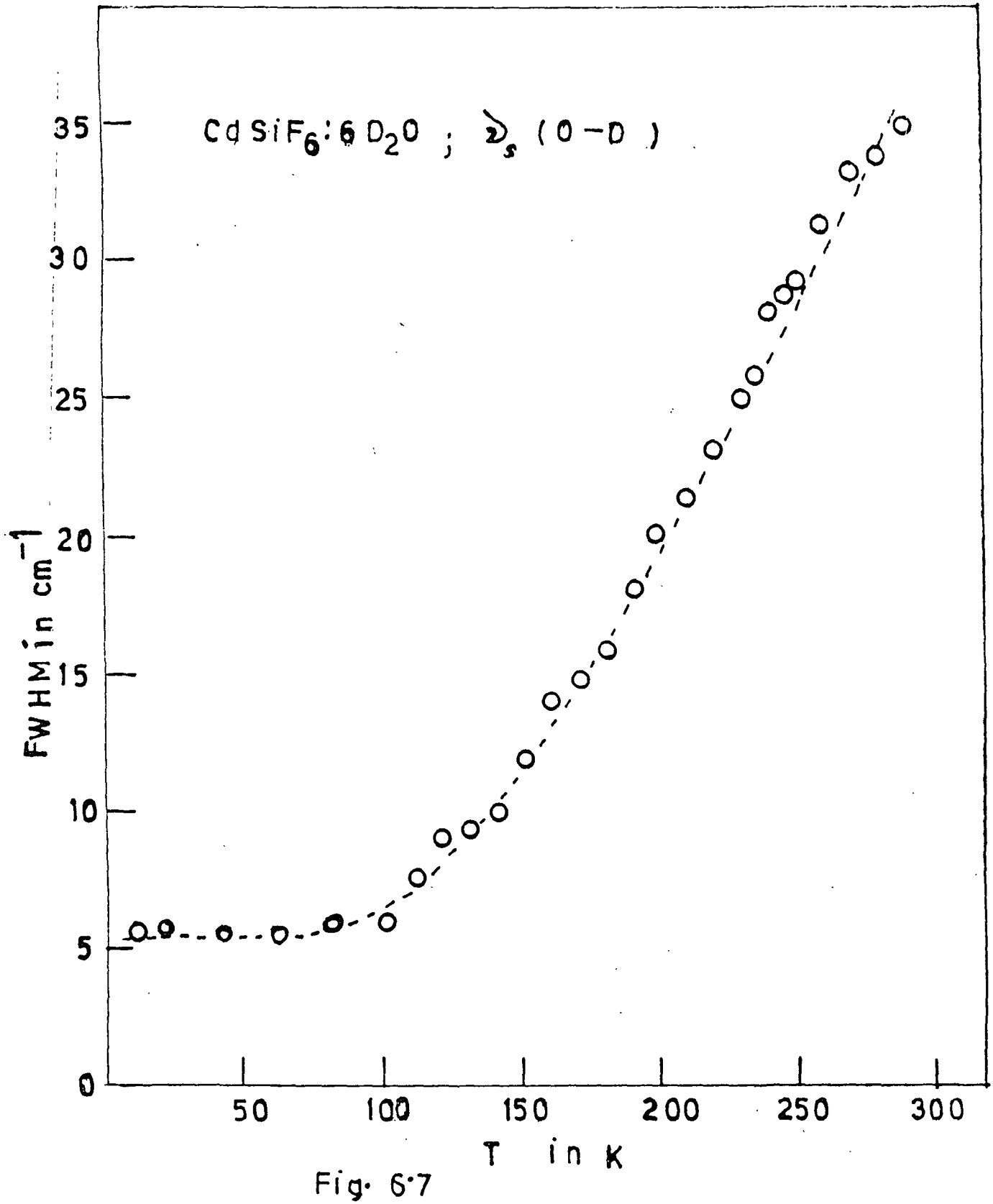

Fig. 6·7

Variation of FWHM ($\Delta\nu_{\frac{1}{2}}$) with temperature of ν_s(O-D) band. The dashed line is a fit to the expression

$\Delta\nu_{\frac{1}{2}} = 5.62 + 155 \exp[-U/T]$ with u = 480k.

CHAPTER VII

C H A P T E R VII

Temperature Dependent Raman and Phase Transition Studies of Single Crystals of Deuterated Cadmium Fluoro-titanate

Temperature-Dependent Raman and Phase Transition Studies of Single Crystals of Deuterated Cadmium Fluoro-Titanate ($CdTiF_6:6D_2O$)

7.1 Abstract

A detailed temperature-dependent Raman study of oriented single crystals of deuterated cadmium fluoro titanate ($CdTiF_6:6D_2O$) has been made in the region of internal vibrations and lattice modes. The Raman spectra have been measured from 10k to room temperature (290k) in the $\{x(yy)z\}$ polarization geometry. Changes have been observed in the frequency shift, line width and intensity of some of the bands at about 218k and 110k. Some doubly degenerate modes show splittings at low temperature. These studies suggest that $CdTiF_6:6D_2O$ undergoes two structural phase transitions at 218k and 110k. Hence a rise of 18 and 30k in the high and low temperature phase transitions is observed in case of the deuterated analogue compared to the hydrated (hydrogenated) salt ($CdTiF_6:6H_2O$).

7.2 Introduction

$CdTiF_6:6D_2O$, cadmium fluoro titanate hexa deuterated (here after called CFTHD for convenience) is a deuterated analogue of the salt $CdTiF_6:6H_2O$ (we called it CFTH for convenience in Chapter IV) which undergoes two structural phase transitions - one at 200k and the other at comparatively low temperature 80k [1]. The other members of the systems of general formula $MXF_6:6H_2O/D_2O$ (where M = divalent metal and X = Ti) also undergo phase transi-

tions, i.e. $NiTiF_6:6H_2O$ and $CoTiF_6:6H_2O$ show phase transitions at 120 and 244K respectively [2,3]. Two phase transitions have been detected in $ZnTiF_6:6H_2O$ - one at 217k and the other at 182k [4]. Moreover, when H_2O is replaced by D_2O in the complexes of the general formula mentioned above, there is a rise in T_c (critical temperature) in most of the members of the systems but in case of Zn-salt of the system, there is no change in the T_c for the 182k transition, but the T_c corresponding to the 217k transition changes to 230k on deuteration [4,5]. We have not found much literature on $CdTiF_6:6(H_2O/D_2O)$ regarding its phase transition or single crystal study except Petrakovskaya E A et al [6] in 1984 reported the EPR spectra of CFTH ($CdTiF_6:6H_2O$) doped with MnF_2 at 77k and reported a phase transition at 139k. The critical temperatures at which some members of this class of compounds show structural phase transitions detected by various techniques are shown in Table A1 in the Appendix. In this chapter we shall deal with Laser Raman study of the deuterated single crystals of cadmium fluoro-titanate (CFTHD) with a view to gain some insight about the mechanism of phase transition in these systems.

7.3 Crystal structure and group theoretical analysis

Most of the members of the series of the general formula mentioned in section 7.2 have space group R $\bar{3}$ (C_{3i}^2) whereas a few of them belong to space group R $\bar{3}$m (D_{3d}^5) at room temperature [7] No structural data are available for CFTH or for CFTHD in the

literature to our knowledge. The crystal structure data for the $ZnSiF_6:6H_2O$ mentioned in section 2.5.1 of chapter II show that the system has a unimolecular rhombohedral unit cell of space group R $\bar{3}$ (C_{3i}^2). We can start from the assumption that the CFTH is isostructural with the $ZnSiF_6:6H_2O$ system (as we assumed in Chapter IV) and may belong to either the R $\bar{3}$ or the R $\bar{3}$m space group because most of the members of the general formula belong to a rhomobohedral system. On this assumption group theoretical predictions can be made and compared with the experimental observations based on both space groups and then it can be seen which space group can explain the experimental data correctly. The Figs. 3.1 (a,b,c) in chapter III illustrate the possible structure of CFTH.

The detailed group theoretical analysis has been given in chapter III for this system also. However, we only mention here the total number of Raman bands expected in the spectra. If the system belongs to C_{3i}^2 space group the total number of Raman bands expected is 24 and if the system belongs to the space group D_{3d}^5, the total number of expected Raman bands would be 17. Experimentally it is sometimes difficult to observe all the bands at room temperature[1].

7.4 Experimental procedure

The single crystals of $CdTiF_6:6D_2O$ (CFTHD) were grown from the D_2O solution. The $CdTiF_6:6H_2O$ (CFTH) crystals were dissolved in D_2O in the dehumidified room, and repeated crystallization in D_2O was done. The details for the growth of single crystals of the

salt CFTHD were similar as in the case of $CdSiF_6:6D_2O$ crystals (section 6.3 in chapter VI). The crystals were cut and polished for Raman measurements in the same manner as in case of $CdSiF_6:6D_2O$ crystals [8]. The details of the experimental procedure for measuring Raman spectra are given in chapter II, section 2.6.1 to 2.6.4 [1].

7.5 Results and discussion

The Raman spectra of CFTHD were measured at room temperature (290k) in all the six polarization geometries using 4880 and 5145Å laser lines. The laser power at the sample was kept less than 200 mW to avoid burning of the crystals. The spectra of CFTHD were also measured at various low temperatures upto 10k in the $\{x(yy)z\}$ polarization geometry. Moreover, the Raman spectra were also measured in all the six polarization geometries at 10k.

7.5.1. Room temperature spectra

The Raman spectra of CFTHD were recorded in all the six polarization geometries at room temperature as stated in the above section 7.5. The spectral data of the salt is given in Table 7.1 while Fig. 7.1 shows the Raman spectra at room temperature. Under the space group C_{3i} the A_g and E_g species of the vibrations are expected to be present in all the five orientations of the crystal except in the $\{x(zz)y\}$ orientation where only A_g species of the vibrations are expected to be present. We observed one band at 80 cm^{-1} in the lattice mode region although 4 Raman bands

$(2A_g + 2E_g)$ are expected in the lattice mode region. We also got only one band in case of $CdSiF_6:6D_2O$ in the lattice mode region at room temperature [8]. The spectrum of CFTHD resembles very closely with that of its hydrated (hydrogeneted) analogue CFTH except for some shifts in the position of few bands. Therefore we have taken C_{3i}^2 as the space group of the CFTHD crystal at room temperature in analogy with that of the hydrogeneted system [9]. The relative intensities and assignment of the observed bands are given in Table 7.1. The band at 80 cm^{-1} in the lattice region is of E_g species because it does not appear in the $\{x(zz)y\}$ orientation. There is practically no shift in this band on deuteration and so we associate this band with the libration mode of $[TiF_6]^{2-}$ ion. The next band of medium intensity appears at 166 cm^{-1}. There is a corresponding band at 176 cm^{-1} (medium intensity) in the hydrated analogue CFTH, because the ratio of frequencies of δ(O-Cd-O) of of CFTH and δ(O-Cd-O) of CFTHD is 1.062 which is consistent with the same ratio in case of Zn, Mn and Ni salts and their deuterated analogues in these systems [10,11]. We do not prefer to associate the 166 cm^{-1} band with the 172 cm^{-1} band in the spectrum of CFTH, because the 172 cm^{-1} band is extremely weak and their frequency ratio also does not agree with the expected ratio of 1.06. The next strong band is at 256 cm^{-1} in the spectrum of CFTHD and is assigned as ν_{as}(Cd-O). It is of E_g species and corresponds to the 265 cm^{-1} band in case of its hydrogenated analogue. The ratio of the frequencies bears an acceptable value of 1.03. In case of $CdSiF_6:6H_2O$

and its deuterated analogue the corresponding ratio is also 1.03 [8]. The 297 cm^{-1} band of CFTHD is assigned as deformation mode δ(F-Ti-F) of $[TiF_6]^{2-}$ octahedra, because practically there is no shift in this band on deuteration. It has $(A_g + E_g)$ symmetries. The medium intensity band at 343 cm^{-1} is assigned as ν_s(Cd-O). It is of A_g species and the ratio of ν_s(Cd-O)(H_2O) to ν_s(Cd-O)(D_2O) is 1.032 which agrees well with the same ratio in cases of Zn,Mn-fluoro titanates [10] and Cd-fluoro silicate [8]. The band at 613 cm^{-1} is the symmetric stretching mode of the $[TiF_6]^{2-}$ octahedra. Practically there is no shift in this band from its hydrogeneted salt. The medium intensity bands at 2536 and 2556 cm^{-1} are due to symmetric and asymmetric stretching modes of D_2O. The ratio of frequencies of this mode to its corresponding hydrogeneted salt is found to be 1.37 which is acceptable.

7.5.2 Low temperature spectra

In order to resolve the closely spaced lines, we recorded the Raman spectra at 10k, as in case of its hydrogeneted salt. We found that the lines became sharp and intensities of some of the bands (lines) increased very rapidly and indicated strong temperature dependence. The D_2O stretching modes became clearly resolved. In order to get information about possible change in the T_c and in the structure of the crystal, the spectra at different low temperatures and at 10k in all the six orientations were recorded. Figs. 7.2 and 7.3 give the spectra at different temperatures. At 10k some additional bands appear which were not observed at room temperature.

The spectra were compared with its hydrogeneted analogue at 10k in all the six polarization geometries. The spectral data are given in Table 7.2. In the lattice mode region, there are six bands in the Raman spectra of CFTH but only five bands were observed in case of CFTHD. The bands at 80 and 98 cm^{-1} of very weak and medium strong intensities respectively in case of CFTHD.

A clear shift of 3 and 5 cm^{-1} in these bands is observed on deuteration of the sample. The ratio of these bands of hydrogeneted and deuteriated samples is 1.053 in the lattice mode region. This is slightly less than the ratio of 1.08 in case of CFSH ($CdSiF_6:6H_2O$) and NFSH ($NiSiF_6:6H_2O$) for the similar bands [8]. We, therefore, assign the 77 and 93 cm^{-1} bands as libration modes of $[Cd(OD_2)_6]^{2+}$ ions. The 69 cm^{-1} band which corresponds to 68 cm^{-1} band of CFTH is assigned as the libration mode of $[TiF_6]^{2-}$ ions. The strong band at 172 cm^{-1} and weak band at 165 cm^{-1} correspond to 171 and 182 cm^{-1} bands respectively of CFTH. These bands are assigned as δ(O-Cd-O) modes. There are clear shifts of 6 and 10 cm^{-1} respectively in the A_g and E_g species of δ(O-Cd-O) modes. The frequency ratio of these bands to its hydrogeneted analogue is 1.058 in case of A_g species and 1.036 in case of E_g species. These ratios are consistent with the other members such as Zn, Ni and Cd salts of the systems. In case of ν_{as}(Cd-O) mode there are only 3 and 2 cm^{-1} shifts in the bands at 254 and 268 cm^{-1} respectively on deuteriation. Practically no shift in the position of bands at 300 and 604 cm^{-1} is observed in the spectrum of deuterated sample. We assign these bands as δ(F-Ti-F) and ν_s(Ti-F) modes. The medium

strong band at 365 cm^{-1} appeared with weak intensity at 348 cm^{-1} on deuteriation. We assign this band as ν_s(Cd-O). The frequency ratio of these bands also agrees with the ratio for corresponding bands in case of other systems of the series.

The ν(D-O) stretching modes appeared at 2532, 2546, 2574, 2588 and 2611 cm^{-1} corresponding to the 3452, 3461, 3488, 3503 and 3529 cm^{-1} bands associated with the stretching modes of (H-O) in its hydrogeneted salt (CFTH). The frequency ratios for the hydrogeneted and deuteriated systems is nearly 1.36 which agrees well with other members of the series. The number of Raman bands at 10k in CFTH is nearly equal to the number of bands in case of CFTHD at 10k.

The main features of the temperature dependence of Raman spectra of CFTHD are as follows -

1. Most of the bands became sharp and many shoulders and unresolved components appeared as distinct bands with decrease in temperature as in the case of CFTH.

2. The frequency shift, half-width and Raman intensities of some bands showed sudden changes or anomalous behaviour at low temperature.

3. At low temperature several modes of E_g species in the lattice mode and internal vibration regions split into two components.

4. The broad bands associated with the (O-D) stretching modes at room temperature split into five sharp components at 10 k.

The Fig. 7.3 shows the Raman spectra of $\overset{a}{\lambda}$ single crystal of CFTHD in the $\{x(yy)z\}$ orientation of the crystal at a few selected temperatures. The corresponding Raman spectral data are given in Table 7.3.

In the lattice mode region the band at 80 cm^{-1} at room temperature shows a gradual shift of frequency ($\Delta\nu$) from 110k to 70k and assumes lowest value (71 cm^{-1}) at about 80k. At a temperature of 110k, two more bands appeared at 90 and 113 cm^{-1} in the Raman spectra. The frequencies of these bands increase gradually as the temperature is decreased from 110k to 10k. At 10k the bands shift to 95 and 116 cm^{-1} respectively. The deformation mode δ(O-Cd-O) which appeared at 166 cm^{-1} at room temperature shifts to 170 cm^{-1} at about 220k, thereafter it remains at 170 cm^{-1} down to the temperature of 120k. From 110k it rises and becomes maximum at about 90k, thereafter it decreases gradually up to the temperature of 60k. From 60k to 10k it remains constant at 166 cm^{-1} (Fig. 7.4).

The ν_{as}(Cd-O) mode showed anomalous behaviour between the temperatures of 120 and 60k. Moreover this band splits into two components at 110k. Fig. 7.4 shows the sudden shift in frequencies in the ν_s(Cd-O) and ν_s(Ti-F) modes at about 220k and at 110k. The vibrational modes associated with the $\left[\text{Ti-F}\right]^{2-}$ ion show only slight change at 220k which may be due to corresponding changes in other ν_s(Cd-O) internal modes or due to changes in lattice parameters with temperature. However, we did not observe such changes in case of its hydrogeneted salt (CFTH).

The Raman peak intensities of ν_s(Ti-F), ν_s(Cd-O) and δ(F-Ti-F) bands showed sudden changes at temperatures of about 218 and 110k as shown in Fig. 7.5. In case of ν_s(Ti-F), as the temperature is gradually increased from 10k, the intensity decreases gradually upto 90k from 37.5 units (arbitrary units) to 37.2 units, but at 110k the intensity suddenly drops down to 35.9 units. Thereafter it decreases very slowly upto 200k. Then again at 210k it drops down suddenly to 35.5 units and afterwards the intensity decreases very slowly as shown in Fig. 7.5. Similar is the case for intensities of the bands associated with other two internal modes ν_s(Cd-O) and δ(F-Ti-F). The change in intensities shows a maximum in case of ν_s(Ti-F) and a minimum in case of δ(F-Ti-F) mode. The relative intensities of these modes are also shown in the Fig. 7.5. We have observed sudden change in intensities at two temperatures (218 and 110k) for all the three bands. The full width at half maximum (FWHM) of the bands associated with the symmetric stretching modes ν_s(Ti-F) and ν_s(Cd-O) showed strong temperature dependence. As the temperature is gradually increased from 10k to room temperature the FWHM increases rapidly. The plots of FWHM versus temperature for the two modes are shown in Fig. 7.6. The FWHM in both the cases suddenly increase at 110k and 218k. The nature of the curves in both the cases is very similar. The FWHM of ν_s(Ti-F) mode remains practically constant below 30k. It is 6.0 cm^{-1} at 10k but at room temperature its value is 16.0 cm^{-1}.

If we overlook the points near 110k and 218k, the curve from 40k to 290k is nearly a straight line. This straight line can be fitted to the equation with parameters as:-

$$\Delta\nu_{\frac{1}{2}}\ (cm^{-1}) = 0.0384T + 4.5\ (cm^{-1})$$

where T is in k. Similarly, in case of the $2\nu_s$(Cd-O) mode, if we overlook the values of $\Delta\nu_{\frac{1}{2}}$ (FWHM) near transition temperatures, the curve can be represented by two straight lines - one from 10k to 90k and the other from 150k to room temperature. The first part of the curve can be fitted to the equation -

$$\Delta\nu_{\frac{1}{2}}\ (cm^{-1}) = 19.3 + 0.0134T$$

and the second part to the equation -

$$\Delta\nu_{\frac{1}{2}}\ (cm^{-1}) = 16.4 + 0.0344T$$

where 19.3 and 16.4 are in cm^{-1} and T in k.

7.5.3 Temperature dependence of the line-width of the symmetric stretching vibration of D_2O molecules in CFTHD

The $2\nu_s$(O-D) band of the CFTHD which appears at 2536 cm^{-1} shows anomalous temperature dependence. When the temperature is gradually increased from 10k to room temperature, the line-width of $2\nu_s$(O-D) increases exponentially upto the temperature of 210k as shown in Fig. 7.7. Then there is a sudden increase in the line-width at about 218k. After this temperature the line-width increases

rapidly again. We observed a break in the smooth exponential curve at 218k as seen in the Fig. 7.7. This is indicative of a phase transition at this temperature.

It is well known that a number of physical processes contribute to a given line-shape and the relaxation mechanism of an excited vibrational state may be studied by careful measurements of the line-width of the corresponding Raman bands. The main physical processes contributing to line shape are - (1) population or life-time relaxation of the excited vibrational state, (2) reorientational motion of the molecules or molecular ions and (3) anharmonic interactions.

Under the approximation that the vibrational and rotational motions are statistically independent, it is possible to separate out the line broadening contribution due to reorientational motion from other intrinsic vibrational contributions. The reorientational motion results in the loss of phase coherence and thus contributes to the anisotropic part of the Raman scattering tensor (off-diagonal Raman tensor). The intrinsic vibrational part contributes to the isotropic part of Raman scattering tensor (diagonal components of Raman tensor).

We have measured the line width of the symmetric stretching mode ν_s(O-D) in the diagonal scattering geometry of the Raman spectrum. This mode is of A_g species and results from diagonal part of the Raman scattering tensor. The symmetric Lorentzian line-shape

rules out the possibility of any significant contribution from the reorientational process.

The $[Cd(OD_2)_6]^{2+}$ and $[TiF_6]^{2-}$ ions are bound mainly by hydrogen bonds which are strongly anharmonic. This anharmonicity gives rise to temperature dependence of the vibrational modes in two ways. The first way is due to thermal expansion of the lattice leading to a frequency shift but it does not contribute to line broadening. The second way is due to thermal fluctuations which effect random variation in the crystal potential and hence a coupling between different vibrational modes. This compling causes a frequency shift as well as line broadening.

The excited vibrational state may decay into a number of phonons according to symmetry selection rules due to cubic and quartic terms in the potential energy function [12,13]. The most expected process in the hexa-aquo salts is a decay into deformation mode of the water molecules $\delta(H_2O)$ at $\sim 1650\ cm^{-1}$. For this mode, $\hbar\omega \gg kT$ below 300k and hence this process would not contribute any significant temperature dependence to the line width.

Pure vibrational dephasing of excited state takes place via quartic terms in the expansion of potential function and can be visualized as an elastic scattering process between the excited state and some other state which creates a fluctuation in the energy of the excitation and thus a loss in phase memory (coherence). This process is known as exchange modulation [14a,b] and gives rise

to Arrhenius type of dependence of FWHM on temperature as given in equation 6.1 chapter VI -

$$\text{FWHM } (\Delta\nu_{\frac{1}{2}}) = A + B \exp\left[-\frac{U}{T}\right]$$

where A is a measure of the decay of the excited state via an inelastic three phonon process (here inelastic decay of ν_s(D-O) which will be temperature independent) and B is related to the inelastic decay of the low frequency mode of energy U equal to $\frac{\hbar\omega}{k}$ coupling with the ν_s(D-O). U is called activation energy. The plot in Fig. 7.7 is a fit to the Arrhenius type of relation given above, in which A, B and U are respectively 5.46 cm^{-1}, 175.2 and 455k. The relation so obtained explains the curve correctly upto the temperature of 210k. But from 220k to room temperature (290k), the curve is fitted to the equation :-

$$\Delta\nu_{\frac{1}{2}} = 175.2 \exp\left[-\frac{387}{T}\right]$$

Therefore, the value of U is decreased by 68k at higher temperature.

We, therefore, suggest that the broadening of line from 10 to 210k is due to vibrational dephasing of the excited ν_s(D-O) state by elastic scattering with the thermally excited torsional vibration of D_2O molecules observed at 328cm^{-1} compared to the predicted value of U = 455k.

It is interesting to note that the value of U obtained in our case compares very well with the value of 475k in the case of hexafluoro silicate of Ni by Jenkins and Lewis [15].

7.5.4 Structural phase transformation

From the temperature-dependent Raman studies on the deuterated crystal of CFTHD (from Figs. 7.4 to 7.8), we have observed two structural phase transformations - one at about 218k and the other at 110k. Therefore there is a rise in the critical temperature (T_c) on deuteriation by 18k and 30k respectively in the phase transition temperatures at the high and low temperatures compared to the case of CFTH. The mechanism of structural phase transition in this system appears to be similar as in case of CFTH which is mentioned in section 4.5.3 in chapter IV.

At low temperature the appearance of 5 sharp bands associated with the ν(O-D) vibrational modes and appearance of libration modes indicate that the D_2O molecules become ordered at low temperature below T_c. This also predicts the inequivalence of D_2O molecules in the $[Cd(OD_2)_6]^{2+}$ octahedra at low temperature. At least three different types of D_2O units can be inferred.

In this series of salt, the $[Cd(OH_2)_6]^{2+}$ and $[TiF_6]^{2-}$ octahedra are bound by hydrogen bonds. The hydrogen atoms of the $[Cd(OH_2)_6]^{2+}$ octahedra are bound to the fluorine atoms of the $[TiF_6]^{2-}$ octahedra as illustrated in Figs. 3(f & g) in chapter III. It is known that the strength of hydrogen bonding becomes weaker when hydrogen is substituted by deuterium due to heavier mass of deuterium and to its lower electron affinity in comparison to hydrogen. As the first transformation at higher temperature takes place due to ordering of the H_2O/D_2C molecules and distortions in

the $[Cd(OH_2)_6]^{2+}$ octahedra, this ordering may occur at somewhat higher temperature in deuterated salt compared to the hydrogenated system due to weakening of H-bonding strength. In other words, the $[Cd(OD_2)_6]^{2+}$ octahedra gets distorted at an earlier temperature when the sample is cooled from room temperature than the distortion in the $[Cd(OH_2)_6]^{2+}$ octahedra. Therefore there is a rise in T_c on substitution of D_2O in place of H_2O in most of the systems of this series of general formula mentioned in the section 7.2 in this chapter [5,16-20].

The second phase transition takes place due to the distortion in the $[TiF_6]^{2-}$ octahedra. As the two octahedra $[Cd(OD_2)_6]^{2+}$ and $[TiF_6]^{2-}$ are bound by hydrogen bonds, the substitution of H_2O by D_2O weakens the H-bonding strength which may result in the increase of bond strength between the Ti and F atoms in the $[TiF_6]^{2-}$ octahedra i.e. decrease in bond length between Ti and F. As the temperature is reduced below 220k, the lattice contracts further and the Ti^{4+} ion does not fit into the octahedron of the $6F^-$ ions. This process may occur at slightly higher temperature in the deuterated salt compared to the hydrogenated system. Therefore, the $[TiF_6]^{2-}$ octahedra may be distorted at an earlier temperature when it is bound to the $[Cd(OD_2)_6]^{2+}$ octahedra than when the same is bound to the $[Cd(OH_2)_6]^{2+}$ octahedra. Therefore the second phase transition takes place at higher temperature in case of deuterated salt than its hydrogenated salt. Some support for this hypothesis comes from the observed higher frequency for the ν_s(Ti-F) A_g mode at 607 cm^{-1} and

lower frequencies for the ν_{as}(Ti-F) E_g and δ(F-Ti-F) A_g modes at 407 and 296 cm^{-1} in the deuterated salt compared to the values at 603, 419 and 300 cm^{-1} for ν_s(Ti-F), ν_{as}(Ti-F) and δ(F-Ti-F) modes respectively in the hydrogenated salt at low temperature.

7.5.5 Low temperature phase structure

In want of X-ray or neutron diffraction data of the crystal structure of CFTHD, it is not possible to say much about its space group at low temperature below 110k from Raman polarization data alone. From the observations shown in Fig. 7.4 and Fig. 7.8 it is obvious that the space group must be lower than C_{3i} having no degenerate representations. The spectra at 10k of this salt (CFTHD) resembles the spectra of its hydrated salt at the same temperature. The space group at 10k in case of its hydrated salt has been established as C_{2h}^5 in the monoclinic series [17]. We therefore, infer that the low temperature space group should be C_{2h}^5 in this case (CFTHD).

7.6 References

[1] Thakur G and Verma A L, J. Raman Spectrosc. 17, 207 (1986).

[2] Jenkins T E and Lewis J, Spectrochim. Acta 37A, 47 (1981).

[3] Bose M, Roy K and Ghoshray A, Proc. Nucl. Phys. and Solid State Phys. Vol 24C pp 389 (1981), BARC, Bombay.

[4] Choudhury P, Paul B, Saha S and Ghosh B, Proc. Nucl. Phys. and Solid State Phys. Vol 24C pp 323 (1981) BARC, Bombay.

[5] Bose M, Roy K and Ghoshray A, J. Phys. C 16, 645 (1983).

[6] Petrakovskaya E A, Abakumova V S and Kochirova A G, Chem. Abs. 103(26) (1985), Abs No. - 226032u.

[7] Hamilton W C, Acta Crystallogr. 15, 353 (1962).

[8] Thakur G and Verma A L, Spectrochim.Acta 45A, pp 615, (1989).

[9] Thakur G and Verma A L, J. Raman Spectrosc. 20, pp 000 (1989).

[10] Choudhury P, Ghosh B, Patel M B and Bist H D, J. Raman Spectrosc. 16(3), 149 (1985).

[11] Jenkins T E and Lewis J, Physica Scripta 18, 351 (1978).

[12] Bellows J C and Prasad P N, J. Chem. Phys. 70, 1864 (1979).

[13] Hess L A and Prasad P N, J. Chem. Phys. 72, 573 (1980).

[14a] Harris C B, Skelby R M and Cornellius P A, Phys. Rev. Lett. 38, 1415 (1977).

[14b] Thakur G and Verma A L, to be communicated.

[15] Jenkins T E and Lewis J, J. Raman Spectrosc. 11, 1 (1981).

[16] Choudhury P, Ghosh B, Lamba O P and Bist H D, J. Phys. C. 16, 1609 (1983).

[17] Choudhury P, Ghosh B, Patel M B and Bist H D, Proc. of III Symp. on "Laser and its application" Bist H D and Goel J S (Eds.), Dec 16 (1983) I.I.T. Kanpur.

[18] Choudhury P, Ghosh B, Patel M B and Bist H D, J. Phys. C 17, 5827 (1984).

[19] Bose M, Roy K and Ghoshray A, J. Phys. C 17 (30) 5277 (1984).

[20] Bose M, Roy K and Ghoshray A, Proc. of D.A.E. Symp. 23C, pp 834 (1980). New Delhi.

[21] Bose M, Roy K and Ghoshray A, Proc. of D.A.E. Symp. 24C, pp 389 (1981) BARC, Bombay.

[22] Ghosh B, Chatterjee N, Das A N, Datta Roy S K and Paul A, J. Phys. C 10, L527 (1977).

[23] Bose M, Ghoshray A, Basu A and Roy K, J. Phys. C12, L771 (1979).

Table 7.1

Raman data of $CdTiF_6:6D_2O$ (CFTHD) at room temperature (290k) at different polarization geometries. A comparison of the data with that of the $CdTiF_6:6H_2O$ (CFTH) has been shown .

{y(xx)z}		{y(zy)z}		{x(yy)z}		{x(zz)y}		{x(zx)y}		Assignment
CFTH	CFTHD	CFTH	CFTHD	CFTH	CFTHD	CFTH	CFTHD	CFTH	CFTHD	
1	2	3	4	5	6	7	8	9	10	11
-	-	-	-	-	-	-	-	-	-	
56e	-	-	-	55e	-	-	-	-	-	
67e	-	66e	-	67e	-	-	-	-	-	Lattice modes
82vw	80w	84e	-	83s	80s	-	-	-	-	
125e	-	134e	-	131e	-	131e	-	-	-	
172e	-	-	-	172e	-	172e	-	-	-	
176m	166m	-	166vw	176m	166m	178e	-	-	-	δ (O-Cd-O)
183sh	-	180vw	-	-	-	-	-	-	-	
265s	256s	261w	256w	261m	256m	275sh	-	266vw	255w	ν_{as} (Cd-O)
304m	297m	293w	297w	300s	297s	305s	296s	299vw	297w	δ (F-Ti-F)
354m	343m	-	-	354w	343w	354vw	343m	-	-	ν_s (Cd-O)
-	-	-	-	453e	-	-	-	-	-	

Table 7.1 continued...

Table 7.1 continued

1	2	3	4	5	6	7	8	9	10	11
611vs	613vs	611m	613m	613vs	613vs	614vs	613vs	614w	614w	ν_s(Ti-F)
-	-	-	-	-	-	-	-	-	-	
3477s	2536m	-	2536vw	3480s	2536m	3485s	2536s	3470vw	2540vw	ν (H-O)/(D-O)
-	2556m	-	-	-	2556m	-	-	-	-	

e = extremely weak, vw = very weak, w = weak, m = medium,
s = strong, vs = very strong, sh = shoulder

Table 7.2

Spectral data in six polarization geometries of $CdTiF_6:6D_2O$ (CFTHD) at 10k.

Compared with that of $CdTiF_6:6H_2O$ (CFTH) at 10k

{y(xx)z}		{y(zx)z}		{y(zy)z}		{x(yy)z}		{x(zz)y}		Assignment
CFTH	CFTHD	CFTH	CFTHD	CFTH	CFTHD	CFTH	CFTHD	CFTH	CFTHD	
1	2	3	4	5	6	7	8	9	10	11
58e	-	-	-	58e	-	56e	-	-	54e	Lattice modes
68vw	69vw	-	-	-	-	67e	69e	-	67vw	
80e	77vw	-	72vw	80e	77vw	80vw	79e	-	-	
98m	93ms	98vw	92w	97vw	93w	95m	94w	95vw	92m	
113w	113vw	113e	115e	112e	-	114e	116vw	114vw	-	
121vw	-	-	-	-	-	121vw	-	-	-	
-	130vw	-	-	-	137vw	131e	-	131e	-	
171vw	142vw	172e	141vw	172vw	-	171w	165vw	172m	-	δ (O-Cd-O)
182m	172s	182vw	171m	181w	171m	181m	172m	183m	172m	
192sh	-	-	-	-	-	190w	184w	200e	-	
215e	229sh	-	-	-	-	-	-	211vw	-	
254m	248ms	254w	248m	254w	248w	254s	251ms	255w	248ms	$2\delta_{as}$ (Cd-O)
266m	260ms	268w	261w	268w	263w	268s	266ms	269e	260sh	

Table 7.2 continued.....

Table 7.2 continued ...

1	2	3	4	5	6	7	8	9	10	11
285w	-	287w	-	286w	279sh	285m	276sh	286vw	-	
300m	296s	300w	293s	301w	293s	300s	296s	299s	294s	δ (F-Ti-F)
313w	-	313w	332e	314m	328e	314m	328e	318vw	-	
365m	348w	363w	348w	364w	348vw	363s	353w	362w	355m	ν_s (Cd-O)
389e	-	389vw	-	-	-	-	-	381vw	-	
419vw	407vw	416e	411e	-	-	419w	-	-	-	ν_{as} (Ti-F)
454vw	-	-	447vw	-	452vw	-	-	-	-	
604vs	607vs	604m	607s	603w	608s	603s	607vs	604s	607vs	ν_s (Ti-F)
-	-	-	-	-	-	-	-	3429e	-	
3446s	2464vw	3445w	-	3444w	2492w	3446s	-	3446vw	2458vw	
3452s	2532s	3451w	2534s	3451w	2534m	3451s	2532s	3451w	2536vs	ν_1 and ν_3 of $\frac{(H-O)}{(D-O)}$
3461w	2548s	3461w	2547s	3461w	2548ms	3461w	2546ms	3462m	2548sh	
3488sh	2570s	3488sh	2571s	3487vw	2570s	3486vw	2574vs	3487m	2576vs	
3503vs	2588vs	3499vs	2596s	3497m	2581s	3497vs	2588ms	3497vs	2588sh	
3506sh	2613w	3505sh	2613w	-	2590s	3506sh	2611m	-	-	
3530m	2625vw	3532m	-	3529w	2613ms	3529m	2628w	3530w	2616m	

e = extremely weak, vw = very weak, w = weak, m = medium, ms = medium strong, s =strong, vs = very strong, sh = shoulder

Table 7.3

Spectral data of $CdTiF_6:6D_2O$(CFTHD) at a few selected different temperature in $\{x(yy)z\}$ orientation(temperature in k)

10	18	30	40	50	60	70	80	90	100	110	120	170	190	200	210	220
69	68	68	-	-	-	-	-	-	-	-	-	-	-	-	-	-
79	80	78	-	76	78	75	71	71	74	76	-	-	-	-	-	-
-	-	-	-	-	-	-	-	-	-	-	79	80	80	80	80	80
95	95	95	94	95	94	91	94	94	94	91	-	-	-	-	-	-
115	120	116	115	116	118	112	114	-	116	109	-	-	-	-	-	-
-	142	-	138	-	152	-	-	-	-	-	-	-	-	-	-	-
166	167	166	167	168	167	-	-	-	-	-	-	-	-	-	-	-
176	177	175	176	175	176	175	174	175	175	173	171	173	170	170	171	170
184	183	181	187	-	-	-	-	188	-	-	-	-	-	-	-	-
-	-	-	-	205	214	-	-	-	-	-	193	192	-	-	-	-
251	248	249	250	249	249	246	247	254	252	250	255	256	256	256	256	256
266	261	261	263	262	262	263	261	-	263	262	-	-	-	-	-	-

Table 7.3 continued.....

Table 7.3 continued

10	18	30	40	50	60	70	80	90	100	110	120	170	190	200	210	220
276	278	281	280	280	280	-	-	-	-	-	-	-	-	-	-	-
296	296	297	298	298	299	293	297	298	297	296	299	298	298	295	297	297
328	328	328	328	-	-	-	-	-	-	-	-	-	-	-	-	-
357	357	357	358	358	358	357	359	359	359	358	350	348	347	345	346	343
607	607	607	607	607	607	607	607	607	607	607	613	613	613	613	613	613
-	-	-	-	-	-	2461	-	-	-	-	-	-	-	-	-	-
2532	2533	2534	2534	2534	2534	2534	2534	2535	2535	2535	2536	2536	2536	2536	2536	2536
2547	2549	2549	2549	2548	2549	2547	2549	2549	2548	2548	2558	2560	2560	2559	2561	2560
2574	2569	2570	2571	2570	2570	2572	2571	2573	2572	2573	2573	-	-	-	-	-
2588	2589	2589	2590	2587	2586	2589	2589	2589	2589	2589	2589	-	-	-	-	-
2611	2615	2612	2612	2611	2612	2612	2614	2614	2614	-	-	-	-	-	-	-
2626	2627	2627	-	-	-	-	-	-	-	-	-	-	-	-	-	-

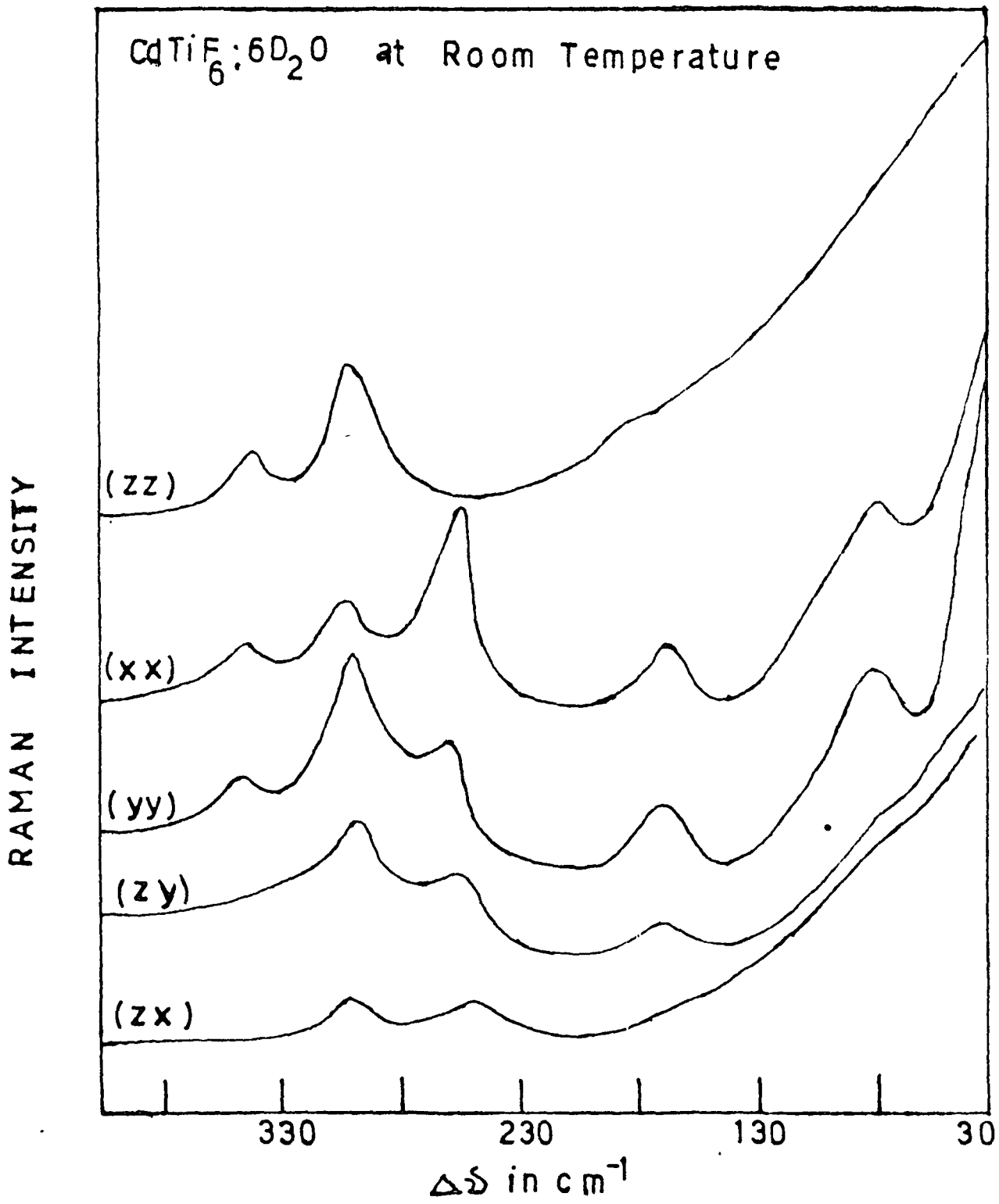

Fig. 7.1

Raman spectra of $CdTiF_6:6D_2O$ (CFTHD) at room temperature in a few selected polarization geometries in the region 30 to 400 cm^{-1}.

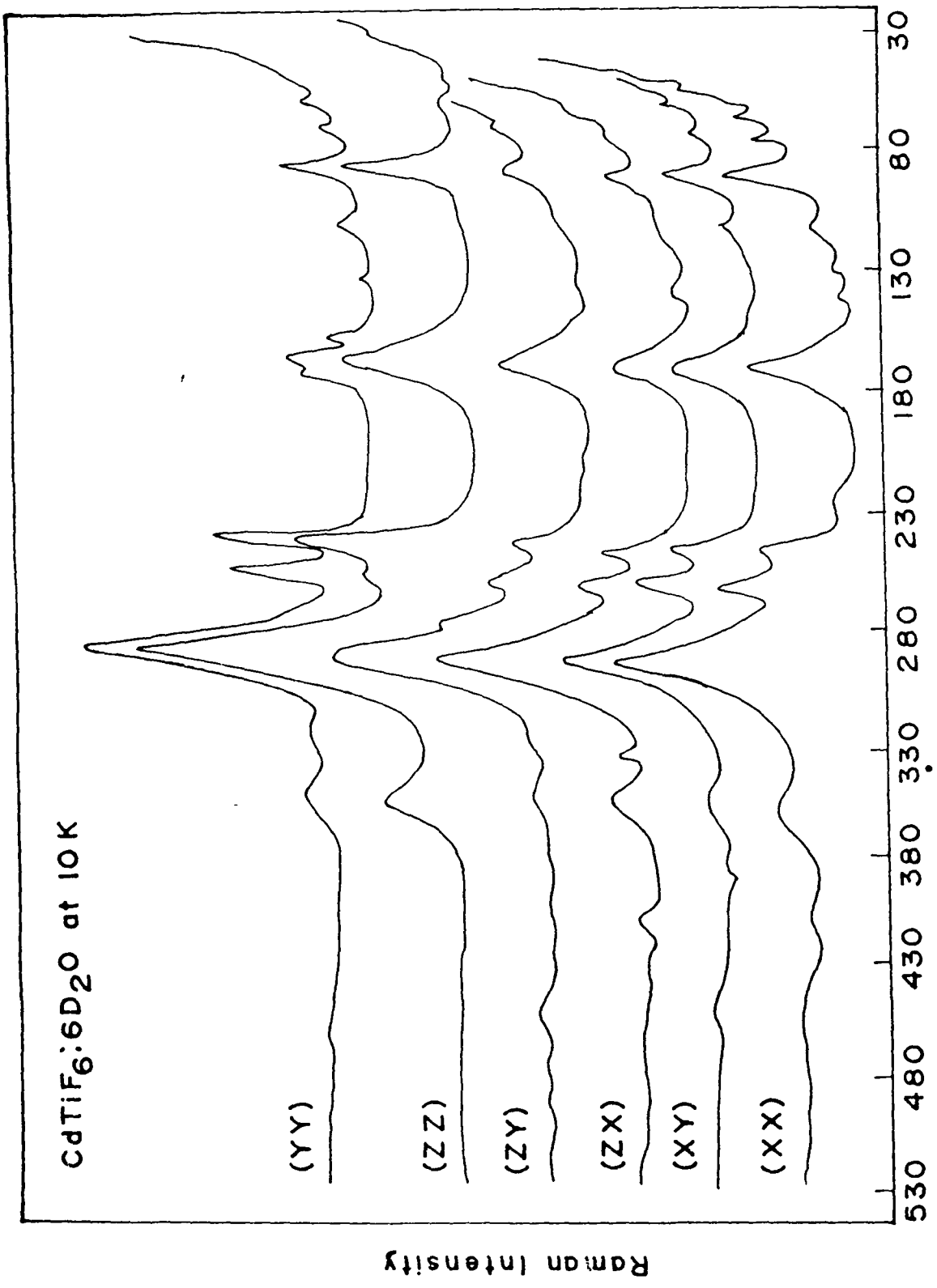

Fig. 7·2 (a)

Raman spectra of CFTHD at 10k in six polarization geometries in the region 30 to 530 cm^{-1}.

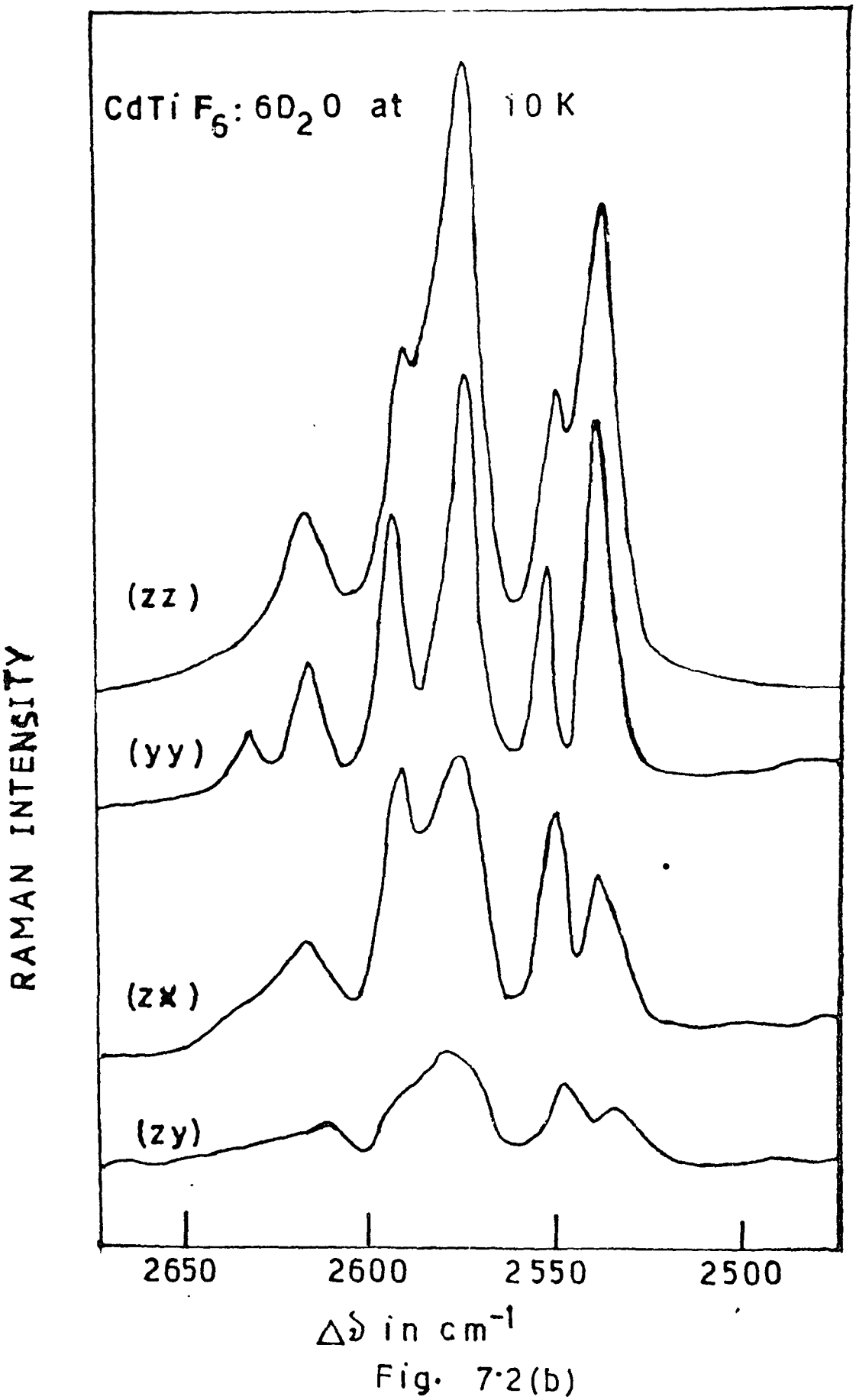

Fig. 7·2(b)

Raman spectra of CFTHD at 10k in a few selected polarization geometries in the region 2500 to 2650 cm^{-1}.

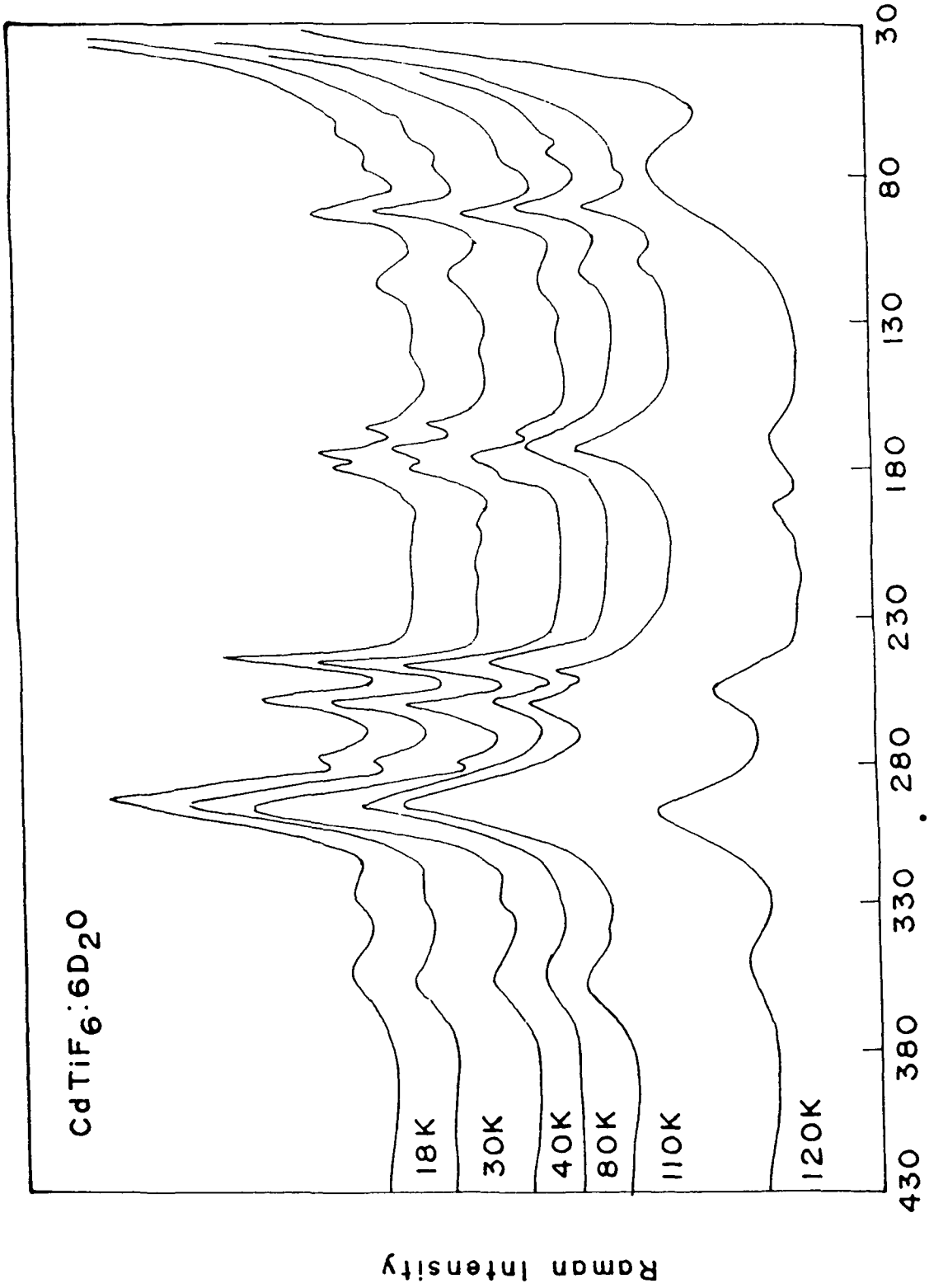

Fig. 7.3 (a)

Raman spectra of CFTHD at different temperatures in the {x(yy)z} orientation in the region 30 to 430 cm^{-1}.

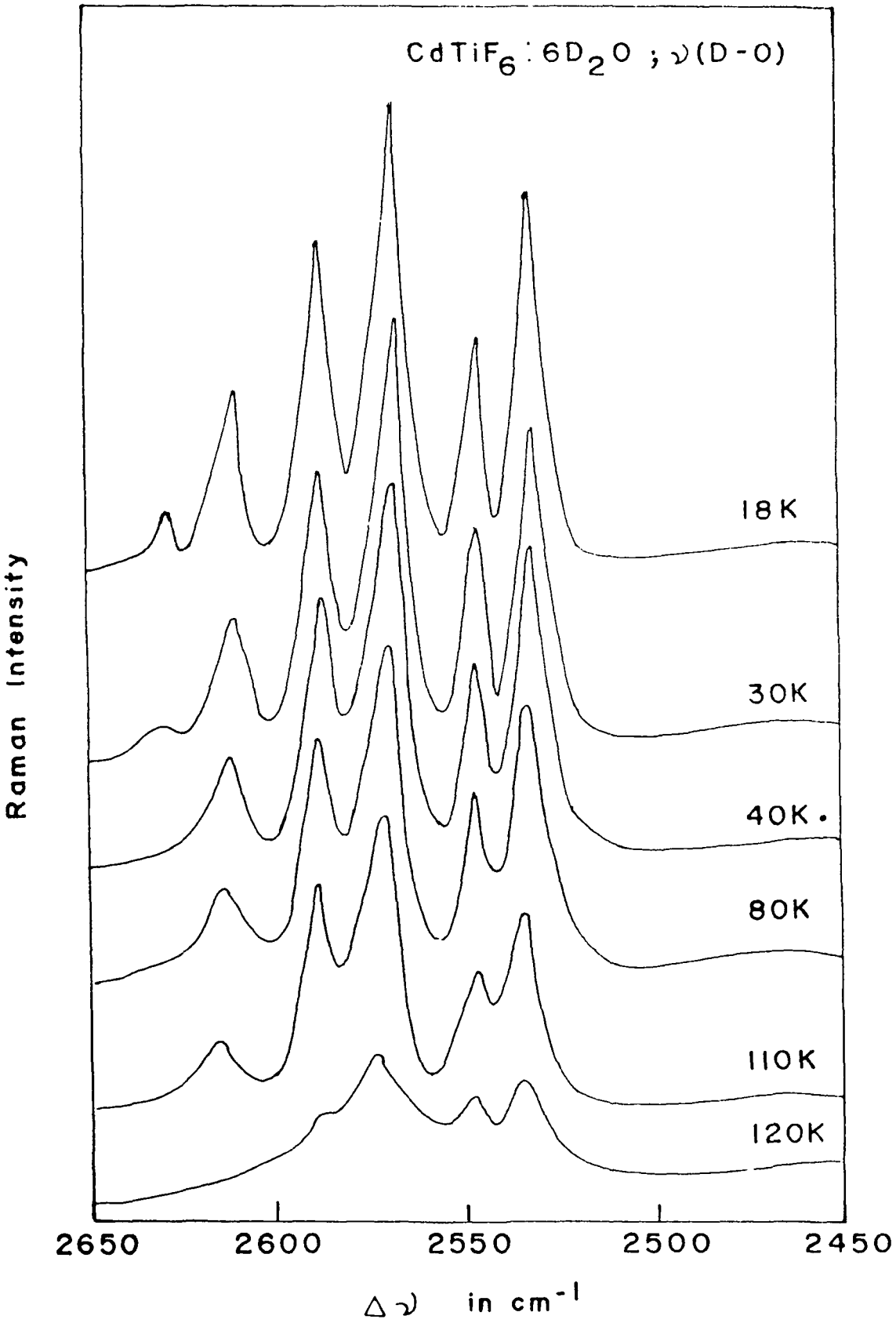

Fig. 7·3(b)

Raman spectra of CFTHD at different temperature in the $\{x(yy)z\}$ orientations in the region 2450 to 2650 cm^{-1}.

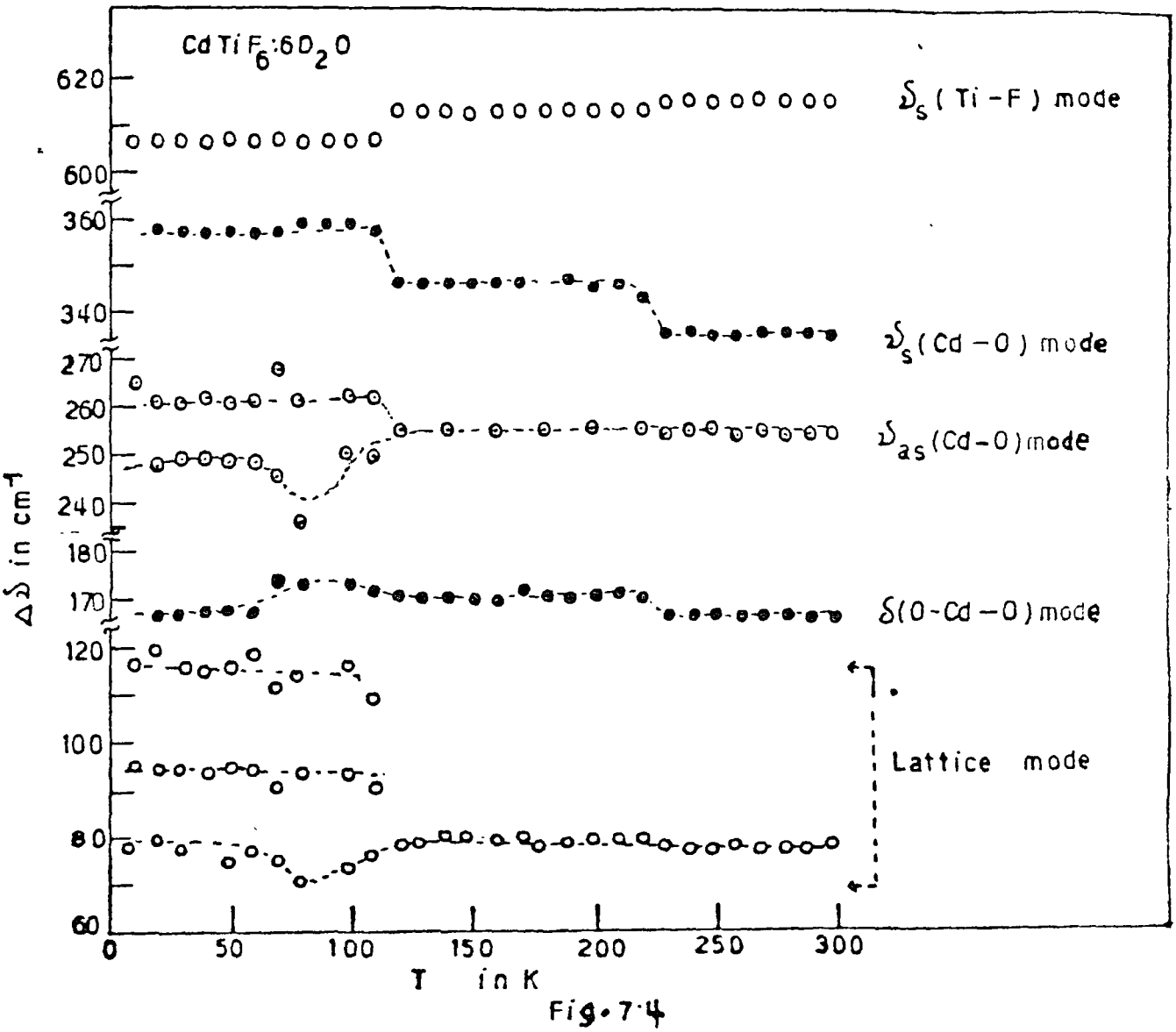

Fig. 7·4

Frequency shift of few Raman bands for CFTHD as a function of temperature

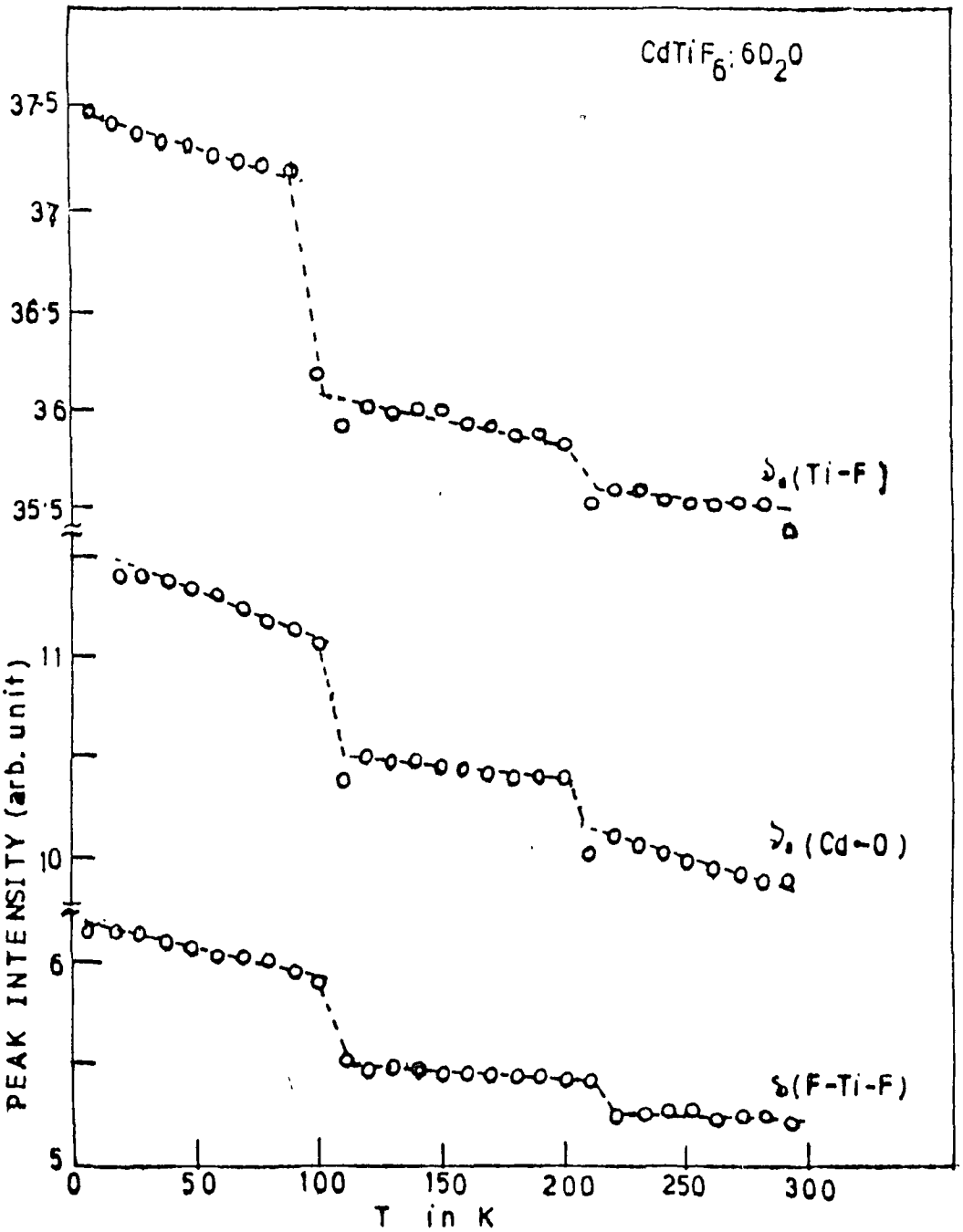

Fig. 7·5

Variation of peak intensity of a few bands as a function of temperature.

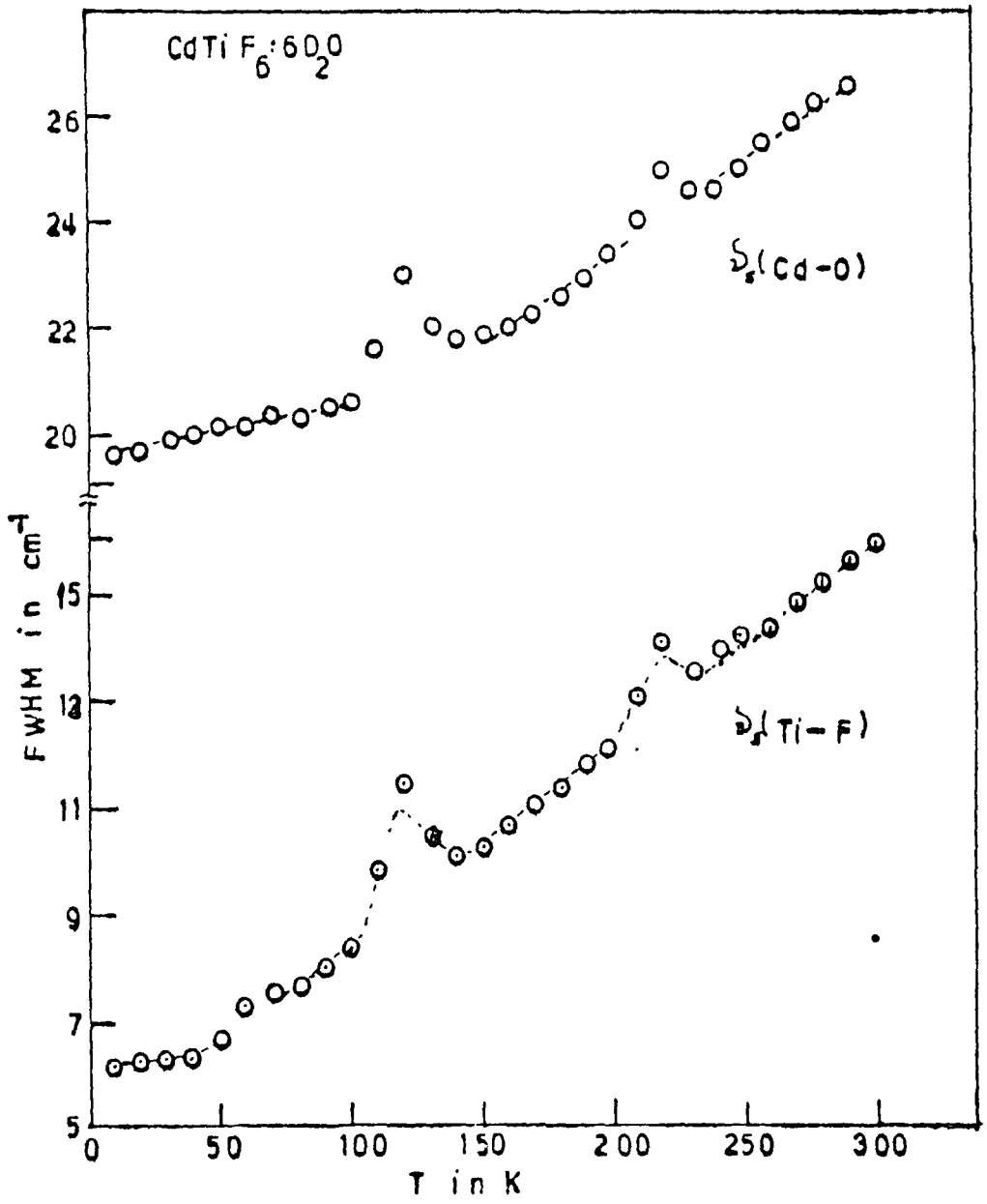

Fig. 7.6

Variation of FWHM ($\Delta\tilde{\nu}_{\frac{1}{2}}$) of $\tilde{\nu}_s$(Cd-O) and $\tilde{\nu}_s$(Ti-F) modes of CFTHD with temperature.

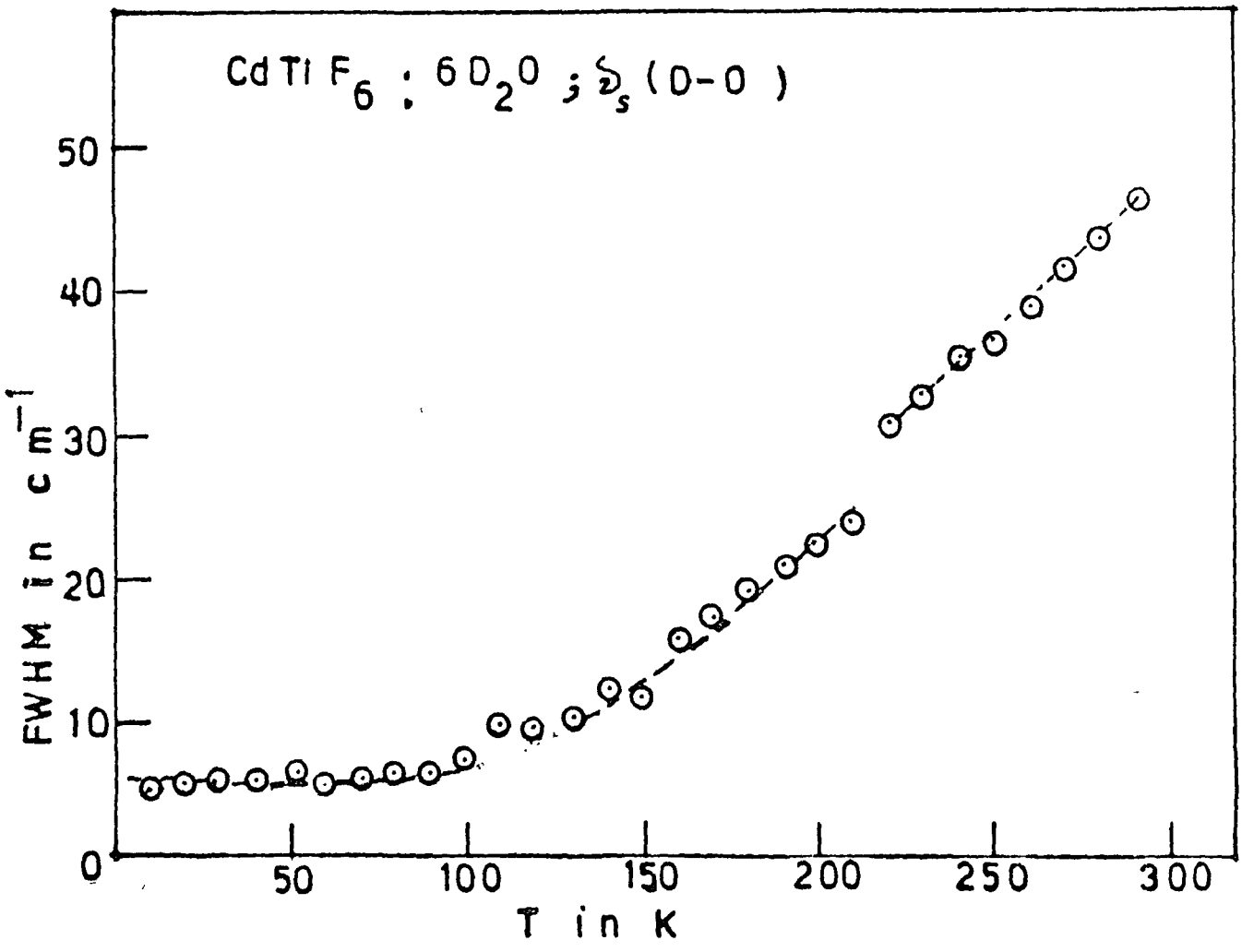

Fig. 7·7

Variation of $\Delta\tilde{\nu}_{\frac{1}{2}}$ of $\tilde{\nu}_s$(D-O) mode the $\{x(yy)z\}$ geometry of CFTHD as a function of temperature.

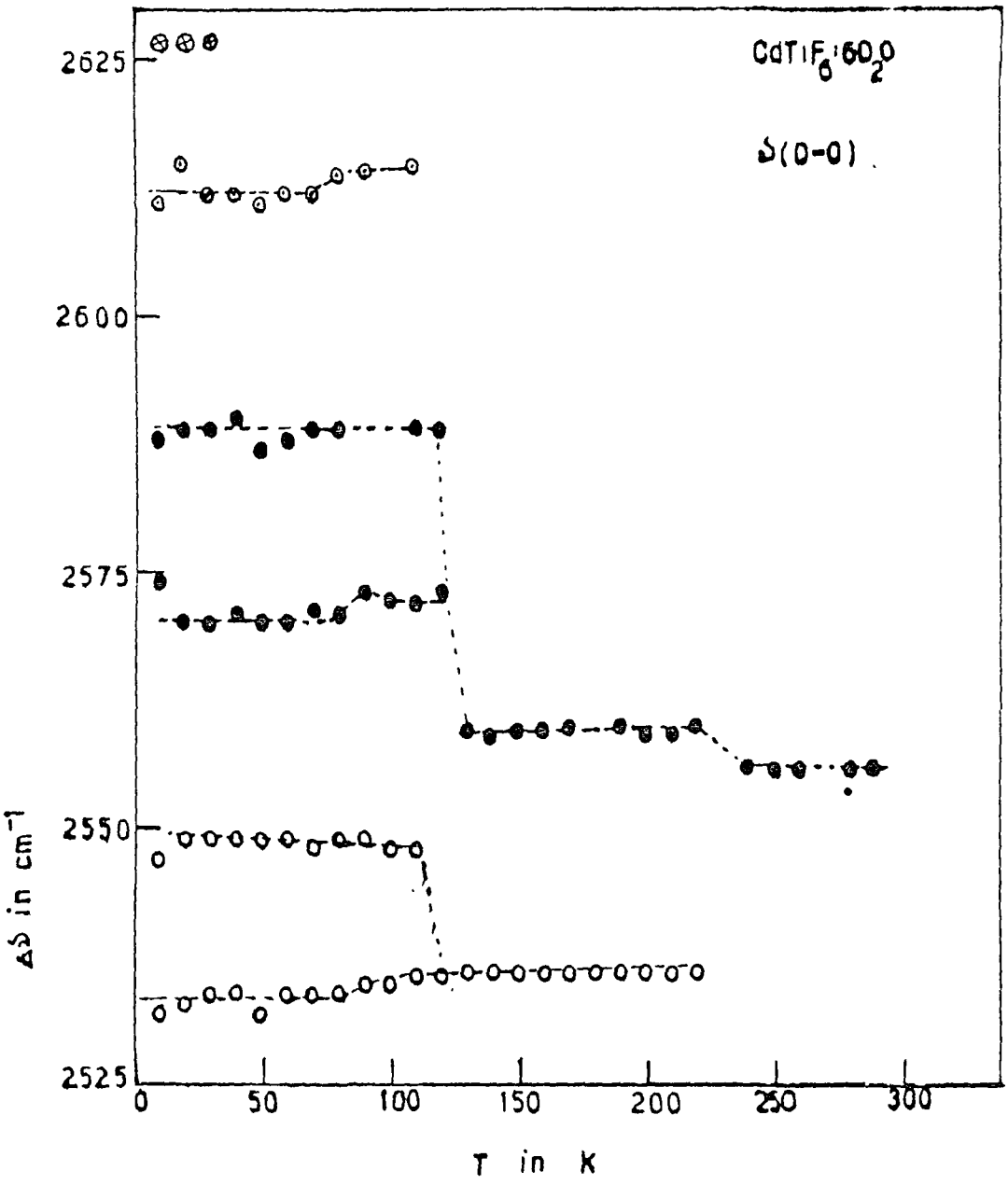

Fig. 7·8

Frequency shift of δ (D-O) modes on variation of temperature for CFTHD.

CONCLUSION

Conclusions and Suggestions for Further Research Work on this Class of Materials

Conclusion - This research work has been discussed in Chapter II and in Chapters IV to VII. The Chapters I and III give General Introduction and Theoretical Aspects relating to the work.

A new experimental arrangement for preparation of H_2TiF_6 acid in laboratory has been developed during the course of this work. A modified solution method for the growth of single crystals of highly hygroscopic hexafluoro silicates and titanates of divalent metals has been devised by us.

The Raman spectra of single crystals of $CdSiF_6:6H_2O$, $CdSiF_6:6D_2O$, $CdTiF_6:6H_2O$ and $CdTiF_6:6D_2O$ at room temperature and at 10k in all the six polarization geometries along with temperature dependent studies from 300 to 10k in specific geometries have been made for the first time in this study.

$CdSiF_6:6H_2O$ crystal undergoes a structural phase transition at 220k. The deuterated analogue of this crystal shows a structural phase transition at 235k. In case of $CdTiF_6:6H_2O$ crystal, we have discovered two phase transitions - one at 200k and the other at 80k. In case of its deuterated analogue, there is a rise in T_c^s by 18k in the high temperature and by 30k in low temperature phase transition temperatures compared to the hydrogenated system.

The high temperature phase transition is triggered by distortions in the $\left[Cd(OH_2)_6\right]^{2+}$ octahedra in all the systems ($CdSiF_6:6H_2O/D_2O$ and $CdTiF_6:6H_2O/D_2O$) investigated in this study. The low temperature structural phase transitions, in case of $CdTiF_6:6H_2O/D_2O$ systems, are triggered by similar distortions in the $\left[TiF_6\right]^{2-}$ octahedra.

The room temperature space group of these crystals ($CdXF_6:6H_2O/D_2O$ where X = Si, Ti) has been established to be C_{3i}^2 ($R\bar{3}$). The space group of the low temperature phase in these systems is proposed to be C_{2h} in monoclinic series of the crystal class.

The anomalous behaviour of the full width at half maximum (FWHM) of the ν_s(O-D) mode as a function of temperature from room temperature to 10k has been explained in terms of pure vibrational dephasing of the excited ν_s(O-D) state due to coupling with the thermally excited torsional vibration of D_2O molecules.

The IR spectra at room temperature of $CdSiF_6:6H_2O$ and $CdTiF_6:6H_2O$ between 200 to 4000 cm^{-1} region have been measured for the first time. The IR spectra at room temperature of $CdSiF_6:6D_2O$ and $CdTiF_6:6D_2O$ between 1800 to 3800 cm^{-1} have been measured which have helped to establish the room temperature space group of the systems.

Suggestion for further research on these systems

In order to confirm and support the structural and phase transformation information on these systems, the X-rays, neutron diffraction, magnetic resonance, specific heat etc, studies at

different temperatures shall be of great help. Further Laser Raman studies on similar systems at different temperatures alongwith temperature-dependent infrared measurements on single crystals of these and other systems shall help greatly in arriving at comprehensive picture of the mechanism of structural phase transformations in this class of compounds.

A P P E N D I X

Table A1

Table Previous studies of phase transition in the system of general formula $MXF_6\ 6(D_2O/H_2O)$ with critical temperature T_c

M	X	H_2O/D_2O	T_c (K)	Method/technique	Ref
Zn	Si	H_2O		IPOCPL, Raman	[1, 2]
Zn	Ti	H_2O	180, 182, 173, 185	EPR, NMR, Dielec, Raman	[3–7]
Zn	Ti	D_2O	182, 180–200, 182, 230	NMR, Raman	[4, 8, 9]
Ni	Si	H_2O	100–270	Dielec	[9(a)]
Ni	Si	H_2O	--	IPOCPL, Raman, EPR	[1, 10, 11]
Ni	Ti	H_2O	121, 120, 122–126	FSR, Raman, NMR	[12, 2, 12(a)]
Ni	Ti	H_2O	134 137, 136	EPR, Magn Susc	[13–15]
Ni	Ti	D_2O	129	NMR	[16]
Co	Si	H_2O	143–173	X-ray	[18]
			246, 259, 246, 240, 230	Magn Aniso, IPOCPL, EPR	[17, 19, 1, 23, 24]
Co	Si	D_2O	263, 262	Magn Aniso, ir, NMR	[20, 21]
Co	Ti	D_2O	262, 261	2D NMR	[22, 25]
Mn	Si	H_2O	223, 143–173 230	OB, X-ray, IPOCPL	[26, 18, 1]
			No 1st order but 2nd order S P T	Nir	[27]
Mn	Ti	H_2O	144	ir	[7]
Mn	Ti	D_2O	200	Raman	[28]
Fe	Si	H_2O	240, 225 230	IPOCPL EPR, X-ray, DSC, DTA	[1, 23, 29–37]
Fe	Ti	H_2O	275	DSC	[33]
Mg	Si	H_2O	298, 302, 298	X-ray, DSC EPR IPOCPL •	[38, 31 1]
Mg	Ti	H_2O	318	EPR	[31]
(Cu, Zn)*Si		H_2O	255–228	DSC	[39]
(CoMg)*Si		H_2O	243 253	Nir	[40]

IPOCPL = Interference Pattern of Convergent Polarized Light
OB = Optical Birefrigerence
*Cu and Co = Diluted with Zn and Mg ions
S P T = Structural Phase Transition

References for Table-A 1

[1] Poulet H and Mathieu J, C.R. Acad. Sc. Paris, t-286(12) Series B, 331 (1978).

[2] Jenkins T E and Lewis J, Spectrochim. Acta 37A, 47 (1981).

[3] Rubins R S, Chem. Phys. Lett. 28, 273 (1974).

[4] Afanasyev M L, Lybzikov A F, Menshikov V V and Zeer E P, Chem. Phys. Lett. 60, 279 (1979).

[5] Choudhury P, Bal B, Saha S, and Ghosh B, Proc. of Nucl. Phys. and Solid State Phys. Vol 24C, pp 323, Dec. 28 (1981), BARC, Bombay.

[6] Jayaram Geetha and Sivarama Sastry G, Chem. Phys. Lett. 97, 431 (1983).

[7] Choudhury P, Ghosh B, Lamba O P. and Bist H D, J. Phys. C 16, 1609 (1983).

[8] Choudhury P, Ghosh B, Patel M B and Bist H D, Proc of 3rd Symp. on "Laser and its application" Bist H D and Goel J S (eds.) Dec. 16 (1983), I.I.T. Kanpur.

[9] Bose M, Roy K and Ghoshray A, J. Phys. C 16, 645 (1983).

[9a] Rammetveit R and Svare I, Physica Scripta 17, 27 (1978).

[10] Jenkins T E and Lewis J, Physica Scripta 18, 351 (1978).

[11] Rubins R S and Haghighatijou T, J. Phys. Chem. Solids 43 (5), 491 (1982).

[12] How T and Svare I, Physica Scripta 9, 40 (1974).

[12a] Cheung H M and Lichti R L, J. Phys. C 18, 6157 (1985).

[13] Rubins R S, Griffin B C and Burris R, J. Chem. Phys. 64 (8), 3349 (1976).

[14] Rubins R S, Bull. Ann. Phys. Soc. 20, 386 (1975).

[15] Karnezos M and Friedbero S A, J. Appl. Phys. 49, 1382 (1978).

[16] Bose M, Roy K and Ghoshray A, J. Phys. C 17 (30), 5277 (1984).

[17] Majumdar M and Datta S K, J. Chem. Phys. 42(1), 418 (1965).

[18] Kodera E, Torii A, Osaki K and Watanabe T, J. Phys. Soc. Japan, 32, 863 (1972).

[19] McLellan A G, and Datta S K, Nat. Seminar on Cryogenics, New Delhi, Abst No = 18. (1975).

[20] Ghosh B, Chatterjee N, Das A N, Datta Roy S K, and Pal A, J. Phys. C 10, L627 (1977).

[21] Bose M, Ghoshray A, Basu A and Roy K, J. Phys. C 12, L771 (1979).

[22] Bose M, Roy K, and Ghoshray A, Proc. of DAE Symp. 23C, pp 834 (1980) New Delhi.

[23] Sthanapati J and De D K, Phys. Stat. Sol(a) 68, K123 (1981).

[24] Roychoudhury Manashi and Pal A K, Indian J. Phys. 55A, 419 (1981).

[25] Bose M, Roy K and Ghoshray A, Proc. of DAE Symp. 24C, 389 (1981).

[26] TSujikawa I and Couture L, J. Phys. Radium 16, 430 (1955).

[27] Datta Sunil K and De Debabala, Indian J. Cryog. 4(1), 39 (1979).

[28] Choudhury P, Ghosh B, Patel M B, and Bist H D, J. Phys. C 17, 5827 (1984).

[29] Rubins R S, J. Chem. Phys. 60, 4189 (1974).

[30] Jehanno G and Varret F, Acta Cryst. A 31, 857 (1975).

[31] Rubins R S and Jani S K, J. Chem. Phys. 66, 3297 and 3948 (1977).

[32] Chappert , J. Physique, 38, 411 (1977).

[33] Rubins R S, unpublished data.

[34] Vollard U, Hösl S and Spiering H , Solid State Commun., 27, 49 (1978).

[35] Rubins R S, J. Chem. Phys. 70, 4383 (1979).

[36] Chevrier , Acta Cryst. A 37, 578 (1981).

[37] Orland P and Rigamonti A, Phys. Stat. Sol. (a) 82, K129 (1984).

[38] Syoyama S and Osaki K, Acta Cryst. B 28, 2626 (1972).

[39] Sukhariviskii , Ukr. Fiz. Zh., 27 (9), 1418 (1982) Chem. Abst. 98 (4) Abst No. 25759.

[40] Datta S K, and De Debabala, Indian J. Phys. 52A, 499 (1978).

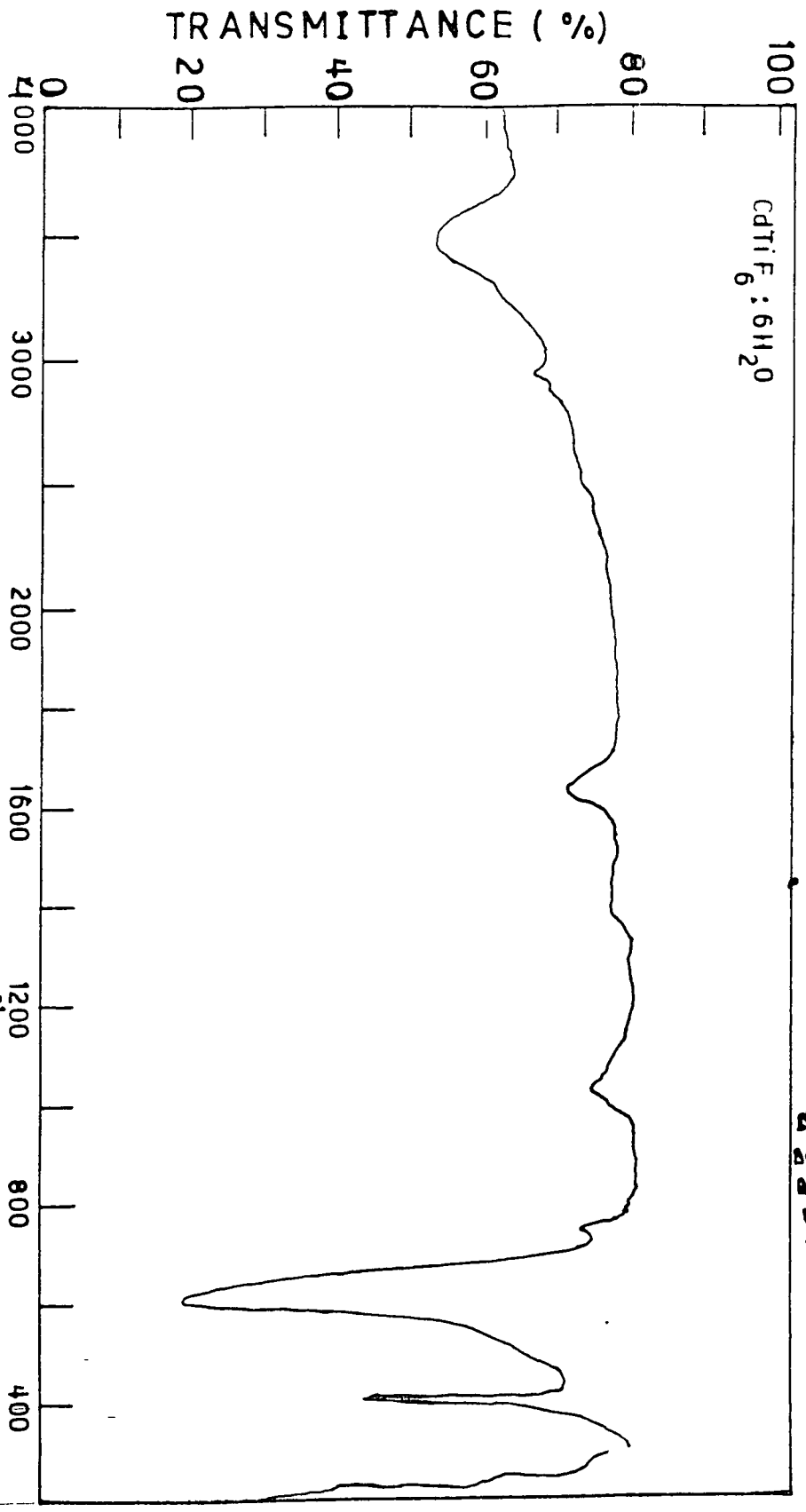

Fig. A1

IR of $CdTiF_6 : 6H_2O$ at room temperature